Spatial and Temporal Stratal Evolution of an Ancient Deep-Marine Channel-Levee Complex, Neoproterozoic Isaac Formation, Windermere Supergroup, British Columbia, Canada

Patricia Fraino

Thesis submitted to the University of Ottawa

in partial fulfillment of the requirements for the M.Sc. degree in Earth Sciences

Faculty of Science
University of Ottawa

Abstract

At the Castle Creek study area a superbly exposed slope channel system (Isaac channel complex 1; ICC1) crops out. ICC1 is ~ 220 m thick, exposed 5 km along strike and consists of four vertically-stacked channel units (LC, UC1-UC3). Based on lithological changes and grain size analysis, two styles of channel fills and stacking patterns are recognized – a disorganized stack of aggradational channel fills (LC, UC1 and UC2) and an organized lateral-offset stack of laterally accreting channel fills (UC3). Changes in channel stacking pattern are interpreted to be related to the combined effects of long- and short-term changes in relative sea level (RSL) that controlled the granulometric make-up and volumetric potential of shelf sediment storage. Episodes of abundant coarse shelf sediment caused flows to adopt a plug-like density structure that promoted riverine-like lateral accretion in channel bends. Conversely, when sediment was sourced principally from the hinterland, flows were highly stratified, which promoted channel aggradation.

Résumé

Dans la région d'étude de Castle Creek, un système de chenaux de pente (ensemble du complexe du chenal Isaac 1; ICC1) est superbement exposé. ICC1 a une épaisseur d'environ 220 m, est exposé sur 5 km parallèlement à l'orientation des strates et consiste en quatre unités de chenal empilées verticalement (LC, UC1-UC3). Basés sur les changements lithologiques et une analyse de granulométrie, deux styles de remplissage de chenaux et motifs d'empilage sont reconnus – un empilage désorganisé de remblai de chenal formé par aggradation (LC, UC1 et UC2) et un empilage organisé, latéralement décalé, de remblai de chenal formé par accrétion latérale (UC3). Des changements en motif d'empilage des chenaux sont attribués à la combinaison des effets de changements à long et à court terme du niveau marin relatif. Cette dernière variable contrôle la constitution granulométrique et le potentiel volumétrique de stockage des sédiments de la plate-forme continentale. Des épisodes d'abondance de sédiments grossiers sur la plate-forme continentale ont provoqué la formation de structures de densité "en bouchon" dans les courants, favorisant l'accrétion latérale de type fluviale dans les courbes des chenaux. Contrairement, quand le sédiment provenait principalement de l'arrière-pays, les courants étaient hautement stratifiés, favorisant l'aggradation des chenaux.

Extended Abstract

At the Castle Creek study area (British Columbia, Canada) a superbly exposed, thickly developed and areally expansive channel complex set in the Windermere turbidite system, here termed Isaac channel complex 1, or simply ICC1, crops out. Detailed documentation of the lithological composition and stratigraphic relationships of inter- and intra-channel fills allows for a comprehensive examination of the complex history of erosion and deposition in a slope-channel system. ICC1 overlies a sequence boundary that separates mixed carbonate-siliciclastic strata (first Isaac carbonate; FIC) from siliciclastic strata of ICC1 and represents the reintegration of sediment delivery from the cratonic hinterland. ICC1 is 220 m thick, is exposed over 5 km along strike and consists of four vertically-stacked channel units: lower channel unit (LC), and three upper channel units (termed UC1 through UC3).

Channel fills of LC, UC1 and UC2 are ~ 4 - 12 m thick and bounded on their margins by erosional basal surfaces that locally scour levee deposits composed of thin-bedded, fine-grained, upper division turbidites, although in the case of LC, channel fills onlap an erosional surface incised at least 30 m deep into strata of the FIC. Channel fills comprise amalgamated, thick-bedded, very coarse-grained sandstone and conglomerate in their axis that fine and thin upward and laterally towards their margins. In addition, strata in LC, UC1 and UC2 show a progressive decrease in modal grain size, but collectively exhibit a polydispersed granulometry (platy- to mesokurtic). Based on lithological and microscopic analysis, channels in LC, UC1 and UC2 are interpreted to have been filled by (vertically) density-stratified flows with a high-density axial part, which deposited amalgamated, coarse-grained sandstone, and low-density, lower energy margins that deposited finer and thinner-bedded strata. Because density-stratified flows experience intense mixing with the ambient fluid, transport capacity is exceeded and results in higher net rates of

sedimentation in the channel compared to over the interchannel areas. This causes the local channel gradient to be reduced, which eventually forces avulsion and channel displacement to a topographically lower (hydraulically more favourable) area on the seafloor, which overtime becomes manifest as a disorganized stacking pattern (sensu McHargue et al., 2011).

In contrast, UC3, which is up 30 m thick, comprises at least six channel fills that are up to 10 m thick and filled with coarse-grained sandstone and conglomerate that show little upward or lateral change in grain size or bed thickness. Additionally, channels exhibit well-developed lateral-accretion surfaces and contain deposits with a moderately-sorted, centrally concentrated (leptokurtic) granulometry. Flows are interpreted to have been poorly density stratified with a basal, coarse-grained layer of more or less uniform sediment concentration. This plug-like density profile resembles that in open channel flows (i.e. rivers) and caused the lower, depositionally important part of the flow to operate much like a river, which in channel bends promoted continuous lateral migration of individual channels, and in the longer term, the systematic lateral-offset stacking of successive channels.

The systematic temporal trend in channel stacking pattern and associated stratal architecture in ICC1 is interpreted to be as consequence of changes in the make-up of the sediment supply, specifically grain size and grain sorting, and their collective influence on the density structure of the channel-confined turbidity currents. These changes are a consequence of an upward change from a poorly-sorted hinterland- to a better-sorted shelf-dominated sediment supply associated with a long-term (possibly 3rd order) sea level rise. Transgression progressively expanded the size of continental shelf and therefore its sediment storage potential, in particular the retention of coarse sediment, which then came to dominate the granulometry of sediment transported to the shelf edge during shorter term (4th / 5th order) sea level falls. With the systematic

development of these two end-member grain size populations were two distinctly different kinds of turbidity currents that gave rise to two end-member channel architectures and stacking styles.

Acknowledgments

This thesis would not have been possible without the help of numerous individuals along the way and I am grateful to every one of them. First and foremost, I would like to thank my supervisor Bill Arnott for giving me the opportunity to work on this project that has been looked at by several people over many years. I'd like to think we finally gave ICC1 its well-deserved ending. Thank you for your guidance, knowledge, for always being enthusiastic and fun when discussing anything focussed on deep-marine sedimentology, for the best and often eye-opening discussions and for the many hours you spent editing my (mediocre-at-best) writing. I hope I can carry all the knowledge that you taught me and your enthusiasm for geology wherever life takes me.

I would like to thank Clement Bataille and Don Cummings for taking the time to serve on my defense committee and providing feedback to improve this thesis.

To Dr. Lilian Navarro for being a mentor since day one, for getting me started on the right foot in my first field season, taking notes and samples, and for the long adventures to the north side. Thank you for your countless hours of discussions about channel 1, guidance and availability to answer many of my questions and the moral support throughout this entire thesis. To my field assistant Liam Jaspere, thank you for taking on this adventure with me in 2019! for your tireless help to collect data, carry my samples, go back to camp if I forgot something, to the many chats about life, geology and biology, endless Shrek quoting, for being an incredible scale and for your astonishing quick math skills (#1310). You made my life much easier in the field.

To the Windy girls: Celeste Cunningham, Simona Ruso, Mary Macquistan and Jessie Kehew for the being helpful in the field, for the many coffee runs and the endless intellectual conversation in the field and office such as what constitutes being inside and which Shania Twain song is the best. To the soon-to-be (ish) Dr. Jag Ningthoujam, thank you for the many hours of discussion about matrix-rich sandstone, for always stopping me on the way to the bathroom to talk about Markov's chain analysis, for the geological map of the Cloridorme Formation, hang in there, just remember all work and no play makes Jack a dull boy. To the rest of the windy group, Dr. Mike Tilston and Dr. Omar Al-Mufti thanks for your support, your questions and comments during Friday meetings, which were very helpful! I would like to thank the Windermere Consortium and

the following partners for their intellectual and continued financial support Anadarko/OXY, Equinor, Husky, NSERC and the University of Ottawa.

I would like to thank all my fellow graduate students for making my time at the University of Ottawa and moving to a different province an amazing experience. Also, special thanks to Genevieve Huyer for her constant input on figures and her awesome CorelDraw skills that I will never have.

Last, but not least, I would like to thank my friends and family. Particularly my parents, Patricia Guasti and Sergio Fraino and my sisters Valeria and Catherine for being there for me, sticking by my side when I decided to move ~ 3400 km away from home. Thank you for your support, many face-time and phone calls, for moral support and allowing me to pursue my passion.

Table of Contents

List of Figures

Chapter 1: Thesis Introduction

Chapter 2: Facies Descriptions and Interpretations of a Deep-Marine, Base-of-Slope, Channel-Levee System, Neoproterozoic Windermere Supergroup, British Columbia.

Chapter 3: Characterization of Stratal Elements in a Deep-Marine, Base-of-Slope, Channel-Levee System, Neoproterozoic Windermere Supergroup, British Columbia.

Chapter 4: Spatial and Temporal Evolution of a Base-of-Slope Channel Complex Set, Isaac Formation, Neoproterozoic Windermere Turbidite System, Cariboo Mountains, British Columbia, Canada.

Chapter 5: Conclusions and Areas for Future work

Appendix A: Drone Photomosaics and Stratigraphic Sections

List of Tables

List of Abbreviations

2-D	Two dimensional
3-D	three dimensional
δ13Ccarb	Carbon isotope composition of carbonate carbon (inorganic)
Cal	Calcite
CC	Castle Creek study area
CC-SE	Castle Creek southeast
CC-South	Castle Creek south
CC-NW	Castle Creek northwest
cm	Centimeter
EN2	Ediacaran δ13Ccarb negative excursion 2 China (Gaskiers glaciation)
F1	Structureless, normally-graded and ungraded sandstone and conglomerate
F2	Traction-Structured Sandstone
F3	Graded, planar-laminated or massive siltstone to massive, structureless mudstone.
F4	Matrix-supported conglomerate
FIC	First Isaac Carbonate
FSST	Falling Stage Systems Tract
HST	Highstand Systems Tract
HS	Hill Section study area
ICC1	Isaac Channel Complex 1
km	Kilometer
LC	Lower Channel Unit
LST	Lowstand systems tract
Ma	Million years ago (datum)
mm	Millimeter
m	Meter
MTD	Mass Transport Deposit
Mus	Muscovite
Myr	Million years (duration)
OFP	Old Fort Point Formation

Plag	Plagioclase
Qtz	Quartz
RSM	Rhythmically intercalated sandstone and sandy mudstone cross-stratified sandstone
SB	Sequence Boundary
Ser	Sericite
SIC	Second Isaac Carbonate
SR	Isolated single set cross-stratified sandstone
SS	Single set cross-stratified sandstone
T_a	A division of Bouma Sequence: massive to structureless sandstone
T_b	B division of Bouma Sequence: planar-laminated sandstone
T_c	C division of Bouma Sequence: ripple cross-stratified sandstone
T_d	D division of Bouma Sequence: discontinuous interlaminated silt-mud couplets
T_e	E division of Bouma Sequence: structureless mudstone
T_{LC}	Thin-bedded, upper division turbidites succession above the Lower Channel Unit
TST	Transgressive Systems Tract
T_{UC}	Thin-bedded, upper division turbidites succession above the Upper Channel Units
UC	Upper Channel Units
UC1	Upper Channel Unit 1
UC2	Upper Channel Unit 2
UC3	Upper Channel Unit 3
WSG	Windermere Supergroup

Chapter 1: Thesis Introduction

1.1 Thesis Rationale

One of the most distinctive geomorphic elements on the continental slope are submarine channels. Like their subaerial counterparts (rivers), submarine slope channels are responsible for transporting sediment, in addition to pollutants and nutrients in modern systems, from the continent into the deep sea. Despite their importance, their inaccessibility in modern systems (i.e. water depth) has resulted in a poorly developed understanding of their internal stratigraphy and how these elements evolve in time and space, and the ultimately the deposited sedimentary record. While significant advances have been made using high-resolution seafloor bathymetric maps, high-quality three-dimensional seismic and core datasets, much remains unknown about the lithological make-up and larger-scale architecture of channel systems at the sub-seismic scale. In addition, the destructive nature of the flows, namely turbidity currents that build up the sedimentary record (Piper and Normark, 2009) in the deep marine realm, makes it difficult to link transport processes and the depositional record in the modern, and by extension, the ancient sedimentary records. To help bridge this gap, deep marine channel deposits preserved in the ancient sedimentary record provide important insight into the internal complexities resulting from the interplay of channel incision, aggradation and lateral migration.

One of the many examples of deep-marine turbidite systems in the sedimentary record is the well-exposed, recently deglaciated, base-of-slope to basin floor deposits of the Neoproterozoic Windermere turbidite system (Ross and Arnott, 2007). Unique to this system is the vertically-dipping orientation and superbly exposed nature of the strata, which provides an unparalleled opportunity to document lithological characteristics on spatial scales the range from millimeters to kilometers. The principal objective of this thesis is to document these characteristic in Isaac

Channel Complex 1, hereafter simply ICC1, in order to better understand the sedimentological and stratigraphic controls that build-up slope channels in the sedimentary record. Moreover, Quaternary slope channel complexes developed under icehouse conditions have been linked to potential systematic changes in the sediment supply during regression-transgression cycles (i.e. Jobe et al., 2015; Manley and Flood, 1988; Samuel et al., 2003). Like the Quaternary, icehouse conditions during the Neoproterozoic were punctuated by multiple glacial and inter-glacial episodes (Young, 2013), and therefore provides an opportunity to explore factors like changes in sediment supply for through-going turbidity currents as controlled by large-scale allogenic drivers like climate and eustasy. This, in turn, can be linked to architectural evolution of ICC1 and therein provide a robust model for similar modern and ancient continental slope channel systems.

1.2 Windermere Supergroup

1.2.1 Location of the Windermere Supergroup

The Windermere Supergroup (WSG) is an unconformity-bounded, 2-9 km thick succession of Neoproterozoic (740-569.9 Ma) metasedimentary rocks associated with the break-up of Rodinia and subsequent formation of the Proto-Pacific Ocean (McMechan, 2015). The WSG is exposed locally from northwestern Mexico and the western United States, continuously throughout most of southwestern Canada, and again locally in the Yukon-Alaska border region (Figure 1.1A) (Ross and Arnott, 2007). In Mexico and the United States the WSG comprises siliciclastic continental and shallow marine strata (Link et al., 1003), siliciclastic deep-marine strata in the southern Canadian Cordillera (Campbell et al., 1973; Ross et al., 1995; Ross and Arnott, 2007), and carbonate-rich shallow-marine and upper continental slope strata in the Mackenzie Mountains of northwestern Canada (Figure 1.1B).

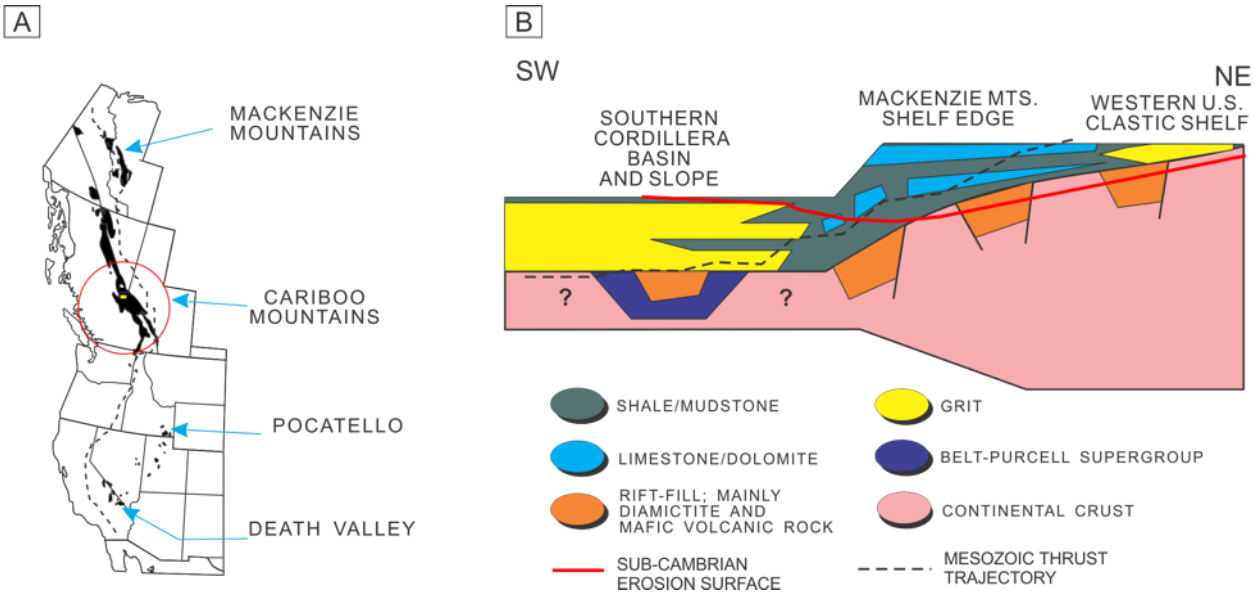

Figure 1. 1. *(A) Areal distribution of exposed rocks of the Windermere Supergroup (WSG) from northern Mexico to northern Canada. The deep marine portion of the WSG is delineated by the red circle with the yellow rectangle indicating the study area (modified from Ross et al., 1995). (B) Schematic cross-section of western North America ca. ~ 600 Ma. In the western United States strata of the WSG consist of shelf deposits compared whereas in Mackenzie Mountains they comprise shelf-edge and upper slope facies. In the southern Canadian Cordillera, on the other hand, strata consist of deep-marine base-of-slope and basin floor deposits. The red line marks the sub-Cambrian erosion surface (modified from Ross and Arnott, 2007) --- an erosion surface that has removed some of the stratigraphic succession in the eastern part of the greater Windermere basin.*

1.2.2 Development of the Windermere Supergroup and Regional Stratigraphy

During the Neoproterozoic (1000-544 Ma) most of the continental landmasses were joined into the supercontinent Rodinia, which was completely assembled by ~ 825 Ma, and at the time extended from the northern polar region to the equator, with Laurentia (ancestral North America) close to its centre (Figure 1.2A; Li et al., 2013; Hoffman, 1991). The break-up of Rodinia began at ~780 Ma and continued throughout the rest of the Neoproterozoic (Figure 1.2B-D; Li et al., 2013). This created an extensive passive continental margin along the margin of the expanding

paleo-Pacific (Panthalasssa) Ocean between Gondwana and western Laurentia, which coincided with the onset of WSG deposition (Ross, 1991; Ross et al., 1995).

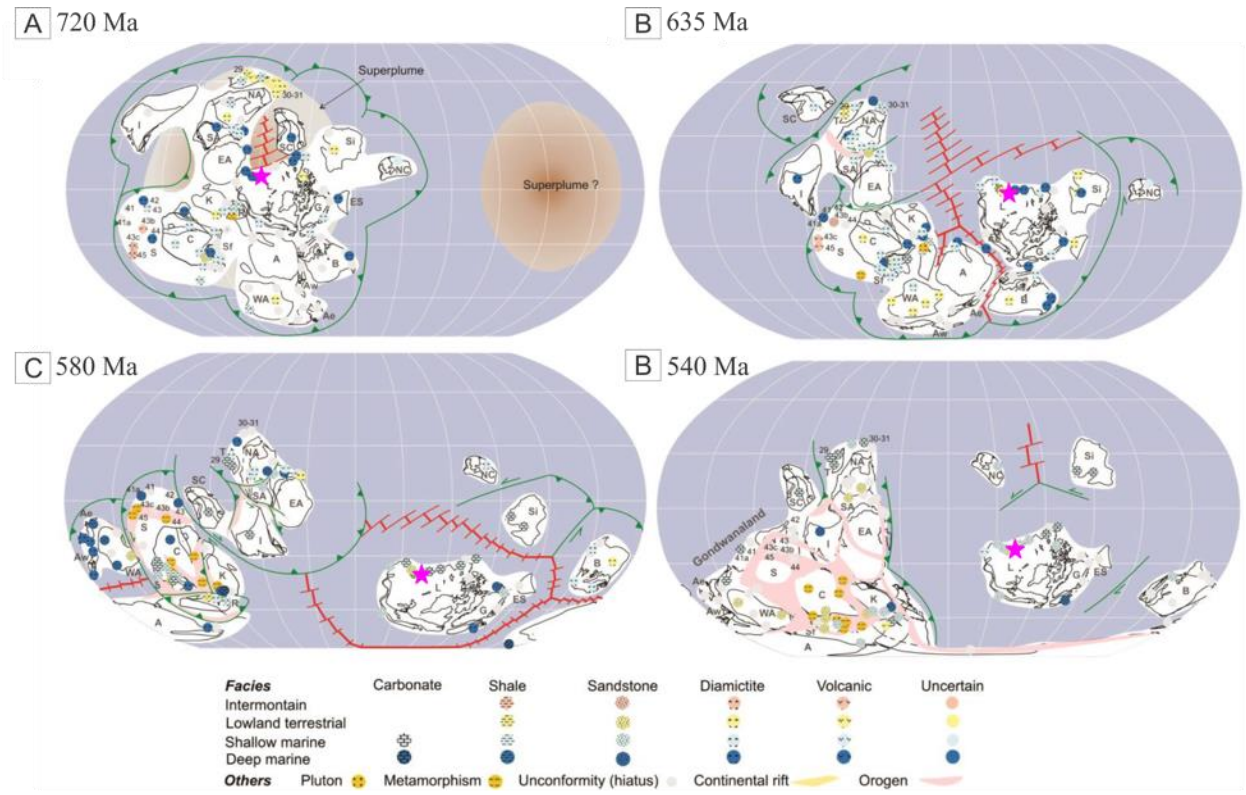

Figure 1. 2*. Global paleogeographic reconstruction by Li et al. (2013) showing the pattern of continent dispersal at four periods during the Neoproterozoic: (A) 720 Ma; illustrating the breakup of the low-latitude Rodinia supercontinent (B) 635 Ma; termination of Rodinia rifting and onset of Marinoan glaciation; note the north-facing continent margin of Laurasia. (C) 580 Ma; termination of Rodinia rifting and initiation of Gondwana and Gaskiers glaciation; (D) 540 Ma; formation of the Godwanaland assemblage. Approximate location of the Windermere margin indicated by pink star.*

As a result of deformation associated with the Mesozoic Cordilleran Orogeny the present-day position, geometry and thickness of the WSG has been post-depositionally altered. During the late Jurassic to Late Paleocene allochthonous terrane accretion and orogenesis created five belts that make up the North American Cordillera termed the Insular Belt, Coast Belt, Intermontane Belt, Omineca Belt and Foreland Belt (Figure 1.3) These belts are oriented sub-parallel to the

north-northwestern trend of the Cordillera and have undergone a variety of deformational styles such a thrust faulting, strike-slip faulting and significant tectonic discontinuities (Stewart, 1972). Nevertheless, within both the foreland Fold and the Thrust Belt and the Omineca Belt in the southern Canadian Cordillera, rocks of the WSG are well exposed and have undergone lower grade metamorphism (sub-greenschist and greenschist facies) and provide an opportunity to conduct detailed sedimentological investigation (Murphy, 1987; Ross and Arnott, 2007).

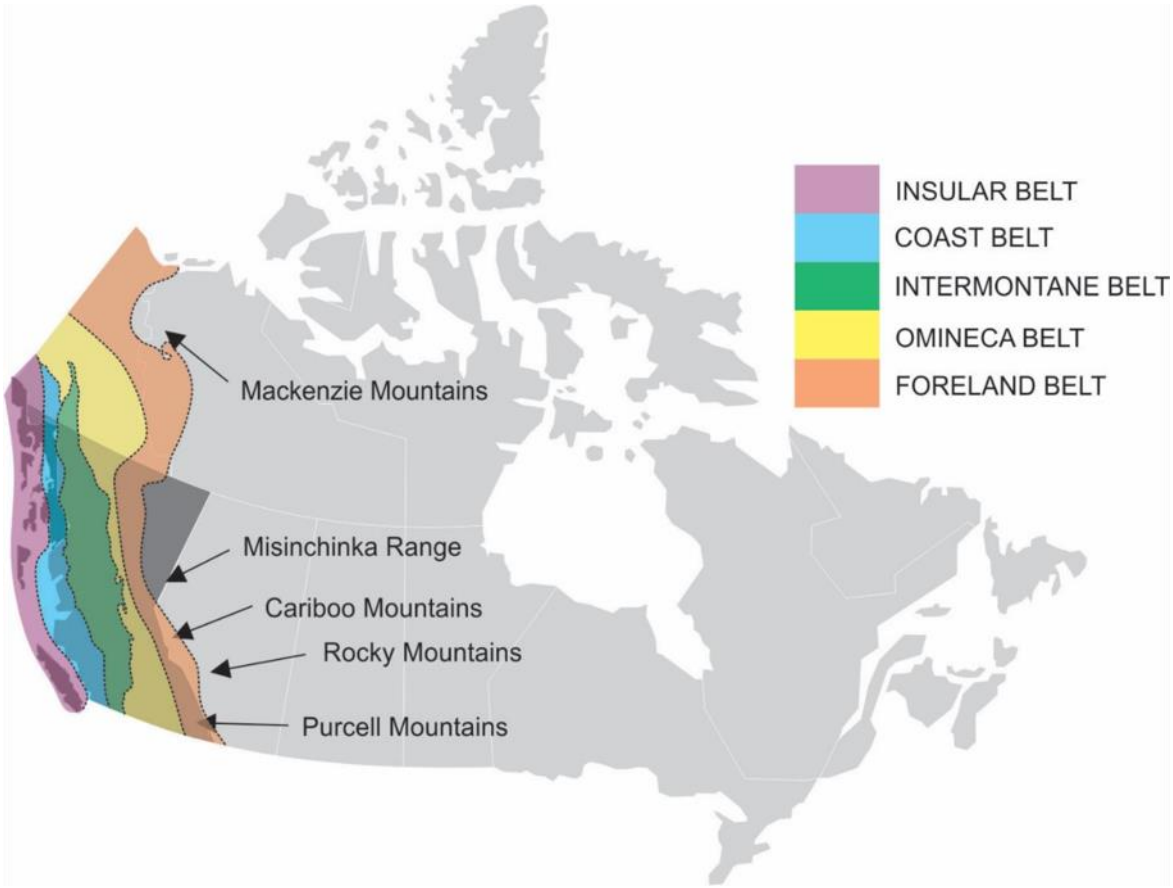

Figure 1. 3. *Map of western Canada showing the five tectonic belts that make up the Canadian Cordillera -- the result of mountain building events related to collisional tectonism and accretion of allochthonous terranes along western Laurentia between 185-50 Ma. From west to east they are the Insular Belt, Coast Belt, Intermontane Belt, Omineca Belt and the Foreland Belt (modified from Davis, 2011).*

The WSG unconformably overlies metasedimentary rocks of the 1.5-1.4 Ga Belt-Purcell Supergroup in southeastern British Columbia and northwestern United States, 2.2-0.73 Ga crystalline basement of the Deserters Gneiss in north-central British Columbia or Malton Gneiss in east-central British Columbia (Evans et al., 2000; Murphy, 1990), and in turn is unconformably overlain by siliciclasitc strata of the Gog Group (Campbell et al., 1973; Ferguson 1994). In the southern Canadian Cordillera, accumulation of the WSG comprises two well-defined tectonostratigraphic sequences: syn-rift and overlying post-rift (Figure 1.4).

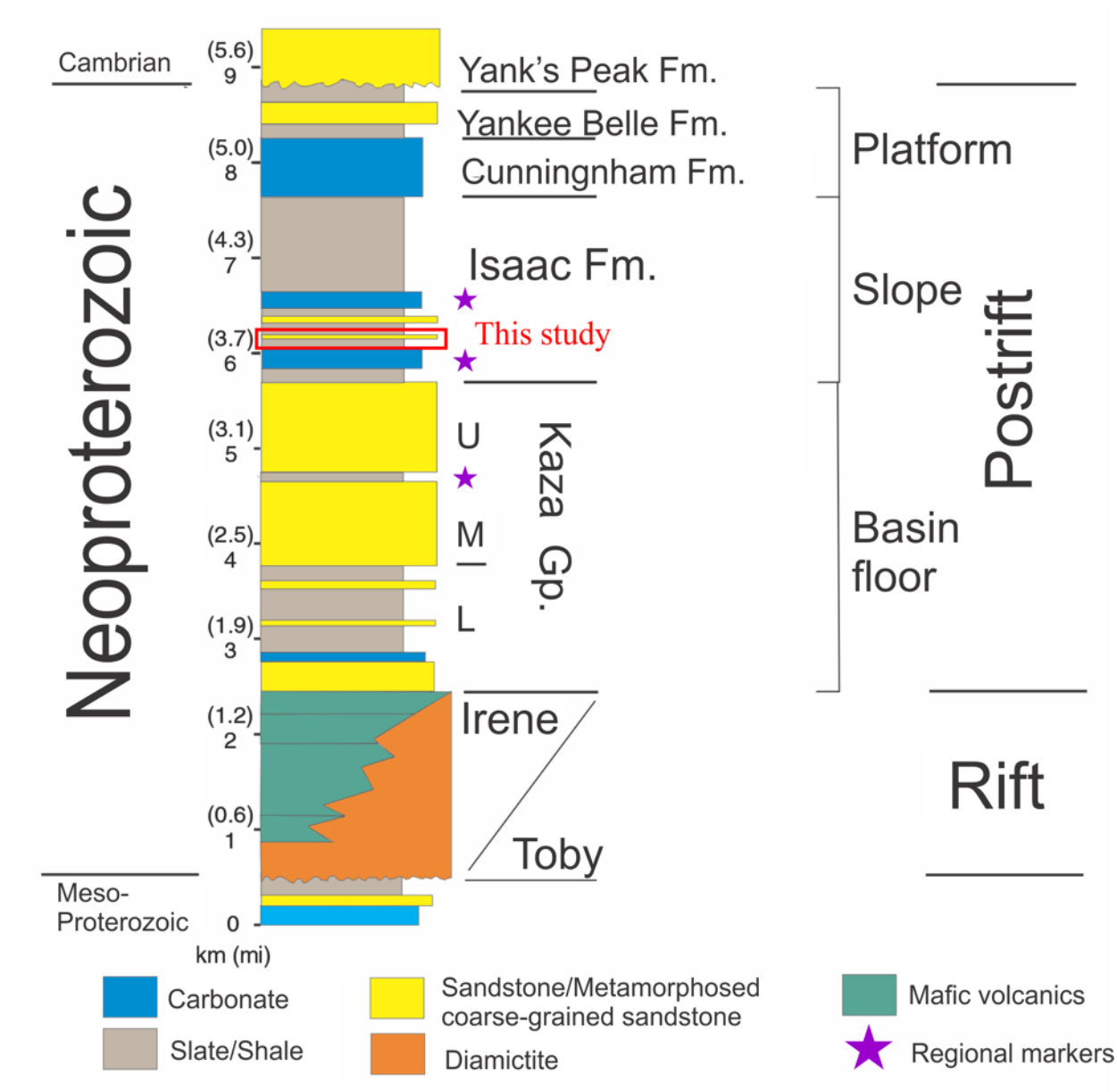

Figure 1. 4. *Generalized stratigraphic column of the Windermere Supergroup in the southern Canadian Cordillera. The WSG comprises syn-rift (Irene and Toby formations in the Purcell Mountains) and the overlying post-rift succession (Kaza Group, Isaac, Cunningham and Yankee Belle formations in the Cariboo Mountains). This study focuses on Isaac Channel Complex 1, which is a base-of-slope, channel-levee system within the Isaac formation indicated by the red box (modified from Ross and Arnott, 2007). Regional markers from bottom to top are Old Fort Point (OFP), 1st Isaac Carbonate (FIC) and 2nd Isaac Carbonate (SIC), respectively (denoted with a purple start) (See discussion in 1.2.5).*

The basal syn-rift sequence consists of up to 2.5 km-thick, glaciogenic diamictites interbedded with mudstone, sandstone, limestone and conglomerate of the Toby Formation intercalated with tholeiitic volcanic rocks of the Irene Formation, and represents deposition during the rifting of Laurentia from the Rodinia supercontinent (Ross et al., 1995). Direct ages from the basement rocks in the Canadian Cordillera and indirect ages from correlative units of the Toby and Irene formations in British Columbia and western United States range from 726-684 Ma, suggesting synchronous deposition and igneous activity during Rodinian rifting (Lund et al., 2003; Fanning and Link, 2004; Li et al., 2013).

The overlying post-drift sequence comprises coarse-grained, sandstone-rich turbidites intercalated with mudstone, minor carbonate intervals and one diamictite (Vreeland Formation) and host of one of the world's best outcrop examples of deep-marine sedimentary rocks (Ross et al., 1995; Ross and Arnott, 2007; Smith, 2009). The 5-7 km post-rift succession represents a succession of deep-water sedimentary strata termed the Windermere turbidite system that accumulated along the Laurentian margin of the proto-Pacific miogeocline in response to decreasing rates of thermally driven subsidence (Ross, 1991; Ross and Arnott, 2007). In the western Rocky Mountains post-rift strata are termed the Miette Group, the Horsethief Creek Group in the Purcell Mountains and the Kaza and Cariboo groups in the Cariboo Mountains (Figure 1.5)

(Ross and Arnott, 2007). Moreover, the exposed part of the Windermere turbidite system covers an area of at least 80,000 km^2 (palinspatically restored), and therefore, is dimensionally comparable to modern passive-margin turbidite systems like the Amazon and Mississippi fans, and also the largest known ancient turbidite system (Figure 1.6) (Ross et al., 1995; Ross and Arnott, 2007).

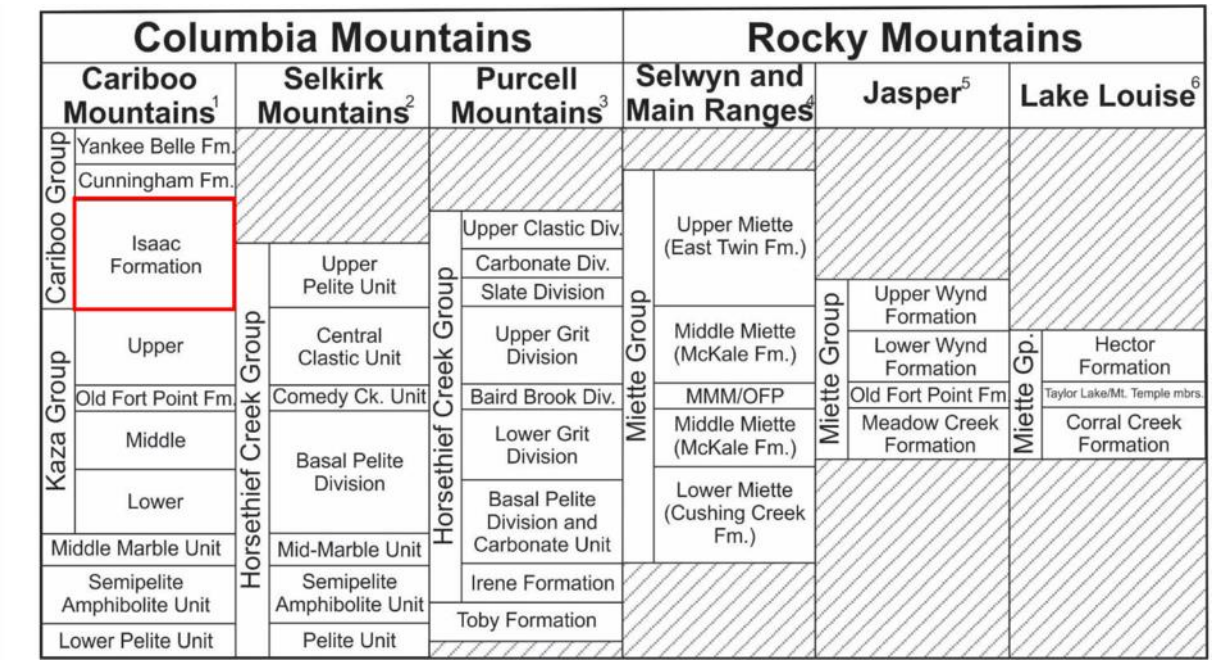

Figure 1. 5. *Stratigraphic nomenclature of the Windermere Supergroup in the southern Canadian Cordillera. Red box indicates strata of this study (from Ross and Arnott, 2007).*

Deep-water strata of WSG crop out extensively and are located in east-central British Columbia. The area is located in the Omineca Belt and is bounded to the east by the Fraser River and the Quesnel Highlands to the west. The Kaza Group makes up the basal 2-4 km of the post-rift succession and is subdivided into three stratigraphic units: Lower, Middle and Upper. The Lower Kaza Group is mudstone-dominated, whereas the Middle and Upper are sandstone-rich and separated by the Old Fort Point Formation (OFP) (Ross and Murphy, 1988; Ross, 1991; Ross et

al., 1995; Smith 2009; Smith et al., 2014) (For more detail see section 1.2.5). Rocks of the Kaza group correlate with the Horsethief Creek Group in the northern Purcell Mountains, which overlies rift-related diamictite of the Toby Formation or mafic volcanic rocks of the Irene Formation (Aalto, 1971). Although the contact between rift and post-rift rocks is not exposed in the Cariboo Mountains, the Kaza Group is presumed to be overlain by the regionally extensive Toby Formation and/or subordinate Irene Formation. The Kaza Group is interpreted to represent basin-floor sedimentation along the passive margin of the Neoproterozoic, and in the case of the Middle and Upper Kaza Group composed primarily of sand-rich depositional lobe deposits (Meyer and Ross, 2007; Terlaky and Arnott, 2014).

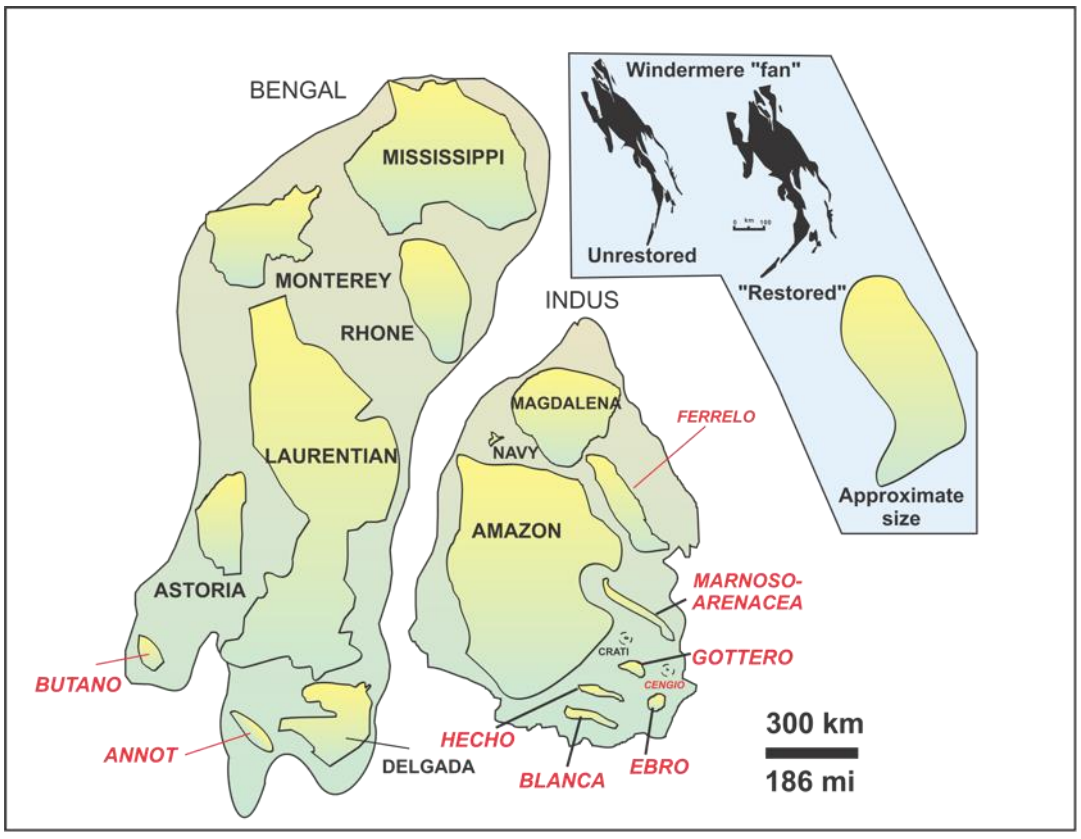

Figure 1. 6. *Size comparison of the restored Windermere turbidite system (Windermere "fan") with modern (black text) and ancient (red text) turbidite systems (Ross, 2001 modified from Barnes and Normark, 1985).*

The overlying Cariboo Group is up to 5 km thick in the Cariboo Mountains and is subdivided into three stratigraphic units. The up to 2.4 km-thick Isaac Formation conformably overlies the Upper Kaza Group and is composed primarily of mudstone (levee deposits) that encase laterally discontinuous coarse-grained sandstone units, some > 100 m thick, in addition to common mass transport deposits (slide, slumps and debrites) and are interpreted to represent base-of-slope leveed-channel complexes (Ross and Arnott, 2007).

Conformably overlying the Isaac Formation are the Cunningham and Yankee Belle formations, which are interpreted to be upper slope and shallow-marine, high-energy shelf deposits (Ross et al., 1995). The Cunningham Formation is up to 550 m thick and comprises oolitic intraclastic limestone with minor mudstone, siltstone and shale (Rowe, 2003). The Yankee Belle, in turn, is composed of up to 900 m of alternating limestone, siltstone, sandstone and shale (Gabrielse and Campbell, 1991). Collectively, the succession of basin floor to continental shelf deposits of the Kaza and Cariboo groups forms a several-km-thick, upward-shallowing succession interpreted to represent the progradation of the passive continental margin of Laurentia into the developing proto-Pacific miogeocline (Figure 1.4; Ross, 1991; Ross et al, 1995; Ross and Arnott, 2007).

Post-depositional uplift and significant regional sub-Cambrian erosion has removed much of the upper part of the Windermere succession in the eastern part of the southern Canadian Cordillera (Devlin and Bond, 1988; Ross and Murphy, 1988). Accordingly, there is a significant unconformity between the Windermere Supergroup and the overlying lower Cambrian Yank's Peak Formation in the Cariboo Mountains or equivalents in the lower in the lower Gog Group of the northern and southern Rocky Mountains, and the Hamill Group in the Purcell Mountains.

1.2.3 Geochronology Constraints

The WSG succession in the southern Canadian Cordillera is poorly dated due to the lack of volcanic rocks and the absence of fossils, the predominantly siliciclastic lithology that lacks suitable material for conventional radiometric dating (Ross et al., 1989; Smith et al., 2011) and the lack of zircons in exposed volcanic rocks (Lund et al., 2003). Nevertheless, highly precise radiometric ages on rocks that uncomformably underlie and overlie the Windermere constrain the maximum and minimum ages of deposition of the turbidite system. Maximum depositional ages were obtained from in the Deserts Range of northern British Columbia, which yielded 728 ± 8 Ma (Evenchick et al., 1984). This is further supported by U-Pb zircon dates from basement orthogneiss in southern British Columbia in the Monashee Mountains dated at 740 ± 36 Ma (Parrish and Scammel, 1988). Moreover, zircon dates from volcanic rocks in Idaho yielded an age of ~ 685 Ma and are considered to be equivalent to rift-related rocks of the Irene Formation (Figure 1.5; Lund et al., 2003). The only direct date reported in the WSG is from an organic-rich mudstone in the Geikie Siding Member of the OFP in the Jasper area which yielded an age of 607.8 ± 4.7 Ma using Re-OS isochron techniques (Kendall et al., 2004). The minimum age of deposition is constrained to U-Pb zircon date of 570 ± 5 Ma from synrift volcanics near the base of the Hamill Group (Figure 1.5; Colpron et al., 2002). Based on these constrains the Windermere turbidite system was active for a maximum of ~210 Ma, although that about half of the succession was deposited in as little as ~ 40 myr.

1.2.4 Sediment Provenance and Paleoflow

The deep-marine Windermere basin in the southern Canadian Cordillera was part of a longitudinal dispersal system that transported sediment from southeast to northwest based on regional facies patterns, sediment provenance and paleocurrent (Resort 1967; Arnott and Hein,

1986; Ross and Parrish, 1991; Ross 2001; Ross and Arnott, 2007). The source of siliciclastic sediment has been determined using uranium-lead dating on detrital zircons in the WSG. Here, all detrital zircons are characterized by a distinctive bimodal distribution of 1.65-2.26 Ga (Paleoproterozoic) and > 2.5 Ga (Archean) ages suggesting that sediment was sourced from fluvial drainage of the southern Canadian Shield and northwestern United States (Ross and Parrish, 1991). This is further supported by consistent paleocurrent direction from ripple and dune cross-stratification, cobble imbrication and less commonly flutes throughout the Windermere turbidite system (Figure 1.7) (Arnott and Hein, 1986; Ross and Arnott, 2007).

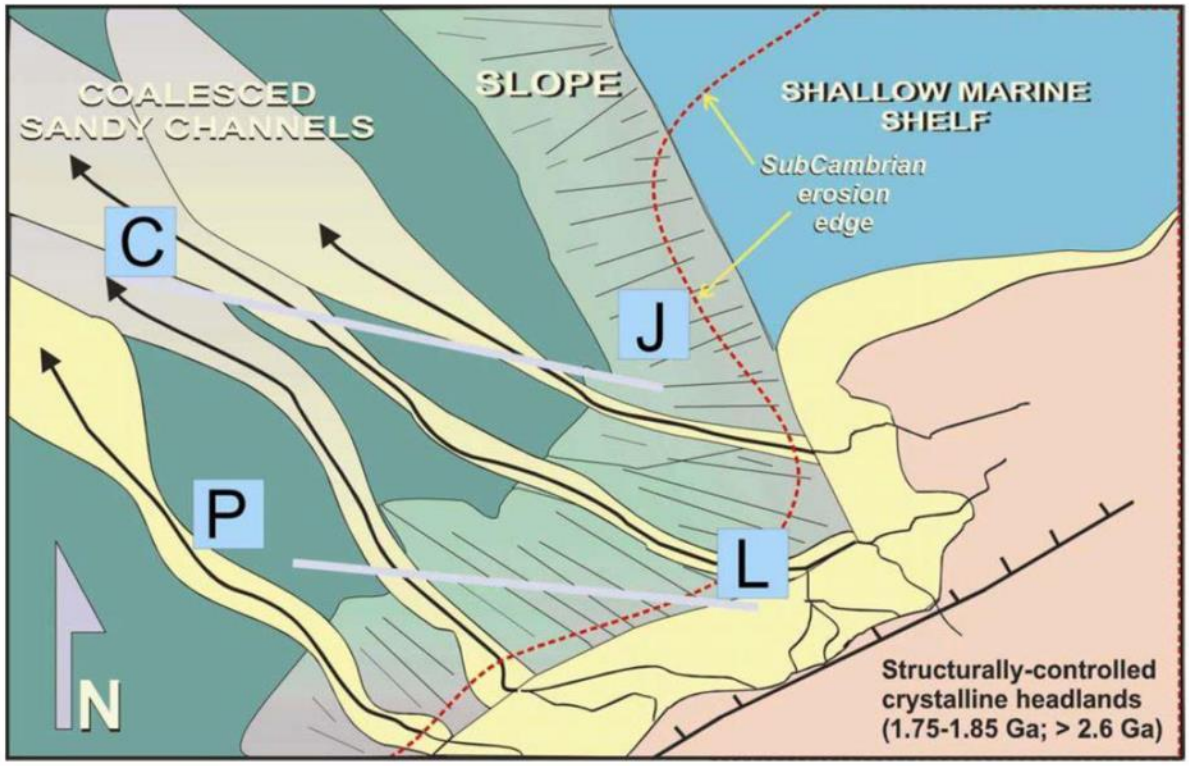

Figure 1. 7. *Schematic paleogeographic reconstruction of the Windermere turbidite system in the southern Canadian Cordillera. Paleoflow was toward the northwest (present day coordinates) from the upper slope in Lake Louise (L) to the lower slope and base-of-slope in Jasper (J) and Purcell (P) regions, respectively, and then onto the basin floor in the Castle Creek study area (C) (Ross, 2000).*

1.2.5 Regional Markers of the Windermere Supergroup

In the southern Canadian Cordillera three distinctive, areally extensive lithostratigraphic markers are used for regional correlation: The OFP of the Kaza Group and two carbonate-rich intervals in the Isaac Formation informally termed the first (FIC) and second (SIC) Isaac carbonates, respectively (Ross et al., 1995; Ross and Arnott, 2007).

The OFP is approximately 50 to 450 m-thick and consists mostly of thin-bedded siliciclastic and carbonate turbidites intercalated locally with distinctive purple and green slate and a black shale horizon and is stratigraphically the lowest regional marker (Ross and Arnott, 2007; Smith et al., 2014). The OFP unit represents a major transgressive event and associated highstand deposition related to a post-glacial eustatic rise from the melting of the Neoproterozoic Marinoan ice sheet (Ross et al., 1995; Smith, 2009; Smith et al., 2014).

The FIC and SIC range from ~ 10- 260 m-thick. The FIC is characterized by three laterally extensive, decameter-thick units composed of very thin- to thin-bedded calcareous turbidites made-up of black to greenish brown siliceous calcilutite and very fine- to fine-grained siliceous calcarenite intercalated locally with up to ~ 20 m-thick granule siliceous calcirudite (conglomerate) to medium-grained siliceous calcarenite. Interbedded with these carbonate units are up to ~ 60 m thick succession of siliciclastic mud dominated, fine-grained, thin-bedded turbidites. Stratigraphic position and inorganic carbon isotopic ($\delta^{13}C_{carb}$) analysis suggest that the FIC preceded the 580 Ma Gaskier glaciation during an elevated sea-level that flooded the continental shelf and enhanced carbonate sediment production on the platform (Ross and Arnott, 2007; Cochrane et al., 2019). The SIC is lithologically similar to the FIC but with local intercalated sheets of quartz arenite (Ross and Ferguson, 2003) and like the FIC suggests a period of elevated sea level.

1.3 Castle Creek Study Area

The Neoproterozoic Supergroup in the northern Cariboo Mountains of east-central British Columbia is a world-class example of an ancient passive margin turbidity system comprising of a complete succession of basin floor to slope turbidites deposits (Figure 1.8A; Ross, 1991). At the Castle Creek study area, strata of the WSG consist of rocks of the Upper Kaza Group overlain by the Isaac Formation (Cariboo Group) that are exposed over 2.5 km perpendicular to bedding, 7 km parallel to bedding and where strata are vertically (89^{o}) dipping (Figure 1.8B). Recent deglaciation (< 100 years) has removed most surface debris and polished the surface smooth, and therefore provides the opportunity for sedimentological and stratigraphic documentation of strata from the mm/cm- to km-scale.

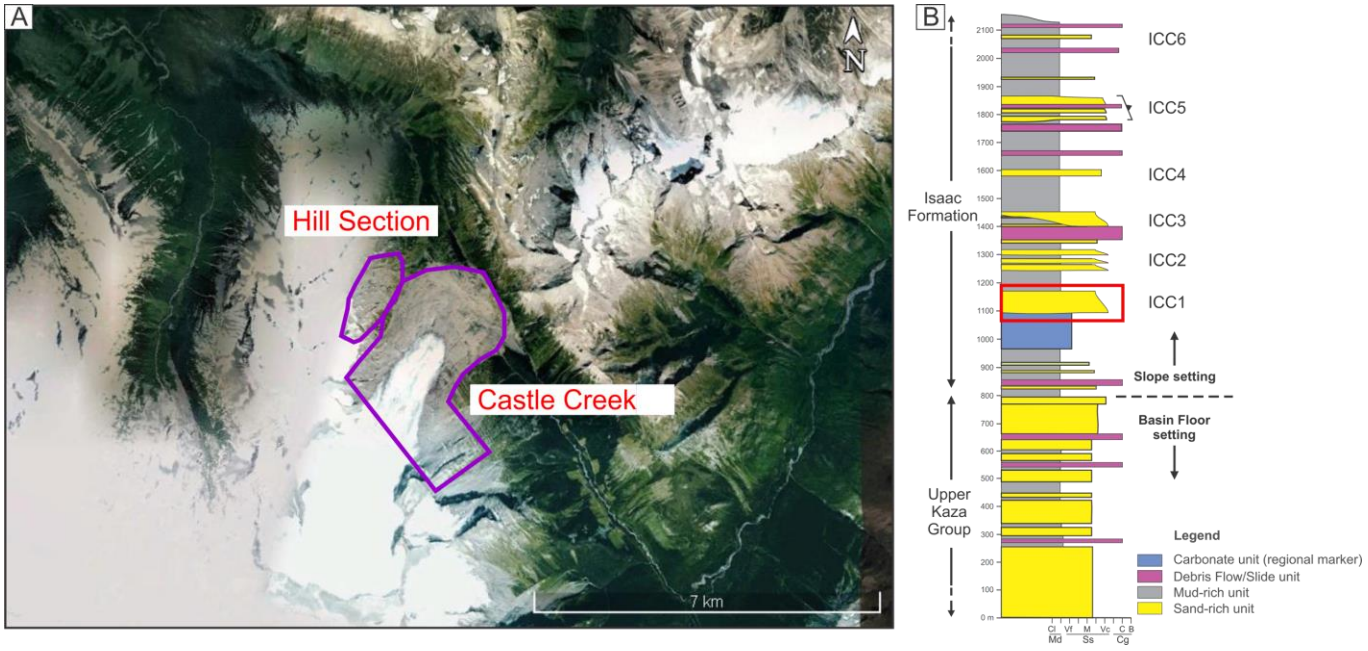

Figure 1. 8. *(A) Satellite image near McBride, British Columbia with the study areas indicated in purple polygons – Castle Creek and Hill Section. (B) Composite stratigraphic column of the Castle Creek study area in the Cariboo Mountains with ICC1 outlined in the red rectangle.*

Rocks in the Cariboo Mountains, including those at Castle Creek, have undergone four episodes of deformation (D1-D4) and at least two low-grade metamorphism (M1 and M2) events (Murphy and Rees, 1983; Murphy, 1987a, b) that are interpreted to be associated with collision and accretion of terranes along the western margin of North America from the mid-Jurassic to Tertiary (Murphy, 1987). A pre- to early metamorphic D1 event produced northwest-trending, northeast-verging, recumbent, isoclinal local folds with cleavage development parallel to bedding in addition to M1, which consists of low-grade metamorphism (Ross & Arnott, 2007). A syn-metamorphic D2 event produced northwest-trending, south-west verging overturned folds and reverse faults that also is associated with the onset of M2 that is manifest as metamorphic minerals that overprint D2 structures (Murphy and Rees, 1983). The late- to post-metamorphic D3 crosscuts and refolded D1 and D2 structures into northwest-trending, open and upright folds with associated reverse faults. The final phase, D4, is post-metamorphic and refolds all previous deformation structures (D1-D3) into metre to decametre, northeast-trending, steeply inclined upright folds with tight inter-limb angles and chevron hinge zones (Campbell et al., 1973; Ferguson, 1994; Reid et al., 1997). Regional metamorphism peaked between D2 and D3, at temperatures between ~ 350-450 and pressures ranging from 4-9 kbar (Lee, 2016). Moreover, lower greenschist metamorphism has caused quartz grains in grain-supported sandstone to display bulging recrystallization and locally even subgrain boundary rotation in more cemented samples (Popovic, 2016). In contrast, samples with mudstone-dominated matrix have been recrystallized to muscovite and chlorite, and therefore the mineralogical make-up of the detrital clay mineral matrix is unknown (Terlaky, 2014; Lee, 2016).

1.4 Previous Work

Early work on the WSG focused on regional mapping (1:250 000 and 1: 50 000 scale), which includes the Castle Creek study area (Campbell et al, 1973; Ross and Ferguson, 2003) and the regional stratigraphy, deformation and metamorphism in the general McBride area (Murphy and Ross, 1983; Murphy, 1987; Ross, 1991; Ross et al., 1995; Reid et al., 2002). More recent sedimentological, stratigraphic, geochemical and architectural analyses of the deep-marine turbidite system in the Castle Creek study area have been conducted by The Windermere Consortium, which is an industry-, government-, and academic-funded research initiative based at the University of Ottawa. To date, graduate student research has focused on a wide range of deep-marine depositional elements including slope mass-transports (i.e. Laurin, 2005; Arnott et al., 2011), slope and base-of-slope channel-levee complexes (Navarro et al., 2007; Arnott 2007; Gammon et al., 2007; O'Byrne et al., 2007; Schwarz and Arnott, 2007a,b ; Musa-Caleca, 2008; Dumouchel., 2015; Cochrane, 2018), basin floor-deposits (Meyer, 2004; Meyer and Ross, 2007; Rocheleau, 2011; Terlaky, 2014; Popović, 2016; Terlaky et al., 2016), avulsion splay deposits (Angus, 2016; Wearmouth, 2018), and levee deposits (Khan, 2012; Bergen, 2017; Billington., 2019), in addition to 21 undergraduate theses.

1.5 Isaac Channel Complex 1 (ICC1)

ICC1 it one of at least seven leveed slope channel complex that crop out at the Castle Creek study area (Fig 1.8A-C). ICC1 abruptly overlies the FIC, which is a mixed carbonate-siliciclastic succession. Based on recent findings by Cochrane (2019) and Navarro (2005, 2016), the mixed carbonate-siliciclastic unit was deposited during a long term (3rd order) eustatic rise that led to the initiation of a well-developed carbonate platform. During this time, carbonates were resedimented from the platform and transported downslope by turbidity currents and debris flows. This, then,

was followed by a dramatic eustatic fall associated with the onset of the Gaskier Glaciation (Cochrane, 2019) that terminated the downslope supply of locally derived carbonate and palimpsest siliciclastic sediment and restored sediment delivery from the (cratonic) hinterland. The related lowstand is manifested stratigraphically as siliciclastic strata of ICC1, which forms a unit that is 220 m-thick and exposed over 5 km along strike.

1.5.1 Thesis Objectives and Structure

The principal objective is to document and interpret the sedimentological and stratigraphic architecture of inter- and intra-channel fills to better elucidate the processes of erosion, by-pass, and deposition. More specifically, to illustrate the spatial and temporal distribution of lithofacies, lithofacies assemblages and stratal elements that populate the complex depositional record of a leveed slope-channel system. This can then be used to compare the architectural variability of ICC1 to modern and ancient channel deposits, and ultimately address the architecture and heterogeneities in subsurface reservoirs and reservoir models (i.e. barriers, baffles and areal extent of potential reservoirs).

Note that parts of ICC1 have been previously studied in the M.Sc. research of Navarro (2005) and Iain Gerald Dumouchel (2012), B.Sc. thesis of Dave Anthony (2011) in addition to geochemical analysis done in mudrocks by Milczarek (2018). This thesis, therefore, is a compilation of their data (i.e. rock samples, stratigraphic sections, and geochemical trends) in addition to new data, especially those from newly deglaciated areas. Additionally, this study is the first to report research of ICC1 at the Hill Section (Figure 1.9).

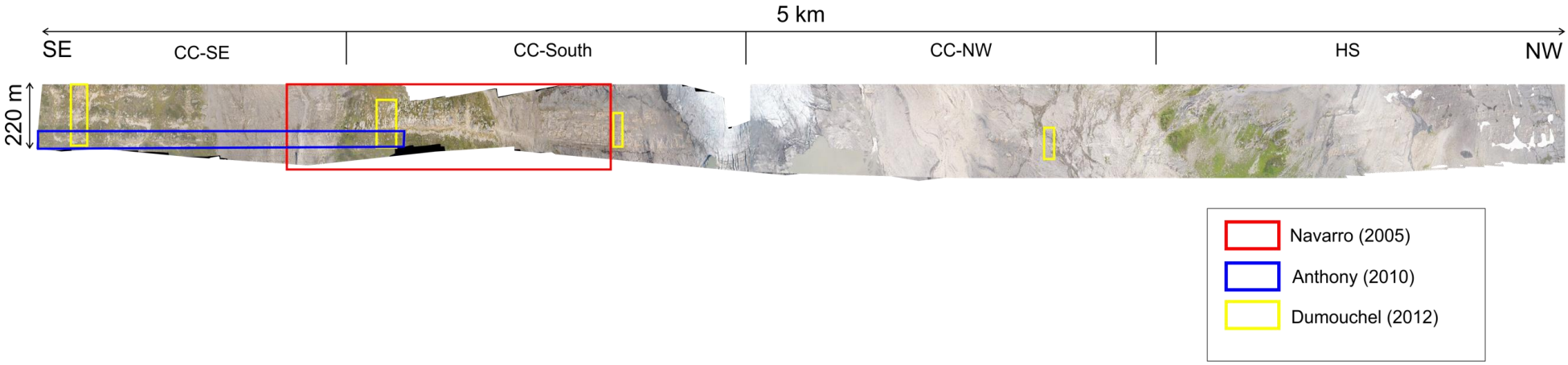

Figure 1. 9. *Drone Photomosaic of ICC1 at the Castle Creek study area, herein subdivided into three sections (CC-SE, CC-South and CC-NW) and the Hill Section (HS). Note the highlighted boxes indicating study area location from previous studies by Navarro (2005), Anthony (2010) and Dumouchel (2012).*

This thesis is written in traditional format: chapter 1 provides an overview of the regional and local geology as well as study methods and a literature review of sediment-gravity flows; chapter 2 is a detailed lithological and petrographic description of all facies; chapter 3 describes the vertical and lateral distribution of stratal elements that make up ICC1; chapter 4 describes the spatial and temporal evolution of ICC1 in a sequence stratigraphic context and provides insight into factors that influence the stratigraphic evolution of submarine channels; and chapter 5 summarizes the study conclusions and proposes areas for future research.

1.5.2 Methodology

Fieldwork at Castle Creek was conducted and assisted by Dr. Lilian L. Navarro and Liam Jasperse over the summers of 2018 and 2019 (~12 weeks total). At the Castle Creek study area a total of 43 stratigraphic logs (~ 20-220 m thick) were measured at cm-scale in channel fills and associated deposits recording lithology, grain size, bed thickness, internal primary and secondary sedimentary structures, basal contacts, mudclast characteristics (size, shape, abundance, and orientation) and where possible, paleocurrent measurement. Correlation between logs was performed by walking out and significant surfaces in the field and mapping them on high resolution drone photomosaics captured by a DJI Phantom 3 Professional drone. These data then formed the basis for illustrating the m- to km-scale distribution of stratal elements in the study area.

In addition, a total of 20 samples were collected for thin section analysis to assess mineralogy, alteration and microstructure composition of the various facies (see chapter 2). Twelve of these thin sections, specifically coarse-grained sandstone, were point counted using an Olympus mechanical rotating stage. In each thin section ~ 300-500 points were assessed for grain size and mineralogy every 0.5 mm. Grain size was categorized using the Udden-Wentworth grain size classification scale (Udden, 1914; Wentworth, 1922). These data were then hand-plotted using a

semi-log graph (Folk and Ward, 1957) to obtain quantitative data needed for statistical analysis (Figure 1.9; see Appendix B).

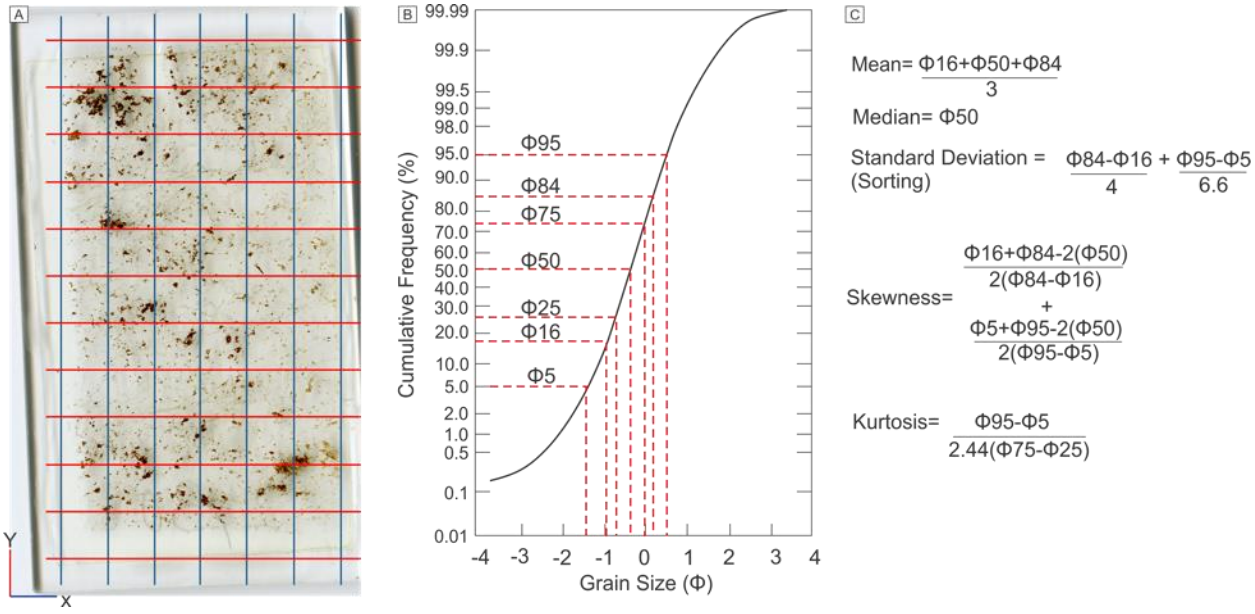

Figure 1. 10. *(A) Example of the sampling grid used for point counting where up to 500 points were measured to assess mineralogy composition and grain size. (B) Example of measured grain size data plotted on a semi-log graph to obtain phi-values needed for statistical analysis. Note that the horizontal axis is plotted in phi units, which is the millimetric (base 10) grain size converted to base 2 units. Also, note that from left to right grain size decreases. (C) Mathematical equations used in this thesis for statistical analysis (from Folk and Ward, 1957).*

1.6 Deep-Marine sedimentation processes and their association deposits

The dominant agents for transporting and depositing sediment in the deep sea are sediment gravity flows (Gani, 2004; Shanmugan, 2000). Sediment gravity flows are differentiated from fluid gravity flows based on the main constituent that makes up the flow. In a fluid gravity flow, the fluid, being air or water, is moved by gravity, which in turn causes sediment to be moved. In contrast, sediment gravity flows are made up of suspended sediment, which creates a density gradient between it and the surrounding ambient fluid and initiates movement (Middleton and

Hampton, 1973; Terlaky, 2014). Since the 1950s it has been recognized that sediment gravity flows in the modern oceans are initiated near the continental shelf break and positions lower on the continental slope by triggering mechanisms like earthquakes or local slope overstepping (Girardclose et al., 2007), hyperpycnal river outflows or local storm re-suspension near the shelf edge (Piper and Normark, 2009). However, sediment gravity flows typically evolve downslope due to changes in gradient, fluid entrainment, erosion, deposition, and flow expansion (Mulder and Alexander, 2001), and therefore characteristics of the final deposit are generally a poor indicator of the initiation process (Piper and Normark, 2009). Nevertheless, in terms of volume, a single sediment-gravity flow can transport more than 100 km^3 of sediment 100s to 1000s of kilometers across the sea floor and at speeds of up to 100 km/h (Talling et al., 2012, Talling et al., 2014). Despite sediment gravity flows being the principal agent moving enormous amounts of sediment into the deep sea, a physical mechanistic understanding remains poorly developed. In part this relates to their infrequent nature but mostly their powerful and destructive nature, which often completely destroys monitoring instruments (Talling et al., 2013). Much of our current understanding, therefore, comes from descriptions in the ancient geological record and carefully controlled laboratory experiments.

1.6.1 Sediment-Gravity Flows

Due to the complexity of sediment-gravity flows, the wide variety of depositional processes and added complexity of deformation and diagenesis makes interpreting the original flow conditions based on characteristic in the sedimentary record difficult (Mulder and Alexander, 2001). This complexity has led to nomenclature in the scientific literature in which numerous schemes have been devised to classify sediment-gravity flows based on sediment concentration (Bagnold, 1962), flow rheology (Postma, 1986; Shanmugam, 2000), sediment-support

mechanisms (Middleton and Hampton, 1973) and a combination of rheology and sediment-support mechanisms (Lowe, 1982). Generally, it is accepted that sediment-gravity flows can be subdivided into two end-member kinds, namely turbidity currents and debris flows, but also a variety of intermediate flow types. To capture the key parameters and variations between flows, Mulder and Alexander (2001) proposed a comprehensive classification scheme based on flow behaviour, grain-size distribution, and grain-support mechanisms in which they proposed two end members: cohesive flows and non-cohesive frictional flows (Figure. 1.10).

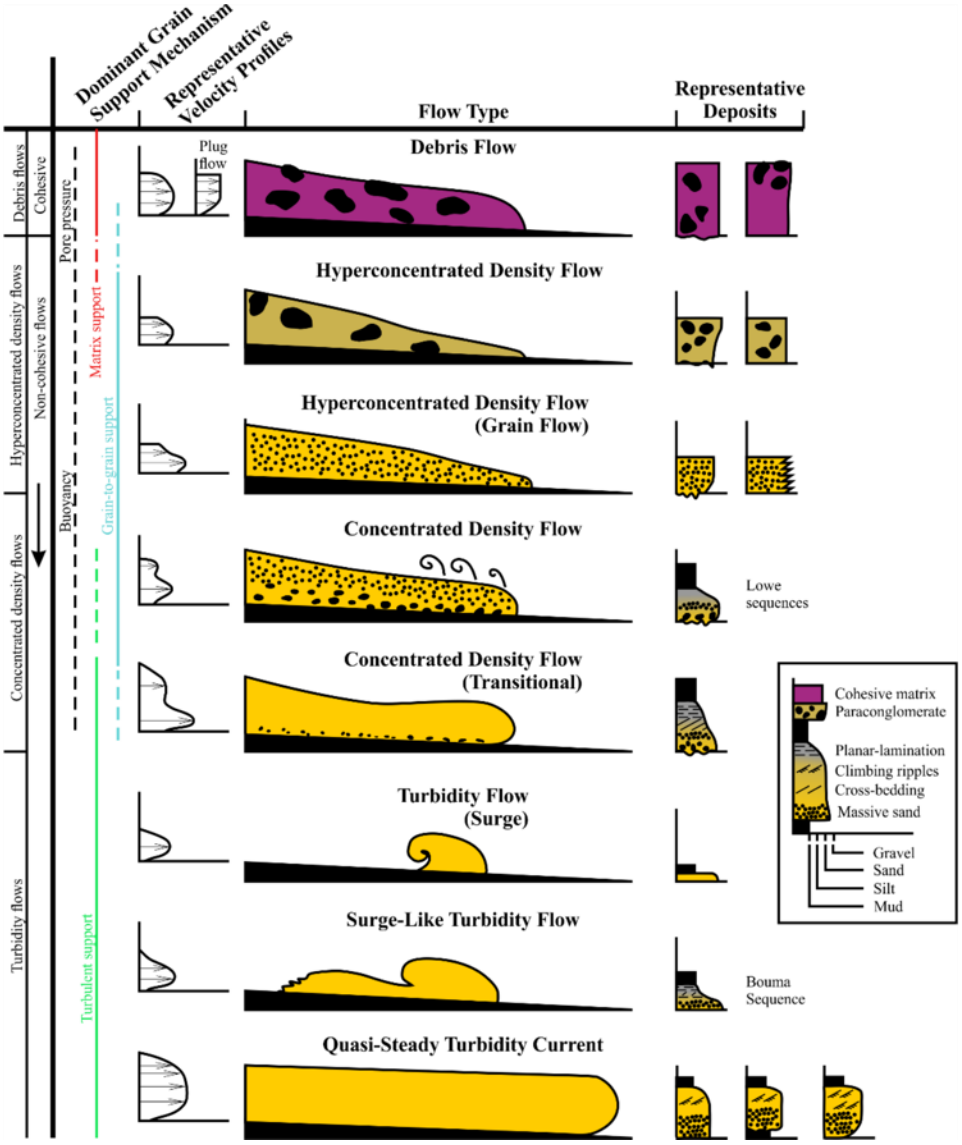

Figure 1. 11. Schematic diagram showing the classification scheme for subaqueous sediment-gravity flows. Classification is divided into two types: cohesive flows and non-cohesive frictional flows, where the latter is subdivided into hyperconcentrated flows, concentrated flows and turbidity currents. Also indicated are the dominant grain-support mechanisms, idealized velocity profiles, idealized flow shape and representative sedimentary logs (redrawn by Billington (2019) from Mulder and Alexander (2001)).

1.6.1.1 Cohesive Flows

Cohesive flows, namely debris or mud flows, are sediment gravity flows with pseudoplastic rheology and a laminar flow state. Cohesion is provided by the interaction between adjacent clay particles that possess a weakly negative electrostatic surface charge. This interaction allows weak electrostatic bonds to form and a network structure of aggregated clay particles to form, which then increases the fluid viscosity and consequently the flows develop mechanical strength, termed matrix strength. In addition to matrix strength, mechanics like particle-particle interaction, buoyancy effect, hindered settling and elevated pore fluid pressure collectively aid in maintaining larger particles in suspension (Table 1; Mulder and Alexander, 2001). Over time, debris flows may transform partially or fully through mixing and dilution at the head (Hampton, 1972) and/or entrainment along the upper boundary of the body or by passage through a hydraulic jump (Fisher, 1983; Weirich, 1988), which can cause flow strength to be reduced and the flow to transform to another kind of sediment gravity flow like a hyperconcentrated density or concentrated density flow if particles larger than medium silt are sufficiently abundant (Hampton, 1972).

Debris flows have been shown in modern system to runout for distances of up to several hundreds of kilometres and deposit poorly sorted and commonly massive sediment (Gardner and Kidd, 1983). These deposits commonly display flat (non-erosional) basal contacts due to turbulence damping by the fine-grained, cohesive matrix. These features have been attributed to hydroplaning (Mohrig et al., 1998), a process whereby a layer of ambient fluid builds up between

the bed and the base of the flow resulting in a dramatic reduction in basal drag (Mohrig et al., 1998; Mulder and Alexander, 2001).

1.6.1.2 Non-cohesive frictional flows

Unlike cohesive flows, frictional (non-cohesive) flows are composed of discrete particles that generally do not interact electrostatically, although some contain clay particles may impart limited cohesive strength to the flow. For the most part, frictional flows are Newtonian fluids and therefore lack yield strength. Mulder and Alexander (2001) recognized three kinds of frictions flows: hyperconcentrated density flows, concentrated density flows and turbidity currents. Each subdivision is differentiated by the dominant sediment-support mechanisms, which includes grain-to-grain interaction, buoyancy, fluid turbulence, pore pressure, and bed support (Figure 1.11; for more detail see Table 1). On the other hand, factors influencing the dominant sediment-support mechanism are sediment concentration, flow conditions, sediment type and grain size distribution (Mulder and Alexander, 2001).

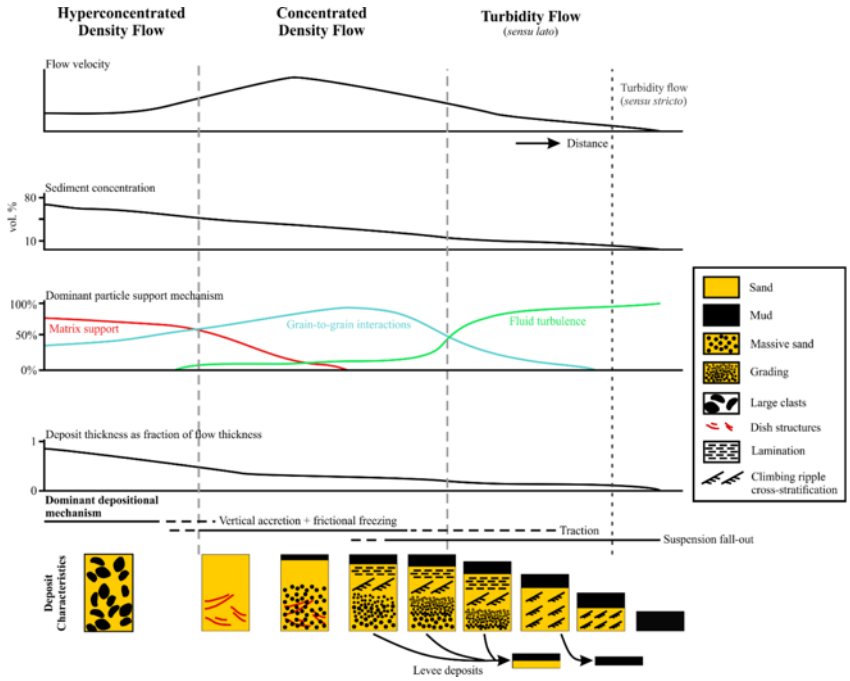

Figure 1. 12. *Diagram illustrating the changes in flow characteristics of frictional flows across the entire continuum. Flow types are differentiated based on differences in sediment concentration, which in turn influences the flow behaviour and depositional characteristics (redrawn by Billington (2019) from Mulder and Alexander (2001)).*

Name	Sediment support mechanism
Fluid Turbulence	Coherent movement of fluid masses at an angle to the main axis of flow in order to minimize a momentum gradient. Turbulence intensity increases with the velocity gradient and is capable of suspending sediment if the strength of the upward component of turbulent motion equals or exceeds the downward settling velocity of the particle due to gravity (Middleton and Hampton, 1973).
Hindered Settling	Reduced particle settling velocity due to increased drag imposed by upward moving fluid/sediment mixture that increases with sediment concentration (Davies, 1968).
Buoyancy	Displacement of a fluid by a falling particle generates an upward force on the particle that is equal to the mass of the displaced fluid volume (Lowe, 1979).
Dispersive Pressure	Collision between solid particles generates a dispersive force that helps maintain the particles in suspension, but also causes the flow to dilate. Grain-to-grain interactions become increasingly important as sediment concentration increases (Bagnold, 1962).
Matrix Strength	Ionic surface charges and large surface area:volume ratio of clay particles cause them to become aggregated into larger masses by weak van der Waal's forces. At sufficiently high concentration, the aggregated clay minerals form a sufficiently strong particle network capable of supporting the weight of larger grains (Mulder and Alexander, 2001)

Table 1. 1 *List of particle support mechanisms that individually or in combination act in sediment gravity flows. Adapted from Dumouchel (2012).*

1.6.1.2.1 Hyperconcentrated Density Flows

Hypercontracted density flows consist of a similar sediment water ratio to cohesive flows; however hyperconcentrated density flows are more depleted in cohesive particles and/or are more internally sheared. Hyperconcentrated flows consist of more than 25% sediment volume concentration and commonly are highly erosive (Mulder and Alexander, 2001). Due to the high sediment concentrations, grain-to-grain collision are an important mechanism for suspending sediment, which greatly reduces buoyancy effects. Frictional freezing resulting from grain-to-grain interaction is the main depositional mechanism and deposits consist of massive, coarse silt, sand

or gravel that locally is inversely graded. Additionally, hyperconcentrated flows may transform downslope into concentrated flows if the flows become sufficiently diluted by fluid entrainment and fluid turbulence becomes more energetic and inflates the sediment suspension (Mulder and Alexander, 2001).

1.6.1.2.2 Concentrated Density Flows

Compared to hyperconcentrated flows, concentrated density flows have a lower sediment concentration (10-25% by sediment volume) and exhibit a change in sediment-support mechanism from primarily buoyancy and inertial forces to grain-to-grain interactions generating dispersive pressure (Kneller and Branney 1995). The sediment concentration varies depending on sediment size, sorting, relative density and composition, thus making it difficult to determine a single threshold condition for the flows or resulting deposits (Mulder and Alexander, 2001). Reduced sediment concentration results in greater entrainment of ambient water causing flow dilution and fluid turbulence to be the dominant support mechanism.

Deposition takes place progressively by differential grain settling of large and/or denser particles first, eventually building up a massive or normally graded sand to gravel beds. In 1982, Donald Lowe developed a six-part (R_1, R_2, R_3, S_1, S_2, S_3) classification of concentrated density flow deposits with gravel-rich (R) and sand-rich (S) end members (Figure 1.12). Gravel-rich R1 consist of structureless gravel, R2 is inversely-graded deposited by traction carpet deposition, and R3 comprises normally-graded gravel deposited from suspension (Lowe, 1982). In sand-rich strata, S1 is formed by bed load transport and is either planar- and/or cross-stratified sandstone, S2 is deposited by traction carpet deposition as sedimentation rate increases, and S3 is the equivalent to Bouma Ta division (See section 2.3.3 for more detail).

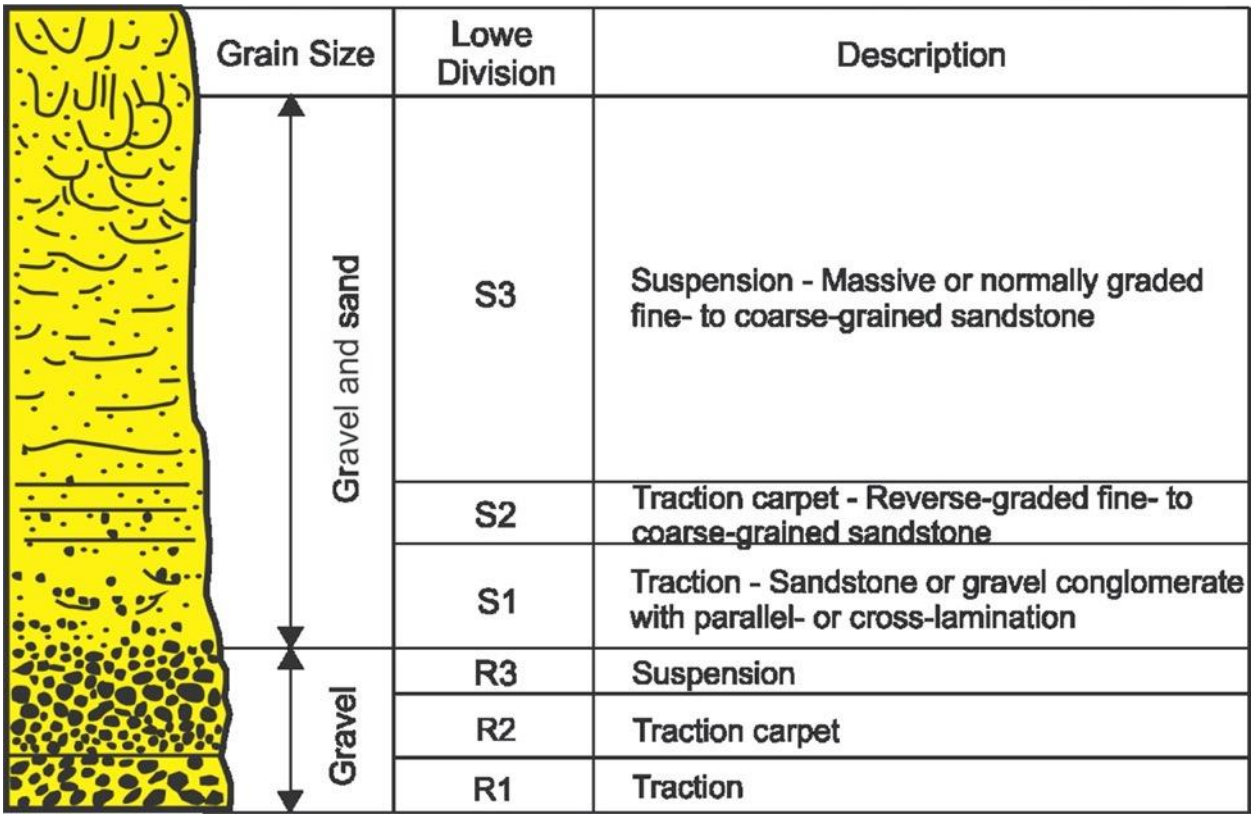

Figure 1. 13. *Idealized Lowe sequence for high-density turbidity currents showing typical grain size profile and sedimentary structures (redrawn by Angus (2016) from Lowe (1982)). The S3 division is equivalent to the Ta division of a classical Bouma turbidite.*

1.6.1.2.3 Turbidity Currents

Turbidity currents are the most common type of frictional flow and are thought to be the principal agent transporting sediment into the deep marine (Arnott, 2010; Khan, 2012). Turbidity currents behave as Newtonian fluids in which the upper threshold of sediment concentration is <9%, which is termed the Bagnold limit (Bagnold, 1962). In such a flow the main particle-support mechanism is fluid turbulence as grain-to-grain interaction is less influential due to ambient fluid entrainment and consequent dilution (Figure 1.11). Above the Bagnold limit, particles become so closely spaced that fluid turbulence begins to be dampened and other particle-support mechanisms like dispersive pressure, hindered settling and buoyancy become increasingly important (Mulder and Alexander, 2001; Arnott, 2010).

An idealised turbidity current exhibits a longitudinal structure that exhibit three distinct, but not sharply bounded parts: head, body and tail (Figure 1.13). The head is characterized by an overhanging nose that forms as a result of basal friction and mixing with the surrounding ambient fluid along and beneath the head and carries sediment-rich fluid back towards the body (Arnott, 2010). In order to be sustained, the body of the flow must continuously supply sediment to the head, which moves 30-40% faster than the head. Moreover, the three parts of a turbidity current consist of different sediment populations. This in turn, causes the flow to be longitudinally

differentiated by grain size with coarse sediment becoming concentrated in the lower part of the head as finer sediment is displaced up and backwards into the body, and eventually forming a dilute fine-grained low-density sediment dispersion that makes up the tail of flow (Arnott, 2010; Kneller and Buckee, 2000).

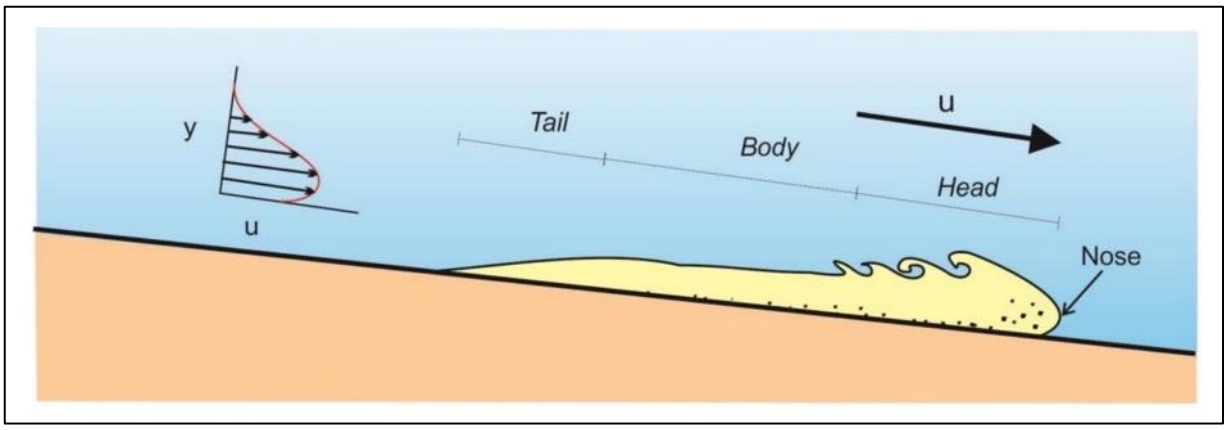

Figure 1. 14. *Longitudinal structure of a turbidity current consisting of a well-defined, head, body and tail. The head has an overhanging nose due to frictional forces exerted along the upper and lower boundaries of the flow (Kneller and Buckee, 2000). The velocity profile shown on the left indicates that flow velocity increases upward from the bed and is highest at approximately 20-30% of the flow thickness and then decreases further upward (Mulder and Alexander, 2001). Illustration from Navarro (2016).*

The deposit from a turbidity current is termed a turbidite. Bouma (1962) was the first to describe the idealized vertical succession of what now is termed the classical, or Bouma sequence, which is interpreted to be deposited by a decelerating low-density (< 9% volume sediment concentration) turbidity current. An ideal Bouma sequence comprises five divisions labelled T_a to T_e divisions (Figure 1.14). The T_a division comprises massive or graded, structureless, coarse- to medium-grained sandstone interpreted to be deposited rapidly from suspension. Their structureless nature is attributed to high rates of suspension fallout that inhibits the development of tractional sedimentary structures (like planar lamination or cross-stratification) (Arnott and Hand, 1989). The overlying T_b division consists of planar-laminated, medium to fine sandstone and indicates

reduced rates of sediment fallout and more prolonged bed surface transport. Recent work by Tilston et al. (2015) suggests that planar laminations form by traction transport on a surface that lacks the requisite bed defects to initiate the development of angular bedforms like ripples or dunes. The T_b division, in turn, is overlain by cross-stratified, fine- to very fine-grained sandstone interpreted to be deposited by migrating current ripples (Khan, 2012). Interlaminated sandstone/siltstone and mudstones make up the T_d division, which forms by mixed traction and suspension sedimentation processes (Lowe 1982). Lastly, the T_d division is capped by the mudstone T_e division deposited by fine-grained suspension fallout (Lowe, 1982).

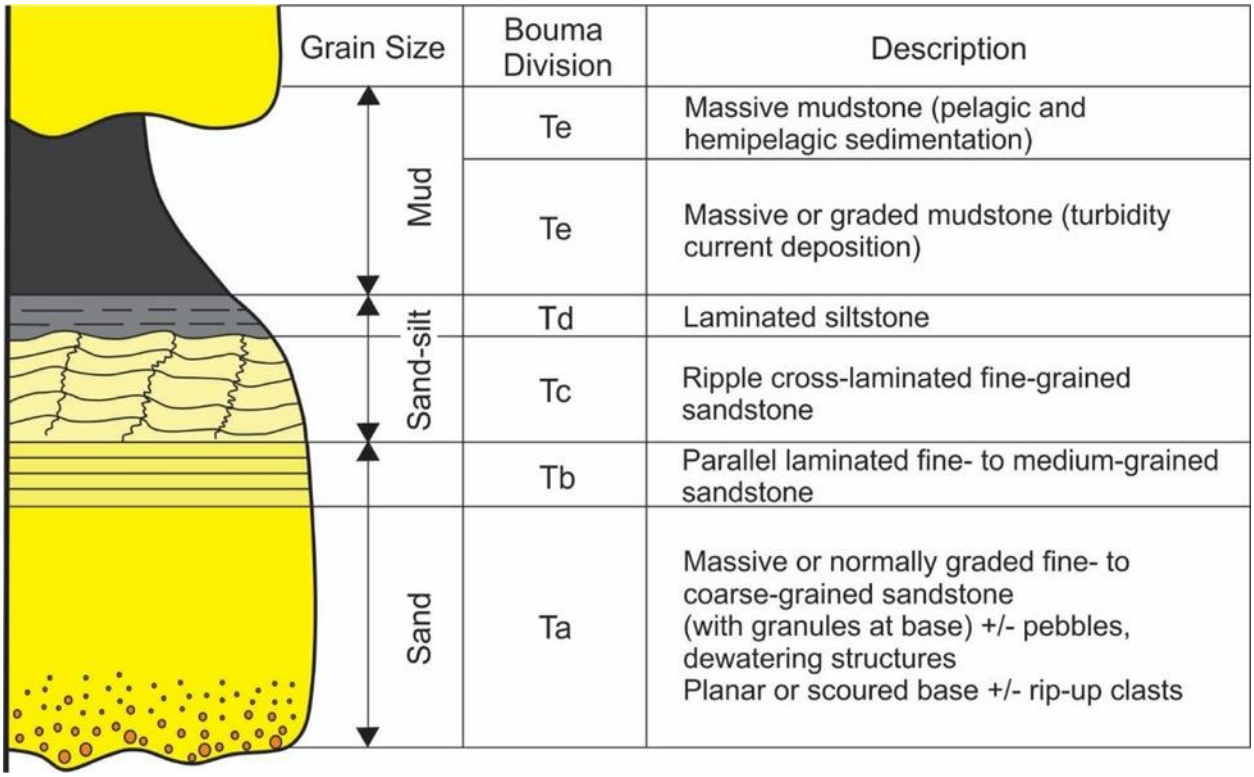

Figure 1. 15. *Idealized Bouma sequence for a low-density turbidity current showing typical grain size profile and sedimentary structures (redrawn by Angus (2016) from Bouma (1962)).*

1.6.1.3 Mass-movement Deposits

In contrast to frictional and cohesive flows, mass movements, namely slides and slumps, are gravity induced coherent masses of sediment that move downslope along discrete failure planes (Shangmugam, 2006). Mass movements are triggered when gravity exceeds the tensile strength of the sedimentary mass. Movement continues downslope until the resisting forces, mainly friction along the base, exceed the downslope gravitational force and en-masse deposition occurs. Typically, a slide mass glides over a planar basal shear surface or detachment surface with little or no internal deformation (Stow, 1986; Shanmugam et al., 1995). As a slide moves downslope, it may evolve into a slump in which the mass moves along an upward-concave basal detachment surface with the development of a wide range of internal deformational structures with evident contortion and rotation (Stow, 1986). Eventually the internal mixing of ambient fluid into the slide or slump causes it to inflate and particles to become suspended in the fluid, which now is considered a turbidity current (Figure 1.15; Shanmugam, 2006).

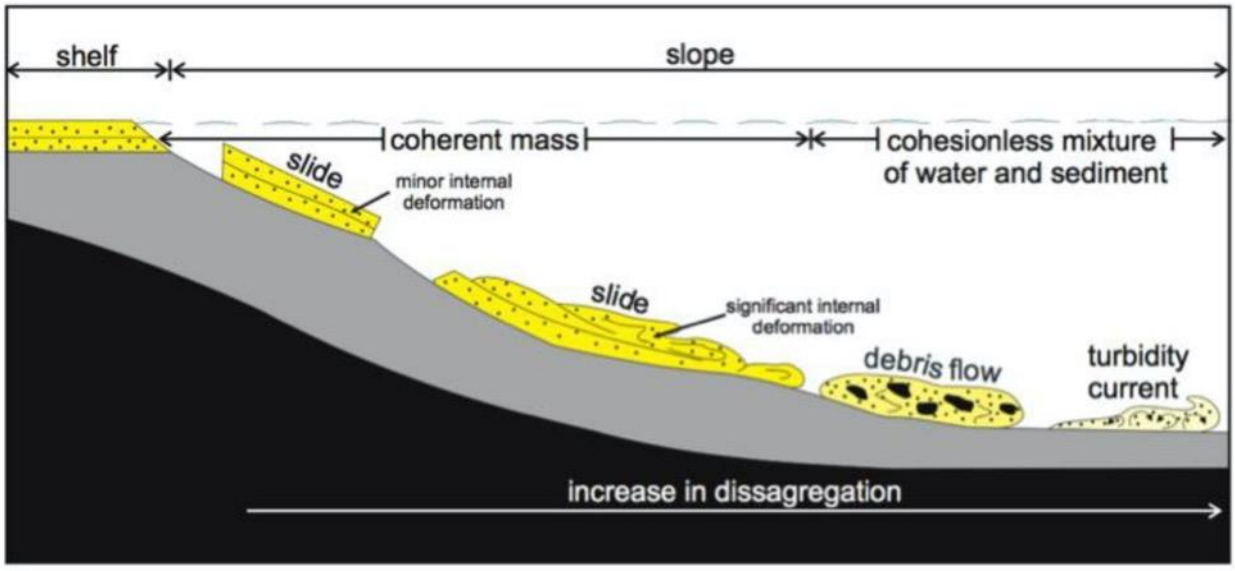

Figure 1. 16. *An idealized downslope evolution of a remobilized sediment pile into a frictional sediment gravity flow. At the shelf edge gravitational failure of local seafloor forms a coherent slump or slide that then disaggregates and transform initially into a cohesive debris flow, but with further ingestion and internal mixing of ambient fluid, transforms into a fully evolved frictional sediment gravity flow termed a turbidity current (redrawn by Khan (2012) from Shanmugam et al. (1994)).*

Chapter 2: Facies Descriptions and Interpretations of a Deep-Marine, Base-of-Slope, Channel-Levee System, Neoproterozoic Windermere Supergroup, British Columbia.

Rocks that make up ICC1 comprise five facies: (1) structureless, normally-graded or massive sandstone and conglomerate, (2) traction-structured sandstone, (3) mudstone and siltstone and (4) matrix-supported conglomerate. Although strata have experienced low-grade greenschist facies metamorphism (200 - 250^{o} C) primary physical sedimentary structures are well preserved and therefore terminology applied to sedimentary rocks will be used to describe these strata. Additionally, metamorphism has transformed detrital clay minerals to chlorite and mica, namely muscovite and sericite (Popovic, 2016). Bed thickness classification follows Ingram (1954): very thin-bedded (1 - 3 cm), thin-bedded (3 - 10 cm), medium-bedded (10-30 cm), thick-bedded (30 - 100 cm), very thick-bedded (> 100 cm). Additionally, grain size is categorized using the Udden-Wentworth grain size classification scale (Udden, 1914; Wentworth, 1922), and turbidites are described following the five-part internal subdivisions of Bouma (1962).

2.1 Facies 1 (F1): Structureless, normally-graded and ungraded sandstone and conglomerate

2.1.1 Macroscopic Characteristics

Facies 1 (F1) comprises 39% of ICC1 stratigraphy and is subdivided into two subfacies. F1.1 (31% of stratigraphy) consists of thin- to very thick-bedded (10 – 650 cm), ungraded and normally graded sandstone and conglomerate (Figure 2.1A-D) that at most can be traced along strike for a few tens of meters. At their base beds consist of dispersed granule or pebble conglomerate in a matrix of medium- to coarse-grained or coarse- to very coarse-grained sandstone that then grades upward to medium- and coarse-grained sandstone. In contrast, ungraded beds comprise coarse-grained sandstone, or rarely, lower medium- to fine-grained sandstone with

dispersed very coarse sand and quartz granules. Beds are typically amalgamated with bases identified by an abrupt change in grain size and locally by visible scours or load structures. Soft sediment deformation structures are observed locally and include (1) sandstone injections up to 30 cm long and 15 cm wide that intrude sub-horizontally into fine-grained Tcde turbidites, and (2) flame structures that range from 2 - 10 cm in length.

F1.2 (6% of stratigraphy) comprises massive, structureless medium- to very thick-bedded (18 - 600 cm), mudstone-clast-supported conglomerate (Figure 2.1E-F). Clasts range from granules to boulders (0.5 - 10 cm thick and 5 - 40 cm long), but uncommonly are up to 2 m long and > 30 cm thick. Siliciclastic mudstone and rare carbonate-cemented mudstone clasts are sub-rounded to rounded and oriented sub-parallel to bedding. Rarely, clasts are angular and composed of fragments of very thin-bedded, fine-grained, upper division turbidites (Tcde). Mudstone clasts occur in the lower and less commonly middle and upper part of the bed. Matrix is composed of medium- to coarse-grained sandstone, and like F1.1, basal contacts are loaded or shallowly scoured. Beds typically extend for several meters along strike, and rarely over several tens of meters.

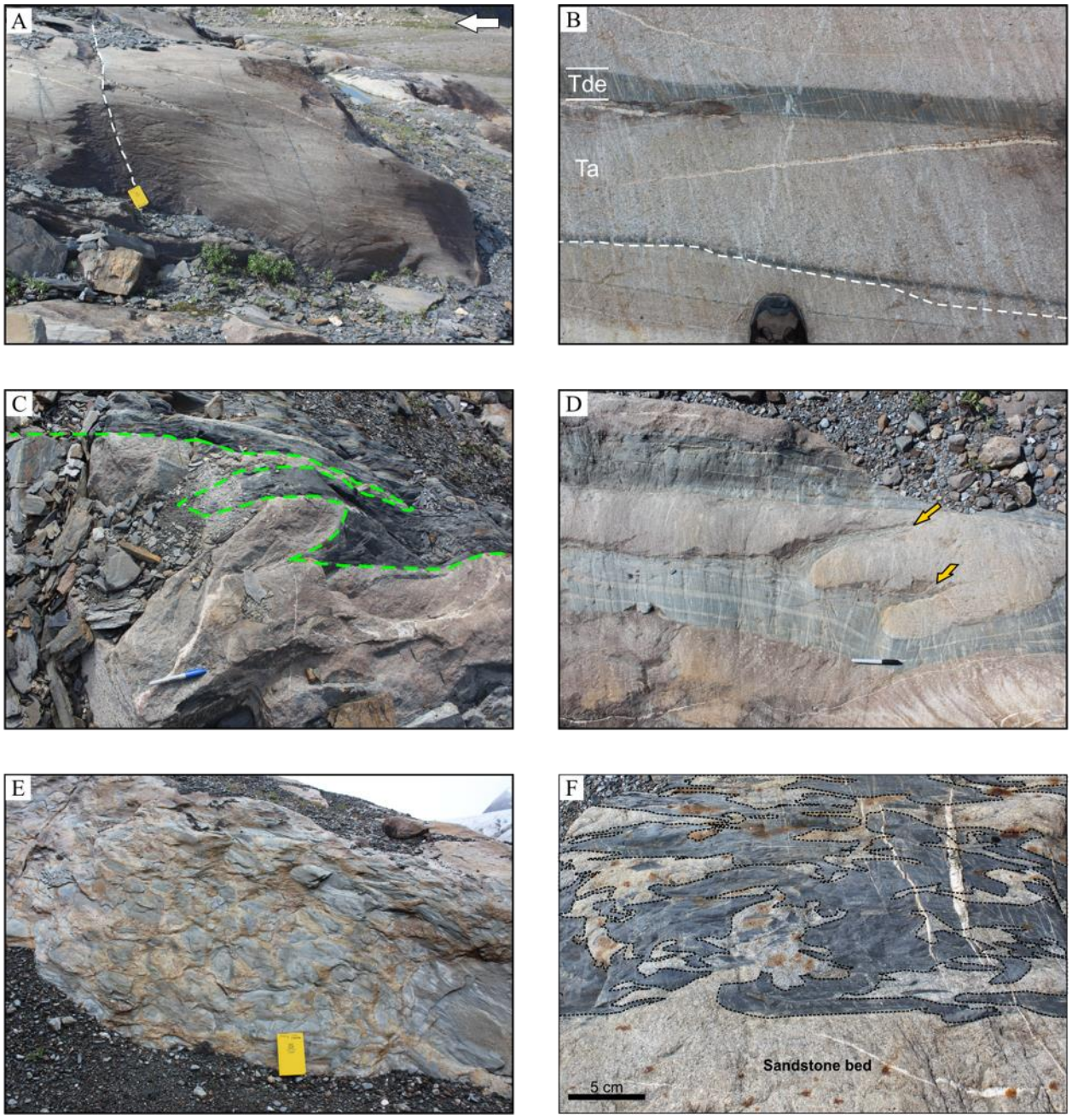

Figure 2. 1. *Representative photos of F1.1 [A-D] and F1.2 [E-F]. (A) Very thick-bedded, granule conglomerate grading upward to coarse-grained sandstone. Dashed white line indicates the top of the bed. White arrow indicates stratigraphic way-up. (B) Medium-bedded, normally-graded, coarse-grained sandstone that fines upward to medium sandstone capped by interlaminated siltstone and very fine-grained sandstone. Note the undulose base that locally coincides with a thin black band representing a metamorphic (Mesozoic) solution seam. (C) Massive, ungraded, coarse-grained sandstone injected into fine-grained Tcde turbidites (dashed green line) forming*

two laterally-tapering sills. (D) Well-developed flame structures (indicated by yellow arrows) along the base of an ungraded, coarse-grained sandstone. Note the downward deflection of the grey-coloured turbidite bed caused by foundering of the overlying sandstone (E) Basal bedding plane of a coarse-grained sandstone with abundant, well-rounded, siliciclastic mudstone clasts. Note the subparallel orientation of the clasts. (F) Mudstone clasts in a coarse-grained sandstone matrix. Note the irregular shape and brecciation of large mud clasts, and the absence of a preferred (clast) fabric. The sandstone is interpreted to represent sediment that was forcibly injected from the underlying sandstone bed into the overlying mudstone forming a complex network of sill and dykes.

2.1.2 Microscopic Characteristics

In thin section, F1 is moderately- to poorly-sorted with sub-angular to sub-rounded, equant to elongate sand grains (Figure 2.2A-D). The sand grains comprise coarse sand to granule monocrystalline quartz (70%) with minor feldspar (2%) and polycrystalline quartz (3%). Quartz grain boundaries commonly exhibit bulging recrystallization indicating deformation temperatures of 280-400^{o}C (Lee, 2016), in addition to sub-grain rotation that creates fine to medium sand grains with relatively straight grain boundaries and straight extinction (Stipp et al., 2002). In contrast, feldspar grains are commonly altered to sericite or calcite and typically are finer-grained than the quartz grains. The intragranular space is filled with silt-sized quartz, recrystallized matrix (mainly muscovite and sericite), chlorite, which typically forms sand-sized porphyroblasts (10%), and iron-rich sparry calcite cement.

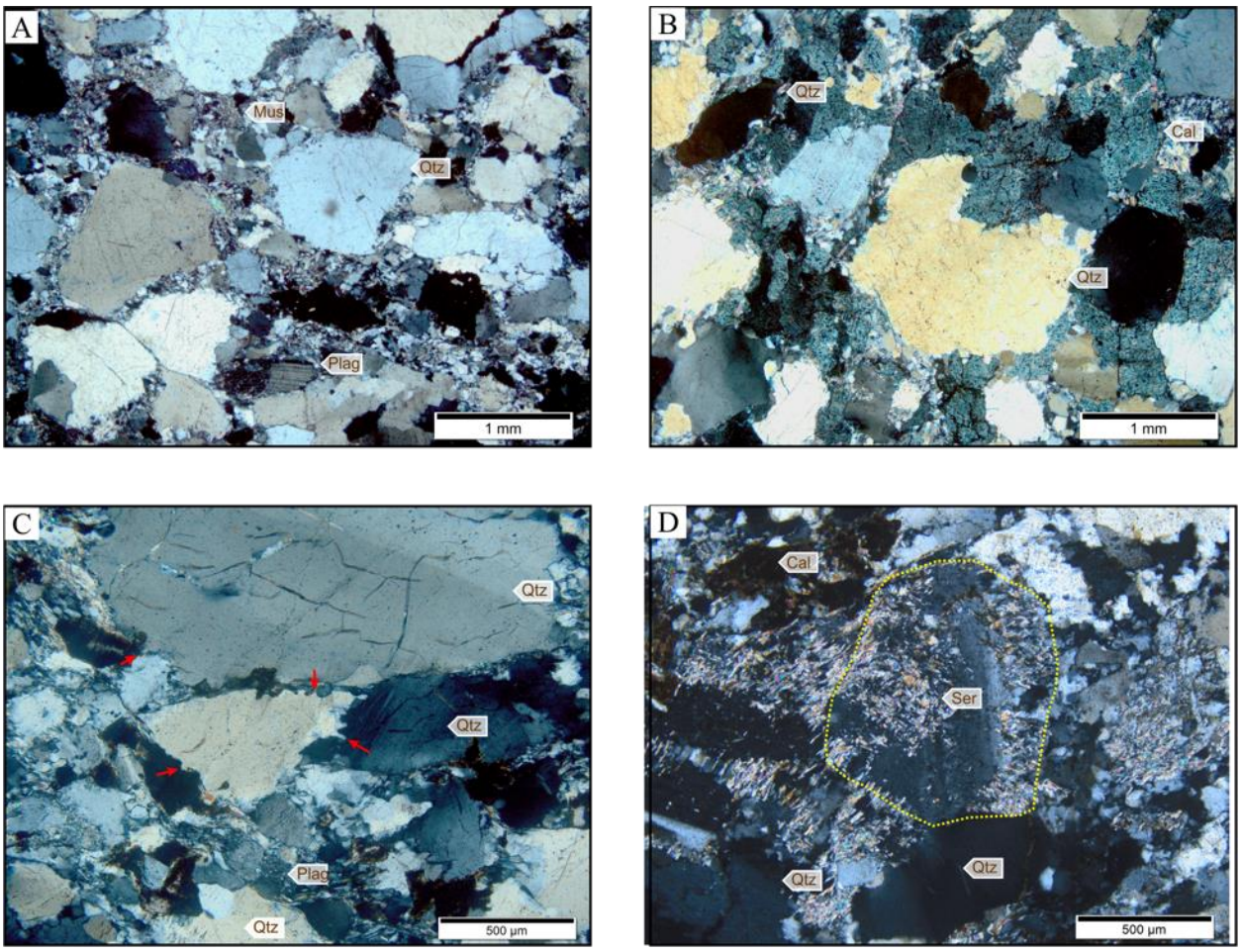

Figure 2. 2. *Photomicrographs of F1 strata. (A) Coarse-grained, poorly-sorted sandstone in XPL. The sample is dominated by sub-rounded detrital quartz (Qtz) framework grains and less common plagioclase (Plag) dispersed in a matrix of quartz silt and recrystallized muscovite (Mus). (B) Poorly-sorted, coarse-grained sandstone comprising sub-angular quartz (Qtz) grains cemented by coarse crystalline, iron-rich calcite (Cal) (20% by volume). (C) Example of coarse-grained sandstone in which the quartz (Qtz) grains exhibit grain bulging along their boundaries. (D) Subarkose in which a plagioclase grain (encased by yellow polygon) has been partly altered to sericite (Ser).*

2.1.3 Interpretation

Strata of F1 correspond to the T_a division of Bouma (1962) or S_3 division of Lowe (1982) and are interpreted to be deposits of high-density turbidity currents (Lowe, 1988), or similarly, concentrated or hyper-concentrated flows (Mulder and Alexander, 2001). Deposition of F1 occurs from suspended particle settling (Alexander and Mulder, 2001), either slowly and progressively from quasi-steady flows (Kneller and Branney, 1995), or rapidly from highly depletive flows (Arnott and Hand, 1989). Nevertheless, irrespective of fallout rate, near-bed conditions, which most probably reflect high sediment concentration, inhibited the formation and amplification of bed-surface defects that ultimately would have evolved into angular bed forms, which with downflow migration, would have formed cross-stratified tractional sedimentary structures (Arnott and Hand, 1989; Venditti et al., 2005; Tilston et al., 2015). Rarely, beds are capped by a 1 - 2 cm-thick siltstone-mudstone layer (Tde; F3) indicating deposition during the final flow stages as the dilute tail of the flow deposited mud by full suspension settling (Lowe, 1982) or later hemipelagic fallout (Meyer, 2004). The lateral discontinuity of mudstone caps in addition to common scour surfaces are associated with sea floor scouring by turbulent eddies related to the event that deposited the overlying sandstone bed. Basal flame structures, on the other hand, indicate not only gravitational loading of the more-dense sand-rich bed on a poorly consolidated, lower density mud-rich layer, but also a short recurrence interval between successive turbidity currents.

In comparison to F1.1, F1.2 consists of clast-supported mudstone-clast conglomerate that are variously interpreted based on clast shape. F1.2 strata consisting of well-rounded, dispersed mudstone and carbonate-cemented mudstone clasts indicate that flows were strongly erosional and based on their rounded morphology were most probably sourced from upflow (upslope) erosion of the local muddy seabed. In contrast, F1.2 strata composed of angular, irregularly shaped

mudstone clasts are interpreted to be associated with in situ brecciation caused by the intrusion of coarse-grained sand that formed an interconnected network of sills and dykes that fractured and fragmented the intruded siltstone and mudstone beds. Mobilization of the coarse sand was a consequence of elevated of pore fluid pressure that eventually, and catastrophically, exceeded the tensile strength of the adjacent low permeability silt and mud strata. Movement of the fluid-sediment mixture continued until the fluid pressure gradient became sufficiently depleted, causing the fluid flow to stop and the fracture network to become filled with now immobile sand.

2.2 Facies 2 (F2): Traction-Structured Sandstone

2.2.1 Macroscopic Characteristics

Facies 2 (F2) makes up 28% of ICC1 stratigraphy and comprises three subfacies. F2.1 (27 % of total stratigraphy) consists of very thin- to medium-bedded (2 - 35 cm thick), planar-laminated medium- to coarse-grained sandstone that grades upward to fine-grained sandstone, which then is sharply overlain by small-scale, cross-laminated very fine- to fine-grained sandstone capped by structureless siltstone (T_{bde} or T_{bcde}; Figure 2.3A-D). The fine- to very fine-grained cross-laminated unit is typically composed of 2-3 non-climbing ripple sets, although single sets are observed. Rarely, planar laminated strata exhibit a gradual upward increase in clay content capped by pinstripe laminated very fine-grained sandstone and siltstone overlain by a massive mudstone cap (1 - 2 cm thick). Basal contacts are sharp and planar but in places undulatory with flame structures and uncommonly overlie coarse-grained structureless sandstone (F1.1).

Beds are also composed exclusively of cross-laminated sandstone overlain by structureless or massive siltstone and mudstone (T_{cde}). Cross-laminated sandstone can be divided into two types: isolated single set (SR) and single set (SS). SR consists of 0.1 - 0.5 cm thick, very fine-grained sandstone that crops out as isolated formsets overlain sharply by a structureless mudstone (0.5 – 1

cm thick). In contrast, SS consists of 0.5 - 5 cm thick, typically fine-grained sandstone cross-sets that are sharply overlain by a structureless siltstone (1 - 5 cm thick). Commonly, 2 to 5 non-climbing SS stack to form cosets that range from 5 - 15 cm thick and are overlain sharply by structureless or planar-laminated siltstone (2 - 15 cm thick) capped by a structureless massive mudstone (1 - 2 cm thick).

F2.2 makes up 1% of ICC1 and comprises rhythmically intercalated sandstone and sandy mudstone (RSM; Figure 2.3E-F). RSM comprises thin- to medium-bedded (3 - 15 cm thick), fine- to medium-grained, planar-, wavy- or cross-laminated sandstone interstratified with sandy mudstone overlain abruptly by massive mudstone (T_{de}). If more than one style of lamination is present planar- or wavy-laminated sandstone typically occurs in the lower part of the bed and is separated from the overlying cross-laminated part by a laterally continuous, 0.5 - 1 cm thick mud layer. Cross-laminated sets that are sand-rich in their upper part feather into mud in their (downflow) trough and cross-stratification dips more shallowly compared to SS.

F2.3 makes up 2% of ICC1 and consists of medium- to thick-bedded (10 - 120 cm), large-scale cross-stratified sandstone. Less commonly strata transition abruptly downflow from planar-stratified to large-scale cross-stratified sandstone (Figure 2.4A-B). Basal contacts are usually undulatory and erosive, although planar contacts are observed. Beds consist of coarse- to very coarse-grained sandstone with common dispersed, sub-rounded granule to pebble quartz grains and mudstone intraclasts that range from 1 - 3 cm thick and 1 - 2 cm long. F2.3 has a distinctive reddish color, which in this case is related to the oxidation of a pervasive ferroan calcite cement. Cross-stratification typically occurs as a single set that ranges from 12 - 30 cm thick, although cosets comprising 2 - 3 sets are observed. Cross-stratified sandstone is rarely overlain by planar- or cross-stratified sandstone (F2.1), but more typically sharply overlies and is overlain by

structureless, normally-grade sandstone (F1.1). Beds pinch and swell but can be traced continuously for a few to several tens of metres along strike.

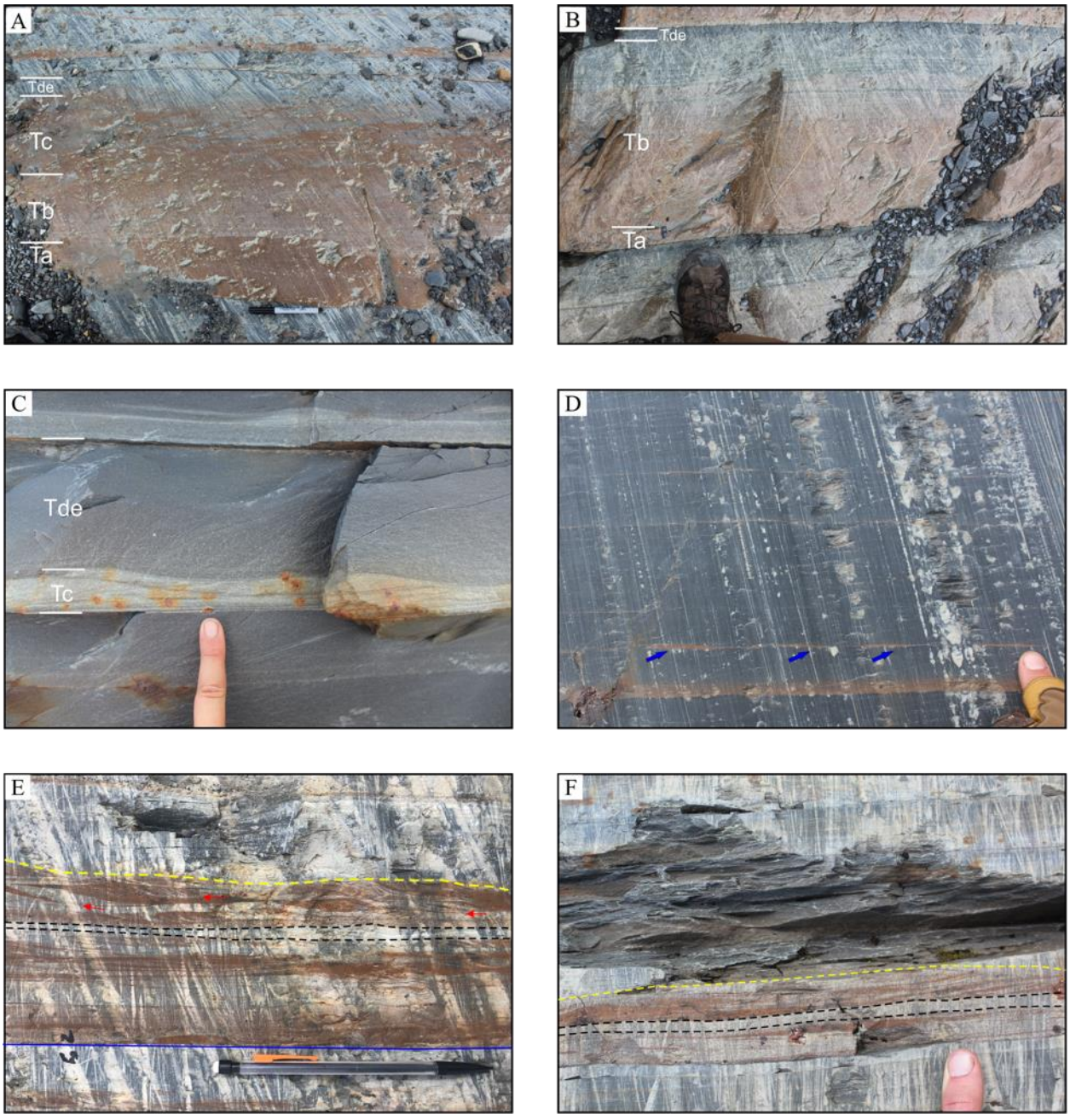

Figure 2. 3. *Representative photos of F2.1 [A-D] and F2.2 [E-F] in outcrop. (A) Medium-bedded, T_{abcde} turbidite. The T_c unit comprises multiple stacked ripples up to 2 cm thick and capped by a thinly-laminated silty mudstone (T_{de}). (B) Thick-bedded, upper medium-grained Tabde turbidite. Note the gradual upward increase in clay content in the planar laminated (T_b) part (indicated by*

the progressive upward darkening), which then is overlain by pinstripe-laminated fine-grained sandstone and siltstone capped sharply by a massive mudstone (T_{de}). (C) Thin-bedded, fine-grained T_{cde} turbidite. Note that the T_c division consists of a single ripple cross-stratified formset overlain sharply by a massive, structureless mudstone. (D) Very thin-bedded, fine-grained, single set (starved) ripple (indicated by blue arrows; T_{cde} turbidite). (E) Flat-based, medium-bedded, fine-grained, wavy- to low-angle laminated sandstone intercalated with mudstone. Note the sharply bounded, 0.5 cm thick, laterally continuous mud layer (denoted by black dashed line) that separates low-angle from high-angle cross-lamination. In the cross-laminated upper layer, note the lateral feathering of the sand-rich upper part into mud in the trough (red arrows). This, then, is overlain by a thinly-laminated siltstone (T_{de}). (F) Thick (up to 1 cm), laterally continuous mud layer (denoted by black dashed lines) sandwiched between wavy- and low-angle cross-laminated sandstone.

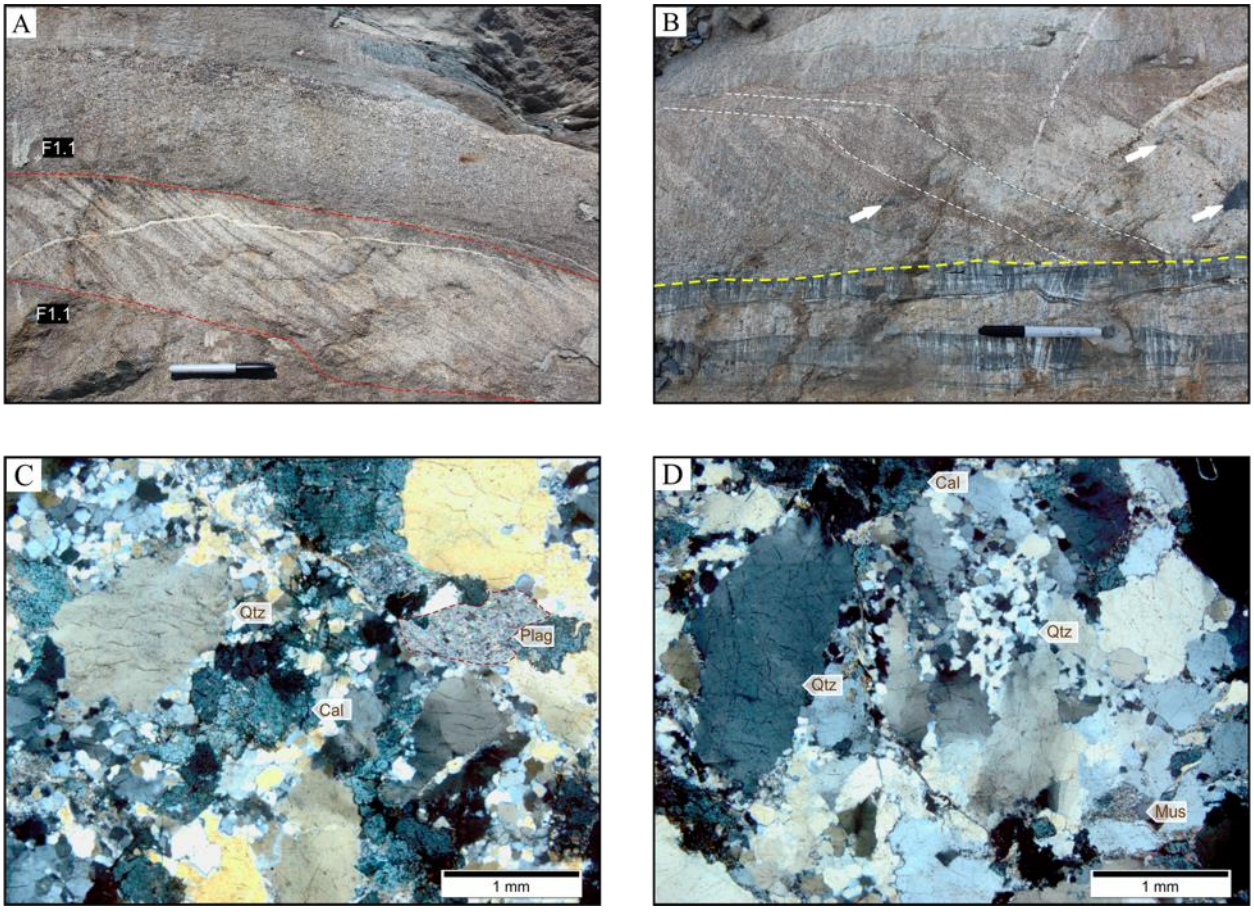

Figure 2. 4. *Representative photos of F2.3. (A) Medium-bedded, coarse-grained, cross-stratified sandstone (F2.3) bounded above and below by coarse-grained strata of F1.1 (red dashed lines). (B) Planar- passing abruptly downflow into cross-stratified, coarse-grained sandstone (some highlighted in white), white arrows point to dispersed mudstone clasts. Note the sharp base (yellow dashed line) with the underlying mudstone bed. (C-D) Cross-polarized photomicrographs of cross-*

laminated sandstone. Framework grains are mostly mono- and polycrystalline quartz (Qtz) dispersed with abundant subgrains and a matrix of quartz silt and muscovite with local patches of iron-rich calcite (Cal) cement.

2.2.2 Microscopic Characteristics

In thin section, planar- and cross-stratified sandstone (F2.1) are mineralogically similar and consist of subangular to subrounded fine- to medium-grained framework grains of monocrystalline quartz and less common plagioclase with a matrix of quartz silt, muscovite, sericite, sand-sized chlorite porphyroblasts and extensive iron-rich calcite cement. Cross-laminated sandstone is commonly poorly sorted with a pervasive calcite cement (Figure 2.5A-B). Moreover, planar-laminated sandstone comprises alternating sharp-bounded matrix-rich and matrix-poor lamina (Figure 2.5C-D): matrix-poor laminae consist mainly of framework grains and 30% recrystallized matrix whereas matrix-rich laminae comprise up to 70% matrix.

Cross-stratified sandstone (F2.3; Figure 2.4C-D) typically consists of ~ 75% framework grains, 10 - 20% matrix (muscovite, chlorite, sericite and silt-sized quartz), and up to 15% carbonate cement (calcite and minor dolomite). Framework grains consist primarily of subangular to subrounded, mono- and polycrystalline quartz (480 - 720 um). Quartz grain boundaries commonly exhibit dynamic quartz recrystallization due to bulging recrystallization or subgrain rotation in addition to sutured boundaries and uncommon overgrowths due to strain-induced pressure dissolution of silica at grain-on-grain contacts. Feldspar (orthoclase and plagioclase) makes up a minor portion of the framework grains (3% of the total volume) and where present is partly to fully altered to sericite or calcite. In contrast, the matrix is composed of detrital clay that has been altered to muscovite and sericite mixed with silt-sized quartz grains (< 62.5 um) and common chlorite porphyroblasts.

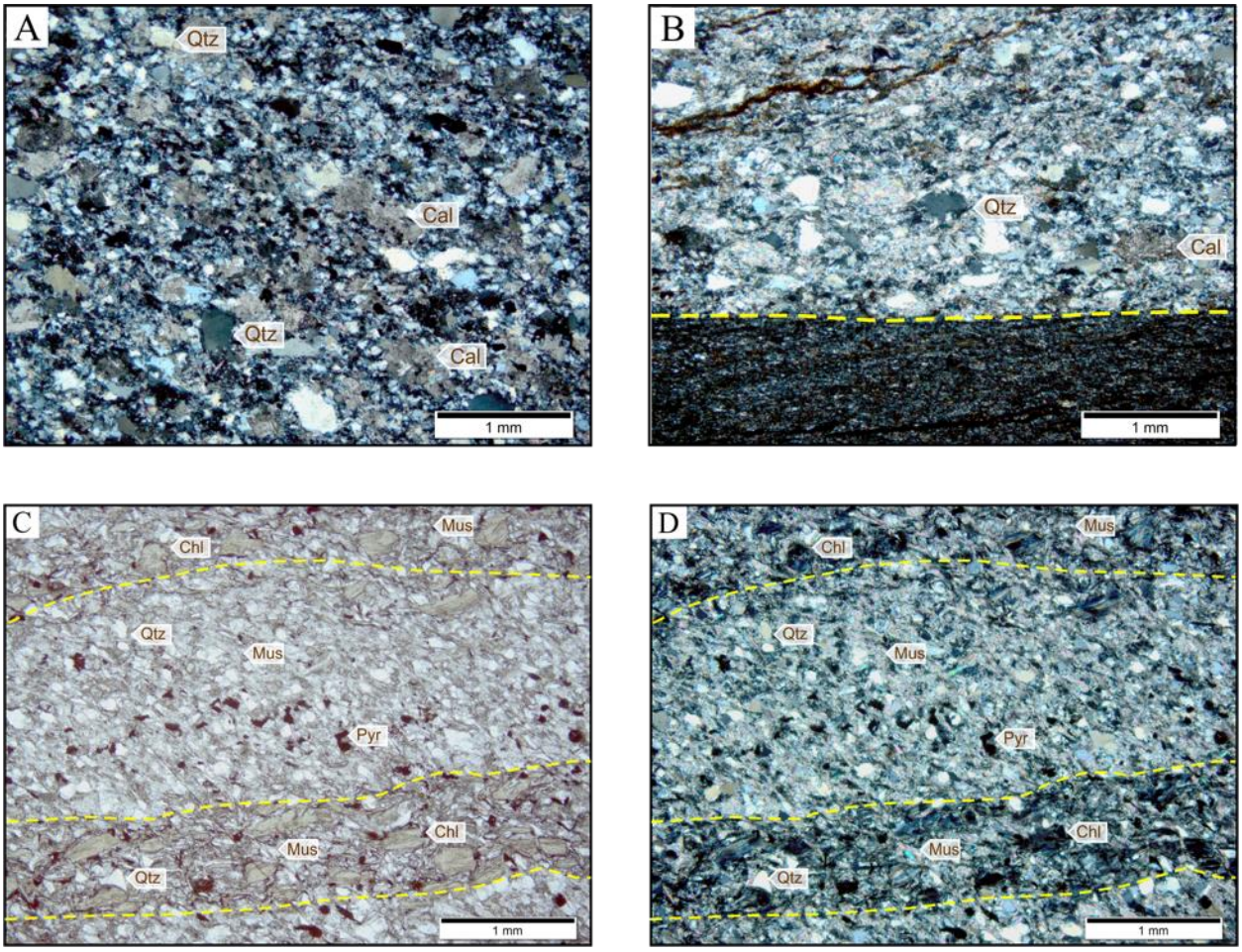

Figure 2. 5. *Photomicrographs of F2.1. (A-B) Cross-laminated fine-grained sandstone consisting of fine-grained quartz (Qtz) grains dispersed in a matrix of quartz silt, muscovite (Ms) and sericite (Ser). Note also extensive patches of iron-rich (15%) calcite (Cal) cement. (B) Note the sharp basal contact (yellow dashed line) with the underlying mudstone composed of muscovite and sericite with dispersed silt-sized quartz grains and medium-grained chlorite porphyroblasts. The apparent (inclined upward to the right) fabric in the mudstone is tectonic cleavage. (C-D). Photomicrographs in plane- and cross-polarized light, respectively, of planar-laminated sandstone. Note the sharp contacts (yellow dashed lines) between chlorite-rich and chlorite-poor laminae. Chlorite-rich laminae comprise fine-grained quartz (Qtz), abundant medium-grained chlorite (Chl) porphyroblasts and minor recrystallized matrix (Muscovite, Mus). Chlorite-poor laminae, on the other hand, are made up of fine-grained quartz (Qtz) dispersed in a matrix of recrystallized muscovite (Mus) with dispersed pyrite (Pyr) grains.*

2.2.3 Interpretation

F2.1 beds are interpreted to represent incomplete, mostly upper division, Bouma turbidites deposited from decelerating turbulent flows composed of clay- to coarse-grained sand suspended

by fluid turbulence (Lowe, 1982). Most basal contacts are sharp and planar indicating that flows generally became immediately depositional.

The planar-laminated part of some F2.1 beds is interpreted to represent the T_b division of a classical Bouma sequence, whereas the small-scale cross-laminated unit is interpreted to represent the T_c division and the thin, siltstone-mudstone unit is interpreted to represent Td/e division (F3, see section 2.3 for detail). The T_b division is interpreted to have been deposited by flows with lower sediment rate fallout, and most likely also lower sediment concentration compared to those that deposited the T_a division of F1 strata (Arnott and Hand, 1989). Planar laminae indicate that conditions in the near-bed region were unfavorable for the establishment and amplification of angular bedforms, possibly because flow speed and/or sediment concentration was initially too high to form the requisite bed defects needed for ripples or dunes (Southard and Boguchwal, 1990; Sumner, 2008; Arnott, 2012; Tilston et al., 2015). These defects change the pattern of fluid flow in the near-bed region that then leads to flow separation, defect amplification, and ultimately the growth of angular bed forms (Venditti et al., 2005). Recent work by Venditti et al., (2005) showed that bed defects can developed spontaneously and everywhere on a flatbed experiencing general bed-surface sediment transport, and not only downflow of a single pre-existing defect. Initiation of these defects is associated with a near-bed hydrodynamic (Kevin-Helmholtz) instability that develops along the interface between the slow moving, bed-load layer and overlying less dense, faster moving near-bed fluid (Venditti et al., 2006). The waveform shape of the perturbed interface causes a spatially regular alternation of areas of sediment transport and accumulation that quickly and uniformly build up the bed defects. It is from these defects that current ripples formed and accordingly the ripple cross-stratified (T_c) part of the deposit. Similar to F1, the laminated siltstone and structureless mudstone that caps the underlying sandstone

formed by late stage settling from the fine, low density tail of the flow or post-flow hemipelagic fallout (Lowe, 1982; Meyer; 2004).

Although superficially similar to F2.1, strata of F2.2 exhibit a distinctive rhythmic intercalation of sandstone and sandy mudstone, in addition to consistently low-angle cross-stratification and wavy lamination. Collectively these features suggest a more complex history of flow conditions, flow deceleration and styles of deposition compared to those that formed strata of F2.1. Similar to F2.1, the planar- and cross-laminated sandstones are interpreted to have been deposited under bedload transport on the bed, the latter being associated with requisite hydraulic conditions and amplification of near-bed surface defects that evolved into downstream-migrating ripples. However, the intricate interstratification of mud and sand lamina, in addition to the thick interstratified mud layers, suggest that with time, and waning flow conditions, mud concentration increased substantially and came to profoundly alter flow conditions and accordingly bed-form morphology (Baas and Best. 2002). As a result, bedload transport sequestered sand in the ripple crest but expanding flow over the downflow trough caused abundant mud to also be deposited. With continued reduction of flow speed, the near-bed hydrodynamic instability although still capable of generating bed defects, was unable to cause sufficient amplification of the defect to alter sediment transport patterns on the up- and downflow sides of the defects. As a consequence, a wavy bed remained the stable bed state.

Flat-based, high-angle cross-stratified sandstone of F2.3 are interpreted to be the remnants of downflow migrating subaqueous dunes. Like ripples in strata of F2.1, suspended-sediment was concentrated in the basal part of the flow and allowed for the development of the hydrodynamic instability needed to form bed-surface defects, but because of higher flow velocity evolved instead into dunes. Notably, dune cross-stratification is rare in the deep-marine sedimentary record, which

according to Arnott (2012), may be a consequence of deleterious near-bed sediment conditions in sand-transporting turbidity currents moving at speeds conducive to the formation of dunes. The lateral discontinuity of dune cross-stratified strata could be a consequence of insufficient supply of sand to build up an expansive array of bed-surface dunes. However, these features almost always overlie an areally extensive graded sandstone (F1.1) suggesting that the availability of cohesionless sand was virtually limitless. Dunes were formed by the tractional reworking of the underlying T_a part of the bed, and represent waning flow conditions and a change from direct suspension deposition (T_a) to bed-load transport. The discontinuous nature of cross-stratified strata is most likely the result of local post depositional erosion associated with the next sedimentation event.

In addition, some high-angle cross-lamination sandstone beds are interpreted to be pseudodunes (Arnott and Al-Mufti, 2017). These cross-stratified features, although superficially similar to the cross-stratification formed by migrating subaqueous dunes, represent the migration of a steep depositional front into an isolated seabed scour. In their model Arnott and Al-Mufti hypothesized that the scours formed by erosion beneath an upflow-migrating zone of flow expansion or the combined erosive effect of downward-directed coherent turbulent flow structures and locally generated turbulence. Nevertheless, irrespective of origin of the scour, once formed the near-bed flow conditions changed from net erosion to net deposition as a length of planar-stratified sandstone at the upflow end of the scour abruptly transitioned into a prograding high-angle cross-stratified set that infilled the scour.

2.3 Facies 3 (F3): Graded, planar-laminated or massive siltstone to massive, structureless mudstone.

2.3.1 Macroscopic Characteristics

Facies 3 (F3) makes up 33% of ICC1 and is composed of very thin- to medium-bedded (0.5 - 10 cm), planar-laminated or massive siltstone overlain sharply by structureless mudstone (Tde turbidites; Figure 2.6A-C). This facies is easily recognized in the field due to its distinctive colour change from light grey (interlaminated very-fine sandstone and siltstone) to dark grey (structureless mudstone cap). Strata comprising F3 commonly stack to form packages up to 20 beds thick or as a single layer that abruptly overlies F1 (2%) or F2 (98%), respectively. Basal contacts are generally sharp and planar.

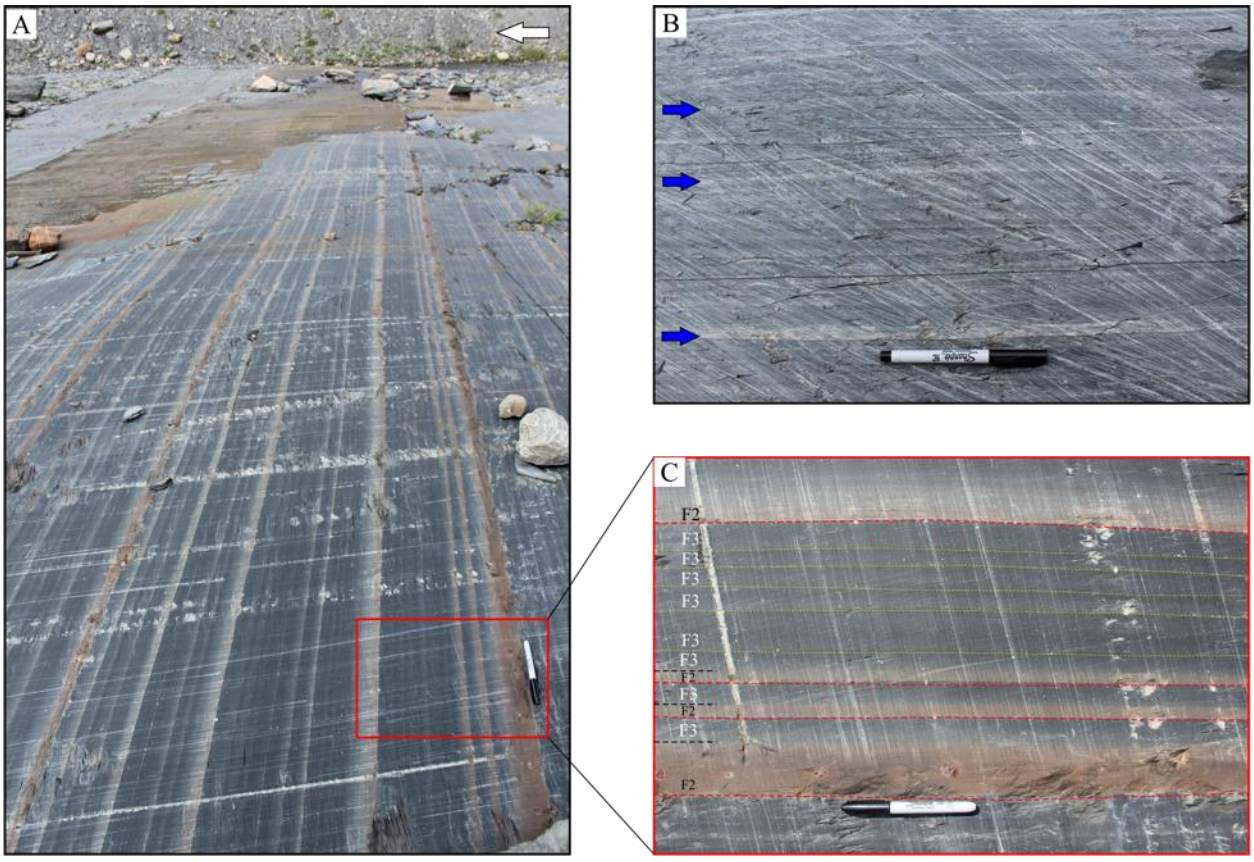

Figure 2. 6. *Representative examples of Facies 3 (F3). (A) Flat-based, thin-bedded, laterally continuous siltstone to mudstone beds intercalated with fine-grained (T_{cde}) sandstone (F2.1). White arrow indicates stratigraphic up. (B) Very thin-bedded siltstone (light grey) to mudstone (dark grey) intercalated with very fine-grained, thin-bedded, cross-laminated sandstone (T_{cde}, indicated by blue arrows). (C) Sharp, planar base (red dashed lines) of an upward-fining and -thinning T_{cde} succession overlain sharply (yellow dashed line) by massive siltstone (light grey) and mudstone (dark grey). Note the progressive upward-thinning of F3 beds and thickening of the mud-rich upper part of each F3 bed.*

2.1.3.2 Microscopic Characteristics

In thin section, F3 strata are composed of 30% grains and 70% recrystallized matrix (muscovite, chlorite porphyroblasts and silt quartz grains), and < 1% carbonate cement. Grains are usually sub-angular to sub-rounded, very fine- to fine-grained quartz. F3 is planar laminated (Td) with a distinctive dark and light banding (Figure 2.7A-C), which then is overlain by a sharp-based, poorly-sorted, structureless mudstone with dispersed silt quartz grains. Light-coloured bands consist of well-sorted, very fine- to fine-grained sand and fine-grained chlorite porphyloblasts dispersed in matrix. Dark laminae contain more recrystallized clay and fewer dispersed very-fine and silt-sized quartz grains compared to the light bands. Stratigraphically upward alternating sand and mudstone laminae progressively fine (decrease in sand:clay ratio) and thin (2 - 5 mm up to 1 mm).

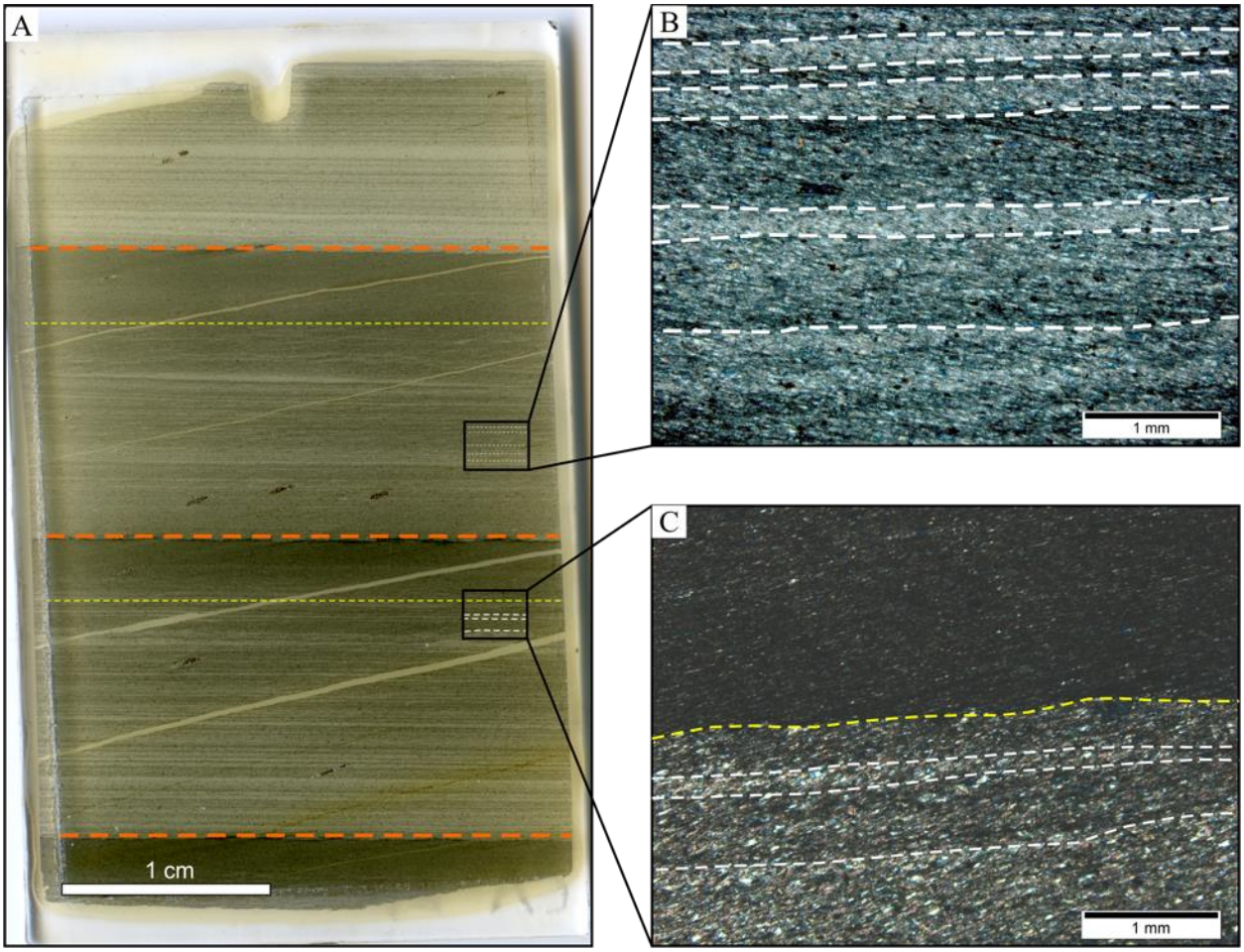

Figure 2. 7. *Photomicrographs of F3. (A) Thin section photo of three sharp based (orange dashed lines) F3 beds. In thin section, strata of F3 exhibit a distinctive alternation of planar laminated sandy mudstone and muddy sandstone (separated by white dotted lines) that collectively fine and thin upward, and are then capped sharply by a structureless mudstone (above yellow dashed lines). (B-C) Photomicrographs of thinly-laminated sandy mudstone and muddy sandstone (indicated in white dashed lines). Note that in figure (C) the planar-laminated unit is sharply capped (yellow dashed line) by a poorly-sorted mudstone with dispersed quartz silt grains.*

2.3.3 Interpretation

Strata of F3 were deposited by fine-grained, low-concentration, low-energy turbidity currents and are interpreted to represent the T_{de} part of a classical (Bouma) turbidite. The T_d division comprises a rhythmic interlamination of plane-parallel very fine-grained sandstone and siltstone. This millimetric interlamination of comparatively coarse- and fine-grained layer has been attributed to alternating hydraulic conditions in the near-bed viscous sublayer of a low-energy

turbidity flow (Stow and Bowen, 1978). In this model, coarse silt settles into the boundary layer as individual grains whereas finer silt and mud settle as flocs. As particles approach the bed increased shear breaks up the flocs but coarse silt grains continue to settle building up a silt lamina on the bed. However with the continued disaggregation of clay aggregates, near-bed clay concentration eventually reaches a threshold whereby clay particles reflocculate and form large aggregates capable of withstanding shear break-up. This then leads to particle gelling and deposition of a clay-aggregate-rich layer that blankets the underlying silt-rich layer (Stow and Bowen, 1978). The mudstone unit that sharply overlies the T_d division is interpreted to be the T_e division formed by pure suspension fallout from the dilute tail of the flow (Lowe, 1982) or by later hemipelagic fallout (Meyer, 2004). Alternatively, the sharp-based, structureless, poorly- to moderately-sorted mudstone cap could represent rapid en masse deposition from a highly-viscous fluid mud layer (McAlly et al., 2007) that formed during the latter part of the sedimentation event.

2.4 Facies 4 (F4): Matrix-supported conglomerate

2.4.1 Macroscopic Characteristics

Facies 4 (F4) makes up < 1% of ICC1 and comprises medium- to thick-bedded (30 - 548 cm) strata with quartz granules and pebbles and mudstone clasts dispersed in a silty mudstone matrix (Figure 2.8A-B). Mudstone clasts are 1 - 5 cm thick and 5 - 10 cm long and typically oriented with their long axis parallel to the base of the bed. Basal contacts are commonly sharp and planar.

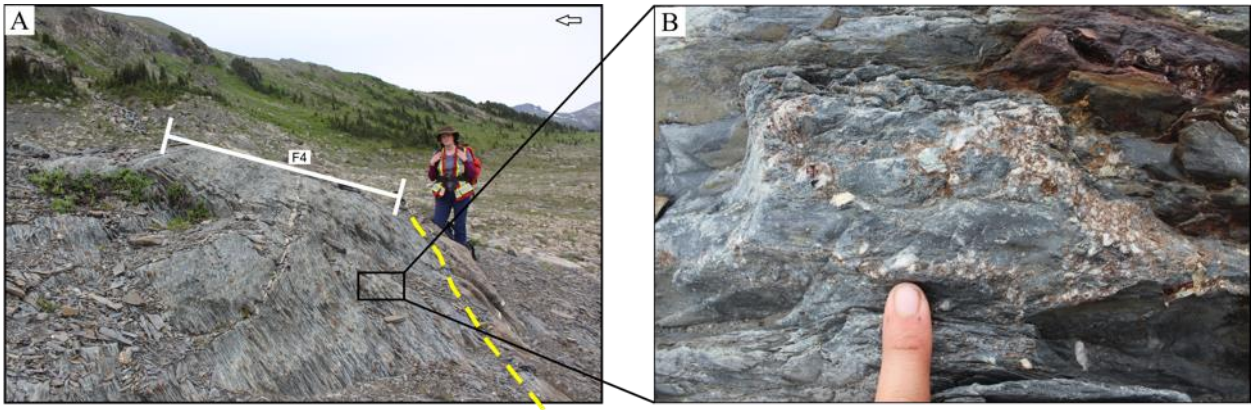

Figure 2. 8. *Representative examples of Facies 4 (F4). (A) Sharp, planar base of a F4 bed overlying a massive T_a sandstone (F1.1); contact indicated by dashed yellow line. White arrow indicates stratigraphic up. (B) Very coarse sand and granule quartz grains dispersed in a silty mudstone matrix.*

2.4.2 Interpretation

Based on the absence of internal stratification and grading, the sharp and irregular nature of the upper and lower contact, and the presence of mudstone clasts and coarse and very coarse sand grains dispersed in a matrix of silt-rich mudstone, strata of Facies 4 are interpreted to have been deposited by cohesive gravity flows, namely debris flows (Mulder and Alexander, 2001). Grains dispersed in the silty mudstone matrix were supported by cohesive strength afforded by the electrostatic surface charge of clay particles, in addition to elevated pore pressure and buoyancy effects provided by the mud matrix (Mulder and Alexander, 2001). Deposition occurred en masse

when basal friction and forces resisting internal shear, mainly the viscosity of the fluid-matrix mixture, equalled or exceeded the downslope gravitation force (Iverson, 1997; Mulder and Alexander, 2001). En masse deposition, in addition to limited internal grain mobility, explains the poorly sorted and chaotic nature of these deposits, which most probably resembles the grain size distribution within the parent flow (Mulder and Alexander, 2001). Also, due to matrix strength during, but also following movement, the thickness of the deposit resembles the thickness of the parent flow (Iverson, 1997).

Chapter 3: Characterization of Stratal Elements in a Deep-Marine, Base-of-Slope, Channel-Levee System, Neoproterozoic Windermere Supergroup, British Columbia.

3.1 Deep- Marine Channels and Levees Overview

Deep-water channels are a major geomorphologic feature on modern continental slopes and are the main conduit for supplying terrigenous detritus by sediment-gravity flows into the deep sea (Mutti and Normark, 1987; Covault et al., 2014). Over the past few decades the sedimentological understanding of deep-water channels has advanced with the acquisition and interpretation of high-resolution 3D seismic data from modern and ancient turbidite systems (e.g. Amazon fan, Mississippi fan, Bengal fan, amongst others) (Figure 3.1A). In addition, outcrop and core studies in the ancient sedimentary record (Figure 3.1B) have provided sub-seismic scale insight into the distribution and stratigraphic make up of stratal elements that populate the deep-marine sedimentary record (Arnott, 2010).

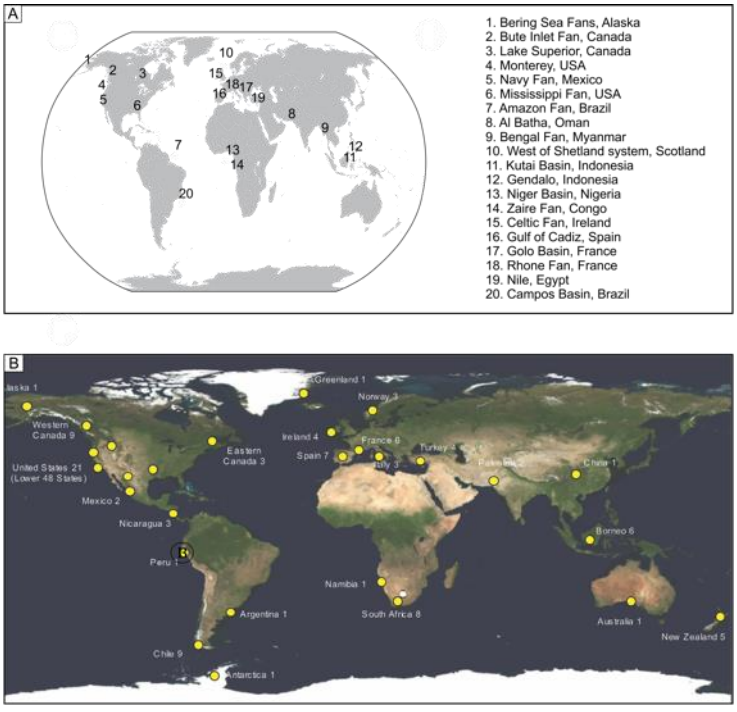

Figure 3. 1. *(A) Distribution of major modern submarine fans (from Pettinga et al., 2018). (B) Location map of ancient deep-water turbidite systems described in the Atlas of Deep-water Outcrops (From Shew et al., 2007).*

3.1.1 Deep-Marine Channels and Their Subaerial Counterparts

In general, deep-marine channels vary from ~ 100 m to more than a few km wide, < 200 m deep and have slopes that range from 0.0001 to 0.02. Fluvial systems, on the other hand, are ~ 200 m wide, are < 20 m deep and have slopes that range from 0.00001 to 0.05, thus making deep-marine channels an order of magnitude wider, deeper and steeper than their subaerial counterparts. This is a consequence of reduced gravity related to buoyancy effects in addition to added friction at the interface between the sediment-laden flow and the overlying ambient water (Konsoer et al., 2013). Nevertheless, despite differences in dimension and inclination, deep-marine channels commonly exhibit a sinuous planform geometry that resembles the pattern of meandering river channels (Figure 3.2). Braided patterns, on the other hand, are rare, and when reported are generally observed in the channel-lobe transition zone (Wynn et al., 2007; Jobe et al., 2016; Foreman et al., 2015).

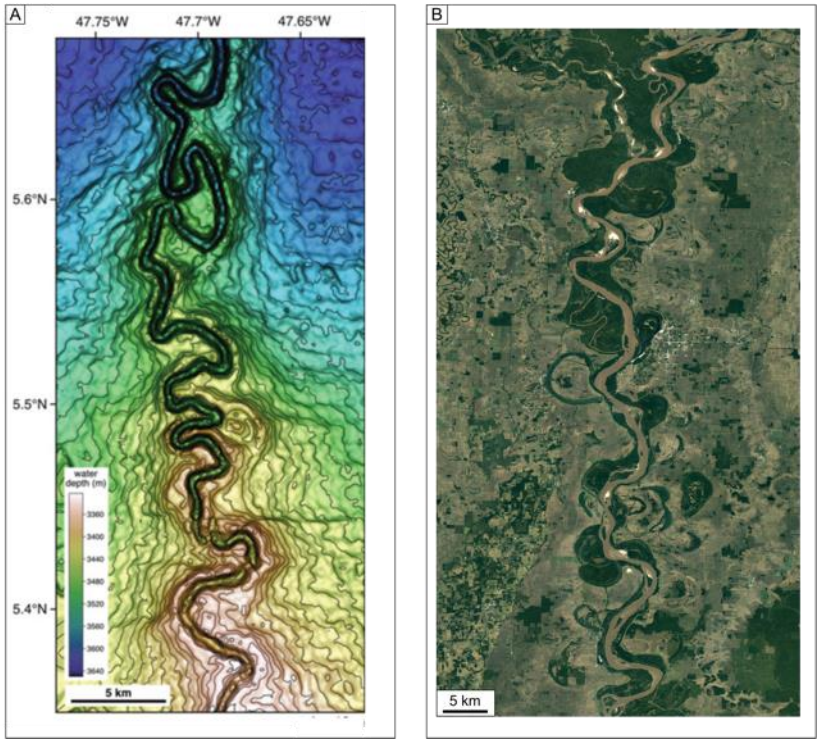

Figure 3. 2. *Similarity in planform geometry of sinuous deep-marine and continental channels. (A) Modern slope channel at 3500 m water depth on the Amazon fan (from Deptuck and Sylvester, 2018). (B) Aerial image of the modern Mississippi River (from Google Earth, 2019).*

The accommodation and depositional architecture of deep-marine channels, like fluvial channels, is governed in part by base level related to an equilibrium profile (Figure 3.3A). In deep-marine channels, base level is determined by gravity base, which represents the furthest point that a turbidity current can flow along a transport pathway (Kneller, 2003). Where base level remains fixed and the channel is at grade, sediment bypasses and deposits farther downslope. Here, channels are constrained to migrate within a plane parallel to the equilibrium profile, analogous to a meander belt in a sinuous fluvial system. Channels show little or no aggradation, which over time builds up a stratigraphy of one or more laterally migrating channel bodies with uncommon lateral accretion deposits (Figure 3.3B; Kneller, 2003; Arnott, 2010). In modern and ancient turbidite systems three types of channels have been identified: erosional, depositional and mixed erosional-depositional (Clark and Pickering, 1996; Mutti and Normark, 1987; Pickering et al., 1995). Erosional channels form where the flow parameters change in a way that causes the channel profile to lie above the graded profile, which then causes erosion of the substrate and reduction of the channel slope (Figure 3.3C). Erosional channels typically exhibit low sinuosity, occur on steep slopes, and are typically associated with frequent channel avulsion (Kneller, 2003; Clark et al., 1992; Clark and Pickering, 1996). In contrast, aggradational/depositional channels have a channel floor bounded on their margins by depositional levees. Levees build up and over time progressively increase channel confinement. Here, the channel profile is below the graded profile (Figure 3.3D) and therefore the channel and associated levees aggrade to steepen the channel profile.

Moreover, it is widely known that fluvial channels commonly exhibit a sinuous platform. The principal depositional unit in these systems is the point bar with its well-known upward-fining succession of lithofacies (Allen, 1964). In seismic images of the sinuous Green Channel Complex

(Lower, Miocene, Offshore Angola), Abreu et al (2003) reported shingled reflections along the margins of channel fills. These reflections paralleled the inner channel bend, dipped at about 5^{o} - 10^{o}, were 40 m thick, 2 km wide, and were termed lateral accretion packages (LAPs). LAPs were interpreted to be point bar deposits and to be formed by the lateral migration of a single channel (Abreu et al., 2003). The term has been applied to a variety of deposits in outcrop where lateral channel accretion and associated lateral accretion deposition have been interpreted (Wynn et al., 2007; Janocko et al., 2013). However, in comparison to the seismic LAPs described by Abreu et al., the dimension of lateral accretion deposits in outcrop are measured in meters to at most several meters wide, and therefore are an order of magnitude smaller. To highlight the dimensional differences Arnott (2007) introduced the term lateral accretion deposits (LADs) to describe the inner-bend deposits of a single laterally accreting channel, and proposed that the term LAP be used for the systematic lateral-offset stacking of discrete channels.

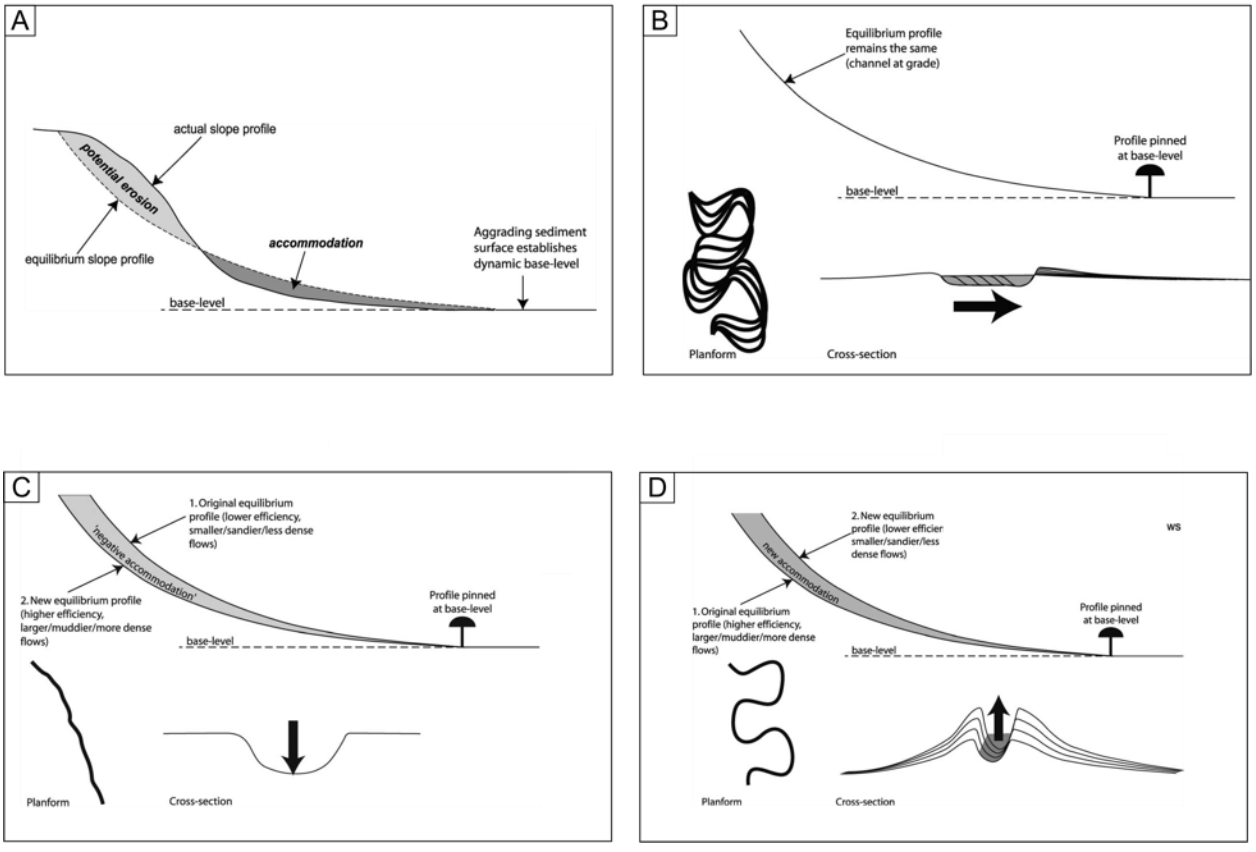

Figure 3. 3. *Adjustment of a channel profile to maintain equilibrium transport conditions. (A) Schematic illustration of equilibrium profile in relation to actual slope profile, such as the floor of the channel or the surface of the slope on which a channel forms (from Samuel et al., 2003). Base level represents gravity base, which is the lowest and generally most distal point that a turbidity current flows along a pathway. Accommodation is the surface to which sediment can theoretically aggrade whereas potential erosion indicates the area of 'negative accommodation'. Additionally, the equilibrium profile dictates where positive and negative accommodation occurs along a channel, which in turn governs the development of the stratal architecture. (B) A channel profile at grade wherein most of the sediment bypasses to areas further downflow and closer to base level (Kneller, 2003). (C) Channel profile above the graded profile results in erosion that flattens the profile (Kneller, 2003). (D) Channel profile that lies below the graded profile aggrades to steepen its profile (Kneller, 2003).*

Nevertheless, despite similarities in planform and other morphological features, the marked differences in the depositional record of deep marine slope channels most probably relates to fundamental differences in the nature of the flows, or more specifically, how sediment is transported. In fluvial systems, sand is commonly transported as bedload and only the finest fraction (mud and finer sand) in suspension, whereas in the deep sea, it is commonly transported in suspension. Furthermore, traction structures like planar- and cross-stratification, which are ubiquitous in fluvial point-bar deposits, are not only comparatively, but also absolutely uncommon in deep-marine point bar deposits. Also, in contrast to subaerial conditions, the small density difference between the flow and surrounding ambient fluid in submarine systems provides buoyancy that enhances superelevation of the flow around bends, resulting in more significant overbank flow (Peakall et al., 2000; Wynn et al., 2007; Khan et al., 2011) and development of levees that are more than an order of magnitude higher and wider than their fluvial counterparts. The lateral tapering of strata away from the channel causes levees to exhibit a distinctive "gull-wing" or wedge-shaped profile on seismic images (Figure 3.4). Additionally, sinuous fluvial channels typically show continuous lateral migration with downflow bend translation and

negligible aggradation. In contrast, deep water channels exhibit more limited lateral migration with significant downflow translation and aggradation (Wynn et al., 2007; Jobe et al., 2016).

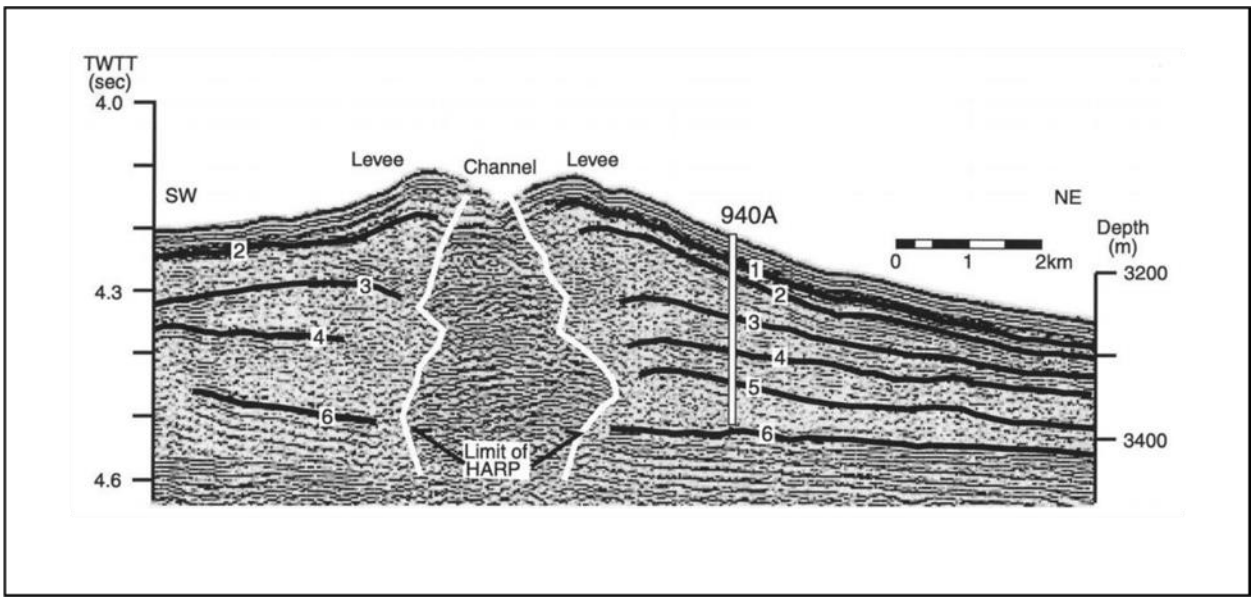

Figure 3. 4. *Seismic profile across a channel-levee complex in the Amazon fan. White lines delineate the margin of the channel. Note how levee deposits on either side of the channel display the characteristic "gull-wing" morphology away from the channel (from Piper and Normark, 2001).*

3.1.2 Channel Evolution and Associated Deposits

Individual submarine channels commonly exhibit a systematic evolution comprising four phases: inception, by-pass, filling and abandonment (Mutti and Normark, 1983; Clark and Pickering, 1996). During inception the channel undergoes net erosion where multiple flows with high transport efficiency scour a sharp-based topographical low that acts as a conduit for flows transporting sediment further basinward (Clark and Pickering, 1996; Arnott, 2010; McHargue et al., 2011). This, then, is followed by channel by-pass where flows neither erode nor deposit sediment except for clast-rich lags and fine-grained laminated mudstone from the tails of incomplete bypassing flows (Clark and Pickering; 1995, McHargue et al., 2011). With time flow efficiency decreases and the channel begins to fill with sediment by a process termed backfilling

(Gardner and Borer, 2000). Channel fills commonly exhibit a systematic succession of lithofacies interpreted to indicate axis to off-axis to margin deposition. Axial strata comprise thick, coarse-grained, amalgamated sandstone (T_a; T_{ab}), whereas channel-margin facies consist of interbedded finer-grained sandstone (T_{bcde}; T_{cde}) and mudstone (T_{de}; T_e) – off-axis strata are intermediate between these two stratal end-members (Clark and Pickering, 1996; Macauley and Hubbard, 2014; McHargue, 2011). Channel abandonment is the final stage of a channel fill, which commonly is associated with an upflow channel avulsion that diverts the channel into a new area of the turbidite system (Posamentier and Kollar, 2003). Channel abandonment is typically characterized by an upward-thinning and -fining sequence comprising fine-grained, thin-bedded turbidites (T_{cde}; T_{de}) that partially or completely fill residual topography (Clark and Pickering, 1996; Peakall et al., 2000; McHargue et al., 2011).

Submarine channels are bounded on their margins by levees formed from overspill, augmented locally by flow stripping (Peakall et al., 2000). During the early stages of channel development, relief between the levee top and channel base is limited and allows the sand-rich basal part of the channelized flows to easily overspill and deposit thick-bedded, coarse-grained, sand-rich strata (T_{abcde} and T_{bcde} turbidite sequence). As the levee aggrades and relief increases, only the upper, more dilute portion of the flow overspills and results in an upward- fining and -thinning succession of thin-bedded, fine-grained turbidites (T_{bcde}; T_{cde}) (Bergen, 2017).

3.1.3 Submarine Channels Stacking Patterns

Deep sea channels commonly exhibit a systematic evolution marked by an early phase of lateral migration of successive channels followed by aggradation with negligible migration (Figure 3.5; Peakall et al.,2000; McHargue et al., 2011; Jobe et al., 2016). McHargue et al. (2011) postulated that channel organization is strongly influenced by the thickness of unfilled channel

element relief at the time of channel abandonment. In their model, early channels have limited relief, and therefore flows are poorly confined. Channels tend to become completely filled mostly with coarse, amalgamated sand-rich strata. With minor compaction, these strata form positive topography that causes younger channels to form in adjacent, topographically lower areas, and ultimately the build-up of a disorganized stacking pattern of amalgamated sand-rich deposits. Additionally, overbank/levee deposits, are poorly preserved because of frequent channel avulsion and erosion by younger channels. In contrast, channels that exhibit greater confinement are typically underfilled. This results in residual negative topography that helps to capture and steer later flows, and ultimately the development of an organized channel stacking pattern. The organized pattern is most commonly reported from the late stage of channel belt evolution and is attributed to flows becoming enriched in mud, therefore less efficient, which then promotes channel and levee aggradation. Similarly, stratigraphic modelling by Sylvester et al. (2011) suggests an initial stage of lateral channel migration with little aggradation that results in numerous crosscutting relationships between individual channels, giving the impression of a relatively disorganized stacking pattern. This is then followed by an aggradational phase and an organized channel thread, and where the change from disorganized to organized is interpreted to be related to a reduction in slope or changes in flow properties caused by delta progradation or changes in relative seal level (Samuel et al., 2003; McHargue et al., 2011).

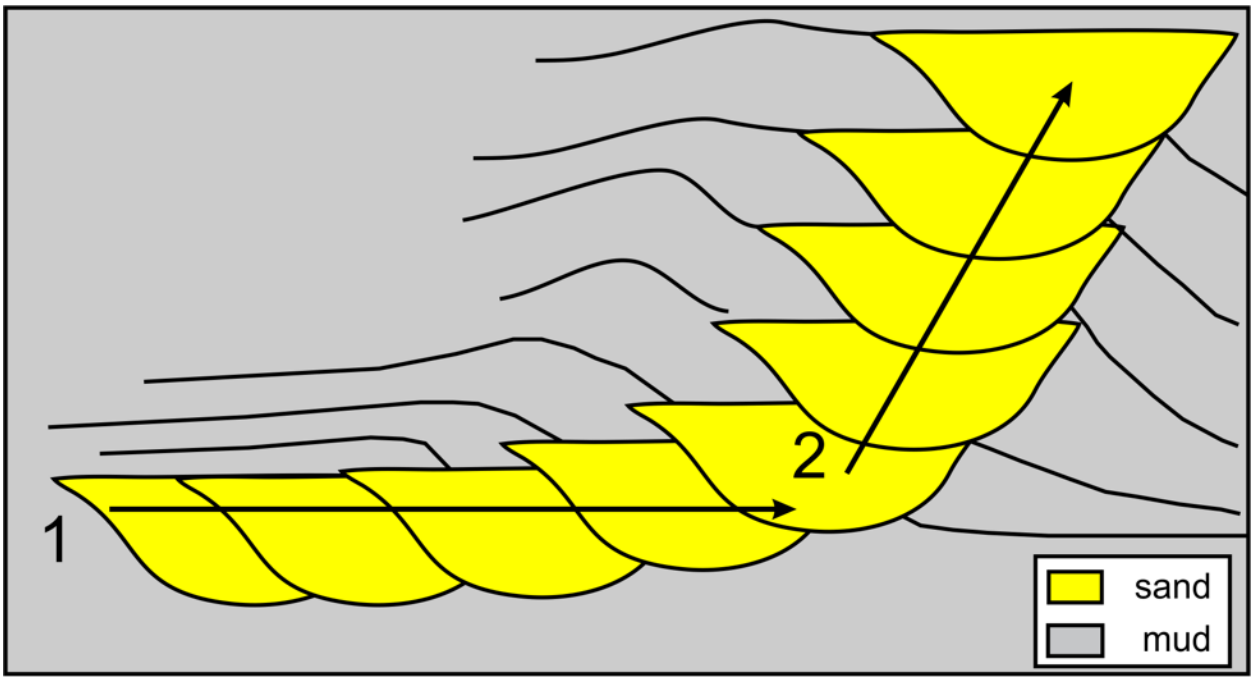

Figure 3. 5. *Submarine channel evolution exhibiting a systematic temporal evolution from (1) lateral migration of successive channels followed by (2) a phase of lateral migration with a significant component of aggradation (from Jobe et al., 2016).*

3.1.4 Classification Scheme

Numerous classification schemes have been proposed to describe the wide range of channelized morphologies observed in deep-marine channel systems (i.e. Clark and Pickering, 1995; Campion et al, 2000; Sprague et al., 2005; McHargue et al., 2011). Here the classification scheme of Navarro (2006) is used to describe the hierarchy of channels that make-up Isaac Channel Complex 1. In this classification a discrete channel fill is defined as sediment deposited in a negative (relief) geomorphic feature through which turbidity currents are at least partly confined and directed downslope (Mutti et al., 2000). Each channel fill is typically less than 10-15 m deep and 100-300 m wide (Figure 1.6A). A channel unit comprises two or more genetically related channel fills (Campion et al., 2000; Sprague et al., 2002). In turn, a channel complex is composed

of two or more channel units exhibiting different stacking patterns. Ultimately, a channel complex set comprises two or more channel complexes, each bounded by a shift of facies or an abandonment surface at its base and top (Figure 1.6B; Abreu et al., 2003).

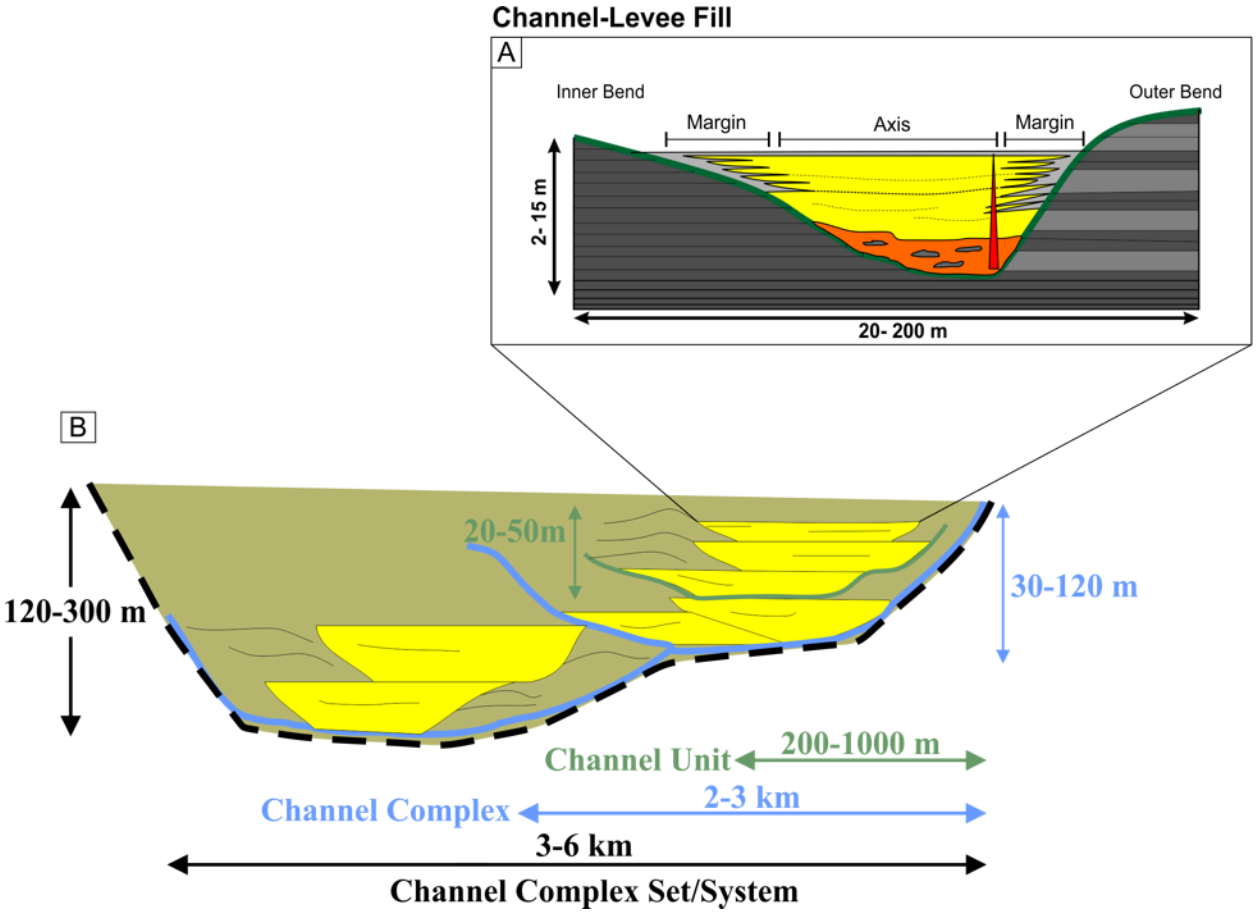

Figure 3. 6. *Channel hierarchy classification of Navarro (2005). This classification is adopted in this study to describe the hierarchical make up of Isaac Channel 1. (a) An individual* ***channel fill*** *consists of a channel-form surface and the sediment that fills it. Axial deposits consist of amalgamated sandstone that become increasingly intercalated with mudstone towards the margins (light grey). Additionally, channel fills fine and thin both vertically and laterally and onlap an incision surface (green) that separates the channel fill from levee deposits. Note that the other bend is steeper than the inner bend levee (redrawn from McHargue et al., 2011). (B)* ***Channel units*** *comprise two or more channel fills, each with a unique stacking pattern but interpreted to be genetically related. In turn, multiple genetically related channel units constitute a* ***channel complex****. Finally, a* ***channel complex set*** *consists of two or more genetically related channel complexes bound on its top by fine-grained abandonment strata or spatially continuous mass transport deposits (i.e. slide/slump or debris flow deposits) (redrawn from Navarro, 2005).*

3.2 Isaac Channel Complex Set 1 Stratal Elements

At Castle Creek, ICC1 is up to 220 m thick and exposed over 5 km along bedding. The study area is divided into four locations, Castle Creek southeast (CC-SE), south (CC-South) and northwest (CC-NW), in addition to the hill section (HS). Identification of stratal elements that make up ICC1 is based on geometry, scale and internal lithological composition – four stratal elements have been identified: channel fill – further subdivided into aggradational and lateral accreting types, channel abandonment elements, levee deposits and debrites (Figure 3.7). Each is described next.

3.2.1 Channel Fill Elements

ICC1 comprises four vertically-stacked channel complexes: lower channel unit (LC) and three upper channel units (UC1-3) (see section 1.4 for hierarchical classification). LC and UC are 30 and 90 m thick, respectively, and separated by a 27 m-thick succession of thin-bedded, fine-grained upper division turbidite deposits in CC-SE (Figure 3.7). LC comprises three channel fills (C1-3), whereas UC1-UC3 consist of multiple channel fills generally filled with amalgamated sandstone. Identifying individual channel fills in the field is difficult and typically based on abrupt increase in grain size and/or presence of mudstone-clast conglomerate. Channel fills are further subdivided into two types: aggradational and lateral accreting.

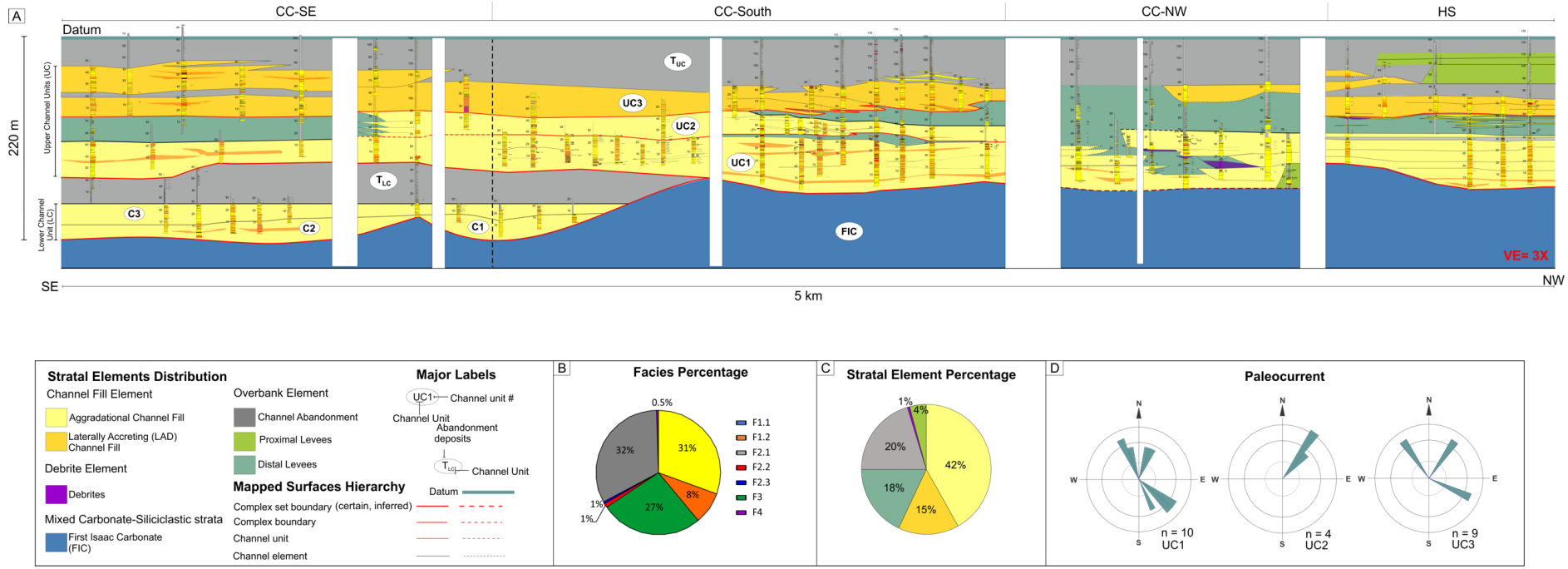

Figure 3. 7. *(A) Architectural panel illustrating the 5 km wide by 220 m thick outcrop belt and the associated stratal elements that make up ICC1. Here, siliciclastic deposits of ICC1 erosively overlie an almost 200 m-thick mixed carbonate-siliciclastic succession informally termed the first Isaac carbonate (FIC). See Appendix A for stratigraphic section location and drone photomosaics. ICC1 is divided into a lower channel unit (LC) and three upper channel units (UC1-3, respectively). Note that the lower channel unit laps out against the FIC, while the upper complex crops out across the entire study area. (B-C) Pie charts illustrate the percent contribution of the various subfacies and stratal elements. (D) Paleocurrent data obtained from ripple cross-laminated sandstone (F2.1) and dune cross-stratified sandstone (F2.3) in the upper channel units.*

3.2.1.1 Aggradational Channel Fill Elements

3.2.1.1.1 Lithological Characteristics

3.2.1.1.1.1 Lower Channel Unit (LC)

The lower channel unit (LC) is confined to the southeast part of the study area (CC-SE) where it is up to 34 m thick and can be traced 1 km parallel to bedding. Siliciclastic strata of LC comprise three channel fills, termed C1 to C3, that onlap a scour at least 30 m deep incised along the top of the thickly developed (~ 250 m) mixed carbonate-siliciclastic stratigraphic marker informally termed the first Isaac carbonate (FIC) (Figure 3.7, 3.8A). Each channel unit overlies a basal scour surface that also is marked by an abrupt increase in grain size, most commonly granule conglomerate with abundant mudstone clasts (F1.2) that can be traced laterally for up to 500 m parallel to bedding. The lowermost channel unit, C1, is 12 m thick with an asymmetrical erosional basal surface that is 250 m wide and incises the top of the FIC. C2 is up to 10 m thick, extends 750 m along strike, and incises both C1 and the FIC. C3 scours C2 and is 15 m thick and exposed for 750 m along strike. In their axis, each channel unit consist mostly of decimetre-thick, amalgamated, pebble and granule conglomerate (F1) with abundant clasts of mudstone and carbonate-cemented mudstone and sandstone (Figure 3.8B). Clast are rounded to semi-angular and oriented with their long axis parallel to the base of the channel. Stratigraphically upwards, clasts become progressively less abundant and sandstone beds generally thin and grade upward to upper medium- to lower coarse-grained sandstone. Along strike coarse-grained strata also show a consistent fining and thinning from coarse, amalgamated sandstone to medium-grained sandstone that become increasingly interbedded with thin- to medium-bedded, upper division turbidites (F2.1 and F3) (Figure 3.8C) that eventually onlap the basal erosional surface. Additionally, strata in the topmost 3 m of C3 become intercalated with fine-grained, upper division turbidites (F2.1 and F3),

which are absent in the upper part of C1 or C2. Sandstone injections are common at the top of C3 and intrude sub-horizontally into the base of a 27 m-thick succession of thin-bedded, fine-grained, T_{cde} and T_{de} turbidites termed T_{LC} (Figure 3.8A)

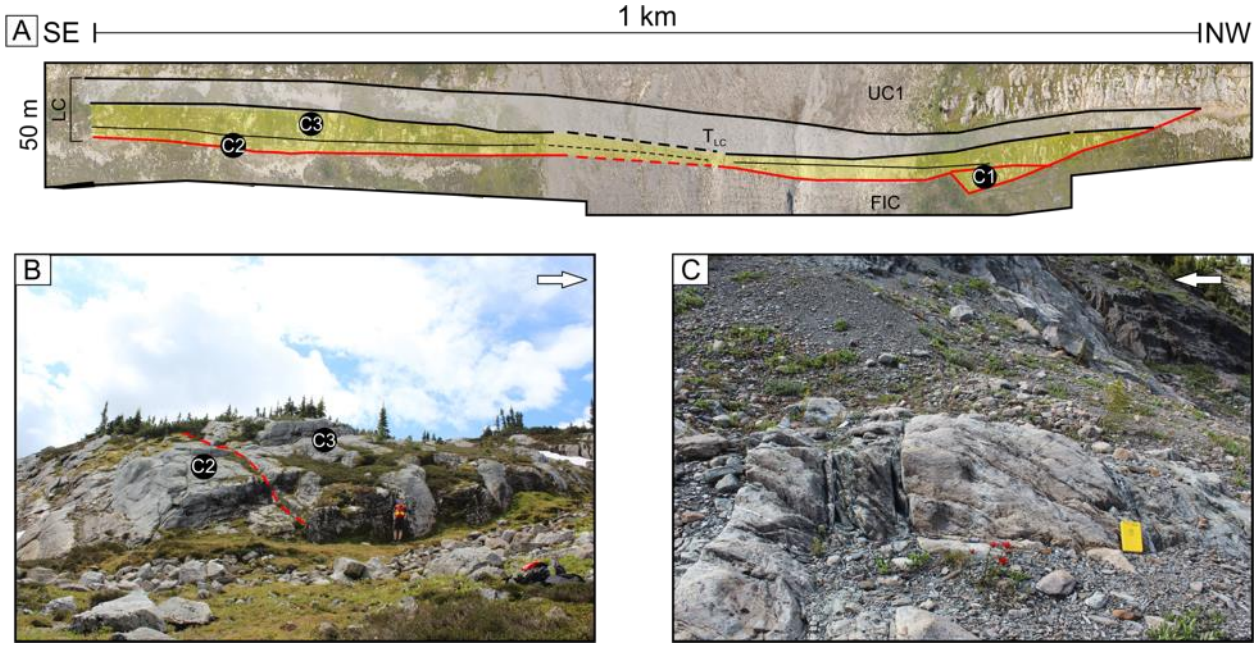

Figure 3. 8. *(A) Interpreted drone image of the Lower Channel Unit (LC) comprising three channel fills (labelled C1-3). Strata of LC are confined to CC-SE where it overlies an erosion surface incised at least 30 m deep into older mixed carbonate-siliciclastic strata (FIC), and in turn is overlain by a thick succession of fine-grained, thin-bedded, upper division (T_{cde} and T_{de}) turbidites (T_{LC}). (B) Axial deposits of channel unit 2 and 3 (C2 and C3, respectively). Here, strata are composed of decimeter-thick beds of amalgamated, very coarse-grained sandstone and conglomerate that progressively fine and thin upward. The red dashed line indicates the base of C3, which in the field is identified by an abrupt increase in grain size. (C) Marginal deposits of C2 consisting of medium-bedded, fine- to medium-grained sandstone intercalated with thin-bedded, fine-grained Tcde turbidites. White arrows in B and C indicate stratigraphic up.*

3.2.1.1.1.2 Upper Channel Unit 1 (UC1)

Upper channel unit 1 (UC1) ranges from 40 - 62 m thick, and is exposed across the entire study area. It sharply overlies T_{LC} in CC-SE and the FIC in CC-South to HS (Figure 3.7). At CC-SE and CC-South, UC1 is made up almost exclusively of amalgamated thick-bedded, granule conglomerate and coarse- to very-coarse grained sandstone (F1) (Figure 3.9A) with negligible upward or along strike change in facies. Strata commonly scour (up to 2 m) underlying sandstone beds in addition to comprising conglomerate with dispersed mudstone and less commonly carbonate-cemented mudstone clasts (F1.2). In CC-South, the topmost 15 m consists of uncharacteristically common (20% of the stratigraphy) medium- to thick-bedded, coarse- to very coarse-grained, dune cross-stratified sandstone and pseudodunes (F2.3). Individual sets are 10 - 40 cm thick and form cosets that are up to 120 cm thick and crop out for a few tens of meter discontinuously along individual stratigraphic horizons. Also, strata pinch and swell along strike and commonly are overlain by thick-bedded, coarse grained sandstone that passively infill the residual topography (Figure 3.9C-D). Additionally, sandstone beds in the topmost 4 m of UC1 fine and thin upward and are capped by up to 10 cm succession of thin-bedded, siltstone and mudstone that extends for up to 20 m along strike.

In CC-NW, UC1 comprises at least four erosionally based channel fills (Figure 3.10A). Channel fills range from 4 to 12 m thick and exhibit a well-defined axis to margin change in facies. Axial deposits comprise amalgamated, thick-bedded, coarse- to very coarse-grained sandstone with local mudstone-clast conglomerate (F1.1 and F1.2) that fine and thin upward to thin- and medium-bedded, fine- to medium-grained T_{abcd} turbidites (Figure 3.10B). Laterally (< 60 m) axial

strata transition from amalgamated, coarse-grained sandstone to medium-bedded, medium-grained, upper division turbidites (F2.1 and F3) (Figure 3.10C).

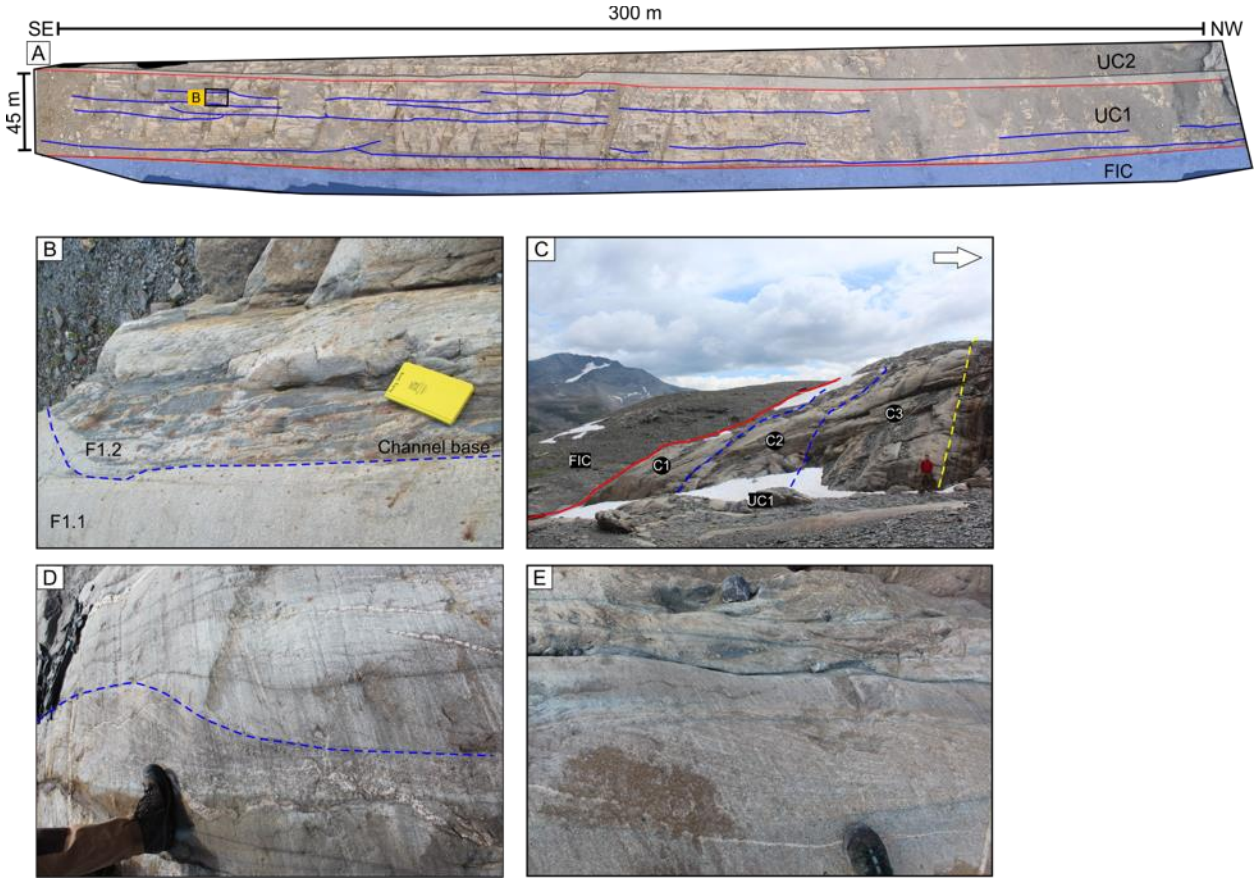

Figure 3. 9. *(A) Interpreted drone photomosaic of UC1 in CC-South. Here, UC1 sharply overlies the FIC and comprises a 45 - 50 m-thick channel unit succession of amalgamated, coarse-grained sandstone, mudstone-clast conglomerate and dune cross-stratified sandstone. Blue lines indicate the base of individual channel fills that commonly are marked by a shallow erosional surface overlain by mudstone-clast conglomerate. (B) Example of a scoured channel base (blue dashed line) overlain by a mudstone-clast conglomerate with a very coarse-grained sandstone matrix (F1.2). (C) UC1 in the HS: similar to UC1 in CC-South, UC1 sharply overlies the FIC and three channel fills are recognized (blue dashed line). Each channel fill comprises coarse-grained, amalgamated sandstone that fine and thin upward but negligibly laterally. (D-E) Examples of dune cross-stratified sandstone. In D note how the overlying coarse-grained, structureless sandstone infills residual topography.*

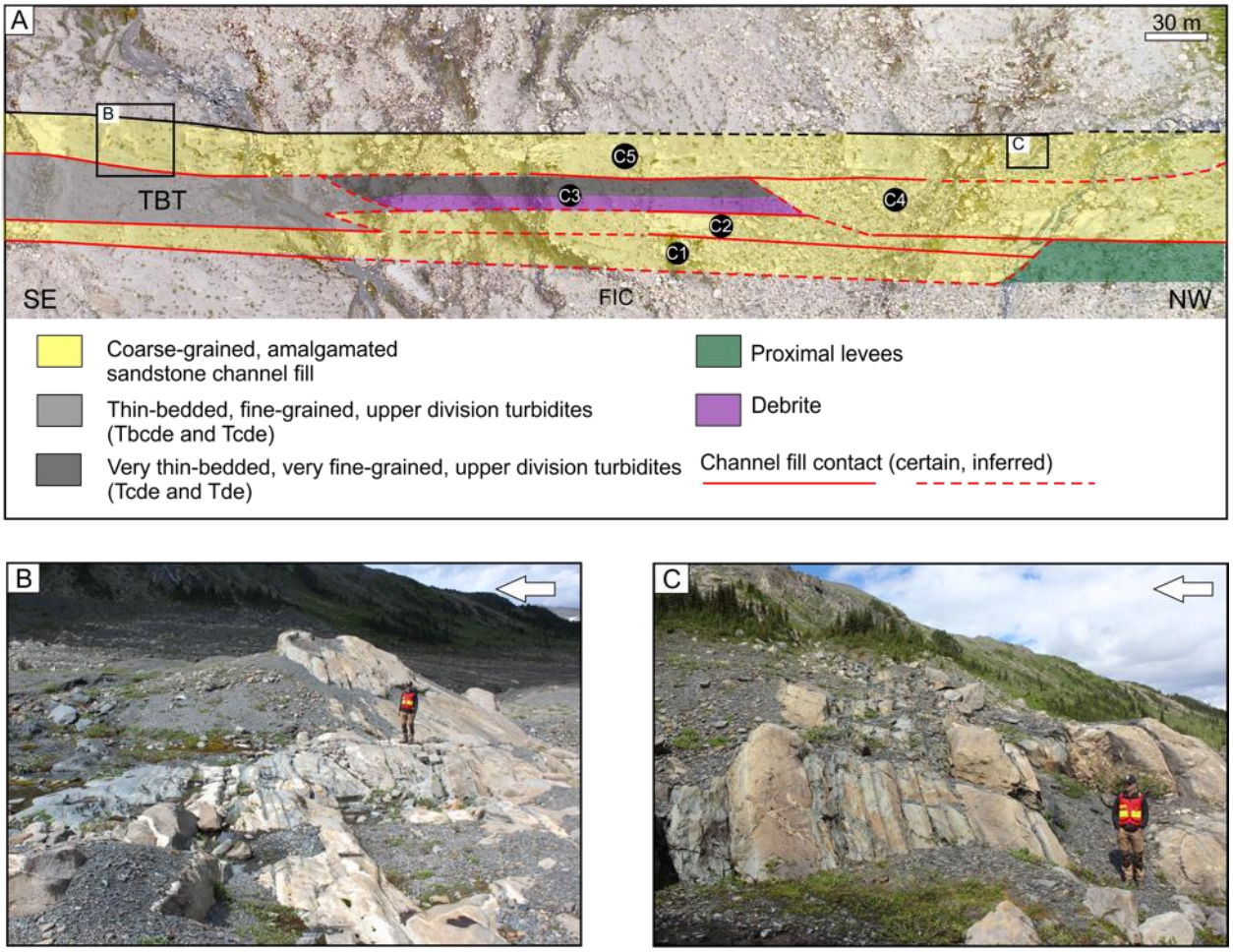

Figure 3. 10. *Example of UC1 channel fills in CC-NW. (A) Interpreted drone photomosaic in CC-NW. Here, UC1 comprises four channel fills (labelled C1-5) with well-defined vertical and lateral fining and thinning trends. Channel fill bases are indicated by red lines (dashed indicates inferred contact); tops indicated by black lines. Note that channel fill 1 erosively onlaps its genetically related levee and directly overlies the FIC. In addition, channel fills C2 and C3 erosively onlap thin-bedded, fine-grained, upper division turbidites (TBT); the former is partially plugged by a debrite (purple polygon) towards its southeast margin. (B) Axial deposits of channel fill C4 (see figure 2.4A for location) comprise thick-bedded, amalgamated, coarse-grained sandstone that fine and thin upwards to medium-bedded, fine- to medium-grained, upper-division turbidites. (C) Marginal deposits of channel fill C4. Thick-bedded, coarse-grained sandstone (T_a) intercalated with medium-bedded, fine-grained T_{bcd} turbidite.*

3.2.1.1.1.3 Upper Channel Unit 2 (UC2)

UC2, is up to 25 m thick, and crops out for 1.5 km between CC-SE and CC-South (Figure 3.7). UC2 comprises at least four stacked channel fills, each overlying a basal erosional surface that scours (up to 1 m) underlying stratigraphy (Figure 3.11). Additionally, coarse-grained sediment at the base of channel fills inject locally into adjacent fine-grained deposits. The channel fills are composed of thick-bedded, coarse- to very coarse-grained sandstone that fine and thin upward. Along strike from the amalgamated channel axis, beds become less amalgamated and interstratified with traction-structured sandstone (F2.1). The top 10 - 50 cm of most channel fills comprises a distinctive grey-coloured, medium-bedded, fine-grained T_{bde} turbidite succession that appears to infill residual topography. These finer-grained strata are laterally discontinuous (< 100 m) where truncated by younger channels. UC2 is overlain by a 12 - 15 m-thick succession of thin- to medium-bedded, upper division turbidites that fine and thin upward (F2.1) and thicken laterally to the northwest, but then are thinned and then completely eroded by UC3 towards the southeast (Figure 3.7).

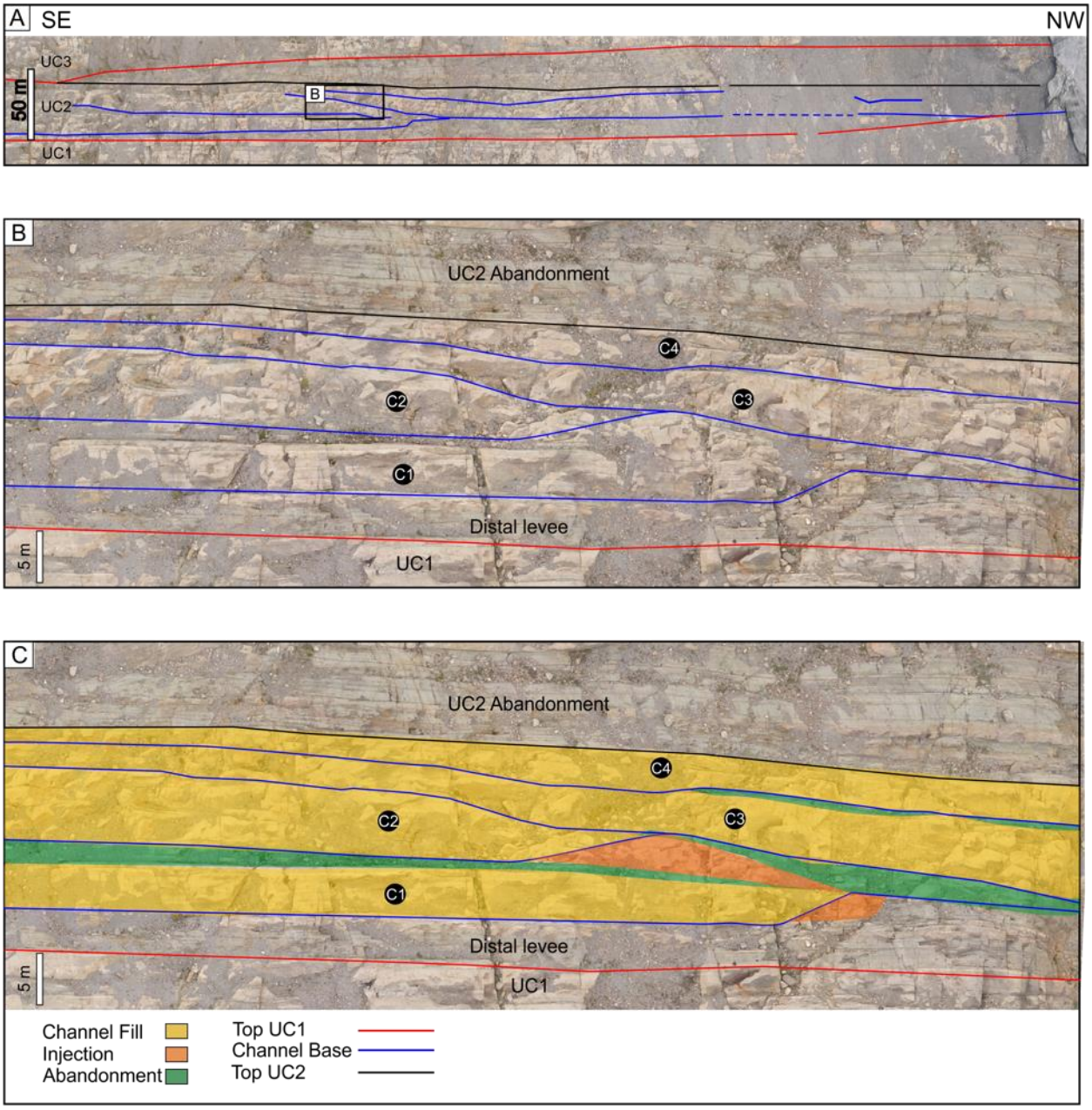

Figure 3. 11. *(A-C) Interpreted drone photomosaics of UC2 in CC-South. Each channel base (blue line) is identified by an abrupt increase in grain size or by a laterally continuous layer of mudstone intraclasts. Channel fills (yellow polygon) comprise decimeter-thick beds of coarse-grained, amalgamated sandstone that fine and thin upward, which in the case of channel 1 and 3 are abruptly overlain by medium-bedded, fine-grained, planar-laminated sandstone with a distinctive green colour in the field (green polygon) indicating elevated chlorite content (which originally were most probably clay minerals). The lateral continuity of these finer-grained beds is < 50 m due to erosion at the base of younger channel fills. Additionally, the base of some channel fills exhibits coarse-grained sandstone injections that have intruded adjacent or underlying fine-grained strata (orange polygons).*

3.2.1.1.2 Microscopic Characteristics

Point counting analysis of thick-bedded, coarse-grained structureless sandstone channel fills of the LC, UC1 and UC2 exhibit a similar mineralogical composition and framework grain size distribution (Figure 3.12A-C). Coarse-grained strata typically comprise 76 - 85% framework grains dominated by quartz with undulose extinctions (91 - 97%). Other sand-size or coarser components include feldspar (1 - 7%), mudstone clasts (<1%) and euhedral pyrite (<1%). Moreover, carbonate cement ranges from 3 - 12% and matrix content, which comprises quartz silt grains and recrystallized clay minerals (i.e. muscovite and chlorite), makes up ~ 9 - 20%. Distinctively, LC is coarser grained than UC1 and UC2 with a modal grain size of 1.32 mm (very coarse sand), median grain size of 0.93 mm (coarse sand) and a mean of 1.60 mm (very coarse sand). In comparison, UC1 has a modal grain size of 1.15 mm (very coarse sand), a median of 0.90 mm (coarse sand) and a mean of 1.25 mm (very coarse sand). Lastly, UC2 has a mode of 1.18 mm (very coarse sand), a median of 0.88 mm (coarse sand) and a mean of 1.13 mm (very coarse sand). The standard deviation (SD) for LC, UC1 and UC2 are, respectively, 1.59, 1.48 and 1.30, suggesting that strata are poorly sorted. Skewness for LC, UC1 and UC2 are 0.1, 0.16 and 0.26, respectively, indicating a progressive change from near symmetrical (LC) to increasingly more positively skewed (i.e. enrichment in coarse sediment) grain size distribution in UC1 to UC2. In addition, kurtosis for LC, UC1 and UC2 are 0.9, 1.02 and 1.06, respectively, and suggests an abundance of particles in the tails of the grain size distribution.

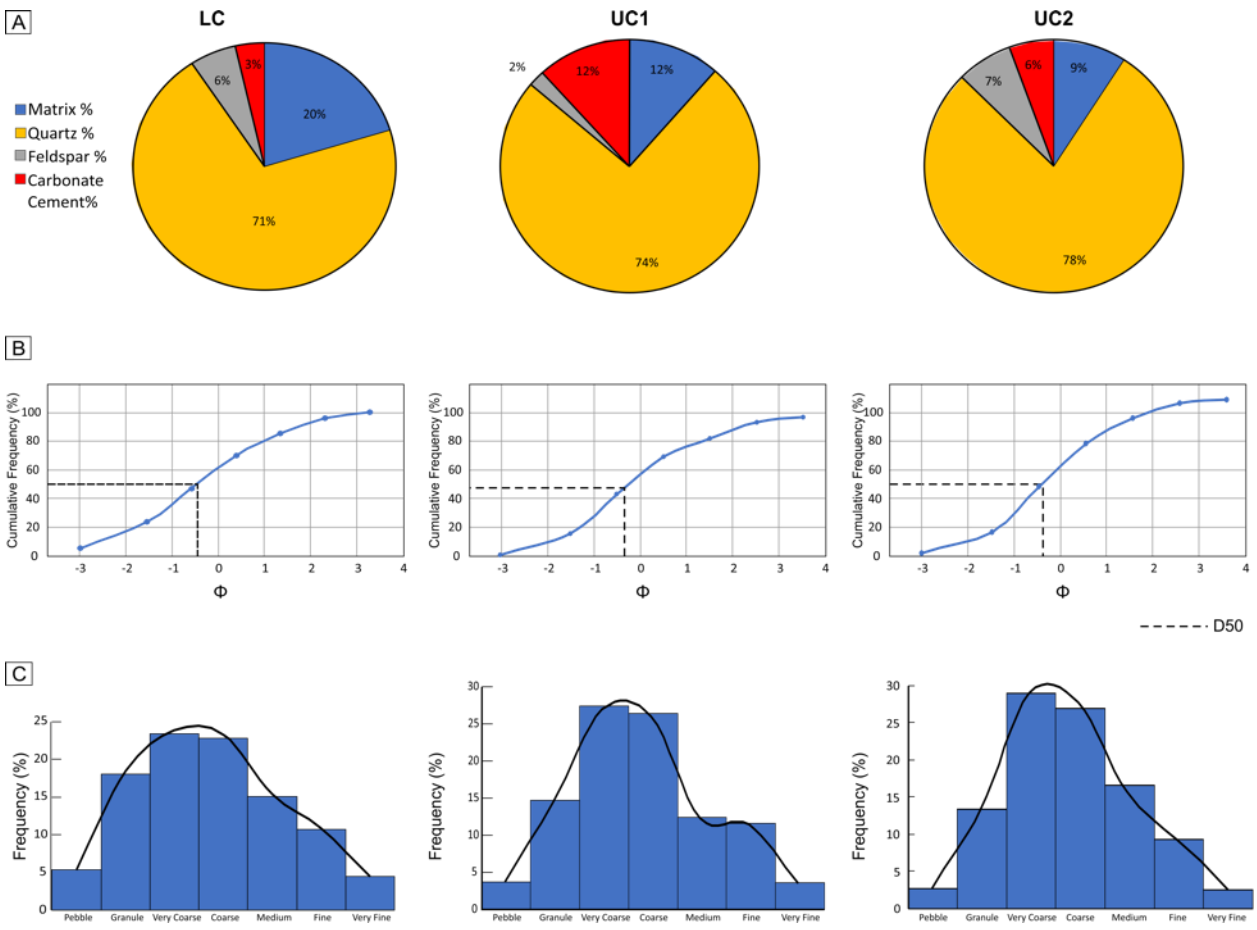

Figure 3. 12. *Grain size distribution in three thick-bedded, coarse-grained, structureless sandstones from aggradational channel units. (A) Pie graphs showing the mineralogy of constituent components. (B) Cumulative frequency curve. Note that grain size is presented in phi values, which from left to right, changes from pebble (-3) to very fine sand (+3). (C) Histograms of framework grain size. Note the polydisperse grain size distribution for all aggradational channels. Also, LC is generally coarser than UC1 and UC2, and UC2 is the best sorted.*

3.2.1.1.3 Aggradational Channel Fill Interpretation

The irregular, erosive basal contact of channel fills of the LC, UC1 and UC2 represent incision by high-energy, high-concentration, sand-rich turbidity currents (Lowe, 1982). Following an initial period of bypass, an amalgamated succession of massive, thick- to very thick-bedded, coarse-grained sandstone to pebble conglomerate with abundant mudstone intraclasts and less common carbonate-cemented mudstone clasts was deposited in the axis of each channel fill. With

time the magnitude of the transiting flow decreased, which is manifest by an upward fining and thinning and deposition of more complete classical turbidites in the uppermost 1-3 m of individual channel fills. In addition to thinning- and fining-upward, channel fills also thin and fine laterally (spatially) over < 100 m from amalgamated T_a sandstone to beds with increasingly more common traction sedimentary structures in their upper part (F2.1) and also interbeds of finer-grained, upper division turbidites (F3).

Strata of aggradational channels exhibit a poorly-sorted grain assemblage with sizes ranging from pebble to mudstone. Such a broad range of grain size would have had a significant effect on the vertical distribution of grains within the sediment transporting turbidity currents, and as a consequence their density profile. Specifically, differences in the settling velocity of the coarse- and fine-grained sediment fractions would have caused the flow to become highly vertically density stratified (Figure 3.13), with coarse-grained sediment being suspended close to the bed overlain progressively, but most probably rapidly, by finer-grained sediment. The high-density core of these density-stratified flows was most likely confined to the deep, axial part of the channel and became progressively more dilute laterally (i.e. toward the channel margins) (Dorrell et al. 2014). Also, stratified flows experience intense interfacial mixing with the surrounding ambient fluid in addition to significant turbulence dissipation related to near-bed sediment concentration and stratification effects (Arnott et al. in review; Tilston 2015; Tilston et al. in review). Collectively these effects caused the current to exceed transport capacity, and as a consequence experience high rates of sediment deposition beneath rapidly collapsing turbulent suspensions (Middleton and Hampton, 1973; Arnott and Hand, 1989). In the channel axis these conditions deposited amalgamated, coarse-grained sandstone and progressively finer, thinner strata toward the channel margin.

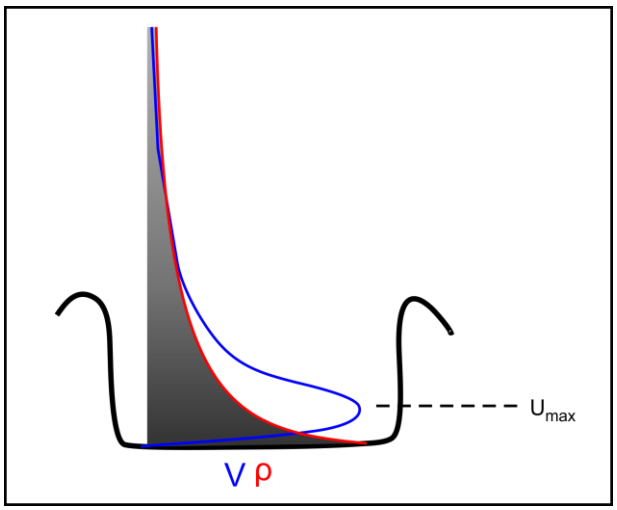

Figure 3. 13*.Cartoon illustrating the velocity (blue) and density (red) profile through a highly-stratified sediment-gravity flow. The grey scale is a qualitative measure of the vertical sediment concentration, which decreases continuously but near the bed rapidly upwards.*

3.2.1.2 Lateral Accreting Channel Fill Elements

3.2.1.2.1 Lithological Characteristics

3.2.1.2.1.2 Upper Channel Unit 3

UC3 is the uppermost channel unit in ICC1 and crops out along the entire length of the study area. In CC-south, UC3 is 30 m thick and consists of at least six channel fills (Figure 3.14A) that show a distinctive lateral-offset-stacking pattern. The channel base is horizontal but the lateral margin on one side of the channel dips at about 8 - 12^{o} to the channel base whereas the other side (northwest) is high angle and erosively scours thin-bedded, fine-grained turbidites (Figure 3.7). Additionally, at the base of some channel fills coarse sediment has been injected into adjacent fine-grained deposits (Figure 3.14B). Individual channel fills are 8 - 12 m thick and filled with thick- to very thick-bedded, coarse- and very coarse-grained sandstone, granule and rare pebble conglomerate and uncommon mudstone-clast conglomerate (F1). Additionally, sandstone beds contain dispersed red-colored sandstone clasts that are cemented with a pervasive ferroan calcite cement. Distinctively channel fills show negligible upward or lateral change in grain size or bed thickness (Figure 3.14C). Characteristically, channel fills thin and then pinch-out obliquely upward where they interfinger with thin-bedded, fine-grained, upper division turbidities (Tcde)

(Figure 3.7). Also, evidence of traction transport (dune cross-stratification or planar lamination) occurs in the upper part near the updip pinchout. The uppermost channel fill in CC-South and CC-SE consists of sharp-based, graded, upper very coarse- to very coarse-grained sandstone with dispersed granules (F1.1) that change little in grain size stratigraphically upward but beds become thinner and interbedded with thin-bedded, fine-grained T_{cde} turbidites (F2.1). In the HS, UC3 consists of two stacked, erosionally-based channel fills. The lower channel fill is 8 m thick but then thins and along strike pinches out abruptly towards the northwest. These strata are then sharply overlain by very thin-bedded, T_{de} turbidite (F3) that conversely thicken from 3 to 10 m toward the northwest. The lower channel fill is then deeply incised (~ 5m) by the upper channel fill, which consists of amalgamated, thick-bedded, coarse-grained sandstone (F1.1) that fines and thins negligibly upward. Both the lower and upper channel fills are interpreted to terminate abruptly against genetically related levee deposits along their northwest margin. Across the entire study area UC3 is overlain by an up to 20 m-thick succession of thin-bedded, fine-grained, T_{cde} and T_{de} turbidites (F2.1 and F3), termed T_{UC} (Figure 3.7).

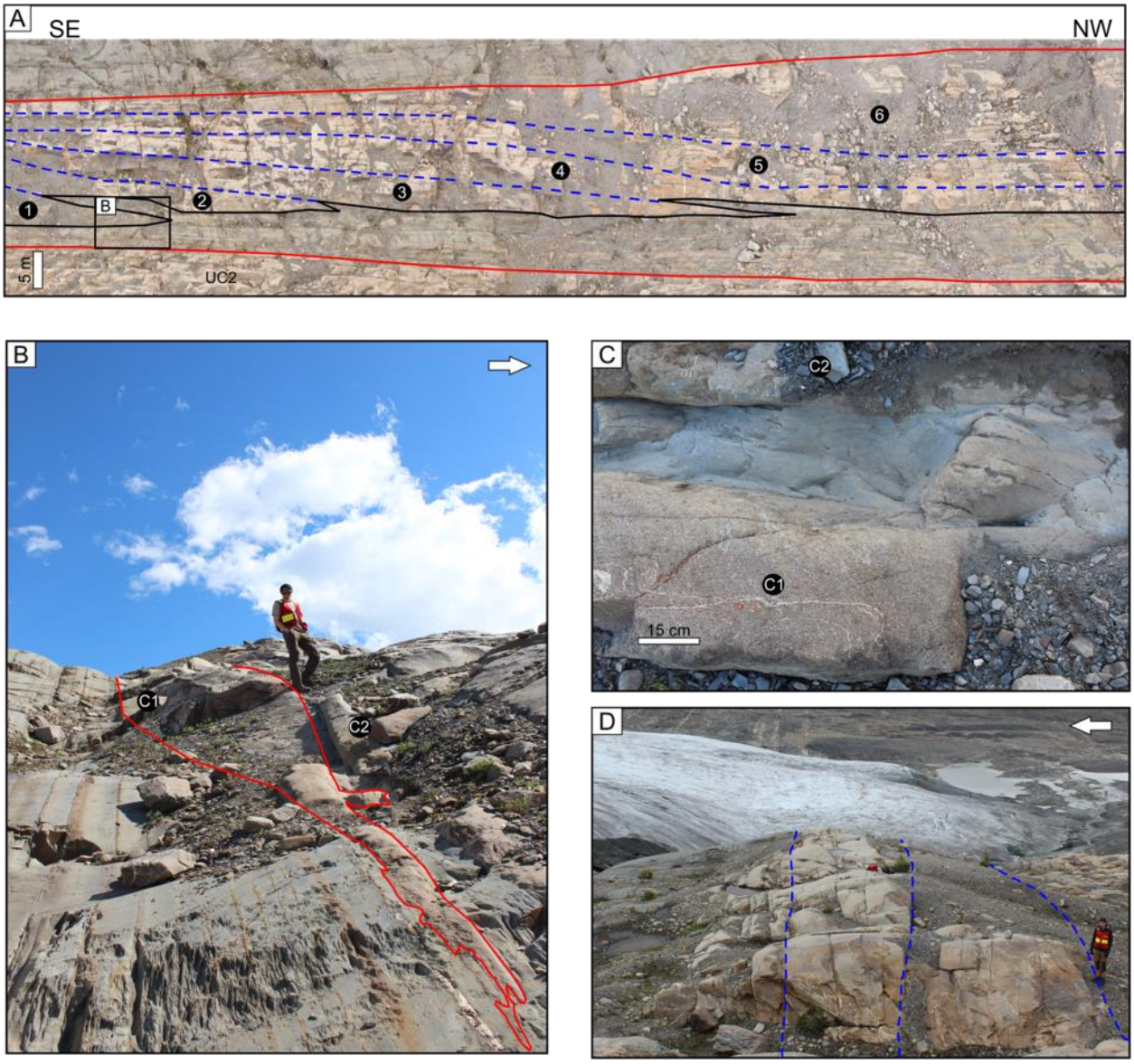

Figure 3. 14. *(A) Interpreted drone photomosaic of UC3 in CC-South. UC3 comprises six laterally accreting channel elements (C1-6) that are up to 12 m thick and filled with coarse- to very-coarse grained sandstone and conglomerate that show negligible upward or along strike change in grain size or bed thickness. Note the lateral offset stacking pattern of successive channel elements and the horizontal (black line) to oblique-upward (dashed blue line) nature of the base of each channel element; regional bedding indicated by the red lines. The locally serrated nature of the basal contact is the result of coarse channel fill sediment has been injected into adjacent fine-grained strata. (B-C) Close-up of a coarse-grained sandstone injection at the base of two channel fills (red lines in B) into adjacent thin-bedded, fine-grained,* T_{cde} *turbidites. Dashed red line indicates the amalgamated contact between the channel fills. (D) Example of thick-bedded, coarse-grained channel fills of UC3. The base of each channel (dashed blue line) is marked by a mudstone-clast conglomerate. White arrows indicate stratigraphic up.*

3.2.1.2.2 Microscopic Characteristics

Thick-bedded, coarse-grained, structureless sandstone of UC3 exhibit a similar mineralogical composition and framework grain size distribution (Figure 3.15A-C). Strata are composed of 58 - 79% framework grains that are dominantly quartz (58 - 76%) and minor feldspar (0 - 4%). Matrix, which consists of quartz silt and recrystallized clay minerals (i.e. muscovite and chlorite) makes up about 11 - 23% of the stratal volume. Intergranular carbonate cement ranges from 10 - 19%. The combined modal, median and mean grain size for UC3 strata are, respectively, 0.71 mm (coarse sand), 0.64 mm (coarse sand), and 0.70 mm (coarse sand). In addition, standard deviation (SD) is 1.02 (moderately sorted); skewness is 0.57 (very coarse sediment enriched) and kurtosis is 1.15, indicative of a leptokurtic grain size distribution (i.e. a deficiency of grains in the tails of the distribution, or similarly, the preferential clustering of grain sizes in the central part of the distribution).

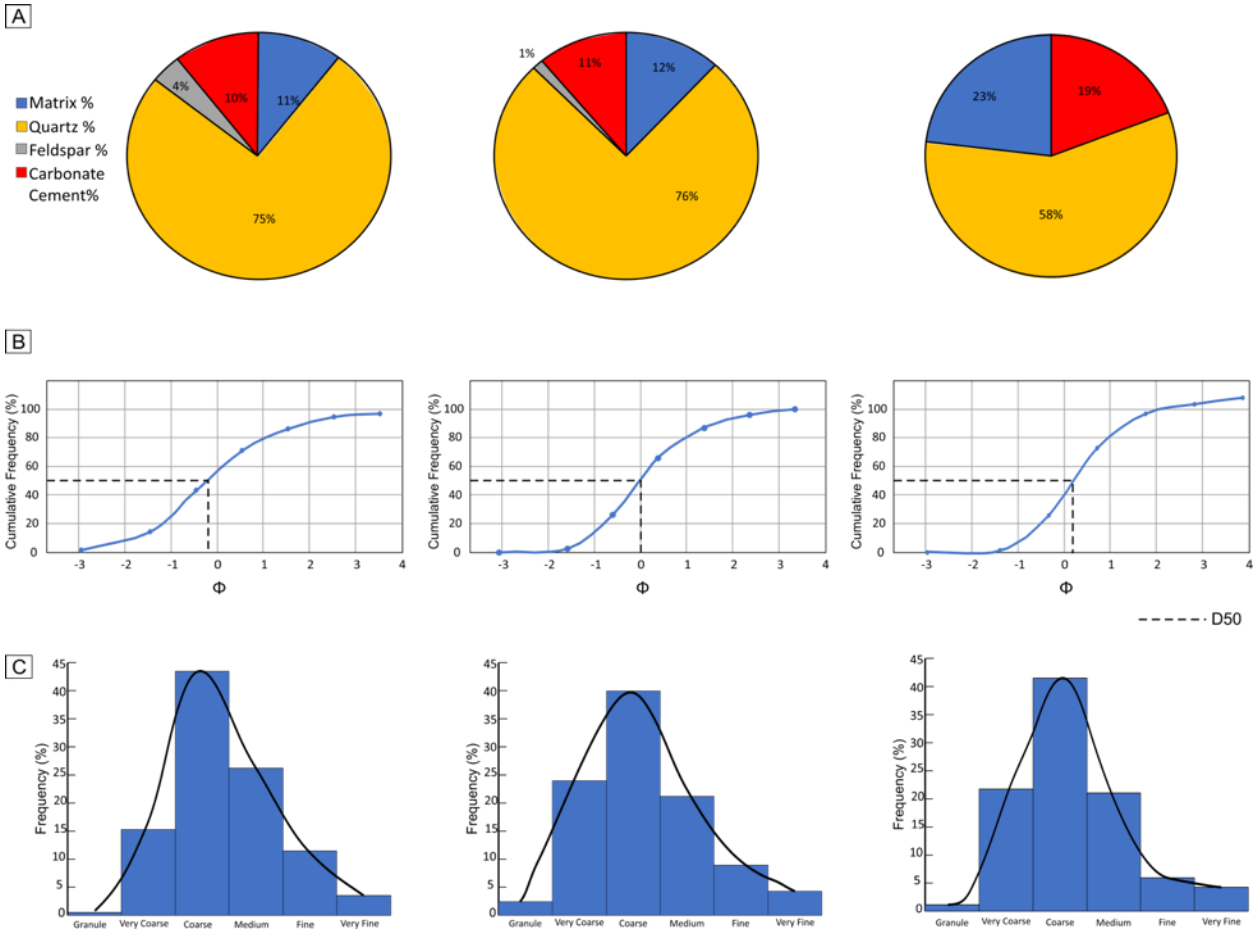

Figure 3. 15. *Grain size analysis of three thick-bedded, coarse-grained, structureless sandstones from laterally accreting channel fills. (A) Pie graphs showing the mineralogical composition of constituent components. (B) Cumulative frequency curve. Note that grain size is presented in phi values, which from left to right, changes from pebble (-3) to very fine sand (+3). Also, note the progressive decrease in D50 (median) and also improvement in sorting (steepening of the curve) stratigraphically-upward (from left to right). C) Histograms showing the narrow range of grain size that centres on coarse sand. Note the progressive left to right narrowing of the central part of the grain size distribution indicating improved sorting stratigraphically upward.*

3.2.1.2.3 Lateral Accreting Channel Fills Interpretation

The inclined character of strata in some of the channel fills, especially those in CC-South, are interpreted to be the result of deposition on the inclined inner bend of a laterally migrating sinuous deep-marine channel. Importantly, not all strata in these channel unit are inclined, which is interpreted to be the result of differences in the position along the exposed sinuous channel, or differences in the orientation of the channel as it intersects the outcrop face (Figure 3.16). For example, the channel axis in channel fills in CC-South are interpreted to be oriented perpendicular to the outcrop surface (Figure 3.16B), whereas channel fill axes in CC-SE, CC-NW and HS parallel the outcrop surface (Figure 3.16C). In CC-South, the base of UC3, is both erosive and also contains several 'steps' and 'terraces' that are interpreted to have formed by the upward and then lateral shift of the succeeding channel fill. In this context, these basal surfaces are not interpreted to represent a single master cut that subsequently was filled, but rather a composite surface resulting from the continuous lateral migration of individual channels superimposed on the aggradation and successive lateral offset stacking of successive channels and their fills (Sylvester et al., 2011).

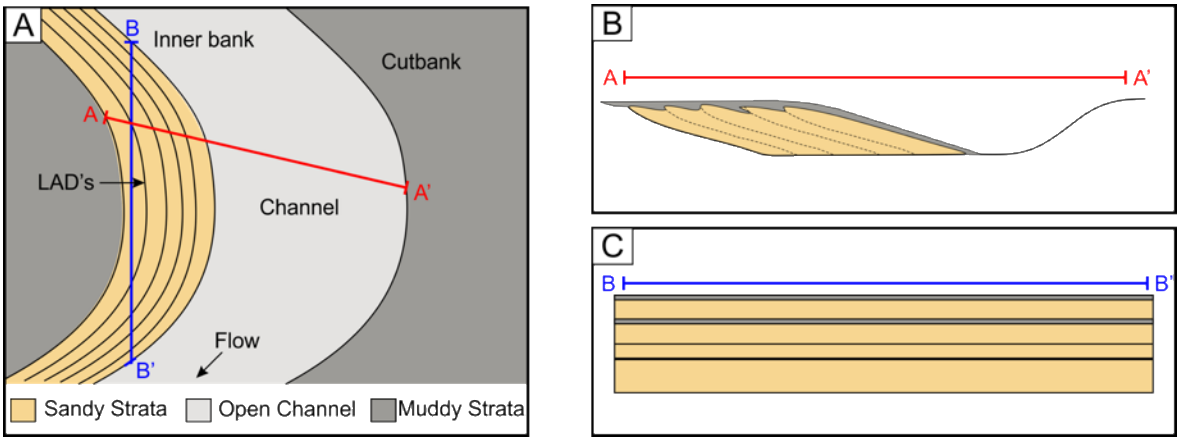

Figure 3. 16. *(A) Cartoon illustrating differences in the character of laterally-accreted strata as a function of the orientation of the exposed outcrop surface versus the orientation of the inner bend of the channel. (B) Strata oriented at a high angle to the trend of the channel exhibit well-developed LADs whereas those oriented parallel to the channel (C) are more or less horizontal (redrawn from Dumouchel, 2015).*

Most notably, UC3 is composed predominantly of coarse and very coarse sandstone that show little to no upward or lateral fining or thinning, and therefore contrasts the polydisperse make up and well-developed upward and lateral fining and thinning trends of aggradational channel fills. This suggests a sediment supply anomalously enriched in coarse-grained sediment, suggesting that these flows, although coarse grained, were better sorted than those that formed and filled aggradational channels (Dumouchel, 2015). More importantly, better sorting would have caused the flows to be less density-stratified and therefore more likely to consist of a ~ uniformly dense coarse-grained basal layer (plug-like) overlain abruptly by a much finer-grained suspension (Tilston et al., 2015; Figure 3.17A). Because of the steepness of the density gradient across the interface, turbulence production would have been suppressed, and as a consequence the extent of energy-consuming vertical mixing (Arnott et al. in review; Tilston et al., 2015). The uniform distribution of coarse sediment would have enhanced hindered settling effects, which in turn inhibited grain settling and promoted flow mobility. More importantly, it resulted in a more or less uniform density profile, which closely resembles the plug-like density profile observed in open channel flows like rivers (Figure 3.17B). Accordingly, in laterally-accreting deep-marine channels, like in rivers, as flows round a channel bend, centrifugal forces results in the upper part of the basal layer to be diverted towards the outer bank, thereby enhancing channel bank erosion. Additionally, owing to the coarse-grained make-up and the inability to lift particles, sediment in the lower part of the flow would follow the channel centerline rather than pile up on the inner bend, which ultimately formed a near-bed secondary flow component that is oriented towards and up the inner

bend surface of a sinuous channel bend, and ultimately, depositional patterns that resemble those observed in rivers (Arnott et al. in review).

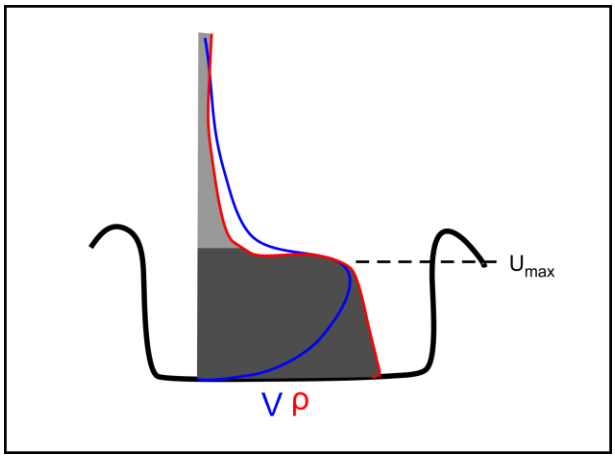

Figure 3. 17. *Cartoon illustrating the velocity (blue) and density (red) profile through a poorly-stratified sediment gravity flow. Here, a plug-like density profile changes little upward but then decreases sharply (indicated by the grey scale). The sharp density gradient at the top of the plug would suppress turbulence production and diminish the strength of the energy-consuming mixing layer.*

3.2.2 Overbank Elements

3.2.2.1 Abandonment Element

3.2.2.1.1 Lithological Characteristics

At the channel fill scale these strata associated with abandonment element are 10 - 30 cm thick, laterally discontinuous (< 50 m) and commonly truncated or completely eroded by an overlying channel fill. These strata comprise very thin- to thin-bedded, fine-grained, upper division turbidites (F2.1 and F3) that fine and thin stratigraphically-upward (Figure 3.18A). However, UC2 channel fills are sharply overlain by thinner, finer-grained T_{bde} turbidites that show no upward fining or thinning and are distinctively grey-coloured due to high chlorite content. At the channel unit scale these strata are 8 - 12 m thick, extend for 300 - 700 m along strike, and gradationally overlie the uppermost channel fill. Strata are composed of fine- to medium-grained, thin- to medium-bedded T_{bcde} turbidites that fine and thin upward into fine-grained, thin-bedded T_{cde} turbidites that drape the topography at the top of individual channel units (Figure 3.18B).

Moreover, abandonment elements are most thickly developed at the top of the lower channel unit (T_{LC}) and at the top of UC3 (T_{UC}), and are 27 and 20 m thick, respectively. Abandonment strata that overlie the lower channel unit (LC) and upper most channel unit (UC3), fine and thin upward with the lower half made up of medium-bedded, fine-grained, T_{bcd} turbidites interbedded with thin-bedded, fine-grained T_{cde} turbidites. Stratigraphically upward, strata consist of T_{cde} turbidites that fine and thin and become increasingly intercalated with T_{de} turbidites. The T_c division is typically less than 2 cm thick and comprises single set ripples and starved ripples that pinch and swell along strike (Figure 3.18C).

Figure 3. 18. *(A) Example of abandonment element above a channel fill (red arrow) in UC1 and comprising thin-bedded, fine-grained upper division turbidites. (B) Abandonment element above UC2 (red arrow) composed of lower medium-bedded, medium-grained T_{bcde} turbidites that fine and thin upward to thin-bedded, fine-grained T_{cde} turbidites. (C) Abandonment element in CC-south above UC3 (contact indicated by white line). Here strata consist of thin-bedded T_{cde} turbidites interbedded with T_{de} turbidites that extend across the entire study area and form a unit up to 20 m thick. White arrows indicate way up.*

3.2.2.1.2 Abandonment Interpretation

The very fine- to fine-grained succession at the top of channel fills and channel units are interpreted to record deposition from low energy turbidity currents. The progressive upward fining and thinning of fine-grained, mostly upper division turbidites coupled with an increase in the thickness and number of siltstone and mudstone beds at all channel hierarchical scales, indicates a progressive reduction in flow energy, transport competence and transport volume related to the

gradual deactivation (i.e. abandonment) of the local (?) channel system (Clark and Pickering, 1995). Alternatively, where these strata abruptly overlie coarse-grained channel fills (i.e. UC2), they may be related to an updip avulsion of the active channel (Posamentier and Kolla, 2003).

3.2.2.2 Levees

3.2.2.2.1 Proximal Levees

3.2.2.2.2.1 Lithological Characteristics

Proximal levees are observed in CC-NW and are onlapped on one side by channel fills of UC1 (Figure 3.19) and channel fills of UC3 in the HS and make up 4% of the stratigraphy. Proximal levees associated with UC1 comprise two packages that are 6 and 10 m thick. Similar to UC1, levees associated with UC3 in the HS comprise two packages and are 5 and 12 m thick. In all cases, proximal levee deposits form packages that can be subdivided into lower and upper parts, the transition being sharp and marked by a dramatic decrease in bed thickness, grain size and sandstone content (Figure 3.19A). The lower part is 2 and 10 m, respectively, and made up of coarse- to medium-grained, medium- to thick-bedded, traction-structured sandstone, including planar lamination and multiset ripple cross-stratification (Figure 3.19B) interstratified with thin-bedded, fine-grained, upper division turbidites. This is then abruptly overlain by the upper part that ranges from 2 - 5 m thick and comprises very thin- to thin-bedded, very-fine to fine-grained upper division turbidites (T_{cde} and T_{de}; F2.1 and F3, respectively) (Figure 3.19C) interbedded with uncommon medium-bedded, medium-grained, traction-structured sandstone (F2.1).

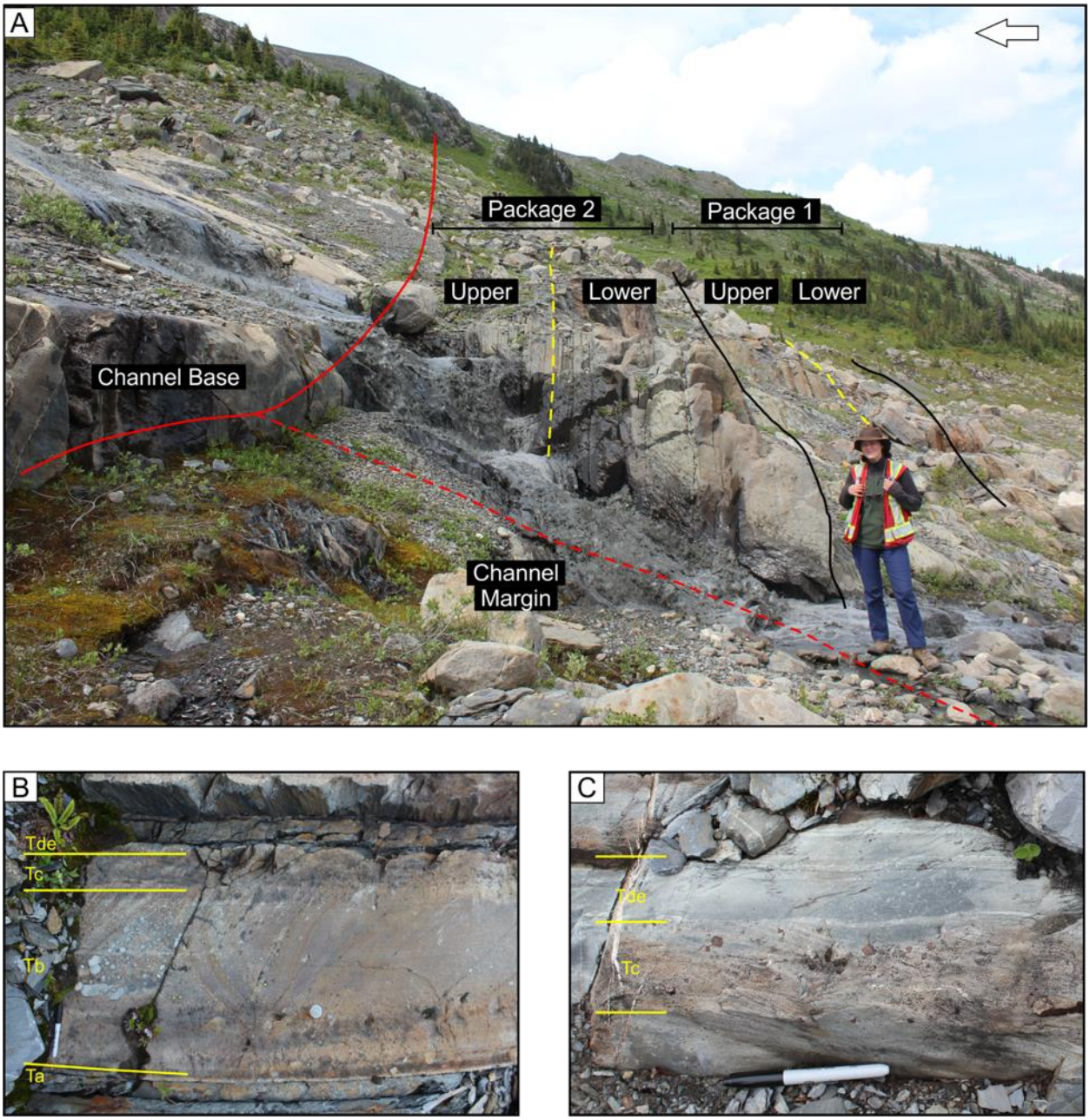

Figure 3. 19. *Proximal levee deposits adjacent to two channel fills in UC1. Strata are divided into two packages (black lines), each composed of two parts – contact between the parts (dashed yellow line) is marked by a dramatic decrease in bed thickness, grain size and sandstone content. In the lower part beds consist mostly of medium- to thick-bedded, upper medium- to coarse-grained, lower division to complete turbidites. In the upper part beds consist mostly of very thin- to thin-bedded, fine-grained, upper division turbidites (T_{cde}) in which the T_c division commonly comprises multi set ripple cross-lamination (Part C).*

3.2.2.2.2.2 Interpretation

Previous work by Khan (2012), Khan and Arnott (2010) and Bergen (2017) showed that proximal levee deposits can form 5 - 20 m-thick stratal packages with distinct upper and lower parts. The lower part was reported to consist of medium- to thick-bedded, upper medium- to coarse-grained sandstone (T_a, T_{ab}) intercalated with very thin- to thin-bedded fine-grained, upper-division turbidites (T_{cde}). This, then, is sharply overlain by a succession consisting of very thin- to thin-bedded upper-division turbidites intercalated with uncommon medium-bedded, lower-division turbidites. Bergen (2017) argued that channel inception initially formed low ridges (incipient levees) along the low-energy margins of the early channel-forming flows. With time (i.e. successive flows) the levee height increased and later flows became progressively more confined (Figure 3.20A). Bergen argued that flows during this early phase of channel development had a plug-like density structure, and as a consequence negligible vertical stratification and high flow efficiency (Tilston et al., 2015; Kneller et al., 2016). In these flows the velocity maximum was elevated well above the height of the incipient levees and allowed the lower sand-rich part of the flow to easily overspill and deposit thick, coarse sandstone beds that make up much of the lower part of each levee package (Figure 3.20B). The intercalated thinner-bedded, upper division turbidites resulted from much finer, lower concentration, and therefore lower energy flows. With time, and ongoing deposition on the margins of successive flows, the height of the now well-developed levees exceeded the height of the velocity maximum, which also closely approximated the abrupt decrease (i.e. rollback) in flow density. This allowed only the finer, upper part of the channelized flow to overspill and in turn deposit the thin, mud-rich turbidites that make up most of the upper part of each levee succession (Figure 3.20C). Uncommon interbeds of thick, coarse sandstone, on the other hand, were deposited by exceptionally large flows where the lower part of

the flow also overspilled. These characteristics resemble those of proximal levees in ICC1, where stratal packages exhibit two well developed and sharply separated parts with similar stratal characteristics, and accordingly are similarly interpreted.

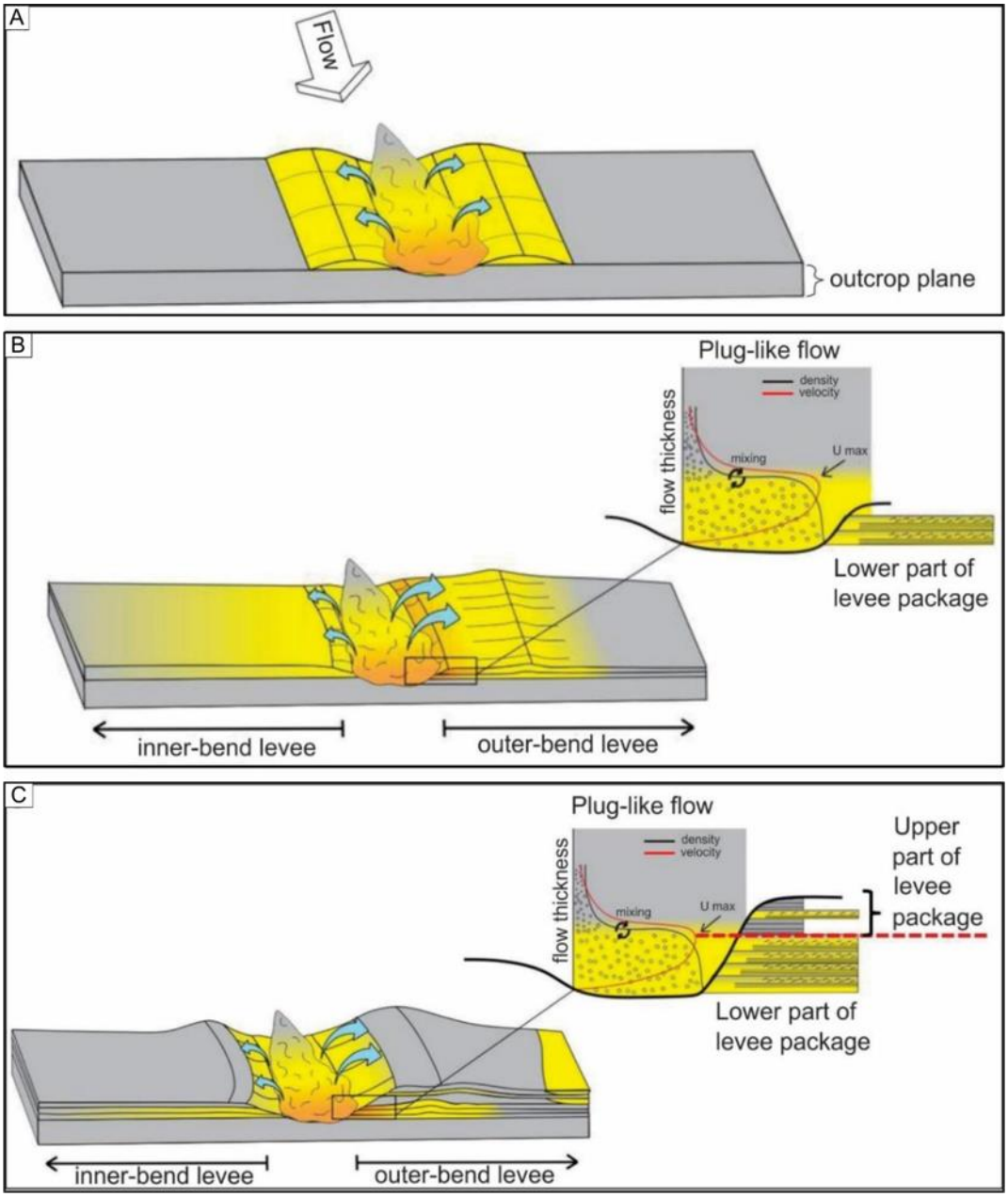

Figure 3. 20. *Schematic model of Bergen (2017) for the deposition of the lower and upper parts of a proximal levee package. (A) The sharp basal contact of each package overlain by coarse-grained turbidites is interpreted to mark channel inception and the base of incipient levees that confined the axial part of subsequent flows. (B). Flows had a plug-like density structure with the height of the velocity maximum elevated above the levee tops. This allowed the coarse, dense, lower part of flows to easily overspill and deposit thick-bedded, coarse-grained turbidites in the lower part of packages. (C) Continued deposition and upward growth of the levee caused the relief between the channel floor and levee crest to exceed the height of the velocity maximum of the average channelized flows. Thus, only the upper, fine-grained parts of currents typically overspilled and deposited the markedly finer upper part of each levee package. Coarse-grained sediment, which was transported in the lower part of the flow, typically remained confined to the channel.*

3.2.2.2.3 Distal Levees

3.2.2.2.3.1 Lithological Characteristics

Distal levees crop out throughout the study area and are commonly inferred to be in erosional contact with aggradational channel fills of UC1 and UC2 (Figure 3.7). Distal levee strata range from 2 – 30 m thick, can be traced for 50 m to < 1 km along strike, and mainly comprise facies of F2.1 and F3. However, in a single occurrence in CC-South, they form a 2 - 6 m thick succession that crops out for 500 m along strike, but is truncated to the southeast and northwest by UC2. Strata comprise five facies, F1, F2.1-F2.3, F3 that are arranged into a lower and upper package. The lower package is 2 - 4 m thick and consists of thin-bedded, fine-to medium-bedded Tcd turbidites (F2.1) that fine and thin upward and become increasingly intercalated with Tde turbidites (F3). The ripple cross-stratified Tc division is 0.5 to 12 cm thick and consists of multiset (up to 3 sets) and uncommon single set varieties. Each bed has a sharp planar base with little evidence of erosion. Additionally, F2.1 beds are intercalated with medium- to thick-bedded, coarse-grained, structureless sandstone (F1.1), pseudodune and dune cross-stratified sandstone with common mudstone intraclasts (F2.3). Basal contacts are loaded, in some cases with flame

structures that are up to 30 cm long. Clastic injections into thin-bedded, Tcd turbidites are also common (Figure 3.21A). Along strike, coarse-grained strata are laterally discontinuous and pinch and swell over distances of ~ 5 m. The upper package sharply overlies the lower package and comprises a 2 m-thick succession of sharp-based F2.2 beds (Figure 3.21B) that fine and thin stratigraphically upward. These strata superficially resemble classical sand-rich turbidites (F2.1), comprise thin-bedded, fine-grained wavy- to cross-laminated sandstone that are rhythmically interstratified with sandy mudstone and then overlain by silty mudstone (F3).

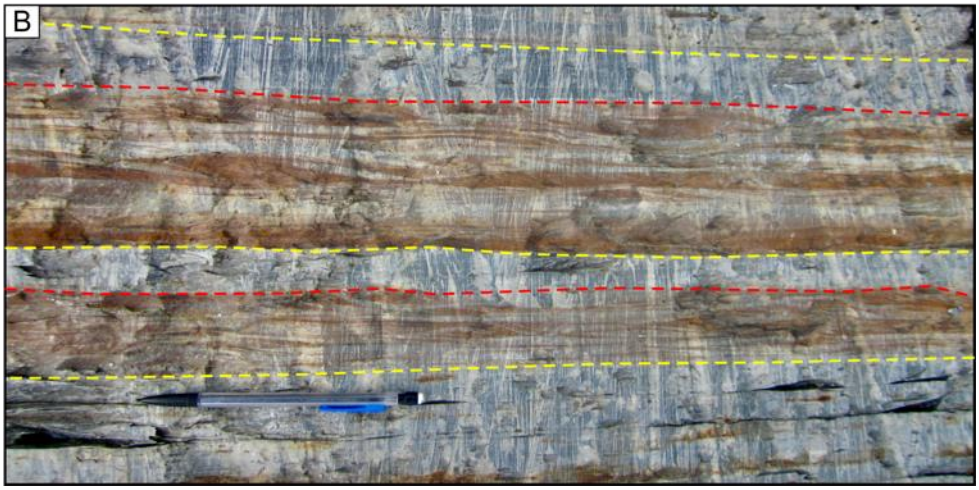

Figure 3. 21. *A) Example of a distal levee succession in CC-South that sharply overlies UC1 and forms an up to 5 m-thick unit composed of thin-bedded, fine-grained* T_{cde} *turbidites (F2.1) intercalated with coarse-grained, structureless (F1.1), cross-stratified sandstone and pseudodunes (F2.3) It is then sharply overlain by a coarse-grained UC2 channel fill that erodes these strata completely < 500 m along strike. White arrow indicates way up. Note the well-developed flame structures (blue arrows) along the base of an ungraded, coarse-grained sandstone, in addition to a coarse-grained, cross-stratified sandstone that thins and eventually pinches out (red arrows). (B) Close-up of two sharp-based (yellow dashed line) F2.2 beds capped by F3 strata (red dashed line). Note also the intricate interstratification of wavy-laminated or low angle cross-laminated carbonate-cemented sandstone (red) and sandy mudstone (grey).*

3.2.2.2.3.2 Interpretation

Distal levee, like proximal levee deposits, are interpreted to represent deposition on the margins of an active channel. Most beds were deposited by low concentration, fine-grained turbidity currents (Khan and Arnott, 2011). The general lack of scoured bed bases and the commonality of multiset ripple cross-stratification suggests that flows became immediately depositional with flow speed in the ripple stability field. Moreover, flows were highly stratified, a consequence of loss of flow confinement and expansion over the levee, which in turn resulted in extensive particle settling. According to the experimental data of Tilston et al. (2015) and the theoretical arguments of Arnott (2012), a highly density-stratified structure is a requisite condition in turbidity current to form the near-bed hydrodynamic instability(s) needed to generate bed-surface defects, which soon after amplify and transform into angular bed forms (ripples), and rarely dunes. Rare interbeds of medium- to thick-bedded sandstone and pseudodunes are likely related to anomalously high-energy, high concentration channel flows that allowed coarser-grained sediment to overspill the levees and travel further from the channel margin. The major difference between distal levee and proximal levee deposits is the absence of the distinctively thick, coarse-grained strata in the lower part of a levee package. Their absence is interpreted to be related to

differences in the distance from the coeval channel. Specifically, distal levee is interpreted to be located further away from the channel margin, and therefore further along the transport pathway, and as a consequence, strata are finer and thinner (e.g. Khan and Arnott, 2010; Bergen, 2017).

Additionally, in distal levees located in CC-South, the abrupt change in lithofacies from classical sand-rich turbidites (F2.1) in the lower package to the intricately interstratified sand-mud turbidites of F2.2 in the upper package is associated with a dramatic change in depositional conditions. These strata, like those in the lower package, and for that matter levee deposits everywhere, were deposited by flows that overspilled the margins of an adjacent channel. However, in this case, overspilling flows were obstructed in the downflow direction by a topographical high that impeded flow away from the channel. The barrier caused the (incident) overspilling flow to form a progressively thickening volume of fluid that eventually developed sufficient density to flow in the reverse direction, which very generally was toward the channel (see also Billington, 2019). Due to dimensional limitations and the 2D nature of the outcrop, in addition to local cover by glacial debris, no evidence of the barrier is observed in outcrop. Nevertheless, it is hypothesized that the barrier could be a mass transport deposit like a slide, slump or debrite, which commonly are reported to form localized positive topography on levees (e.g. Kane et al., 2007; Armitage et al., 2009; Kane et al., 2010). This two-way confinement between the upflow levee crest and the downflow barrier created a local set of unique sedimentological conditions that most profoundly resulted in the trapping and accelerated deposition of fine-grained sediment – a condition here that is recorded by the intricate and rhythmic intercalation of sand and mud strata of F2.2 rather than the more typical classical turbidites (F2.1) observed in the lower package.

3.2.3 Debrite Element

3.2.3.1 Lithological Characteristics

The debrite element is not only uncommon in ICC1 (~1%), but is confined to UC1, and more specifically to the CC-NW and HS study areas. Strata range from 30 - 200 cm thick and are only exposed locally (< 10 m along strike before becoming covered by glacial debris). Strata consist of matrix-supported conglomerate with cm- to m-scale mudstone clasts and quartz granules and pebbles dispersed in a matrix of silty mudstone (F4) – dispersed quartz grains give the debrite a distinctive "starry night" appearance. In three examples, debrites are overlain by thickly developed, coarse-grained, amalgamated channel fills. However, in one case in CC-South, it erosively overlies and on one side is bounded by a channel fill and one the other by fine-grained, thin-bedded, upper division turbidites and on the other side, it is scoured by a channel fill composed of amalgamated, coarse-grained sandstone (Figure 3.22 see also Figure 3.11). This debrite is 548 cm thick, is exposed for ~ 35 m, and is sharply overlain by an up to 400 cm thick succession of very thin-bedded, very-fine grained, upper division turbidites.

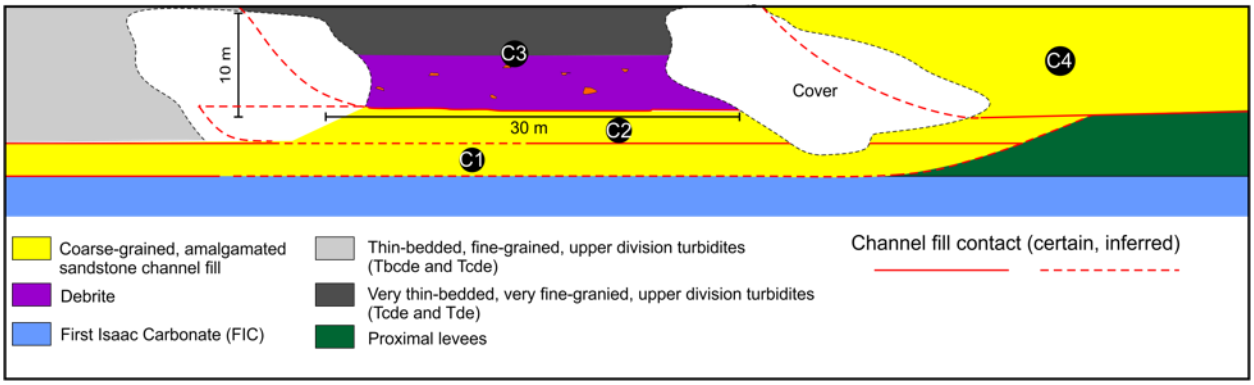

Figure 3. 22. *Line drawing of the debrite channel fill, which on one side (left) deeply scours a thick succession of thin-bedded, fine-grained, upper division turbidites (Tbcde and Tcde) and on the other side is scoured by a channel (C4) filled with coarse-grained amalgamated sandstone. See figure 3.10 for additional detail.*

3.2.3.2 Interpretation

Debrites are interpreted to be the deposits of submarine debris flows, which are cohesive sediment-gravity flows that likely originated from the mechanical transformation of an upslope seabed failure (Arnott, 2010). Mudstone clasts and quartz gravel grains were supported by cohesive strength and buoyancy provided by the silty mudstone matrix that inhibited particle settling and promoted downslope transport (Mulder and Alexander, 2001). Initial slope failure could have been associated with high rates of sedimentation, sediment loading, seismic activity, excess pore pressure and/or eustatic changes (Zhao et al., 2019; Brami et al., 2000; Canals et al., 2004). Deposition, on the other hand, occurred by progressive frictional freezing and expansion of a rigid plug from the top of the flow downward, which upon reaching the base of the flow caused *en masse* deposition. Debrites in UC1 are commonly overlain by channel fills, which is a common association in many deep-marine channel systems (Armitage et al., 2009; Clark and Pickering, 1996; Samuel et al., 2003; Mayall et al., 2006; Arnott et al., 2011) and typically are interpreted to be associated with slope instability caused by shelf-edge unloading and increased pore pressure during falling relative sea level and/or lowstand (Posametier and Kolla, 2003, Arnott et al., 2011). In CC-NW example (Figure. 2.16) the debrite is interpreted to have partly plugged an erosional surface and is interpreted to be a channel plug. Later the channel was abandoned and the remnant topography infilled by very thin-bedded, T_{de} turbidites.

Chapter 4: Spatial and Temporal Evolution of a Base-of-Slope Channel Complex Set, Isaac Formation, Neoproterozoic Windermere Turbidite System, Cariboo Mountains, British Columbia, Canada.

4.1. Deep-Marine Sequence Stratigraphy Overview

Sequence stratigraphy focuses on analyzing facies and geometric characteristics of stratigraphic successions and identifying key surfaces to determine the chronological order of basin filling and erosional events. In general, sequence stratigraphy is generally most easily applied in coastal to shallow-water settings where the stratigraphic response is a manifestation of changes in sediment supply, which is tied to continental weathering, and accommodation on the continental shelf, the latter controlled by the interplay of changes in eustasy and subsidence, or what is termed relative sea level (Catuneanu et al., 2009). Intuitively, it is clear how eustatic changes could control the development of the continental shelf, and in turn the delivery of sediment into the deep sea. Theoretically this apparent intrinsic relationship is abundant and coarse sediment is fed during low relative sea level (RSL) when fluvial systems prograde to the shelf-edge, whereas sediment flux and grain size decreases during high RSL when continental shelves are flooded (Posamentier and Kolla, 2003; Catuneanu; 2006; Catuneanu et al., 2009; Posamentier and Walker, 2006).

Deep-marine siliciclastic turbidite systems, in particular those with a wide shelf and a well-developed shelf-slope break (e.g. passive margin basins), such as the one thought to have existed on the western margin of Neoproterozoic Laurentia, are controlled by changes in shelf accommodation associated with RSL. Although this might be the case on passive continental margins, it is important to note that not all turbidite systems are controlled principally by eustasy, but instead by tectonic, compaction and/or climate factors that are unrelated to sea level position,

such as crustal thinning, mantle-lithospheric thickening, sedimentary and volcanic loading, subcrustal loading, amongst others (Ingersoll, 2012). To date, several models have been proposed that relate a depositional sedimentary continuum, theoretically separated into systems tracts, to sea level fluctuation; the differences between models are based on the stratigraphic surfaces chosen to subdivide the stratigraphy. Nonetheless, irrespective of nomenclatural differences, four genetic units are generally recognized and interpreted to be key for stratigraphic interpretation (Figure 4.1), these are: forced regression (Posamentier et al., 1992), also termed falling-stage systems tract (FSST), normal regression (lowstand and highstand systems tract; LST and HST, respectively) and transgressive systems tract (TST). This four stage system tracts model is used in this thesis to interpret the spatial and temporal evolution of Isaac Channel Complex Set 1 (ICC1), and is discussed next.

During the falling-stage (FSST; Figure 4.1), falling relative sea-level causes the continental shelf to become progressively more exposed as the shoreline shifts downward and basinward (Posametier et al., 1988; Kolla et al., 1995). As a result of subaerial exposure, rivers extend basinward and commonly incise the now-exposed shelf, possibly as far as the shelf margin. This, in turn, results in the expansion of the catchment area and accordingly sediment supply to the distal end of the transport system. If the terminus coincides with the shelf-slope break sediment-gravity flows can be supplied directly to the slope from the up-flow fluvial system (hyperpycnal flow) (Posametier and Kolla, 2003). These flows initially contain high sand:mud ratio and if out grade with the existing slope gradient result in extensive erosion of submarine canyons and channels that excavate along the upper- and middle-slope as sediment is bypassed to the base-of-slope and basin floor. Additionally, falling relative sea level is characterised by widespread gravitational instability along the outer shelf and upper slope due to factors such as hydro-eustatic uplift, stratal

overpressures, seafloor fluid seepage, gas-hydrates decomposition and oversteepened slope gradient (Arnott, 2010). This, in turn, leads to extensive slope failure and mobilization of cohesive dominantly fine-grained slope deposits producing a variety of mass-transport types (i.e. slumps, slides and debris flows).

When sea level reaches its lowest point at the onset of the lowstand system tract (LST; Figure 4.1) sediment supply to the shelf-slope break followed by downslope resedimentation is maximized. The basal contact of the LST marks the sequence boundary (SB), and by definition, the start of the next depositional sequence. Leading up to this point, the ratio of sand:mud in the sediment supply increases steadily as shelf deltas prograde and approach the shelf-slope break. The increase in coarse sediment decreases the flow efficiency of sediment gravity flows and steepens the slope equilibrium profile through deposition. This newly developed accommodation allows mid- and lower-slope regions to aggrade and to temporarily starve the basin floor of sediment causing local retrogradation. Once transport equilibrium is re-established on the slope, the active center of deposition shifts back to the basin floor (Posamentier and Kolla, 2003).

As sea level begins to rise sediment sourced from continental erosion becomes increasingly sequestered in the aggrading coastal plain and deltas (Posamentier and Walker, 2006), causing the deep marine environment to become increasingly starved of clastic sediment input. Gravitational instability along the shelf-edge and upper-slope increases as the equilibrium profile (slope) changes, causing an increase in the frequency of mass-wasting events and related mass-transport deposits (Posamentier and Kolla, 2003). Flows that transport sediment along the shelf and pass over the shelf-slope break have a lower sand:mud ratio and form highly confined, sinuous channel systems with well-developed levees and are highly aggradational (Figure 4.1; Peakall et al., 2000; Kneller, 2003; Abreu et al., 2006).

Associated also with rising sea level and the start of transgression (TST) is the possible initiation and development of a shallow water carbonate platform that then may shed sediment from the platform downslope where it deposits along with relict resedimented siliciclastic and also biogenic suspension sediment (Harper et al., 2015). The presence of carbonate-rich strata in an otherwise siliciclastic dominated deep-marine turbidite system, for example the Windermere Supergroup in the southern Canadian Cordillera, can form important stratigraphic marker horizons that aid not only in sequence stratigraphic modelling, but also regional stratigraphic correlation.

Transgression on the shelf ends when rising sea level is exceeded by sediment supply, marking the onset of the highstand systems tract (HST; Figure 4.1) Now the shelf is at its widest and this restricts the supply of coarse sediment, notably sand and gravel, into the deep sea. Accordingly, the deep-marine becomes a site of slowly accumulating, mostly fine-grained sediment, and quite possibly development of a condensed section. In the case of carbonate shelves, if the rate of rising sea level is sufficiently high and drowns the carbonate shelf factory, carbonate sediment is replaced by fine-grained siliciclastic during the HST and most probably also during the ensuing FSST (Plint and Nummedal, 2000).

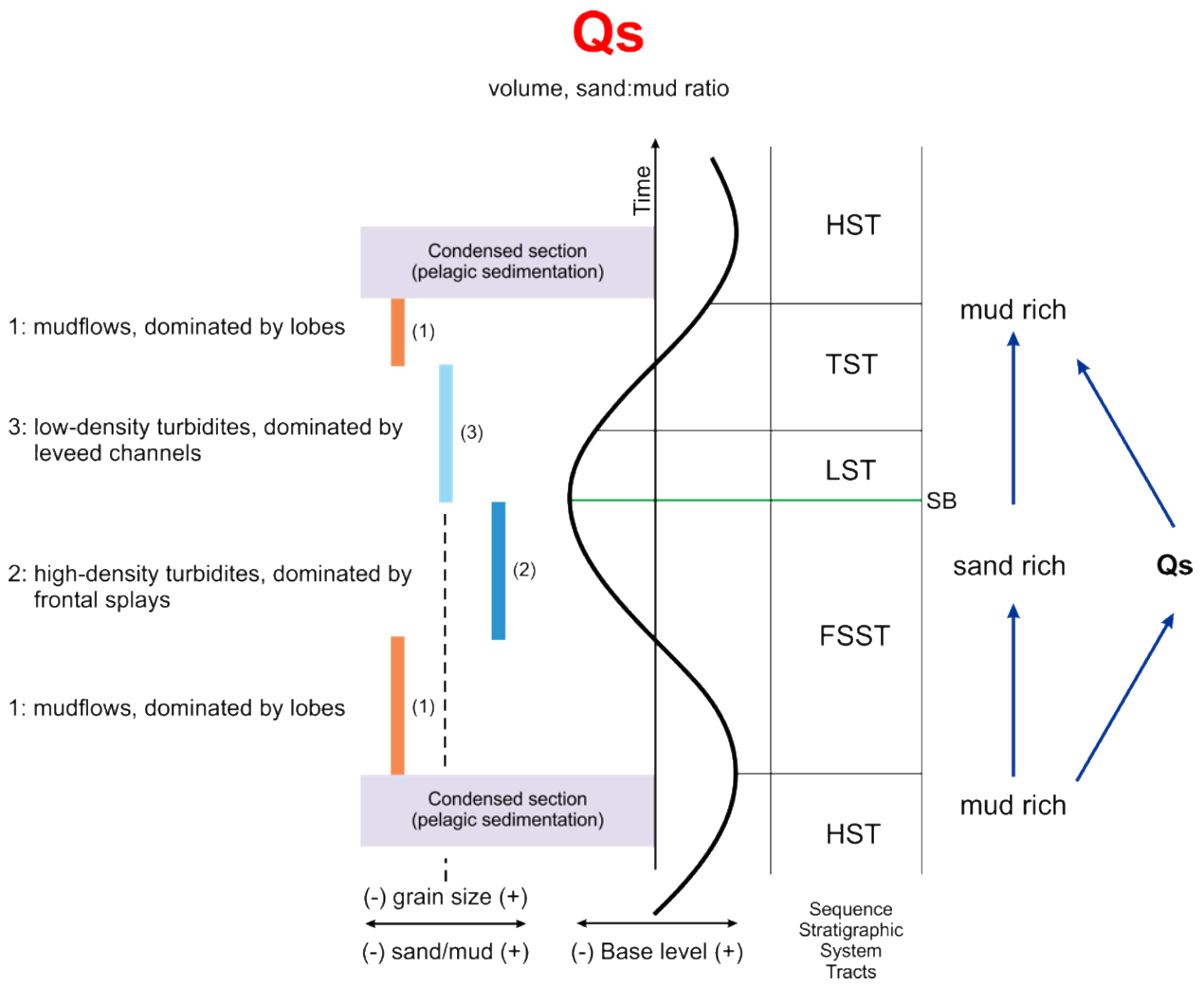

Figure 4. 1. *Idealized model relating dominant type of sediment-gravity flow and deposits that form a deep-marine fan complex. This thesis utilizes four systems tracts: falling-stage (FSST), lowstand (LST), transgressive (TST) and highstand (HST) (sensu Hunt and Tucker, 1992). With falling relative sea level (FSST), widespread gravitational instability on the outer shelf/upper slope results in extensive mass wasting and incision of canyons and slope channels, and bypass of sediment to the base-of-slope and basin floor (1). When RSL reaches its lowest position a new sequence begins, the base marked by a sequence boundary (SB) followed by the LST associated with a high sand:mud ratio and sediment flux (Qs). This causes sediment bypass on the slope and feeds the basin-floor depositional lobes and splays (2). With the ensuing rise of relative sea level (LST to TST), the sand:mud ratio begins to decrease, which enhances levee growth and the development of leveed channel systems (3). As the sediment flux decreases (Qs), the deep-marine part of the system becomes sediment starved. Eventually a condensed interval forms and marks the beginning of the HST (modified from Catuneanu et al., 2009).*

4.2. Evolution of Isaac channel Complex 1

Stratigraphic analysis of ICC1 has helped elucidate the evolution of a deep-marine channel levee complex set, and also identify factors that controlled its development. As discussed next, changes in facies, geometry and distribution of stratal elements are interpreted to be controlled by differences in sediment supply, including grain size and grain size distribution, which are interpreted to be linked to allogenic (external) controls, such as long-term (probably 3rd-order) eustasy and climate changes (Figure 4.2) (e.g. Posamentier and Kolla, 2003; Catuneanu et al., 2009). Additionally, autogenic (internal) mechanisms, such as avulsion rate (e.g. Armitage et al., 2012; Kolla, 2007) and channel migration patterns (e.g. Sylvester et al., 2011) profoundly influenced deposition of the ICC1. Collectively, the combined influence of allogenic and autogenic controls helps to explain the stratal make-up and spatial and temporal trends observed in ICC1.

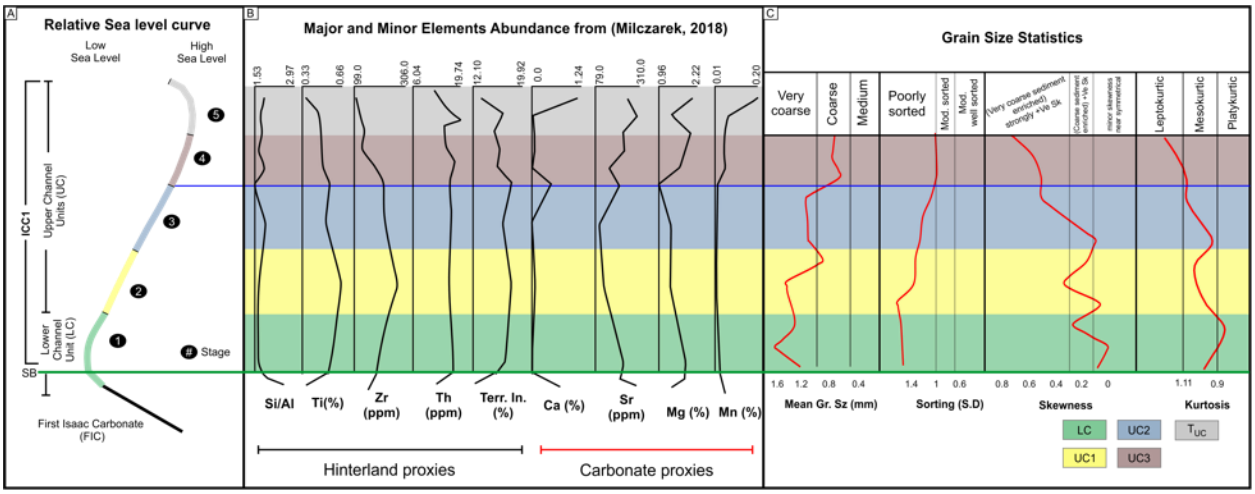

Figure 4. 2. *(A) Summary evolutionary model of ICC1 illustrating long-term (3rd order) changes in relative sea level possibly related to the onset of the 580 Ma Gaskiers glaciation (see text for details). The erosion surface between the FIC and ICC1 marks a 3rd order sea level fall and is interpreted to represent a sequence boundary (SB; green line). Numbers 1-5 indicate the depositional stages associated with the channel units that make-up ICC1. (B) Major and minor element abundance from mudstones in ICC1 (from Milczarek, 2018). Stratigraphically upward, hinterland proxies (Si/Al, Ti, Zr, Th, Terr. In) are high in parts 1, 2 and 3, but then progressively decrease in parts 4 and 5 as carbonate proxies (Ca, Sr, Mg and Mn) increase. (C) Grain size statistics of thick-bedded, coarse-grained sandstone (F1.1) showing mean grain size (mm), sorting (S.D), skewness and kurtosis. Note that stratigraphically upward strata become finer, better-sorted, more coarse skewed, and progressively more enriched in coarse sediment. Also, kurtosis changes gradually from platykurtic to leptokurtic, indicating that grain size becomes increasingly more clustered in the central part of the distribution.*

4.2.1 First Isaac Carbonate (FIC)

ICC1 overlies the regionally-extensive, approximately 200 m thick, deep-marine mixed carbonate-siliciclastic first Isaac carbonate (FIC), which forms a major regional stratigraphic marker within the siliciclastic-dominated Windermere turbidite system (Ross and Arnott, 2007). The FIC consists of three decameter-thick, laterally-continuous, sheet-like, deep-water calciturbidite deposits, informally termed CT1-3, intercalated with decameter-thick, laterally-extensive sheet-like siliciclastic fine-grained deposits incised locally by channels and scours filled with coarse-grained, mixed carbonate-siliciclastic sandstone and carbonate-rich debris-flow

deposits. Stratigraphically upward, these stratal elements exhibit systematic changes in architecture and mineralogical composition (Navarro, 2016; Cochrane 2018; Cochrane et al., 2019). In addition to lithostratigraphic changes, recent work by Cochrane et al. (2019) showed that at the base of the FIC, $\delta^{13}C_{carb}$ is negative (-3.8 ‰ to -5.2 ‰) and stratigraphically upwards progressively increases to +2 to +3 ‰ in the middle of the succession and then declines to -6.3 ‰ at its top. This upward enrichment followed by depletion in $\delta^{13}C_{carb}$ is interpreted to reflect changes in organic productivity and its influence on inorganic carbonate precipitation by the shelf carbonate factory. Additionally, siliciclastic mudstone-rich strata at the top of the FIC exhibit a marked increase in the abundance of terrestrial proxies like Ti, Zr, Al, K, and Na, and a commensurate decrease in carbonate components like Ca, Sr and Mg (Figure 4.2B; Milczarek, 2018). Collectively, these lithostratigraphic and geochemical changes in the FIC suggest a 3^{Rd} order transgression followed by regression that quite possibly was tied to rising and then falling sea level. Superimposed on this long-term change were shorter sea level fluctuations (4^{th} and 5^{th} order) that formed the decametre-thick channel complexes filled with amalgamated, carbonate-cemented, coarse-grained sandstone during periods of lowered sea level (Navarro, 2016).

The upward change in $\delta^{13}C_{carb}$ potentially correlates with worldwide Ediacaran $\delta^{13}C_{carb}$ datasets like in the Doushantuo Formation in south China where several negative $\delta^{13}C_{carb}$ anomalies have been reported, most specifically the EN2 excursion that was suggested to be associated with the 580 Ma Gaskiers glaciation (Tahata et al., 2013). This suggest that the FIC might represent a chemostratigraphic record of $\delta^{13}C_{carb}$ conditions in global seawater immediately before the Gaskiers glaciation (Cochrane et al., 2019), and that ICC1 represents, at least in part or its entirety, deposition during the Gaskiers glaciation, and how possible short- and long-term changes in glacially controlled sea level potentially affected slope-channel evolution.

4.2.2. Stage 1: Deposition of the Lower Channel Unit (LC)

During the falling stage systems tract, and prior to the deposition of the lower channel unit (LC), changes in sediment flux, specifically, the reactivation of voluminous downslope sediment transport resulted in a disequilibrium between currents that transited the slope and the gradient of the slope. Disequilibrium may have been accentuated as the system reverted from a carbonate system with a steeper continental slope, most probably a consequence of early seafloor carbonate cementation, back to a siliciclastic system with an inherently lower angle slope (Ross et al., 1994). Collectively, this would have enhanced gravitational instability, which in turn caused extensive mass wasting marked by erosion and sediment by-pass as the slope profile was being readjusted. Initially, the primary source of sediment remobilized downslope was most probably palimpsest and relict coarse shelf sediment.

The initiation of ICC1 was marked by highly erosive, net-incisional flows, which in the southeast part of the study area is evidenced by a minimum 30 m-deep scour into the FIC (Figure 4.3). After this initial period of erosion and bypass, flows became net-depositional and deposited the lower channel unit (LC) during the late falling stage and early lowstand system tracts (Figure 4.4). At this time, sediment supply was dominated by remobilized coarse palimpsest and relict shelf sediment and eroded older highstand shoreline and continental slope deposits. These sediments occur in the lowermost ~ 8 - 10 m of LC channel fills (C1) and consist of anomalously coarse sediment, including quartz pebbles and clasts of carbonate-cemented sandstone and mudstone. However, stratigraphically upward, channel fills become finer grained (coarse- to very-coarse grained) with a notable absence of these coarse granular components, suggesting that the supply of sediment to the shelf edge had changed, and most probably was now being derived principally from the hinterland. Strata are poorly sorted, enriched in coarse sediment and exhibit a

meso- to playkurtic kurtosis (Figure 4.2C). Turbidity currents composed of this poorly sorted sediment would have been highly density-stratified due to the wide variety of particle size, and therefore settling velocity (Dorrell et al., 2013). Each channel in the LC was filled by density-stratified flows with a high-density axial region that deposited amalgamated, coarse-grained sandstone, and low-density, lower-energy margins that deposited finer and thinner-bedded strata. Because of intense interfacial mixing with the surrounding ambient fluid and turbulence suppression related to near-bed sediment concentration and stratification effects (Tilston et al., 2015; Kneller et al., 2016), sediment transport capacity was exceeded resulting in significantly higher net rates of sedimentation in the channel compared to the interchannel areas (Bryant et al., 1995; Mohrig et al., 2000; Jerolmack and Paola, 2007). Higher rates of aggradation in the channel caused the channel gradient (Kneller, 2003) to be reduced and eventually the channel made hydraulically inefficient, which then forced avulsion to an adjacent, topographically lower, more hydraulically favourable area on the seafloor (Mohrig et al., 2000).

Additionally, because of confinement in the deep scour that incised FIC in the southeast part of the study area, avulsed flows became re-established in close proximity to the deactivated channel. As a consequence, younger channels cannibalized older channel deposits, which is manifest by the disorganized juxtaposition of successive channel fills – a pattern termed disorganized stacking by McHargue et al. (2011) (Figure 4.4C-D). These strata are then overlain by a 27 m-thick succession of fine-grained, thin-bedded, upper division turbidites, indicating a dramatic decrease in flow energy, transport competence and volume most probably associated with a deactivation of at least the local transport system (T_{LC}; Figure 4.4B).

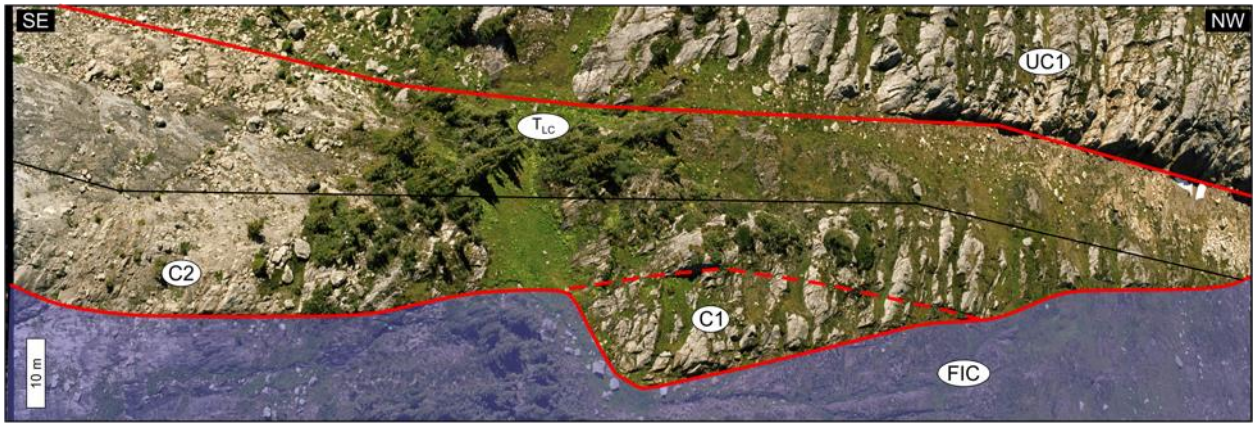

Figure 4. 3. *Aerial photograph of the > 30 m-deep incision (red line) into the top of the FIC during the sea level fall that terminated deposition of the FIC and formed the sequence boundary at the base of ICC1. Note the onlap of channel fills C1 and C2 onto the erosional surface towards the NW; channels separated by dashed red line. Upper red line marks the base of UC1.*

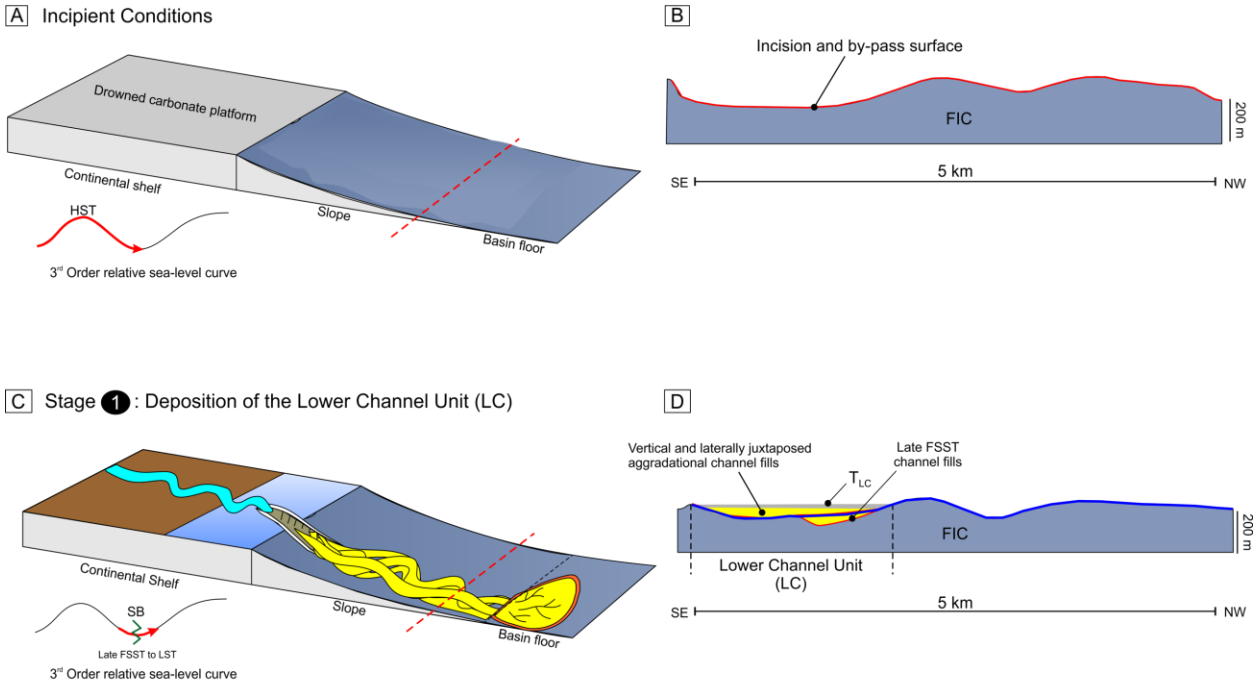

Figure 4. 4. *Schematic diagrams illustrating relative sea level (RSL). (A-B) Prior to the inception of ICC1 an up to 200 m-thick mixed carbonate-siliciclastic succession (FIC) associated with transgression, highstand and subsequent falling RSL. During the falling stage systems tract (FSST), periods of erosion and by-pass incised the FIC and created an at least 30 m-deep scour that became the primary conduit for subsequent turbidity currents. (C-D) The erosive contact between the FIC and ICC1 marks a 3rd order sea level fall, and, therefore a sequence boundary (blue line in D) resulting in the deactivation of the carbonate factory and re-instatement of a*

voluminous supply of coarse terrigenous sediment into the basin. Highly efficient and erosive flows transited topographical lows along the top of the FIC and eventually formed the base of LC. With reduced flow efficiency, channels filled, avulsed and become re-established with only negligible lateral displacement, which becomes manifest as a disorganized stacking pattern; these conditions most probably coincide with the early lowstand. Later, deactivation of at least the local transport system deposited a blanket of mostly thin-bedded, fine-grained, upper division turbidites (T_{LC}).

4.2.3. Stage 2: Deposition of UC1

As sea level continued to rise during late lowstand, the sediment supply was still polydispersed, but now most probably made up of sediment sourced directly from the hinterland. Nevertheless, like LC, strata of UC1 exhibit similar grain size distribution, are poorly sorted, enriched in coarse sediment and exhibit a mesokurtic kurtosis (Figure 4.2C).

Channel fills of UC1, like LC, were aggradationally-filled with a spatially disorganized stacking pattern (Figure 4.5); however, UC1 is composed almost exclusively of 100% amalgamated remnants of the axial sand-rich part of channel fills with rare examples of upward and lateral fining and thinning. This, then, suggest that in comparison to LC, avulsion rates in UC1 were higher, which possibly could be related to greater confinement that caused avulsing channels to exhibit even less lateral displacement, and accordingly extensive cannibalization of older channel deposits. A possible explanation for the confinement could be an areally-extensive, but unexposed mass transport deposit (MTD), such as a debrite, slide or slump. These features are common in the slope deposits of the Isaac Formation throughout the Castle Creek study area, including ICC1, suggesting that gravitational instability and mass wasting was common and that due to the two-dimensionality of the outcrop may cause areally restricted features to be underrepresented along a single outcrop surface, notwithstanding the added possibility of erosion by a younger channel.

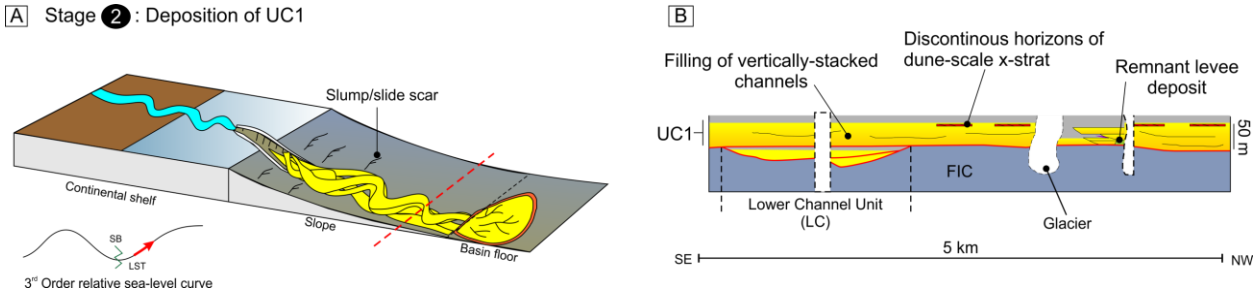

Figure 4. 5. *Schematic diagrams illustrating relative sea level (RSL) and sediment flux into the deep-marine realm. (A) As the lowstand proceeded remobilized coarse-grained palimpsest and relict shelf became a more minor component in a sediment supply that was now becoming dominated by hinterland input. Flows that formed channels in topographical lows experienced high confinement, which is manifest by an up to 50 m-thick succession of amalgamated axial sandstone-rich deposits. Channels completely filled, avulsed, and became re-established with negligible lateral displacement, which over time built up a spatially disorganized pattern of stacked sandstone-rich channel fills (B).*

The uneven surface topography caused by MTD's have been extensively documented in a number of studies (i.e., Armitage et al., 2009; Jackson and Johnson, 2009; Kneller, 2016; Zhao et al., 2019). These studies have indicated that MTD's commonly exhibit significant negative (i.e. erosional scars) and positive relief along their upper surface (Figure 4.6), which then can control not only the location and distribution of younger channel fills, but also the stratal architecture of their fill (Armitage et al., 2009). The absence of an MTD beneath UC1 is interpreted to be a local feature caused by complete erosion by channels that transited the topographical confinement along the top the MTD.

Dune-scale cross-stratification and pseudodunes, which are rare not only in other ICC1 channel units, but also in other channel complexes in the Isaac Formation, are notably common at the topmost 20 m of UC1. A possible interpretation for their common occurrence in UC1, but general absence everywhere else, might be related to topographical confinement formed by the MTD. More specifically, lateral confinement would have increased local flow speed, but most

importantly allowed flow speed to remain elevated during the final stages of a discrete transport event. This would have enhanced bed-surface reworking during the critical waning stages of flow when near-bed density conditions allowed bed-surface defects to develop, and because of moderate flow speeds, allowed dunes to form (rather than the more common ripples in a classical turbidite.

Additionally, similar to LC, the paucity of levee deposits in UC1 is probably an artifact of erosion by younger channels (McHargue et al., 2011) or, alternatively these channels were instead erosionally rather than depositionally confined (see for example Clark and Pickering, 1996).

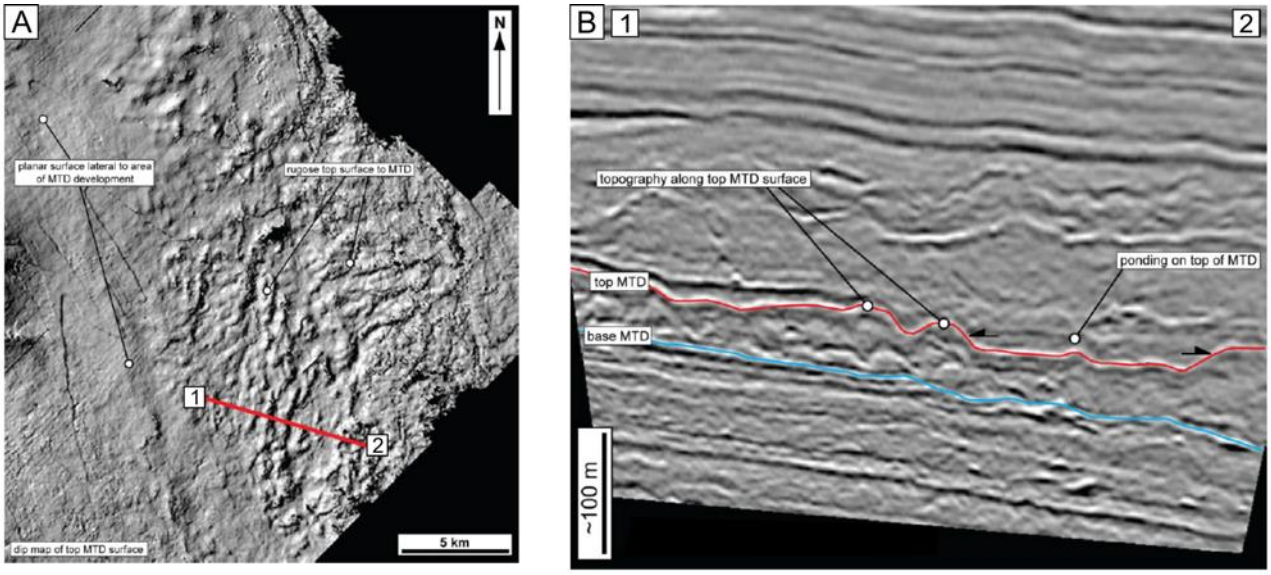

Figure 4. 6. *High-resolution reflection-seismic (A) horizon extraction (i.e. plan view) and (B) cross-section illustrating the uneven surface of a shallowly-buried MTD. MTD's commonly exhibit significant negative and positive relief along their upper surfaces that can be up > 100 m deep and cover areas > 120 km^2. Red line in (A) marks the location of the cross-section in (B). Note the ponded deposits in the cross-section that fill the topographical lows along the irregular surface of the MTD (from Posamentier and Walker, 2006). In the case of the exposed part of UC1 at Castle Creek, however, the MTD was completely eroded locally by channels that flowed along its upper surface.*

4.2.4. Stage 3: Deposition of UC2

With continued sea level rise, and following the abandonment of UC1, UC2 was initiated by a period of channel incision and by-pass. At this time, the sediment supply into the basin progressively changed, more specifically, coarse sediment became sequestered on the proximal shelf and further landward, while hinterland sediment input was also significantly reduced. This is best expressed in the grain size distribution of UC2, which exhibits better sorting than LC and UC1 (Figure 4.2C), shows a decrease in granule and pebble grains, and in the topmost sample shows an abrupt increase in coarse and very coarse framework grains and narrowing of the grain size distribution (more leptokurtic). Like LC, individual channels in UC2 show a well-developed axis to off-axis continuum of facies; namely, axial deposits consisting of coarse-grained sandstone and conglomerate that along strike become progressively finer-grained and increasingly interbedded with thin-bedded, finer-grained turbidites. Additionally, and similar to LC, UC2 channel fills commonly fine and thin upward, suggesting better preservation of the upper part of channel fills.

Like LC and UC1, channel fills of UC2 were aggradationally-filled and successive channels tend to be erosively juxtaposed and form a disorganized nested stacking pattern (Figure 4.7) (cf. McHargue et al., 2011). Compared to UC1, the upward-fining and -thinning is related to increased net in-channel deposition and reduced avulsion rate.

Additionally, and like UC1, the occurrence of one example of distal levee deposits suggest the almost complete erosion of interchannel deposits by younger channels (sensu McHargue et al., 2011).

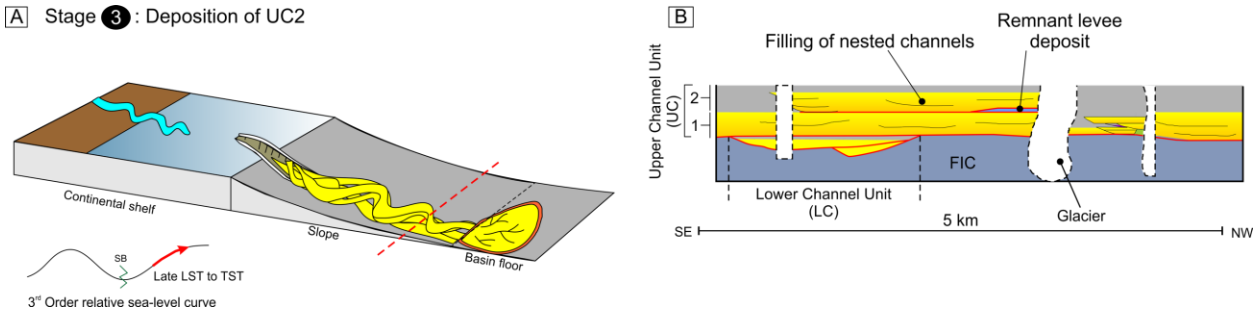

Figure 4. 7. *Schematic diagrams illustrating relative sea level (RSL) and sediment flux into the deep-marine realm. (A) As sea level continued to rise during the late lowstand to transgressive systems tract sediment supply into the deep part of the basin changed as coarse sediment became increasingly sequestered in more proximal subaqueous and subaerial parts of the basin. Nevertheless, like these earlier channels, channels of UC2 filled aggradationally with a spatially disorganized stacking pattern (B).*

4.2.5. Stage 4-5: Deposition of UC3 and abandonment of ICC1.

UC3 is marked by the development of laterally accreting channels filled with coarse- to very coarse-grained sandstone. Unlike the aggradational channel fills of LC, UC1 and UC2, laterally accreting channels of UC3 show little to no upward or lateral fining or thinning. Also, strata are the best sorted, exhibit the narrowest grain size distribution (Figure 4.2C), contain the fewest feldspar framework grains, are the most enriched in carbonate cement, and unlike UC1 and UC2 contain carbonate-cemented sandstone clasts. The occurrence of carbonate cement and carbonate-cemented clasts, the former being the product of recrystallized detrital carbonate grains, indicates the activation of a carbonate platform and flooding of a shallow-water platform. Moreover, major and minor elemental data from abandonment strata above UC2 and then above UC3 (T_{UC}; Figure 4.2B) (Milczarek, 2018) show a steady decrease in hinterland proxies (i.e. Ti, Zr, Th and terrestrial input) but increase in carbonate element proxies (Ca, Mn, Sr and Mg); Sr and Mg showing the best developed trend (Figure 4.2B).

Collectively, the mineralogical, geochemical and grain size characteristics of strata that fill laterally-accreted channels of UC3 contrast those in aggradationally-filled channels (LC, UC1 and UC2). A potential cause for these systemic changes could be related to rising RSL and the effects of transgression. It is well established that sediment that makes up the Windermere turbidite system is sourced from an Archean and Paleoproterozoic cratonic hinterland with a granite-granodiorite composition (Ross and Arnott, 2007). If at least partly coarse crystalline, the weathering product of these rocks would have provided an assemblage of siliciclastic grains that ranged from clay to pebbles – a polydispersed grain size distribution that is more consistent with aggradational channel fills. However, during transgression this polydispersed sediment, which now had become stranded on the flooded shelf, would have been extensively reworked by marine processes, and like conditions on modern continental shelves, sorted according to transport potential. The most mobile sediment fraction, specifically medium sand and finer, tended to follow the retrograding shoreline and built up barrier island complexes and also forced into estuaries filling incised valleys (Plint, 2010; Figure 4.8). Stranded relict, but more importantly palimpsest sediment, became mixed with minor carbonate sediment and formed the principal sediment source for turbidity currents, which would have been transported downslope during superimposed short-term 4^{th} and 5^{th} order sea level falls.

Significantly, these flows consisted of a rather unique assemblage of grain sizes – an anomalous abundance of coarse and very coarse sand. The consequence of this distribution is that flows became poorly density-stratified, comprising a basal layer of ~ uniformly dispersed coarse sand overlain sharply by a much finer-grained, lower-density suspension. The abrupt change in density from the lower to the upper part of the flow would have minimized interfacial mixing and helped to preserve flow momentum sourced mostly in the dense, basal part of the flow, which then

would have allowed these now highly efficient flows to bypass the channel and transport much of their sediment further down-dip (Arnott, 2007; Tilston et al., 2015). Additionally, the more or less uniform density of the basal part of the flow would resembled the structure in an open channel flow, and therefore in channel bends the development of circulation patterns resembling those in rivers. However, bypass conditions were probably interrupted episodically by erosion along the outer bend that promoted lateral expansion on the outer bend side of the channel. Upon entering this expanded region, later flows would have been less efficient and would have deposited coarse sediment along the inner bend (point-bar) of the channel to bring the channel back to equilibrium and therefore to "by pass" conditions (Arnott, 2007; see also van de Lageweg, 2014). Deposition of coarse sediment along the inner bend rather than along the base of the channel, as in aggradational channels, caused the channel to remain an open and hydraulically efficient conduit. Upon abandonment, and then later reactivation of the transport system, the underfilled relief of the original channel became the locus of later flows, and therefore the rejuvenation of the local transport system, and ultimately the development of an organized pattern of laterally-offset-stacked channels and their fills (Figure 4.5; sensu McHargue et al., 2011).

The final deposition stage of ICC1 is marked by a thick blanket of thin-bedded, fine-grained upper division turbidites that represents the local, caused by upflow channel avulsion, or potentially regional, due to continued relative sea level rise, abandonment of the ICC1 channel system.

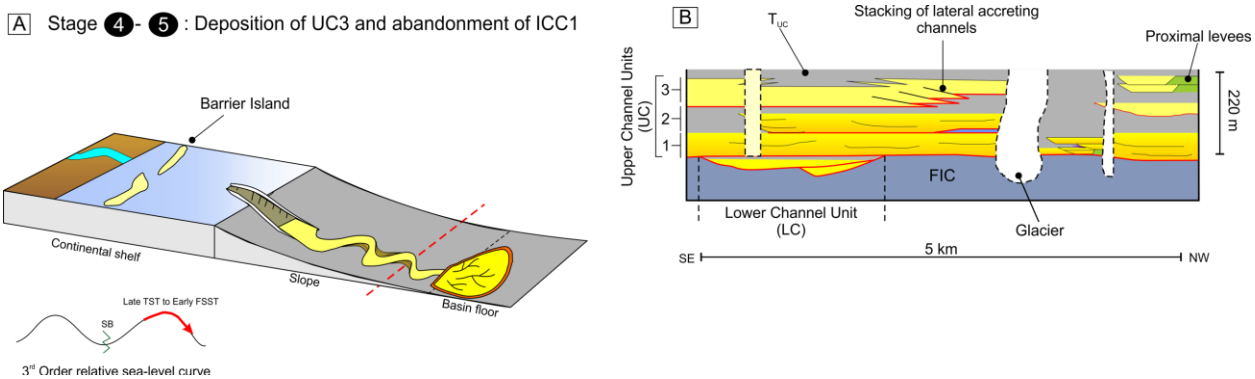

Figure 4. 8. *Schematic diagrams illustrating relative sea level (RSL) and sediment flux into the deep-marine realm. (A) The abrupt shift in stacking pattern from disorganized to organized is associated with late transgressive to early FSST conditions. As sea level rose and later stabilized, ~ coarse sediment became sequestered on the shelf and extensively reworked along late transgressive to highstand shorelines. Sediment being delivered downslope was not only coarse, but significantly moderately well-sorted, which in turn caused flows to have a plug-like density structure resembling that in open channel flows, like rivers. This, then, caused the lower, depositionally important part of the flow to operate much like a river where lateral channel accretion is a common phenomenon. Continuous lateral channel migration caused channels to remain underfilled and therefore the preferential site for later turbidity currents, which in the long term built up an organized pattern of successive lateral-offset-stacked channels and channel fills (B).*

4.3. Comparison to Other Deep-Marine Channel-levee Systems

4.3.1 Comparison to Channel Complexes Within the Isaac Formation

If RSL played a critical role in the spatial and temporal evolution of channel fill in ICC1, then intuitively, other slope-channel complexes in the Isaac Formation (Figure 4.9) should also exhibit similar lithological and geometrical attributes. Due to the lack of age control within the study area, or much of the Windermere turbidite system for that matter, it is not possible to accurately tie changes of stratigraphy with changes in RSL with absolute confidence. However, composition and granulometry of strata in the study area, specifically the occurrence of carbonate, carbonate-cemented sandstone and mudstone clasts, in addition to the abundance of quartz pebbles provides a lithological proxy for interpreting long-term eustatic changes.

Isaac Channel Complex 2 (ICC2) is separated from ICC1 by an up to 75 m-thick succession of fine-grained, very thin to thin-bedded upper division turbidites (TBT). ICC2 comprises at least five laterally accreting (LAD) channel fill complexes that each exhibit an organized stacking pattern (Arnott, 2007; Dumouchel, 2015). Channels are flat-based and filled with ungraded to graded coarse- and very coarse-grained sandstone and granule conglomerate with silty mudstone intraclasts. Like UC3, these channel fills show little change in grain size or bed thickness upward or laterally. In addition, at the top of most channel fills, coarse-grained strata exhibit a distinctive obliquely-inclined interfingering with thin-bedded, fine-grained turbidities and mudstone interpreted to be contemporaneous inner levee deposits (Arnott, 2007). Additionally, major and minor trace elements through ICC2 exhibit a geochemical signature suggesting a mixture of hinterland and shelf provenance. These conditions are interpreted to reflect 3rd order late TST and HST conditions and the input of a mixed supply of siliciclastic sediment with minor carbonate sediment (Milczarek, 2018). A similar pattern of laterally accreting channels exhibiting an organized stacking pattern has also been observed in Isaac units 14 and 21 (Dumouchel, 2015), the top of ICC3 (Huyer 2016), ICC4 (Mussa-Caleca, 2008), and ICC5 (Schwarz and Arnott, 2007a,b).

Thickly-developed channel complexes of ICC3 to ICC5 exhibit a complete upward evolution from aggradationally-filled channels with a disorganized channel pattern to laterally accreting channels with an organized stacking pattern (Navarro et al., 2007; Schwarz and Arnott, 2007a,b). The lowermost stratigraphic succession of ICC3 to ICC5 comprise channel fills, MTD and levee deposits that comprise anomalous carbonate detritus, both as primary carbonate fragments and carbonate-cemented sandstone clasts. For example, the MTD beneath ICC3 is areally extensive, thickly-developed (up to 110 m thick) and contains clasts of oolite and

stromatolite fragments (Arnott et al., 2011). Significantly, the uppermost part of the MTD has elevated Sr, Mg, and Ca contents. This, then, is followed by an abrupt increase in siliciclastic input above the base of ICC3 with a steady decline in carbonate element proxies, but an abrupt increase in siliciclastic indicators (i.e. Zr and Ti) (Milczarek, 2018). These changes, in addition to the rapid upward decrease and then absence of carbonate clasts in strata of ICC3, suggest that just above the base of ICC3 is a sequence boundary (note that the earlier work of Navarro et al. (2007) placed the sequence boundary at the base of ICC3). Similarly, MTDs that underlie ICC4 and ICC5 suggest elevated slope instability and mass wasting that most probably coincided with episodes of falling relative sea level, followed by the reintegration of poorly-sorted, siliciclastic-rich sediment that make up the channel fill for each complex.

The lowermost channel fills in ICC3 to ICC5 are dominated by anomalously coarse sediment (up to pebble conglomerate), and like channel fills of ICC1, namely LC through UC2, these channel fills exhibit well-developed upward, and in many cases, along strike fining and thinning trends (Navarro et al., 2007; Schwarz and Arnott, 2007a,b; Bergen, 2016) suggesting that they too, were filled aggradationally. Notably, these channel fills exhibit common cut and fill features suggesting multiple erosively juxtaposed channel fills with a spatially disorganized stacking pattern. The uppermost channel fills of ICC3, ICC4 and ICC5, exhibit an abrupt change in stacking pattern, and like UC3 of ICC1, comprise laterally-accreting channel fills that show negligible lateral or upward-fining or -thinning. These uppermost channel fills are then followed by a thick succession of thin-bedded, finer-grained, upper division turbidites associated with the local deactivation of the channel system.

Considered collectively, therefore, the lower part of channel complexes in the Isaac Formation consist of a disorganized stack of discrete, aggradationally-filled channels that

individually experienced negligible lateral migration. These channels are associated with late falling stage to early transgressive conditions associated with a long-term 3rd order change of relative sea level. At the top of the channel complex, on the other hand, strata consist of a systematic (i.e. organized) lateral-offset-stack of laterally-accreting channels most likely associated with late transgression–to early sea level fall (FSST). Collectively, this consistent depositional pattern suggests rhythmic, systematic changes in the character of the turbidity currents that transited the system. More specifically, the nature of the currents depended on the granulometric make-up and sorting of the sediment supply, which ultimately was controlled by 3rd order changes of eustasy.

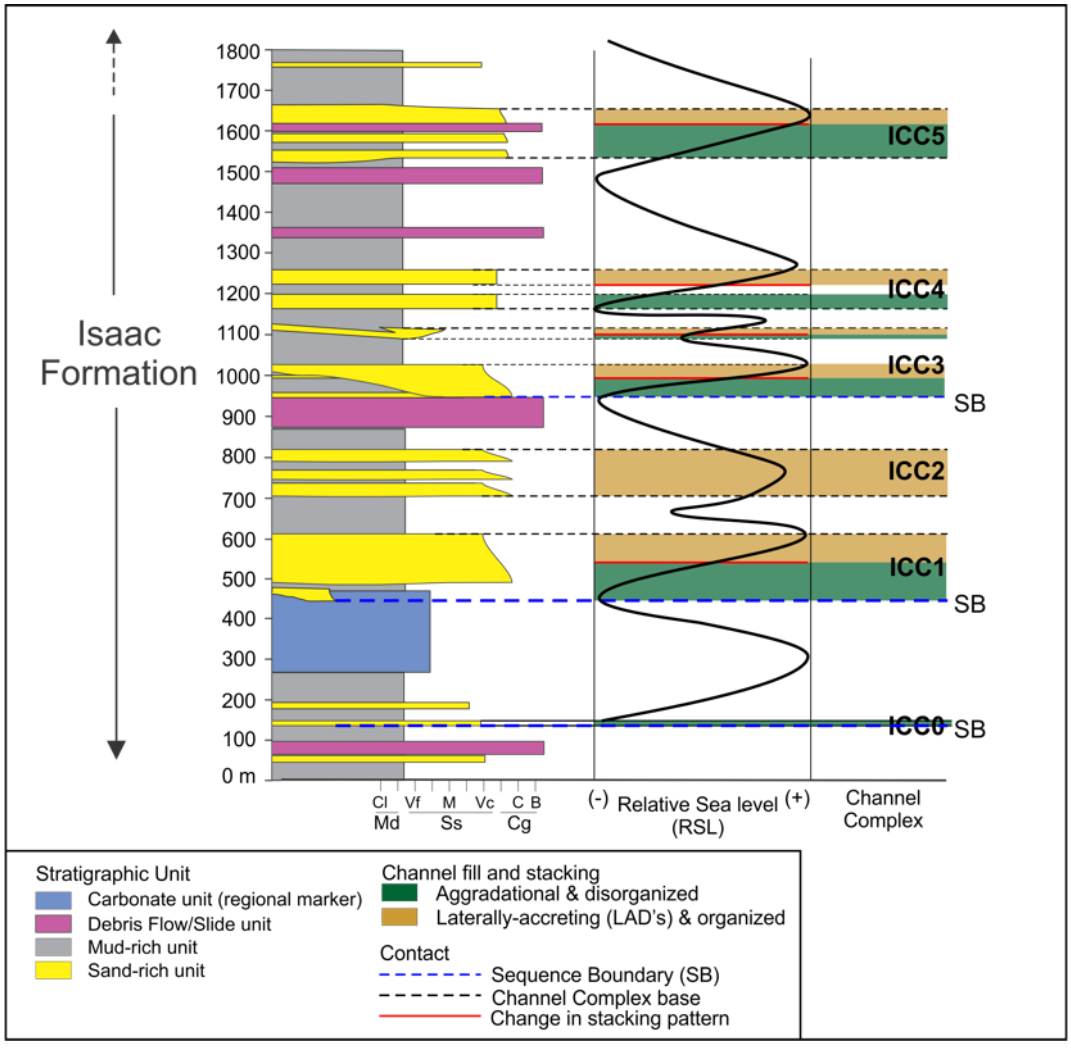

Figure 4. 9. *Generalized stratigraphic column for the Castle Creek study area showing the stratigraphic make-up of the Isaac Formation and relationship to interpreted 3rd-order changes of relative sea level. Note the consistent relationship between the position of RSL and channel-fill type and stacking pattern.*

4.3.2 Comparison with Channel Complex Systems Outside of the Windermere

The stratigraphic architecture of deep-marine slope channels has been well documented in a wide range of basin geometries and tectonic settings (see Table 1 for summary). In general, most of the systems that have been extensively studied document examples of aggradationally-filled channels; however, much less frequently reported from both the modern and ancient sedimentary records are meter- to several meter-scale laterally-accreting channel deposits.

Aggradationally-filled channels of ICC1 are of similar thickness to many of the slope channels described in the literature (see Table 1), which on average are ~ 8 – 12 m thick. However, due to the two-dimensionally of the outcrop and frequent incision by younger channels, widths could not be measured and, therefore, cannot be compared. Additionally, well-documented aggradationally-filled channels exhibit similar stratigraphic patterns, specifically vertical and lateral fining and thinning, which has been attributed to the deposition of strata by highly-stratified turbidity currents (i.e. Camacho, 2002; Kane and Hodgson, 2011; Hubbard et al., 2014). Less well-documented in the literature is the description of grain size characteristics in aggradational channels. However in a recent study of the 'Y Channel' on the western Niger Delta slope, Jobe et al. (2017) provided details of grain size distribution along the channel thalweg (axis), and like coarse-grained strata of aggradationally-filled channels of ICC1, sand-rich axial deposits of the Y channel exhibit a polydispersed grain size assemblage with all sizes, except at the extreme tails (coarse and fine) of the distribution, well represented. Moreover, recent outcrop examination of slope channels in the Los Molles Formation, Neuquén Basin in Argentina (Gan et al., 2019)

provided grain size analysis of channel deposits, and like aggradational channel fills of ICC1, are composed of very poorly- to poorly-sorted sandstone.

Unlike aggradationally-filled channels, LAD's are less well documented. Outcrops in the Rosario Formation, the Solitary channel, the Beacon Channel complex (Brushy Canyon Formation) and the Makarshka Flysch in Croatia are some of the few sedimentological studies that have interpreted deposition in laterally accreting channels (see Table 4.1). For example, the Rosario Formation in the San Fernando Canyon in northern Mexico is one of the best described examples in the literature with LAD's being between 2 and 5 m thick, 60 m wide and comprising thick-bedded, coarse-grained sandstone and conglomerate beds that dip at ~ 10 - 12^{o}. Within the channel fill beds fine and thin upward and also down dip (i.e. toward the channel thalweg) (Dykstra and Kneller 2009). In addition, some LAD's in the Rosario Formation have been reported to overlie aggradationally-filled channel complex and were better sorted than the underlying aggradational channel fills (Li et al., 2018; Kneller et al., 2020) – similar characteristics are observed in strata at the top of ICC1 (i.e. UC3 compared to the underlying stratigraphy).

A feature common to all reported LAD's is that they are commonly filled with coarse-grained sandstone with uncommon granule and pebble conglomerate and generally are distinctively coarser than aggradational channel fills. Therefore, the apparent absence of well-developed lateral accretion deposits in many deep-marine slope systems, may be associated with the lack of a sufficiently coarse, but more importantly, well-sorted sediment supply to alter the density structure of channelized flows and promote lateral channel migration.

Moreover, irrespective of the tectonic setting, at the channel complex and channel complex set scale, the stratigraphic evolution of submarine channels follows two discrete phases. The early stage is characterized by incision and lateral migration of the active channel. At this time, channels

exhibit extensive lateral mobility and migration, with large lateral offset between successive channel fills resulting in a spatially disorganized stacking pattern (i.e. Hodgson et al., 2011; Sylvester et al., 2011; Jobe et al., 2016). This, then, is followed by a later stage where channels migrate laterally but with a significant component of aggradation, resulting in a systematic lateral offset between successive channels and development of an organized stacking pattern. This general spatial and temporal evolution has been observed in many ancient deep-water channel systems worldwide (see Table 1) and attributed to systematic changes in the equilibrium gradient of the slope (Kneller, 2003). More specifically, the change from laterally offset to vertically stacked channel fills is a consequence of the equilibrium profile being initially lowered by large, erosive, efficient sandy flows that causes channel accommodation to be reduced and successive channels to preferentially form along a single horizon, leading to extensive (channel) cannibalization and deposition of a sheetlike, sand-rich layer. Later, accommodation progressively increases as the equilibrium gradient steepens in response to a reduction in flow efficiency, flow magnitude and mud content. This promotes aggradation of the channel floor and development and growth of channel-bounding levees. Under these conditions, channels remain underfilled and younger channels adopt a path that closely mimics the previous channels, and ultimately development of an organized, vertically aggrading succession of successive channels (Samuel et al., 2003; Kneller, 2003; Hodgson, 2011; McHargue et al., 2011; Jobe et al., 2016).

Emphasis on the progressive shift from large, frequent, erosive sandy flows to less frequent, smaller and more depositional muddy flows (i.e. Kneller, 2003; McHargue et al., 2011) has been thoroughly cited in the literature. This then, dictates the spatial and temporal evolution in the rate of net sedimentation in slope channels and their associated equilibrium profile. However, here it is argued that this upward change is instead caused by changes in the make-up of the

sediment supply, specifically grain size and grain sorting and their collective influence on the density structure of the channel-confined turbidity current that plays a critical role on influencing whether channel complexes will exhibit disorganized or organized stacking pattern (sensu McHargue et al., 2011). Ultimately, the upward change in sediment supply is controlled by the comparative volumetric input of hinterland versus palimpsest and relict shelf sediment. The granodiorite-granite composition of the hinterland sediment supply (Ross and Arnott, 2007) would most likely have provided a polydispersed sediment supply consisting of gravel to clay. In contrast, palimpsest and relict shelf sediment, which represents a residuum of comparatively better sorted sediment enriched in coarse-grained sediment, is related to transgressive reworking processes and temporary storage on the shelf. The upward change from hinterland- to shelf-dominated sediment supply is interpreted to be related to a long duration, most probably 3rd-order, rise of relative sea level. Superimposed on the long-term trend are multiple shorter duration (4^{th} / 5^{th} order) changes that were responsible for episodically transporting sediment to the shelf edge for resedimentation downslope and into the deep sea. As RSL rose the comparative contribution of shelf-derived sediment increased and eventually became the principal component in slope channel fills–conditions marked by channel fills in the lowermost part of LC (at the base of ICC1) and throughout UC3 (at the top of ICC1).

Type of Data		Location	Basin Type	Channel fill Dimension (Thickness/Depth by width)*	System Grain Size	Channel fill style		Channel Complex Dimension (Thickness by width)	Stacking Pattern	Controls on stacking pattern	Key References
Outcrop	**Isaac Channel 1**	**Canada**	**Passive Margin**	**Aggradational: 5- 15 m; LAD's: 8- 12 m ***	**mud to pebble**			**30-55 m by 1- 5 km**	**Disorganized --> Organized**	**Turbidity current density and velocity structure variations**	**This study**
Outcrop	Rosario Formation	Mexico	Forearc basin	Aggradational fills: at least 10 m by 300-400 m; LAD's = 2- 12 m by 15- 80 m	mud to cobble			50- 140m by 5- 7 km	Braided channels --> Sinuous Channels (LADs) or just LAD's	Equilibrium profile and accomodation on the slope	Dykstra and Kneller (2009); Janocko (2011); Li et al., (2018);Kneller et al., (2020)
Outcrop	Tres Pasos Formation	Chile	Retroarc foreland basin	6- 15 m, by 300 m	mud to pebble			130 m by 1.5 km	Disorganized --> Organized	Channel abandonment relief and lateral confinement	Macauley and Hubbard (2013)
Outcrop	Karoo Basin	South Africa	Retroarc foreland basin	10- 20 m by 100- 200 m	mud to fine-grained sandstone			30- 50 m by 300- 500 m	Disorganized --> Organized	Equilibrium profile and accommodation on the slope	Di Celma et al.,(2011); Hodgson et al., (2011)
Outcrop	Ross Formation	Ireland	Intracratonic (extensional)	Aggradational fills: avg. 5- 10 m by 100 m LAD's : 15 m by 100 m	fine- to medium-grained turbidites			25-35 m by 2.5- 5 km	LAD's, organized ?		Elliot (2000); Abreau et al., (2003)' lien et al., 2003; Wynn et al., (2007)
Outcrop	Capistrano Formation	USA		3- 20 m by 200- 400 m	mud to cobble			50- 60 m by 1.1- 1.2 km	Aggradational stacking pattern--> lateral migration and vertical aggradation	Seafloor degradation and aggradation	Camacho et al., (2002); Li et al., (2016)
Outcrop	Brushy Canyon Formation	USA	Intracratonic (extensional)	Aggradational fills (base-of-slope): 3- 10 m by 50- 400 m; LAD's: 5- 10m, 100 m	mud to medium-grained sandstone			aggradational: 35 m by 600 m; LAD's: 15-20 m by several 100 m	Aggradationall-filled channels exhibit multilateral fills --> vertically stacked fills	progressive increase of slope confinement restricting lateral movement	Gardner and Borer (2000); Pyles et al., (2010)
Outcrop	Nanaimo Group	Canada	Forearc basin	10- 15 m *	mud to very coarse-grained sand			80- 120 m by 1- 4 km**	laterall offset (migrating) channels--> vertically stacked (aggrading)	Equilibrium profile and accommodation on the slope	Bain and Hubbard (2016); Englert et al. (2020)
Outcrop	Solitary Channel	Spain	Intracratonic (compressional)	25 m by 150 m	conglomerate				LAD's, organized ?		Kleverlaan et al., (1989); Wynn et al., (2007)
Outcrop	Makarska		Passive Margin	6 m by 40 m	pebble conglomerate				LAD's, organized ?		Janocko (2011)
Seimic	Niger Y channel	Egypt	Passive Margin	N/A	mud to coarse-grained sand, uncommon gravel			120 m by 200 to 800 m	lateral migrating channels --> aggradational channels	Changes in sediment supply	Jobe et al., (2015); Jobe et al., (2017)
Seismic	CL3 Indus Fan	Egypt	Passive Margin	10- 50 m, by 120- 500 m	mud to gravel				lateral migration--> aggradation	Increase of inner levee confinement	Deptuck et al., (2007), Sylvester et al., (2011)
Seismic	Bengal Fan	India	Passive Margin	18-30 m by 200- 400m				300- 500 m by 5-15 km	lateral migration-> aggradation		Kolla et al., (2012)
Seismic	Amazon Fan	Offshore Brazil	Passive Margin	2 - 60 m by 1.2- 1.5 km	mut to very coarse-grained sandstone				lateral migration-> aggradation	Equilibrium profile	Pirmez et al., (2000);Pirmez and Ingram (2003)
Seismic	Nile Delta	Egypt	Passive Margin	10- 20 m by 50- 200 m	mud to coarse-grained sandstone				lateral amalgamated channels --> aggradational channels	Equilibrium profile and accommodation on the slope	Samuel et al., (2003); Cross et al., (2009)
Conceptual	Forward Model	N/A	N/A	avg. 13 m by 200 m	N/A			Used at various scales	Disorganized --> Organized	Equilibrium profile and channel abandonment relief	McHargue et al (2011)

*	2D outcrop inhibits accurate estimate of width, only thickness is available.
**	Channel Complex set dimensions
	This study
	Aggradationally-filled
	Lateral-accretion filled

Table 4. 1. *Summary of outcrop, seismic and stratigraphic model examples of deep-marine channel-levee systems.*

4.4 Implication for Reservoir Exploration and Development

Slope channel deposits of ICC1 are comparable in thickness to modern offshore deep-marine systems and, therefore, can be a useful analogue for predicting the stratal architecture of slope channel hydrocarbon reservoirs at the sub-seismic scale.

Each of the two end-member channel fill types recognized in this study would exhibit different reservoir quality characteristics. At the channel fill scale, the sandstone thickness to total stratal thickness, or more colloquially, net-to-gross (N:G) varies from 0.88 to 0.93 in axial strata, but decreases to 0.70 as strata fine, thin and become more interbedded with mudstone in channel margin strata. However, it is important to note that the coarsest axial deposits of aggradationally-filled channels (LC, UC1 and UC2) are characteristically poorly sorted, which would reduce intergranular volume. In contrast, laterally accreting channel fills of UC3 have the highest N:G (0.98), and although on average are slightly finer grained than axial strata of aggradational channels, but still composed of coarse to very coarse sandstone, are notably better sorted (Figure 4.2C and Figure 4.10). Additionally, UC3 channel fills, which are of the order of 10 m thick, show negligible change in grain size or texture upward or along strike over 100s to 1000s of meters, with few or any barriers, and baffles in the form of local clusters of mudstone intraclasts. Moreover, these channels are typically capped by a thickly-developed succession of thin-bedded, upper division turbidites that might provide an effective reservoir seal.

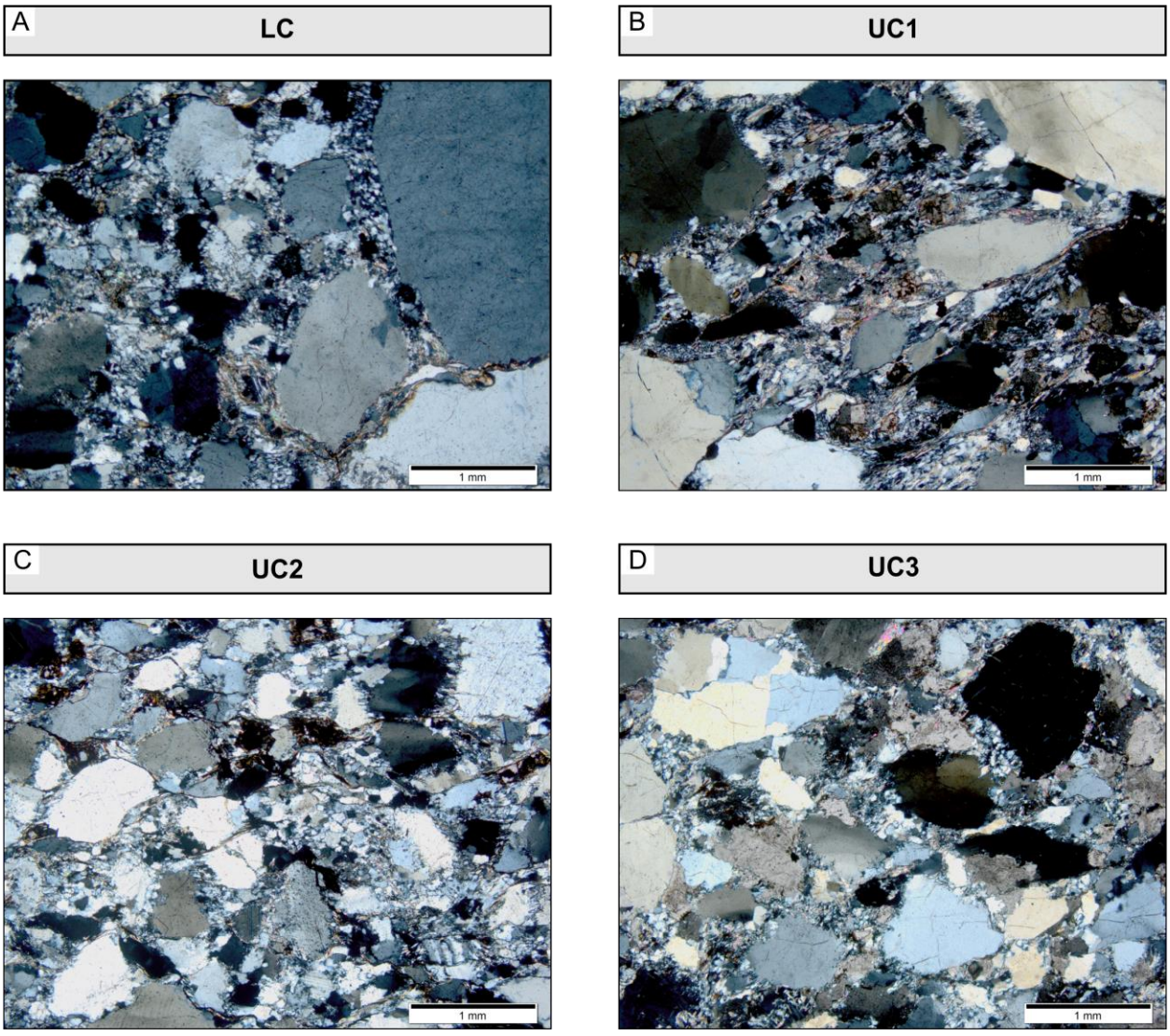

Figure 4. 10. *Representative photomicrographs of thick-bedded, coarse-grained sandstone from each of the four channel units that comprise ICC1. In all examples the principal framework component is quartz grains with variable amounts of calcite cement (highest in UC3). Note the more poorly sorted texture of aggradational channel fills (LC, UC1, UC2) compared to lateral accreting channel fills (UC3). Accordingly, intergranular volume would be highest in laterally accreting channel fills. Also, note the significantly higher intergranular volume filled with calcite cement (grey-brown patches) in UC3 sandstone.*

Chapter 5: Conclusions and Areas for Future work

5.1 Summary

Continental slope channels are the primary conduits for transporting sediment from the hinterland to deeper parts of basins, and in the ancient sedimentary record represent significant hydrocarbon reservoirs. Studies from modern and shallowly-buried deep-water systems have provided significant insight into turbidite channels; however, our understanding of the mechanistic processes and depositional controls responsible for the initiation, fill and abandonment of slope channels remain poorly understood. Accordingly, studies in the ancient deep-marine sedimentary record are potentially the best way to unravel many of these unknowns. At the Castle Creek study area a superbly exposed, thickly developed and areally expansive leveed-channel complex in the Windermere turbidite system, Isaac channel complex 1, or simply ICC1, crops out. Detailed documentation of the lithological composition and stratigraphic relationships of inter- and intra-channel fills allowed for a comprehensive examination of the complex history of erosion and deposition in a leveed slope-channel system.

ICC1 is 220 m-thick, exposed over 5 km along strike, and erosionally overlies mixed carbonate-siliciclastic strata of the first Isaac Carbonate (FIC). ICC1 consists of four vertically-channel units (LC and UC1-UC3). Strata of ICC1 comprise three stratal elements, each composed of a unique combination of stratal geometry, scale and lithological composition. These are: channel fills (aggradationally- and laterally accreting), overbank deposits (abandonment, proximal and distal levees), and debrites.

Siliciclastic strata of LC comprise three nested channel fills, each about 10 to 15 m thick and composed of amalgamated, thick-bedded, very coarse-grained sandstone and conglomerate in

their axis that fine and thin upward and laterally. Strata of LC are confined to the southeast part of the study area where they onlap an erosional surface incised at least 30 m deep into strata of the FIC. The top of LC is mantled by a laterally continuous succession of thin-bedded, fine-grained upper division turbidites interpreted to indicate abandonment of the local transport system. UC, in contrast, is 95 m thick and crops out across the entire study area. UC1 and UC2 are, respectively, 50 m and 25 m thick, bounded on their margins by erosional surfaces that scour fine-grained abandonment deposits and in two places by levee deposits. UC1 and UC2 exhibit common cut and fill characteristics suggesting multiple erosively juxtaposed channel fills that are 4 to 12 m thick. UC1 is dominated by coarse-grained, graded, massive or cross-stratified sandstone that show little lithological change upward or laterally. UC2, on the other hand, comprises nested channel fills that are ~5 to 8 m thick and composed of coarse-grained sandstone that progressively fine and thin upward and laterally. Strata in LC, UC1 and UC2 show a progressive decrease in modal grain size, but collectively exhibit a polydispersed granulometry (platy- to mesokurtic). Based on upward and lateral facies trends, channels of LC, UC1 and UC2 are interpreted to have been filled aggradationally. Turbidity currents that transitted and filled these channels are interpreted to have been highly density-stratified, which resulted in intense interfacial mixing with attendant energy loss and significant deposition.

UC3, on the other hand, is up 30 m thick and comprises at least six laterally-accreting channel fills. Channel fills in UC3 exhibit well developed lateral-accretion deposits that populate a succession of flat-based, lateral-offset-stacked channels that on one side erosionally onlap thin-bedded, finer-grained turbidites, and on the other interfinger obliquely upward with thin-bedded, finer-grained turbidites. Channel fills are up to 10 m thick and filled with coarse-grained sandstone and conglomerate that show little upward or lateral change in grain size or bed thickness.

Distinctively, strata consist of dispersed red-colored sandstone clasts cemented with a pervasive ferroan calcite cement. In comparison to the granulometric make-up of aggradationally-filled channels LC, UC1 and UC2, strata in UC3 channels are better sorted and more negatively skewed. This caused the through-going flows to adopt a more even near-bed density-profile; specifically, a dense, coarse-grained basal layer of more or less uniform sediment concentration overlain abruptly by a much finer grained, lower density suspension (Tilston et al., 2015). This plug-like density profile resembles that observed in open channel flows, and as a consequence caused the lower, depositionally important part of the flow to operate much like a river in channel bends. Here then, lateral accretion, like in fluvial systems, rather than aggradation, dominated and formed the laterally accreting channels and channel fills of UC3.

The Neoproterozoic Era was an exceptional time punctuated by extreme environmental events, including long-term intra- and interglacial periods, which may have played a critical role in shaping the deep-marine sedimentary record along the passive continental margin of Laurentia. Here it is hypothesized that a well-defined shelf-slope break separated the basinward continental slope and basin floor from a variably developed continental shelf. Moreover, the erosive juxtaposition of ICC1 above mixed carbonate-siliciclastic strata of FIC, in addition to internal lithological and geochemical trends, are interpreted to be the stratigraphic manifestation of a 3rd order fall and then rise of relative sea level; the fall coinciding with the onset of the Gaskiers glaciation (Cochrane et al., 2019). Therefore, siliciclastic strata of ICC1 represent the reintegration of a voluminous sediment supply into the deep-water Windermere basin, and therein an unparalleled opportunity to better understanding how external factors, like sea level changes and sediment supply affect the stratigraphic evolution of submarine channels (Figure 5.1).

Calciturbidite deposition at the top of the FIC was interpreted by Navarro (2016), Cochrane (2018) and Cochrane et al. (2019) to coincide with a long-term (3rd order) fall of relative sea level. Attendant early seafloor cementation and lithification would have steepened the continental slope beyond those more typical of siliciclastic systems (Ross et al., 1994). As relative sea level continued to fall erosion and transport bypass dominated on the slope as the system regraded, which in the southeast end of the study area is manifest by a 30 m-deep incision into the top of the FIC. This was then succeeded by the inception and early stages of channel-filling in ICC1. Channel fills in the lowermost ~ 8 - 10 m of LC are filled with a distinctively coarse-grain mix of siliciclastic sediment, in particular abundant quartz pebbles, and dispersed gravel-size carbonate-cemented sandstone and mudstone clasts. These sediments are interpreted to represent the late stages of slope regrading near the end of the 3rd-order relative sea level fall. With the ensuing lowstand, erosion on the slope and shelf diminished, and younger LC channel fills were filled with generally finer sediment that most probably was being principally sourced from the hinterland. Similarly, channel fills of UC1 are interpreted to be associated with lowstand conditions to early 3rd order rise of relative sea level, and sediment being sourced directly from the hinterland. With continued transgression, channel fills in UC2 were filled with sediment sourced from the hinterland but increasingly with palimpsest and relict sediment eroded from the ever-expanding shelf. Considering grain size characteristics and vertical and lateral facies trends, LC, UC1 and UC2 comprise a disorganized stack of discrete, aggradationally-filled channels that individually experienced negligible lateral migration. The polydisperse make-up of these channel fills suggests that flows had a rapidly-diminishing-upward density profile that resulted in intense interfacial mixing, which then reduced transport efficiency and promoted in-channel sedimentation that exceeded sedimentation over the interchannel area. This caused the channel floor to become

superelevated (i.e. Bryant et al. 1995) which in turn promoted avulsion onto a topographically lower, and accordingly more hydraulically efficient area on the seafloor (Figure 5.1) – the stratigraphic manifestation being a disorganized stack of aggradationally filled channels.

In contrast, UC3 comprises an organized lateral-offset-stack of laterally-accreting channels. Geochemical analysis of mudrocks at the base of UC3 and the abandonment deposits at the top of ICC1 indicate a reduction in hinterland proxies (Si/Al, Ti, Zr, Th) and an increase in carbonate proxies (Ca, Sr, Mg and Mn). In addition, grain size analysis indicates that UC3 strata are distinctively better sorted and more coarse-grained skewed compared to those in aggradationally-filled channels. Deposition of UC3, therefore, was most likely associated with late 3rd order transgression, HST to early falling stage conditions. During the long-term transgression relict, but more importantly, palimpsest coarse sediment associated with multiple shorter-term regressive-transgressive cycles built up an increasingly voluminous reservoir of coarse-grained sediment, which then became a major source of sediment delivered to the shelf edge and resedimented downslope during UC3. This coarse and moderately well-sorted sediment would have resulted in highly efficient flow with a plug-like density profile, and therefore negligible interfacial mixing. This caused the flows to function much like that in rivers, and in channel bends develop a circulation pattern that promoted erosion on the outer bend and commensurate deposition on the inner bend. This then caused channels to remain open, hydraulically efficient transport conduits (Figure 5.1), and sedimentation confined principally to the inside margin of channel bends (i.e. point bars).

	Aggradational Channel Fill	Laterally Accreting Channel Fill
Lateral facies trend	well-developed axis to margin (< 100 m) fining and thinning	Negligible lateral fining and thinning
Vertical facies trend	well-developed upward fining and thinning	Negligible upward fining and thinning
Grain size distribution	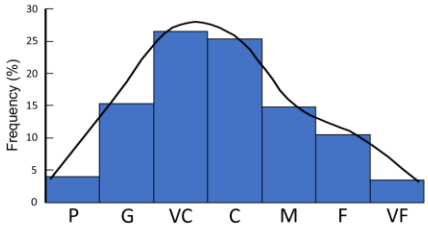	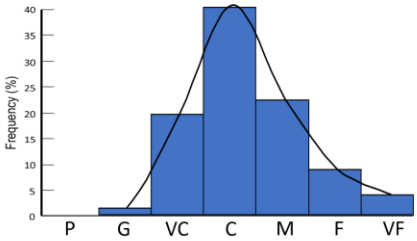
Density and velocity profile	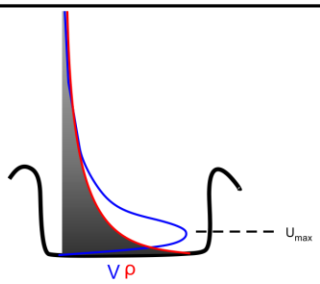	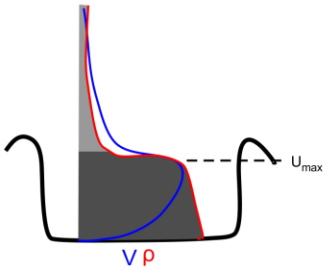
Channel fill style	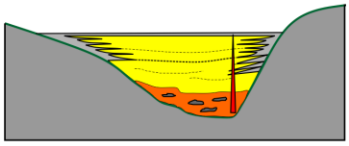	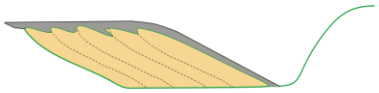
Stacking pattern	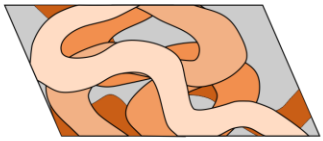	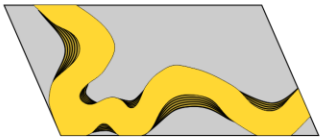
Sequence stratigraphy	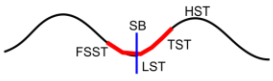	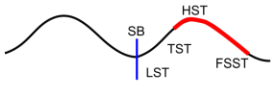

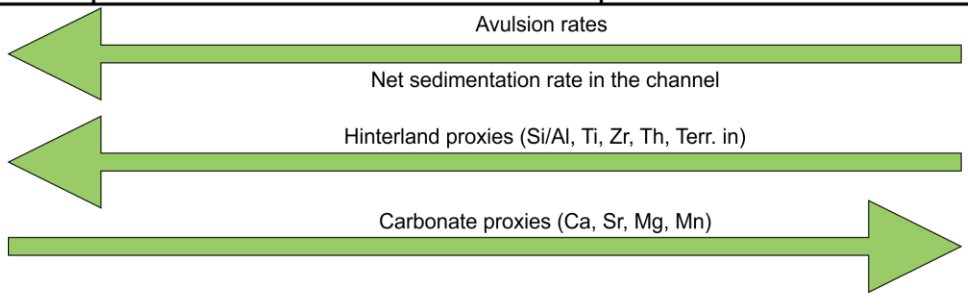

Figure 5.1. *Comparison between aggradationally-filled and lateral-accreting channel fills. Relationship between grain size distribution and nature of channel fill. Aggradational channel fills have a more polydispersed size distribution compared to laterally accreting channel fills. This difference controlled the density, and in turn, velocity structure of the through-going turbidity currents; respectively, a highly stratified profile with Umax close to the bed compared to a plug-like density profile with Umax elevated far from the bed. These differences in flow characteristics influenced how the channels evolved in space and time; specifically, channels filled aggradationally and stacked in a disorganized pattern versus laterally accreting with an organized stacking pattern. Aggradationally-filled channels develop during the long-term (3rd order) late falling stage (FSST) and into the early part of the transgressive systems tract (TST). Laterally-accreting channels develop preferentially during the late transgressive (TST) into the early part of the ensuing falling stage systems tract (FSST).*

Central to the above model is the temporal change of sediment supply to the Windermere turbidite system. Significantly, similar lithological and architectural patterns are observed in other Isaac channel complexes, for example ICC3 (Navarro et al., 2007; Huyer, 2016) and ICC5 (Schwarz and Arnott, 2007), suggesting systematically recurring changes in the granulometric make-up of the sediment supply, which here is interpreted to be tied to the long-term (3rd order sea level) expansion and contraction of the continental shelf, and the associated build-up and then depletion of palimpsest and relict shelf sediment – sediment that was transported to the shelf-slope break by higher frequency sea level changes (possibly 4th and 5th order). These sediments are the result of transgressive reworking and accumulation of a coarse-grained lag of immobile (relict) and partly mobile (palimpsest) sediment (Figure 5.2). On parts of the modern Newfoundland shelf, for example, well-sorted sand and gravel mixed with abraded carbonate detritus makes-up to 30% of sea floor sediment (Piper, 1991). Here, relict is considered to be sediment coarser than upper very coarse sand (least mobile coarse sediment fraction), which in general are uncommon grain sizes in much of the Castle Creek study area. Palimpsest, on the other hand is taken to be sediment between upper very coarse and upper coarse sand (more mobile coarse sediment fraction). Interestingly, Russell (1968) pointed out that very coarse- to granule-size sediment is generally uncommon in most fluvial and shallow-marine sedimentary environments, but especially abundant

along shorelines. Here constant wave agitation results in selective transport of finer and coarser grained sediment, and the preferential accumulation of the intervening grain sizes. During an ensuing transgression this and coarser sediment becomes smeared across and stranded on the now flooded wave ravinement surface, and therein made available for basinward resedimentation during a later regression. It is these grain sizes that are interpreted to constitute the coarse-grained residuum of relict and palimpsest sediment that formed by transgressive reworking during short-term, but more profoundly by the gradual expansion of the shallow-marine realm during the longer-term rise of relative sea level.

Theoretically, during the early stages of the long-term fall of relative sea level (FSST) one of the principal sources of sediment that was mobilized downslope would have been residual palimpsest and relict sediment from the continental shelf, in which the more mobile palimpsest fraction was most probably proportionately more abundant in the through-going turbidity currents. Evidence of mid to early-late FSST channel fills are absent in strata of ICC1, and may only be represented by the erosion surface that separates early channel fills of the lower channel unit and the FIC. However, as noted above, the lowermost 8 - 10 m of channel fills of the lower channel unit (LC) consist of abundant quartz pebbles and granules, and carbonate-cemented sandstone and carbonate clasts, which collectively are interpreted to be coarse shelf sediment that was remobilized downslope during the late FSST. These distinctively coarse-grained strata consist of an anomalous abundance of relict shelf sediment, which most likely reflects the preferential remobilization, and therefore depletion of the more mobile palimpsest fraction during the earlier stages of the FSST (Figure 5.2). The relative abundance of relict sediment then decreases stratigraphically upward as the shelf continued to shrink in areal extent and became progressively depleted of its relict and palimpsest sediment. With the onset of the 3rd order lowstand the shoreline

had progressed to its lowest, most basinward position, which likely coincided with the shelf-slope break and sediment being principally sourced from the hinterland. During lowstand (most of LC and UC1) relict and palimpsest sediment began to once again accumulate during short-term (4^{th} and 5^{th} order) transgression and highstand conditions. However, due to limited accommodation on the shelf, available storage was negligible and much of the accumulated sediment was remobilized downslope during short-term sea level falls. However, as the long-term rise of sea level continued (UC2), shelf width and depth increased and provided a progressively more expansive surface on which relict and palimpsest sediment could be efficiently formed and stored. With continued relative sea level rise and into the HST and possibly as late as the early FSST (UC3), the palimpsest fraction came to overwhelm the relict component and dominate the sediment flux to the shelf edge during superimposed short duration episodes of sea level fall, while the immobile fraction (relict) accumulated and became an increasingly more voluminous part of the shelf sediment reservoir. This sediment was then remobilized and moved basinward during the subsequent long-term sea level fall (Figure 5.2).

These results, therefore, provide insight into the possible control of long- and short-term changes of relative sea level, potentially linked to high frequency, high amplitude glacio-eustatic changes, on the deep-marine sedimentary record. However, much of the current literature links changes in the stratigraphic style during a single depositional sequence to systematic changes in the volume and sand-to-mud ratio of the sediment supply in response to 4^{th} order sea level rise and fall (i.e. Chiocci, 2000; Kneller, 2003). Moreover, sediment supply is interpreted to have remained constant and only substrate stability and the distance from the shoreline to the shelf-slope break changed. Here, however, it is suggested that long-term eustatic changes influenced shelf accommodation (width and depth), and therefore, the potential for sediment storage, particularly

of coarse sediment, on the continental shelf. This in turn, controlled the granulometry of sediment available for through-going turbidity currents on the slope, which profoundly changed the properties of the turbidity currents (density structure) and controlled the channel fill style and the spatial and temporal stacking patterns in ICC1. Understanding these changes, therefore, is key to resolving the spatial and temporal evolution of slope channels, particularly in similar large-scale, shelf-slope-basin floor passive margin systems.

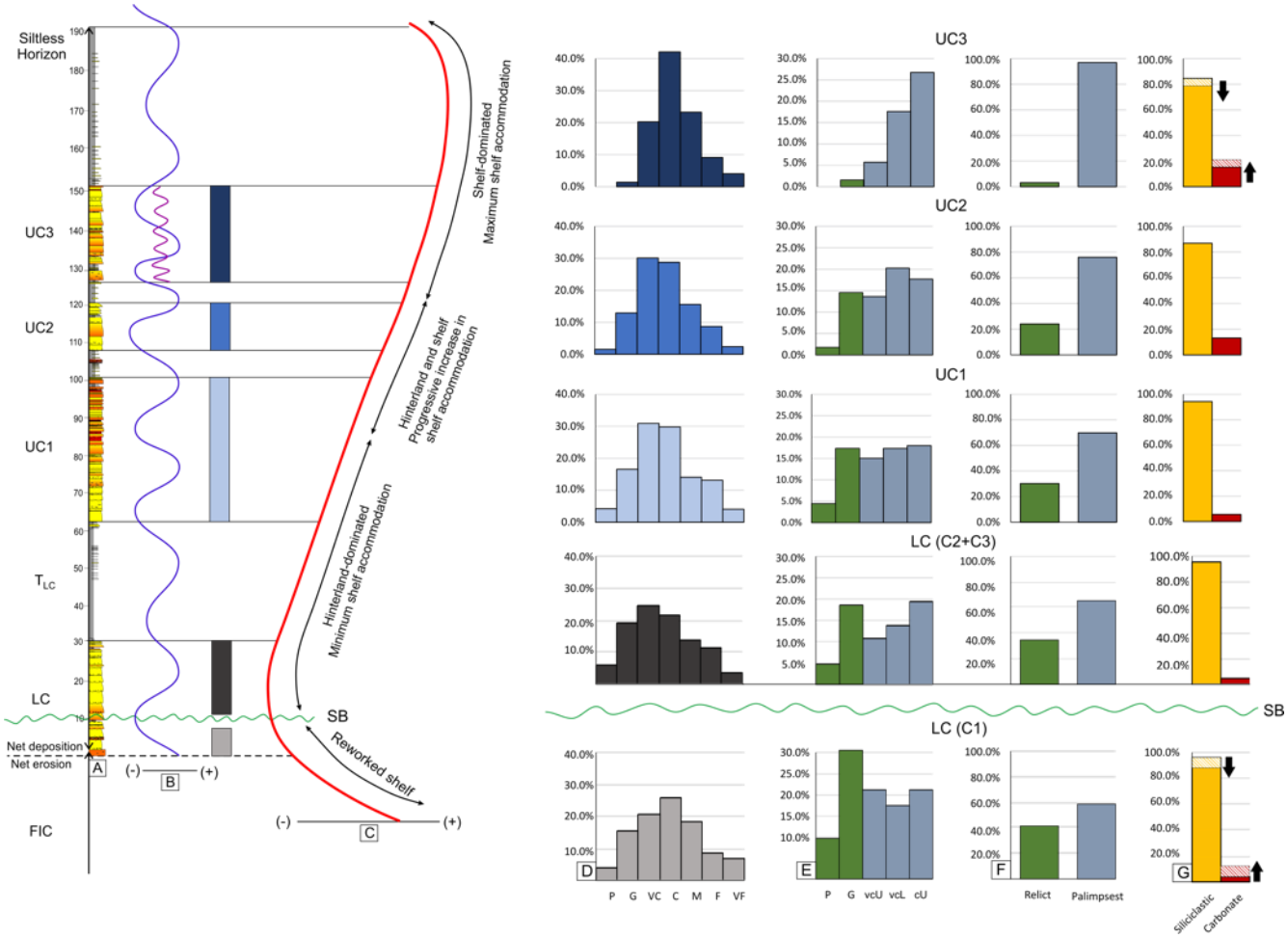

Figure 5. 2. *(A) Schematic stratigraphic section of ICC1. (B) Short-term 4th (blue curve) and 5th (purple curve) order relative sea level curve; high frequency lowstands are interpreted to be the main mechanism that transported coarse sediment to the shelf-slope break. (C) Long-term (3rd order) relative sea level curve. Note that the coloured bars to the left of the curve correlate with individual channel units identified by the same coloured grain-size histogram in (D). Histograms in (D) show the frequency percentage (%) of full grain size distribution; C1 represents the lowermost channel fill of LC and is interpreted to represent the composition of channel fills during late FSST. These strata are then overlain progressively by the channel fills of LC through to UC3. Note that stratigraphically upward the grain size distribution becomes more narrowly confined to the central part of the distribution. (E) Frequency percentage (%) of the coarse sediment fraction (i.e. upper coarse sand and coarser). Note the progressive upward decrease in the coarsest fraction and enrichment in the finer-grained fraction, namely upper coarse and lower very coarse sand. (F) During transgressive reworking the least mobile sediment (green columns in E) represents relict sediment whereas the more mobile coarser fraction (grey columns in E) represents palimpsest sediment. Note the pronounced increase in the palimpsest fraction in UC3, which is interpreted to coincide with the maximum expanse of the shelf during with the late transgressive to early falling stage systems tract of a 3rd order relative sea level fluctuation. (G) Frequency percentage (%) of siliciclastic framework grains and carbonate cement. Stratigraphically upward, carbonate cement decreases in UC1 but steadily increases in UC2 and UC3 (carbonate cement is interpreted to be recrystallized detrital carbonate grains). The cross-hatched area at the top columns LC1 and UC3 represents the contribution of carbonate-cemented sandstone and mudstone clasts to the carbonate fraction. Because these particles are so large, and therefore avoided during sample collection in the field, they are underrepresented in thin section analysis. Nevertheless, visual estimates in the field suggest they represent an important component in channel fills of LC- C1 and UC3.*

5. 2 Areas for future Research

ICC1 crops out at Milk River, which is ~ 20 km along depositional dip from the Castle Creek study area. Future stratigraphic measuring, mapping and sampling could further develop a more regional depositional history for ICC1. In addition, chemostratigraphic analysis of mudrocks by Milczarek (2018) were only collected in Castle Creek south, sampling through mudstone-rich strata above LC and UC1 in Castle Creek southeast could help further refine the sequence stratigraphic framework of ICC1.

While aggradationally-filled channels have been extensively studied in many tectonic settings, laterally-accreted channel fills, on the other hand, remain enigmatic and future studies should focus on documenting the stratigraphic architecture of these channels to create a more robust spatial and temporal model. In addition, a more exhaustive comparison of the granulometric make-up in

aggradational and laterally-accreting channel fills in other Isaac channel complexes, and also elsewhere in the geological record, should also be conducted to build a more statistically significant dataset for comparison between channel complexes of different age and in different tectonic settings.

Additionally, stratigraphic forward modelling (i.e. McHargue et al., 2011; Sylvester et al., 2011) and flume tank experiments (i.e. Peakall et al., 2007; Straub et al., 2008) have increasingly become a tool to better understand channel-filling processes and as predictive models for the spatial and temporal evolution of slope channels. Although results exhibit similar patterns seen in outcrop and seismic data, current models assume that the structure of the through-going turbidity currents remains constant despite interpreted changes in sediment caliber (sand-rich vs. mud-rich flows). Future models and experiments should carefully study the effects of turbidity current structure and its effect on how channel fill and stack, and how those patterns evolve in time and space.

Reference List

Aalto, K.R. (1971). Glacial marine sedimentation and stratigraphy of the Toby Conglomerate (Upper Proterozoic), southeastern British Columbia, Northwestern Idaho and Northeastern Washington, Canadian Journal of Earth Sciences, **8**: 753-787.

Abreu, V., Sullivan M., Pirmez C., Mohrig D., & Mutti E. (2003). Lateral accretion packages (LAPs); an important reservoir element in deep water sinuous channels. *Marine and Petroleum Geology*, 20, p.631–648.

Allen, J. R. L. (1964). The Nigerian continental margin: bottom sediments, submarine morphology and geological evolution. *Marine Geology*, *1*(4), 289-332.

Anthony, D. (2011). Architectural and Depositional Evolution of a Neoproterozoic Deep Marine Slope Channel Complex: Isaac Formation, Windermere Supergroup, southern Canadian Cordillera (unpublihed B.Sc. thesis, University of Ottawa).

Armitage, D. A., Romans, B. W., Covault, J. A., & Graham, S. A. (2009). The influence of mass-transport-deposit surface topography on the evolution of turbidite architecture: The Sierra Contreras, Tres Pasos Formation (Cretaceous), southern Chile. *Journal of Sedimentary Research*, *79*(5), 287-301.

Arnott, R.W.C., and Al-Mufti, O. (2017). Deep-marine pseudo dune cross-stratification – Similar, but not completely different, Journal of Sedimentary Research, **87**: 312-323.

Arnott, R.W.C. (2007). Stratal architecture and origin of lateral accretion deposits (LADs) and conterminuous inner-bank levee deposits in a base-of-slope sinuous channel, lower Isaac Formation (Neoproterozoic), East-Central British Columbia, Canada, Marine and Petroleum Geology, **24**, p.515-528.

Arnott, R. W. C. (2010). Deep-marine sediments and sedimentary systems. In *Facies models 4*, p.295-322. Geological Association of Canada, St. John's, Newfoundland and Labrador.

Arnott, R.W.C. (2012) Turbidites, and the case of the missing dunes, Journal of Sedimentary Research, **82**: 379-384.

Arnott, R. W. C., and Hand, B. M. (1989). Bedforms, primary structures and grain fabric in the presence of suspended sediment rain. *Journal of Sedimentary Research, 59*(6), 1062-1069.

Arnott, R.W., Hein, F.J. (1986). Submarine canyon fills of the Hector Formation, Lake Louise,

Alberta: Late Precambrian syn-rift deposits of the proto-Pacific miogeocline, Bulletin of Canadian Petroleum Geology, **34**: 395-407.

Arnott, R. W. C., Wallace, K., Laurin, J., Shipp, R. C., Weimer, P., & Posamentier, H. W. (2011). Stratal architecture and temporal evolution of a passive margin mass-transport deposit, Neoproterozoic Isaac Formation, Cariboo Mountains, British Columbia, Canada. *Mass-transport deposits in deep-water settings: SEPM Special Publication*, *96*, 221-234.

Bain, H. A., & Hubbard, S. M. (2016). Stratigraphic evolution of a long-lived submarine channel system in the Late Cretaceous Nanaimo Group, British Columbia, Canada. *Sedimentary Geology*, *337*, 113-132.

Bergen, A. (2017). Vertical and lateral facies architectures of slope channels and genetically related levee deposits, Isaac Formation, Neoproterozoic Windermere Supergroup, Cariboo Mountains, B.C. M.Sc. thesis, University of Ottawa, Ottawa, ON.

Billington, T. (2019). Sedimentologic and Petrographic Evidence of Flow Confinement in a Passive Continental Margin Slope Channel Complex, Isaac Formation, Windermere Supergroup, British Columbia, Canada. M.Sc. thesis, University of Ottawa, Ottawa, ON

Bouma, A.H., (1962). *Sedimentology of some Flysh Deposits. A graphic approach to facies interpretation.* Elsevier, Amsterdam, p.168.

Brami, T. R., Pirmez, C., Archie, C., Heeralal, S., & Holman, K. L. (2000). Late Pleistocene deep-water stratigraphy and depositional processes, offshore Trinidad and Tobago.

Bryant, M., Falk, P., & Paola, C. (1995). Experimental study of avulsion frequency and rate of deposition. *Geology*, *23*(4), 365-368.

Clark, J.D, N.H. Kenyon, and K.T Pickering. (1992). Quantitative analysis of the geometry of submarine channels: implications for the classification of submarine fans. Geology, **20**, p.633-636.

Clark, J. D., & Pickering, K. T. (1996). Architectural elements and growth patterns of submarine channels: application to hydrocarbon exploration. *AAPG bulletin*, 80**(2)**, p.194-220.

Camacho, H., Busby, C. J., & Kneller, B. (2002). A new depositional model for the classical turbidite locality at San Clemente State Beach, California. *AAPG bulletin*, *86***(9),** 1543-1560.

Campbell, R.B., Mountjoy, E.W., and Young, F.G. (1973). Geology of McBride map-area, British Columbia, Geological Survey of Canada, Paper 72-35, 103 p.

Campion, K. M., Sprague, A. R., Mohrig, D., Lovell, R. W., Drzewiecki, P. A., Sullivan, M. D., & Sickafoose, D. K. (2003). Outcrop expression of confined channel complexes.

Colpron, M., Logan, J.M., and Mortensen, J.K. (2002). U-Pb zircon age constraint for late

Neoproterozoic rifting and initiation of the lower Paleozoic passive margin of western Laurentia, Canadian Journal of Earth Sciences, **39**, 133-143.

Canals, M., & Lastras, G. (2004). Slope failure dynamics and impacts from seafloor and shallow.

Catuneanu, O., (2006). Principles of Sequence Stratigraphy: Amsterdam, Elsevier 375

Catuneanu, O., Abreu, V., Bhattacharya, J. P., Blum, M. D., Dalrymple, R. W., Eriksson, P. G., & Giles, K. A. (2009). Towards the standardization of sequence stratigraphy. *Earth-Science Reviews*, *92*(1-2), 1-33.

Chiocci, F.L. (2000). Depositional response to Quaternary fourth-order sea-level fluctuations on the Latium margin (Tyrrhenian Sea, Italy), in Hunt, D., and Gawthorpe, R.L., eds., Sedimentary Response to Forced Regression: Geological Society of London, Special Publication 172, p. 271–289.

Cochrane, D. (2018). Stratigraphic and Carbon Isotope Evolution of an Ediacaran Mixed Siliciclastic Deep-Marine Base-of-Slope System, First Isaac Carbonate, Windermere Supergroup, Canadian Cordillera, British Columbia. M. Sc. thesis. University of Ottawa, Ottawa, ON.

Cochrane, D. J., Navarro, L., & Arnott, R. W. C. (2019). Sedimentological and geochemical evolution of an Ediacaran mixed carbonate-siliciclastic continental slope system, Windermere Supergroup, southern Canadian Cordillera, British Columbia, Canada. *Precambrian Research*, *327*, 47-67.

Covault, J. A., Kostic, S., Paull, C. K., Ryan, H. F., & Fildani, A. (2014). Submarine channel initiation, filling and maintenance from sea-floor geomorphology and morphodynamic modelling of cyclic steps. *Sedimentology*, 61**(4)**, p.1031-1054.

Covault, J. A., Sylvester, Z., Hubbard, S. M., Jobe, Z. R., & Sech, R. P. (2016). The stratigraphic record of submarine-channel evolution. *The Sedimentary Record*, *14***(3)**, 4-11.

Cross, N. E., Cunningham, A., Cook, R. J., Taha, A., Esmaie, E., & El Swidan, N. (2009). Three-dimensional seismic geomorphology of a deep-water slope-channel system: The Sequoia field, offshore west Nile Delta, Egypt. *AAPG bulletin*, *93***(8)**, 1063-1086.

Davis, L. (2011). Architecture of deep-marine interchannel deposits: Isaac Formation, Windermere Supergroup (Neoproterozoic), southern Canadian Cordillera, M.Sc. thesis, University of Ottawa, Ottawa, ON.

Devlin, W.J., and Bond, G.C. (1988). The initiation of the early Paleozoic Cordilleran miogeocline: evidence from uppermost Proterozoic-Lower Cambrian Hamill Group of southeastern British Columbia, Canadian Journal of Earth Sciences, **25**, 1-19.

Deptuck, M. E., & Sylvester, Z. (2018). Submarine fans and their channels, levees, and lobes. In *Submarine geomorphology* (pp. 273-299). Springer, Cham.

Di Celma, C. N., Brunt, R. L., Hodgson, D. M., Flint, S. S., & Kavanagh, J. P. (2011). Spatial and temporal evolution of a Permian submarine slope channel–levee system, Karoo Basin, South Africa. *Journal of Sedimentary Research*, *81***(8)**, 579-599.

Dorrell, R. M., Darby, S. E., Peakall, J., Sumner, E. J., Parsons, D. R., & Wynn, R. B. (2014). The critical role of stratification in submarine channels: implications for channelization and long runout of flows. *Journal of Geophysical Research: Oceans*, *119*, **4**, 2620-2641.

Dumouchel, I.W. (2012). Effects of relative sea-level change on the stratigraphic architecture of a passive margin deep-marine channel fill complex, Windermere Supergroup, British Columbia, Canada (unpublished B.Sc. thesis, University of Ottawa).

Dumouchel, I.G. (2015). Stratigraphic Architecture and Depositional History of Laterally-Accreted Channel Fills in the Lower Isaac Formation, Windermere Supergroup, British Columbia, Canada. M.Sc. thesis, University of Ottawa, Ottawa, ON

Dykstra, M., & Kneller, B. (2009). Lateral accretion in a deep-marine channel complex: implications for channelized flow processes in turbidity currents. *Sedimentology, **56***, 1411-1432.

Elliott, T. (2000). Depositional architecture of a sand-rich, channelized turbidite system: the Upper Carboniferous Ross Sandstone formation, Western Ireland, *in* P. Weimer, R.M. Slatt, A.H. Bouma and D.T. Lawrence (Eds.), *Deep-water reservoirs of the world*

Englert, R. G., Hubbard, S. M., Matthews, W. A., Coutts, D. S., & Covault, J. A. (2020). The evolution of submarine slope-channel systems: Timing of incision, bypass, and aggradation in Late Cretaceous Nanaimo

Evans, K.V., Aleinikoff, J.N., Obradovich, J.D., and Fanning, C.M. (2000.) SHRIMP U-Pb

geochronology of volcanic rocks, Belt Supergroup, western Montana: evidence for rapid deposition of sedimentary strata, Canadian Journal of Earth Sciences, **37**, 1287-1300.

Evenchick, C.A., Parrish, R.R., and Gabrielse, H. (1984). Precambrian gneiss and Late Proterozoic sedimentation in north-central British Columbia, Geology, **12**, 233-237.

Ferguson, C.A. (1994). Structural geology and stratigraphy of the northern Cariboo Mountains

between Isaac Lake and Fraser River, British Columbia. Map, University of Calgary, Calgary, AB,. (1997-047810) 157.

Fisher, R.V. (1983). Flow transformation in sediment gravity flows, *Geology. **11**, 273-274.*

Gammon, P.R., Arnott, R.W.C., and Ross, G.M. (2007). Architectural relationship between channels, levees, and debris flows: Isaac Channel 6, Castle Creek South, lower Isaac Formation, Windermere Supergroup, British Columbia, Canada. *In* Atlas of deep-water outcrops: AAPG Studies in Geology 56. *Edited by* T. H. Nilsen, R. D. Shew, G. S. Steffens, and J. R. J. Studlick, CD-ROM, 4 p.

Gan, Y. P., Steel, R. J., Olariu, C., & De Almeida Jr, F. (2020). Facies and architectural variability of sub-seismic slope-channel fills in prograding clinoforms, Mid-Jurassic Neuquén Basin, Argentina. *Basin Research*, *32*(Clinoforms and Clinothems: Fundamental Elements of Basin Infill), 348-362.

Gardner, M. H., Borer, J. M., Bouma, A. H., & Stone, C. G. (2000). Submarine channel architecture along a slope to basin profile, Brushy Canyon Formation, west Texas. *SPECIAL PUBLICATION-SEPM*, ***68***, 195-214.

Hampton, M.A (1975) Competence of fine-grained debris flows. *J. Sed. Petrol.,* **45**, 834-844.

Hubbard, S. M., Covault, J. A., Fildani, A., & Romans, B. W. (2014). Sediment transfer and deposition in slope channels: Deciphering the record of enigmatic deep-sea processes from outcrop. *Bulletin*, *126***(5-6)**, 857-871.

Huyer, G., (2016). Architecture and Stratigraphy of a Neoproterozoic Deep-Marine Slope Channel-Complex Set, Windermere Supergroup, Castle Creek, BC. Unpublished B.Sc. thesis, University of Ottawa, 55 p.

Iverson, R. M., Reid, M. E., and LaHusen, R. G. (1997). Debris-flow mobilization from landslides. *Annual Review of Earth and Planetary Sciences, 25*(1), 85-138.

Jackson, C. A., & Johnson, H. D. (2009). Sustained turbidity currents and their interaction with debrite-related topography; Labuan Island, offshore NW Borneo, Malaysia. *Sedimentary Geology*, *219*(1-4), 77-96.

Janocko, M. (2011). Deep-water sinuous channels: their development and architecture. Ph.D. Thesis (unpublished), University of Bergen.

Janocko, C. A., Nemec, W., Henriksen, S., & Warchoł, M. (2013). The diversity of deep-water sinuous channel belts and slope valley-fill complexes. *Marine and Petroleum Geology*, ***41***, 7-34.

Jensen, J.A., Sickafoose, G.N., (2000). Outcrop expression of confined channel complexes. *In* Deep-water Reservoirs of the World: Gulf Coast Section. *Edited by* P. Weimer, R.M. Slarr, J. Coleman, N.C. Rosen, H. Nelson, A.H. Bouma, M.J. Styzen and D.T. Lawrence. SEPM Foundation 20th Annual Research Conference, pp. 127-150.

Jerolmack, D. J., & Paola, C. (2007). Complexity in a cellular model of river avulsion. *Geomorphology*, *91***(3-4)**, 259-270.

Jobe, Z.R., Hower, N.C., Auchter, N.C. (2016). Comparing submarine and fluvial channel kinematics: Implications for stratigraphic architecture. The Geological Society of America, 44**(11)**, p.931-934.

Jobe, Z. R., Sylvester, Z., Parker, A. O., Howes, N., Slowey, N., & Pirmez, C. (2015). Rapid adjustment of submarine channel architecture to changes in sediment supply. *Journal of Sedimentary Research*, *85***(6)**, 729-753.

Jobe, Z., Sylvester, Z., Pittaluga, M. B., Frascati, A., Pirmez, C., Minisini, D., & Cantelli, A. (2017). Facies architecture of submarine channel deposits on the western Niger Delta slope: Implications for grain-size and density stratification in turbidity currents. *Journal of Geophysical Research: Earth Surface*, *122***(2)**, 473-491.

Kane, I. A., McCaffrey, W. D., Peakall, J. & Kneller, B. C. (2010) Submarine channel levee shape and sediment waves from physical experiments. *Sedimentary Geology*, 223, 75–85.

Kane, I. A., Kneller, B. C., Dykstra, M., Kassem, A., & McCaffrey, W. D. (2007) Anatomy of a submarine channel-levee: An example from Upper Cretaceous slope sediments, Rosario Formation, Baja California, Mexico. *Marine and Petroleum Geology*, 24, 540-563.

Kane, I. A., & Hodgson, D. M. (2011). Sedimentological criteria to differentiate submarine channel levee subenvironments: exhumed examples from the Rosario Fm.(Upper Cretaceous) of Baja California, Mexico, and the Fort Brown Fm.(Permian), Karoo basin, S. Africa. *Marine and Petroleum Geology*, *28***(3)**, 807-823.

Khan, Z.A., and Arnott, R.W.C. (2011). Stratal attributes and evolution of asymmetric inner- and outer-bend levee deposits associated with an ancient deep-water channel-levee complex within the Isaac Formation, southern Canada, Marine and Petroleum Geology, **28**: 824-842.

Khan, Z. (2012). Origin and architecture of deep-water level deposits: Insight from the ancient rock record and experiments, Ph.D. thesis, University of Ottawa, Ottawa, ON.

Kendall, B.S., Creaser, R.A., Ross, G.M., and Selby, D. (2004). Constraints on the timing of Marinoan "Snowball Earth" glaciation by 187Re-187Os dating of a Neoproterozoic, post-glacial black shale in Western Canada, Earth and Planetary Science Letters, **222**: 729-740.

Kleverlaan, K. (1989). Three distinctive feeder-lobe systems within one time slice of the Tortonian Tabernas fan, SE Spain. *Sedimentology,* 36, 25-45.

Kneller, B. C. (2003) The influence of flow parameters on turbidite channel slope Architecture. *Marine and Petroleum Geology*, 20, p.901–910.

Kneller, B., Bozetti, G., Callow, R., Dykstra, M., Hansen, L., Kane, I., & Thompson, P. (2020). Architecture, process, and environmental diversity in a late Cretaceous slope channel system. *Journal of Sedimentary Research*, *90*(1), 1-26.

Kneller, B., Dykstra, M., Fairweather, L., & Milana, J. P. (2016). Mass-transport and slope accommodation: implications for turbidite sandstone reservoirs. *AAPG Bulletin*, *100*(2), 213-235.

Kneller, B., Nasr-Azadani, M. M., Radhakrishnan, S., & Meiburg, E. (2016) Long-range sediment transport in the world's oceans by stably stratified turbidity currents. *Journal of Geophysical Research: Oceans*, 121, 8608–8620, doi:10.1002/2016JC011978.

Kolla, V., Posamentier, H. W., & Eichenseer, H. (1995). Stranded parasequences and the forced regressive wedge systems tract: deposition during base-level fall—discussion. *Sedimentary Geology*, *95*(1-2), 139-145.

Kolla, V. (2007). A review of sinuous channel avulsion patterns in some major deep-sea fans and factors controlling them. *Marine and Petroleum Geology*, *24*(6-9), 450-469.

Kolla, V.,Bandyopadhyay, A.,Gupta, P., Mukherjee, B., Ramana, D. V., Prather, B. E., & Wynn, R. B. (2012). Morphology and internal structure of a recent upper Bengal fan-valley complex. *Application of the Principles of Seismic Geomorphology to Continental-Slope and Base-of-Slope Systems: Case Studies from Seafloor and Near-Seafloor Analogues: SEPM, Special Publication*, *99*, 347-369.

Konsoer, K., Zinger, J., & Parker, G. (2013). Bankfull hydraulic geometry of submarine channels created by turbidity currents: Relations between bankfull channel characteristics and formative flow discharge. *Journal of Geophysical Research: Earth Surface*, *118*(1), 216-228.

Laurin, J. (2005). Depositional history and sequence stratigraphic context of a Neoproterozoic mass transport deposit, Isaac Formation, east-central B.C., B.Sc. thesis, University of Ottawa, Ottawa, ON.

Lee, S.L. (2016). Microstructural and external characterization of a low-grade metaturbidite succession in the Windermere Supergroup, British Columbia, Canada, B.Sc. thesis, University of Ottawa, Ottawa, ON.

Levy, M., Posamentier, H.W., and Drinkwater, N.J. (2011). Architecture of turbidite channel systems on the continental slope: Patterns and predictions, Marine and Petroleum Geology, **28**: 728-743.

Li, P., Kneller, B. C., Hansen, L., & Kane, I. A. (2016). The classical turbidite outcrop at San Clemente, California revisited: an example of sandy submarine channels with asymmetric facies architecture. *Sedimentary Geology*, *346*, 1-16.

Li, P., Kneller, B., Thompson, P., Bozetti, G., & Dos Santos, T. (2018). Architectural and facies organisation of slope channel fills: Upper Cretaceous Rosario Formation, Baja California, Mexico. *Marine and Petroleum Geology*, *92*, 632-649.

Li, Z.X., Evans, D.A.D., and Halverson, G.P. (2013). Neoproterozoic glaciations in a revised global palaeogeography from the breakup of Rodinia to the assembly of Gondwanaland, Sedimentary Geology, **294**: 219-232.

Lien, T., Walker, R. G., & Martinsen, O. J. (2003). Turbidites in the Upper Carboniferous Ross Formation, western Ireland: reconstruction of a channel and spillover system. *Sedimentology*, *50*(1), 113-148.

Link, P.K., Christie-Blick, N., Devlin, W.J., Elston, D.P., Horodyski, R.J., Levy, M., Miller, J.M.G., Pearson, R.C., Prave, A., Stewart, J.H., Winston, D., Wright, L.A., and Wrucke, C.T. (2003). Middle and late Proterozoic stratified rocks in the western U.S. Cordillera, Colorado Plateau, and Basin and Range Province. *In* Precambrian: Conterminous U.S., The Geology of North America: Geological Society of America Decade of North American Geology Series, v. c-3. *Edited by* J.C. Reed, Jr. M.E. Bickford, R.S. Houston, P.K. Link, D.W. Rankin, P.K. Sims, and W.R. Van Schmus, pp. 474-690.

Lund, K., Aleinikoff, J.N., Evans, K.V., and Fanning C.M. (2003). SHRIMP U-Pb geochronology of Neoproterozoic Windermere Supergroup, central Idaho: Implications for rifting of western Laurentia and synchroneity of Sturtian glacial deposits, Geological Society of America Bulletin, **115**: 349-372. Hoffman, P.F. 1991. Did the breakout of Laurentia turn Godwanaland inside-out?, Science, **525**: 1409-1412.

Lowe, D.R. (1982). Sediment gravity flows: II. Depositional models with special reference to the deposits of high-density turbidity currents, Journal of Sedimentary Petrology, **52**: 279-297.

Macauley, R.V., and Hubbard, S.M. (2013). Slope channel sedimentary processes and stratigraphic stacking, Cretaceous Tres Pasos Formation slope system, Chilean Patagonia: Marine and Petroleum Geology, v. 41, p. 146–162, doi:10.1016/j.marpetgeo.2012.02.004.

Mayall, M., Jones, E., & Casey, M. (2006). Turbidite channel reservoirs—Key elements in facies prediction and effective development. *Marine and Petroleum Geology*, *23*(8), 821-841.

McAnally, W. H., Friedrichs, C., Hamilton, D., Hayter, E., Shrestha, P., Rodriguez, H., Sheremet, A., and Teeter, A. (2007). Management of fluid mud in estuaries, bays, and lakes. I: present state of understanding on character and behavior. *Journal of Hydraulic Engineering, 133*(1), 9-22.

McHargue, T., Pyrcz, M.J., Sullivan, M.D., Clark, J., FILDANI, A., Romans, B.R., Covault, J.A., Levy, M., Posamentier, H., Drinkwater, N.(2011). Architecture of turbidite channel systems on the continental slope: patterns and predictions: Marine and Petroleum Geology, v. 28, p. 728–743.

McMechan, M.E. (2015). The Neoproterozoic succession of the central Rocky Mountains, Canada, Bulletin of Canadian Petroleum Geology, **63**: 243-273.

Meyer, L. (2004). Internal architecture of an ancient deep-water, passive margin, basin-floor fan

system, Upper Kaza Group, Windermere Supergroup, Castle Creek, British Columbia, M.Sc. thesis, University of Calgary, Calgary, AB.

Meyer, L., and Ross, G.M. (2007). Channelized lobe and sheet sandstones of the upper Kaza Group basin-floor turbidite system (Windermere Supergroup), British Columbia, Canada. *In* Atlas of deep-water outcrops: AAPG Studies in Geology 56. *Edited by* T. H. Nilsen, R. D. Shew, G. S. Steffens, and J. R. J. Studlick, CD-ROM, 4 p.

Middleton, G.V. and Hampton, M.A., (1973). Sediment Gravity Flows: mechanics of flow and deposition, *in* Middletong, G.V and A.H Bouma, eds., *Turbidites and Deep Water Sedimentation. Short Course Notes,* No **1**, SEPM (Pacific Section), Los Angeles, p. 1-38.

Milczarek, G. (2018). Chemostratigraphic Analysis of Mudrocks and its Implication on Provenance and Sequence Stratigraphy in the Isaac Formation, Windermere Turbidite System, Castle Creek, B.C., Canada: Unpublished B.Sc. thesis, University of Ottawa.

Mohrig, D., Heller, P. L., Paola, C., & Lyons, W. J. (2000). Interpreting avulsion process from ancient alluvial sequences: Guadalope-Matarranya system (northern Spain) and Wasatch Formation (western Colorado). *Geological Society of America Bulletin*, *112*(12), 1787-1803.

Mulder, T., Alexander, J., (2001). The physical character of subaqueous sedimentary density flows and their deposits. *Sedimentology,* **48**, p. 269-299.

Murphy, D.C. (1987a). Kaza Group, eastern wells gray park, British Columbia, Geological Survey of Canada Paper 87-1A, pp. 735-742.

Murphy, D.C., (1987b). Suprastructure/infrastructure transition, east-central Cariboo Mountains, British Columbia; geometry, kinematics and tectonic implications, Journal of Structural Geology, **9**: 13-29.

Murphy, D.C., and Rees, C.J. (1983). Structural transition and stratigraphy in the Cariboo Mountains, British Columbia. *In* Current Research Part A, Geological Survey of Canada Paper 83-1A, 245-252.

Mussa-Caleca, M. (2008). Architecture and depositional history of a Neoproterozoic deep-water slope channel complex in a passive margin setting: Isaac Formation, Windermere Supergroup, southern Canadian Cordillera.: M.Sc. Thesis thesis, University of Ottawa, Ottawa, Ontario.

Mutti, E., & Normark, W. R. (1987). Comparing examples of modern and ancient turbidite systems: problems and concepts, in J. R. Leggett, and G. G. Zuffa, eds., Marine Clastic Sedimentology: Concepts and Case Studies: London, Graham and Trotman, p.1–37.

Navarro, L. (2005). Depositional architecture and evolution of deep-water base-of-slope and slope channel complexes in a passive margin setting: Isaac Formation, Windermere Supergroup (Neoproterozoic) southern Canadian Cordillera. M.Sc. thesis, Université d'Ottawa/University of Ottawa, 272 p.

Navarro, L., Z. Khan, and R. W. C. Arnott, (2007). Depositional architecture and evolution of a deep-marine channel-levee complex: Isaac Formation (Windermere Supergroup), Southern Canadian Cordillera., in T. H. Nilsen, R.D. Shew, G. S. Steffens, and J. R. J. Studlik, eds., Atlas of Deep-water Outcrops., v. CD-ROM: Tulsa, AAPG Studies in Geology 56, CD-ROM, p.22.

Navarro, L. (2016). Stratigraphic architecture depositional processes and reservoir implications of the basin floor to slope transition, Neoproterozoic Windermere turbidite system, Canada: Ph.D. thesis, University of Ottawa, Ottawa, ON.

Normark, W.R., Barnes, N.E., and Coumes, F. (1985). Rhone Fan, Mediterranean. *In* Submarine Fans and Related Turbidite Systems. *Edited by* A.H. Bouma, W.R. Normark, and N.E. Barnes. Springer, New York, U.S.A, pp. 151-156.

Normark, W. R., C. K. Paull, D. W. Caress, W. Ussler, and R. Sliter. (2009). Fine-scale relief related to Late Holocene channel shifting within the floor of the upper Redondo Fan, offshore Southern California: Sedimentology, v. 56, p. 1690-1704.

O'Byrne, C.J.M., Barton, M.D., Steffens, G.S., Primez, C., and Buergisser, H. (2007). Architecture of a laterally migrating channel complex: Channel 4, Isaac Formation, Windermere Supergroup, Castle Creek north, British Columbia, Canada. *In* Atlas of deep-water outcrops: AAPG Studies in Geology 56. *Edited by* T. H. Nilsen, R. D. Shew, G. S. Steffens, and J. R. J. Studlick, CD-ROM, 4 p.

Parrish, R.R., and Scammell, R.J. (1988). The age of the Mount Copeland syenite gneiss and its metamorphic zircons, Monashee Complex, southeastern British Columbia. *In* Radiogenic age and isotopic studies: Report 2, Geological Survey of Canada Paper 88-2, 21-28.

Peakall, J., McCaffrey, W. D. & Kneller, B. C. (2000). A process model for the evolution, morphology, and architecture of sinuous submarine channels. *Journal of Sedimentary Research*, 70, p.434–448.

Peakall, J., Amos, K. J., Keevil, G. M., Bradbury, P. W., & Gupta, S. (2007). Flow processes and sedimentation in submarine channel bends. *Marine and Petroleum Geology*, *24*(6-9), 470-486.

Pettinga, L., Jobe, Z., Shumaker, L., Hower, N. (2018). Morphometric scaling relationships in submarine channel-lobe systems. The Geological Society of America, **46**(9), p.819-822.

Pickering, K. T., Clark, J. D., Smith, R. D. A., Hiscott, R. N., Lucchi, F. R. & Kenyon, N. H. (1995). Architectural element analysis of turbidite systems, and selected topical problems for sand-prone deep-water systems, Atlas of deep water environments, Springer, p. 1-10.

Piper, D. J. W., & Normark, W. R. (2001). Sandy fans – from Amazon to Hueneme and beyond. *AAPG Bulletin*, 85, 1407–1438.

Pirmez, C., & Imran, J. (2003). Reconstruction of turbidity currents in Amazon Channel. *Marine and Petroleum Geology*, 20(6), 823-849.

Plint, A. G., & Nummedal, D. (2000). The falling stage systems tract: recognition and importance in sequence stratigraphic analysis. *Geological Society, London, Special Publications*, *172*(1), 1-17.

Plint, A.G. (2010). Wave- and storm-dominated shoreline and shallow-marine systems, Ch. 8, *in* N.P. James and R.W. Dalrymple (Eds.), *Facies Models 4* (pp. 167-199), Geological Association of Canada.

Popović, N. (2016). Sedimentology and stratigraphy of a matrix-poor to matrix-rich depositional continuum in proximal basin floor strata, upper Kaza Group, Windermere Supergroup, B.C., Canada, M.Sc. thesis, University of Ottawa, Ottawa, ON.

Posamentier, H. W., Allen, G. P., James, D. P., & Tesson, M. (1992). Forced regressions in a sequence stratigraphic framework: concepts, examples, and exploration significance. *AAPG bulletin*, *76*(11), 1687-1709.

Posamentier, H. W., & Kolla, V. (2003). Seismic geomorphology and stratigraphy of depositional elements in deep-water settings. *Journal of sedimentary research*, *73*(3), 367-388.

Posamentier, H. W., and R. G. Walker, (2006). Deep-water turbidites and submarine fans: SEPM Special Publication, v. 84, p. 397–520.

Postma, G., (1986). Classification for sediment gravity-flow deposits based on flow conditions during sedimentation: Geology, v. 14, p. 291-294.

Pyles, D.R., Jennette, D.C., Tomasso, M., Beaubouef, R.T., Rossen, C. (2010). Concepts learned from a 3D outcrop of a sinuous slope channel complex: Beacon Channel Complex. Brushy Canyon.

Reid, L.F., Cook, F.A., and Erdmer, P. (1997). Structural correlation across the suprastructure-infrastructure transition (Cariboo Mountains, British Columbia); possible, impossible or work in progress?, lithoprobe slave Northern cordillera lithospheric evolution (SNORCLE) and cordilleran tectonics workshop; report of the 1997 combined meeting. Lithoprobe Report, 56, 181-182.

Ross, G.M., and Murphy, D.C. (1988). Transgressive stratigraphy, anoxia, and regional correlations within the late Precambrian Windermere grit of the southern Canadian Cordillera, Geology, **16**: 139-143.

Ross, G.M. (1991). Tectonic setting of the Windermere Supergroup revisited, Geology, **19**: 1125-1128.

Ross, G.M., and Parrish, R.R., (1991). Detrital zircon geochronology of metasedimentary rocks in the southern Omineca Belt, Canadian Cordillera, Canadian Journal of Earth Sciences, **28**: 1254-1270.

Ross, W. C., Halliwell, B. A., May, J. A., Watts, D. E., & Syvitski, J. P. M. (1994). Slope readjustment: a new model for the development of submarine fans and aprons. *Geology*, *22*(6), 511-514.

Ross, G.M., Bloch, J.D., and Krouse, H.R. (1995). Neoproterozoic strata of the southern Canadian Cordillera and the isotopic evolution of seawater sulfate, Precambrian Research, **73**: 71-99.

Rowe, C.E. (2003). The Cunningham formation: a ramp to platform carbonate in the terminal Proterozoic of the Cariboo Mountains, British Columbia, M.Sc. thesis, University of Calgary, Calgary, AB.

Ross, G.M., and Arnott, R.W.C. (2007). Regional Geology of the Windermere Supergroup, Southern Canadian Cordillera and Stratigraphic Setting of the Castle Creek Study Area, Canada. *In* Atlas of deep-water outcrops: AAPG Studies in Geology 56. *Edited by* T. H. Nilsen, R. D. Shew, G. S. Steffens, and J. R. J. Studlick, CD-ROM, 16 p.

Russell, R. J. (1968). Where most grains of very coarse sand and fine gravel are deposited. *Sedimentology*, *11*(1-2), 31-38.

Samuel, A., Kneller, B., Raslan, S., Sharp, A., & Parsons, C. (2003). Prolific deep-marine slope channels of the Nile Delta, Egypt. *AAPG bulletin*, 87(4), 541-560.

Schwarz, E., and Arnott, R.W.C. (2007a). Anatomy and evolution of a slope channel-complex set (Neoproterozoic Isaac Formation, Windermere Supergroup, southern Canadian

Cordillera): implications for reservoir characterization, Journal of Sedimentary Research, **77**: 89-109.

Schwarz, E., and Arnott, R.W.C. (2007b). Outcrop characterization of a passive- margin channel-complex set: Isaac Channel 5, Neoproterozoic Isaac Formation, British Columbia, Canada. . *In* Atlas of deep-water outcrops: AAPG Studies in Geology 56. *Edited by* T. H. Nilsen, R. D. Shew, G. S. Steffens, and J. R. J. Studlick, CD-ROM, 15 p.

Shanmugam, G., (2000). 50 years of turbidite paradigm 1950s-1990s: deep-water processes and facies models- a critical perspective. *Mar Petrol. Geol.,***17**, p. 285-342

Shanmugam, G. (2006). Deep-water processes and facies models: Implications for sandstone petroleum reservoirs. Elsevier, New York, U.SA.

Shew, R.D., Steffens, G.S., Studlick, J.R.J. (2007). Introduction: Atlas of Deep-water Outcrops: AAPG Studies in Geology 56.

Smith, M.D. (2009). Stratigraphic and geochemical evolution of the Old Fort Point Fm., southern Canadian Cordillera: The deep-marine perspective of Ediacaran post-glacial environmental change, Ph.D. thesis, University of Ottawa, Ottawa, ON.

Smith, M.D., Arnott, R.W.C., and Ross, G.M. (2014). Physical and geochemical controls on sedimentation along an ancient continental margin: The deep-marine Old Fort Point Formation (Ediacaran), southern Canadian Cordillera, Bulletin of Canadian Petroleum Geology, **62**: 14-36.

Sprague, A. R., M. D. Sullivan, K. M. Campion, G. N. Jensen, D. K. Goulding, D. K.Sickafoose, and D. C. Jennette, (2002). The physical stratigraphy of deep-water strata: a hierarchical approach to the analysis of genetically related elements for improved reservoir prediction, AAPG Annual Convention and Exhibition. Abstracts. : Houston, Texas, p. 10-13.

Stewart, J.H. (1972). Initial deposits in the Cordilleran geosyncline; evidence of a late Precambrian (<850 m.y.) continental separation, Geological Society of America Bulletin, **83**: 1345-1360.

Straub, K. M., Mohrig, D., McElroy, B., Buttles, J., & Pirmez, C. (2008). Interactions between turbidity currents and topography in aggrading sinuous submarine channels: A laboratory study. *Geological Society of America Bulletin*, *120*(3-4), 368-385.

Sylvester, Z., Pirmez, C., & Cantelli, A. (2011). A model of submarine channel-levee evolution based on channel trajectories: Implications for stratigraphic architecture. *Marine and Petroleum Geology*, 28(3), 716-727.

Tahata, M., Ueno, Y., Ishikawa, T., Sawaki, Y., Murakami, K., Han, J., Shu, D., Li, Y., Yoshida, N. and Komiya, T. (2013). Carbon and oxygen isotope chemostratigraphies of the Yangtze Platform, South China: Decoding temperature and environmental changes through the Ediacaran, Godwana Research, **23**: 333-353.

Talling, P. J., D. G. Masson, E. J. Sumnet, and G. Malgesini, (2012). Subaqueous sediment density flows: Depositional processes and deposit types: Sedimentology, v. 59, p. 1937-2003.

Talling, P. J., C. K. Paull, and D. J. W. Piper, (2013). How are subaqueous sediment density flows triggered, what is their internal structure and how does it evolve? Direct observations from monitoring of active flows: Earth-Science Reviews, v. 125, p. 244-287.

Terlaky, V. (2014). Sedimentology, stratigraphy, architecture and origin of deep-water, basin-floor deposits: Middle and upper Kaza Group, Windermere Supergroup, B.C., Canada, Ph.D. thesis, University of Ottawa, Ottawa, ON.

Terlaky, V., and Arnott, R.W.C. (2014). Matrix-rich and associated matrix-poor sandstones: Avulsion splays in slope and basin floor strata, Sedimentology, **61**: 1175-1197.

Tilston, M., Arnott, R.W.C., Rennie, C.D., and Long, B. (2015). The influence of grain size on the velocity and sediment concentration profiles and depositional record of turbidity currents, Geology, **43**: 839-842.

Udden, J. A. (1914). Mechanical composition of clastic sediments. *Bulletin of the Geological Society of America, 25*(1), 655-744.

Van de Lageweg, W. I., van Dijk, W. M., Baar, A. W., Rutten, J., & Kleinhans, M. G. (2014). Bank pull or bar push: What drives scroll-bar formation in meandering rivers?. *Geology*, *42*(4), 319-322.

Venditti, J.G., Church, M., and Bennett, S.J. (2005). Bed form initiation from a flat sand bed, Journal of Geophysical Research, **110**: F01009, 1-19.

Venditti, J.G., Church, M., and Bennett, S.J. (2006). On interfacial instability as a cause of transverse subcritical bed forms, Water Resources Research, **42**: W07423.

Weirich, F.H. (1988) Field evidence for hydraulic jumps in subaqueous sediment gravity flows. *Nature,* **332**, 626-629

Wentworth, C. K. (1922). A scale of grade and class terms for clastic sediments. Journal of Geology*, 30*(5), 377-392.

Wynn, R.B., Cronin, B.T., and Peakall, J. (2007). Sinuous deep-water channels: Genesis, geometry, architecture, Marine and Petroleum Geology, 24, p.341-387.

Appendix A: Drone Photomosaics and Stratigraphic Sections

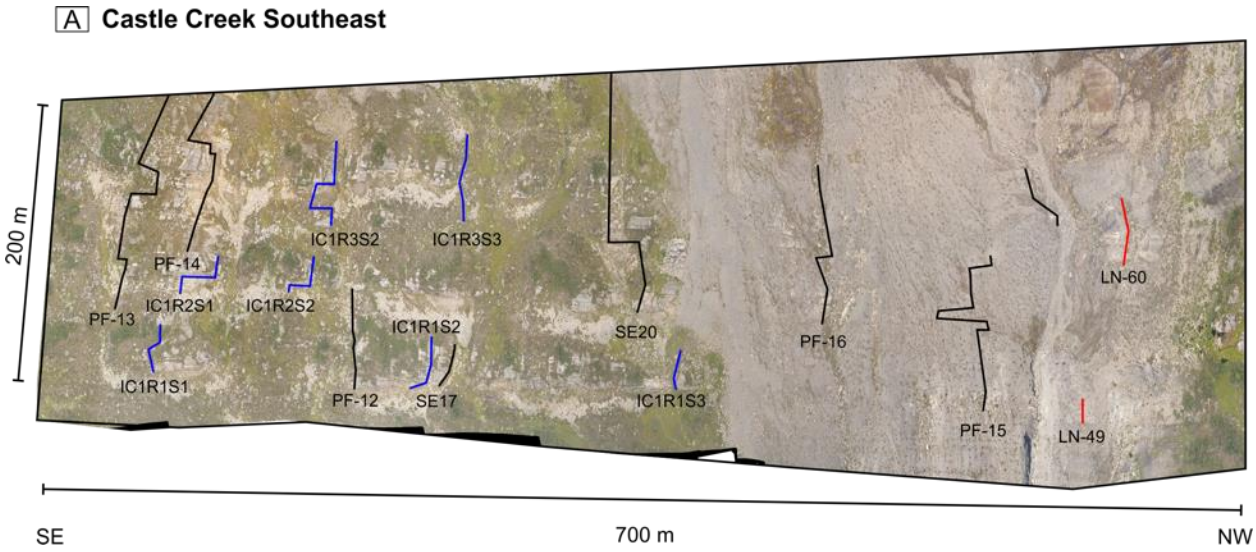

Figure A. 1. *Drone photomosaic from Castle Creek south east and location of measured stratigraphic sections.*

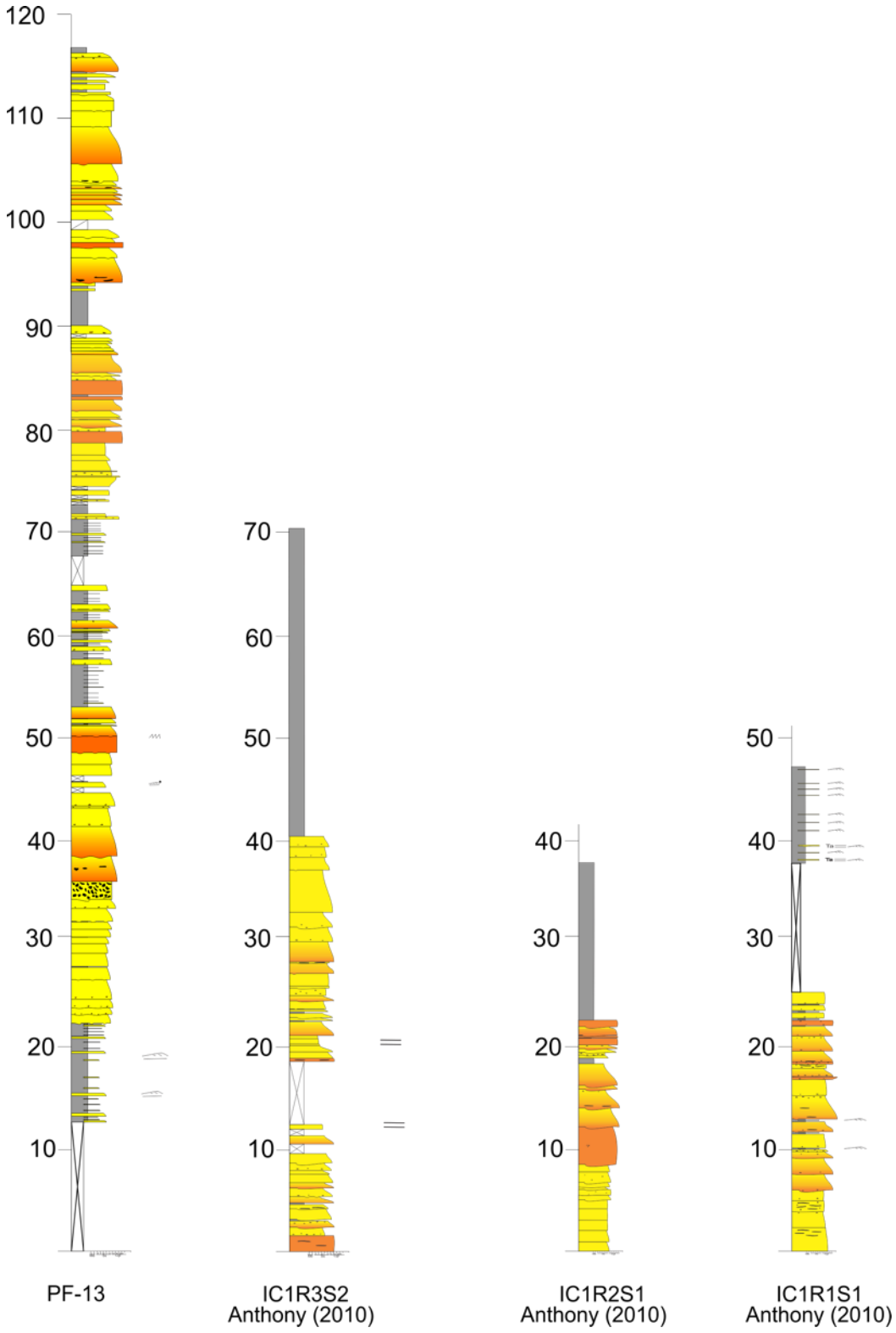

Figure A. 2. *Measured stratigraphic sections in Castle Creek southeast. For log locations see Figure A.1.*

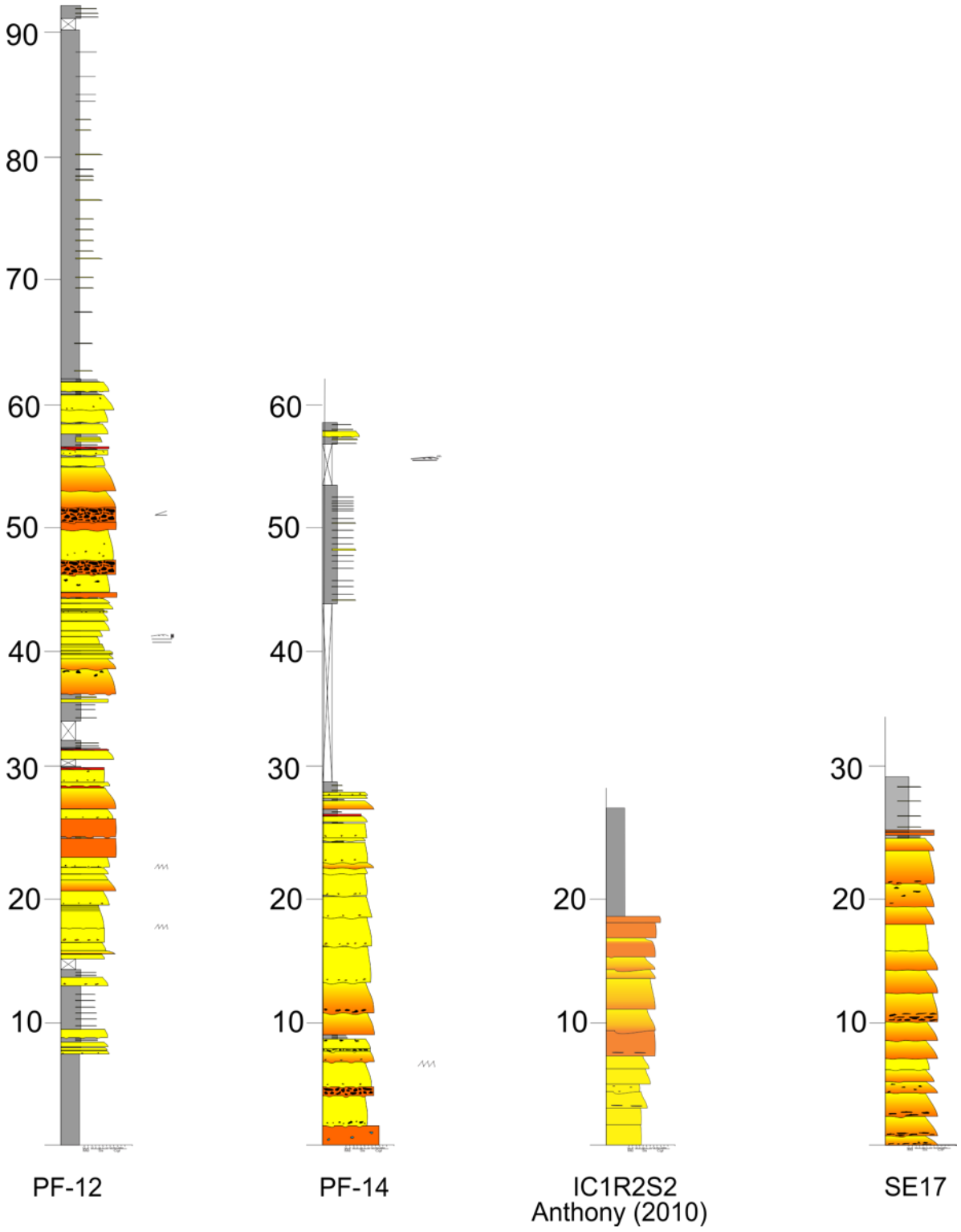

Figure A. 3. *Measured stratigraphic sections in Castle Creek southeast. For log locations see Figure A.1.*

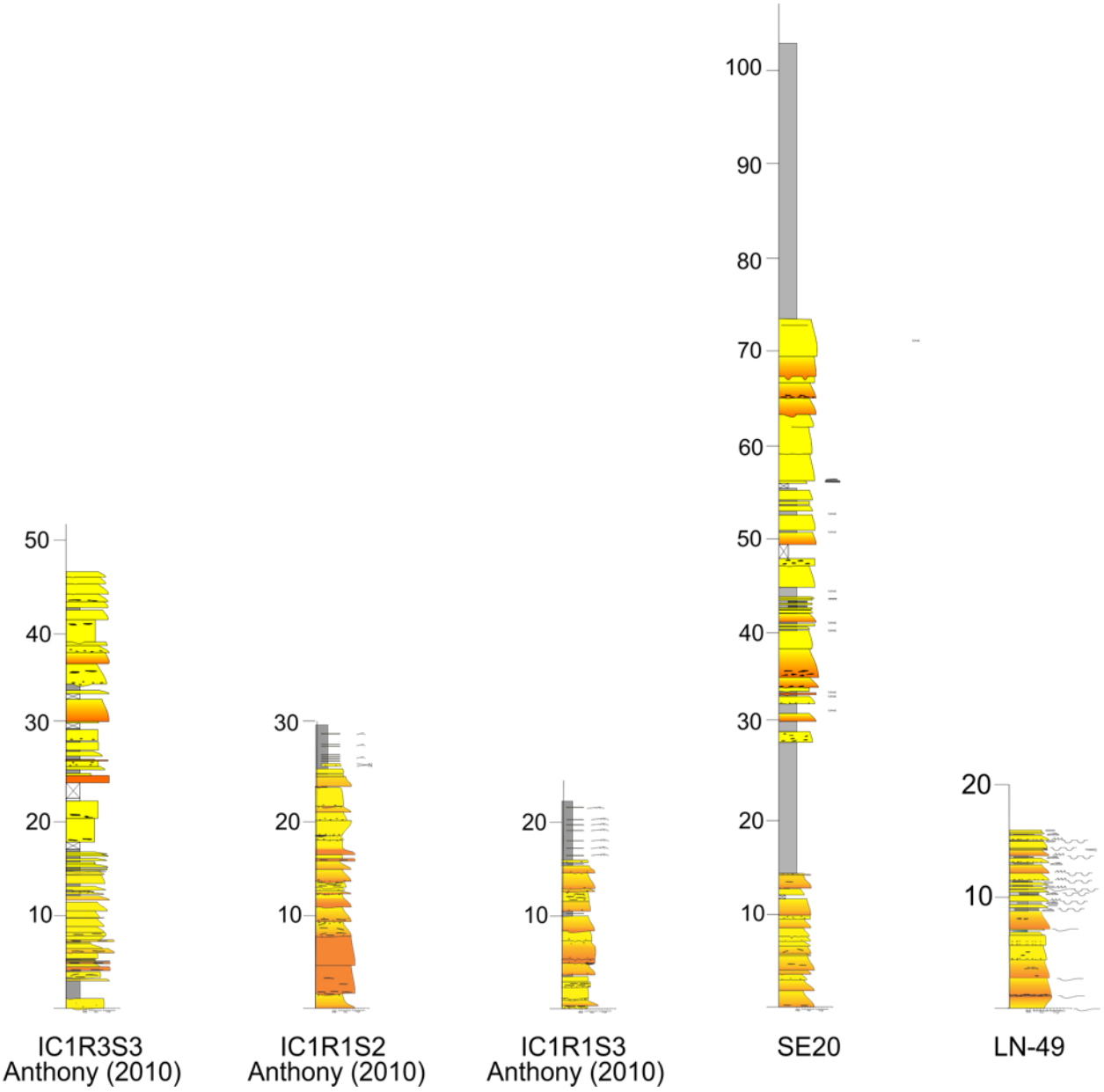

Figure A. 4. *Measured stratigraphic sections in Castle Creek southeast. For log locations see Figure A.1.*

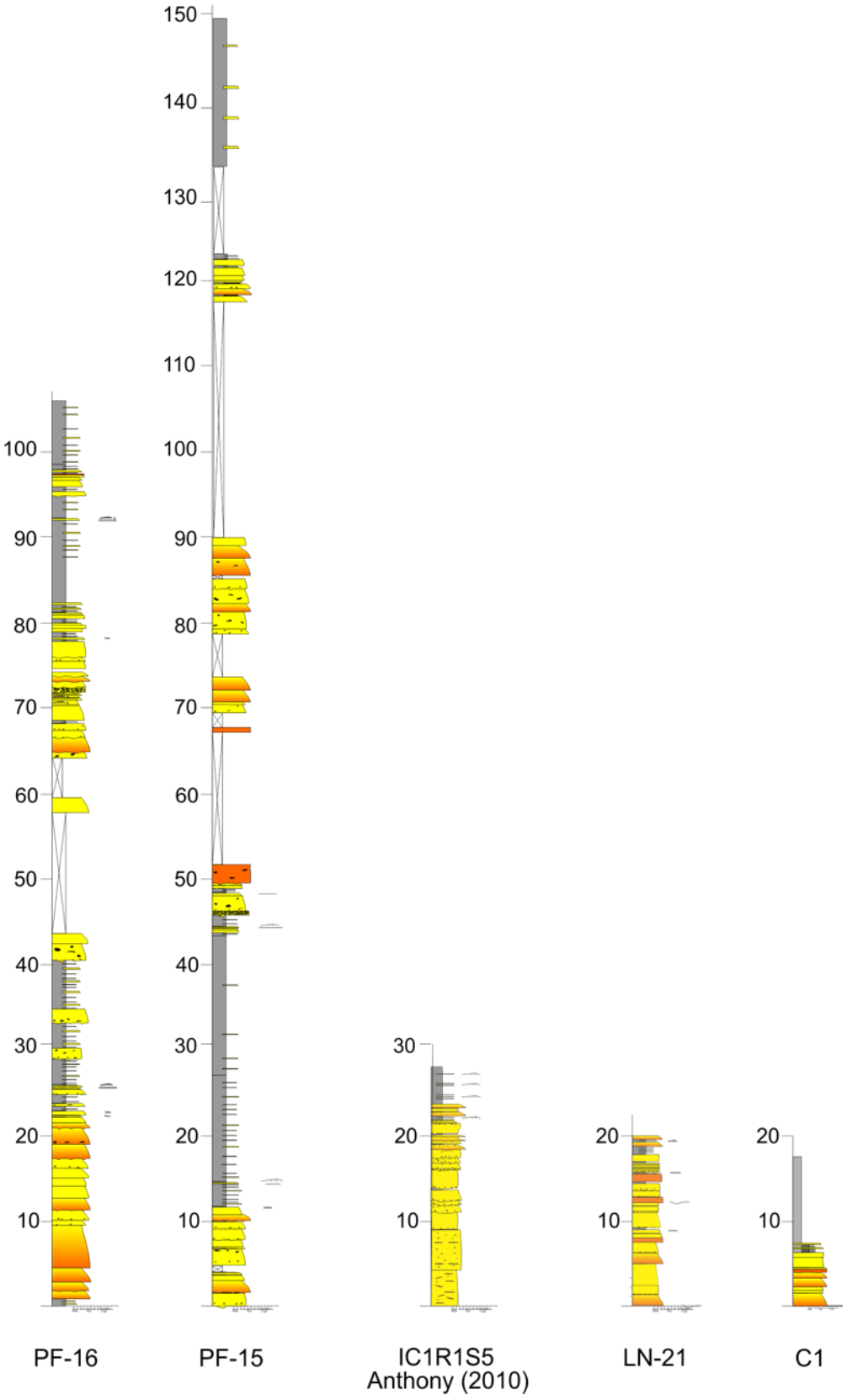

Figure A. 5. *Measured stratigraphic sections in Castle Creek southeast. For log locations see Figure A.1.*

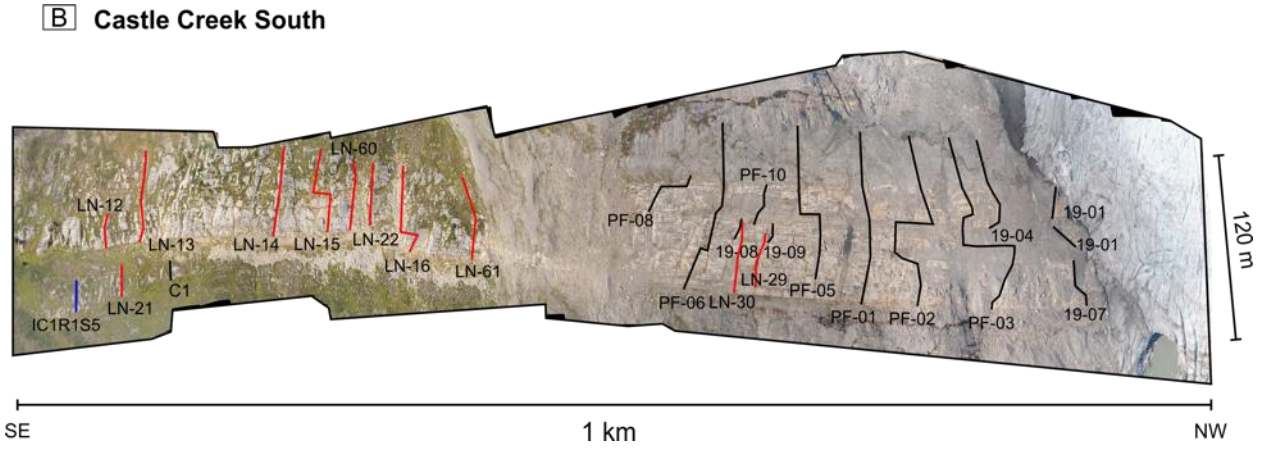

Figure A. 6. *Drone photomosaic from Castle Creek south and location of measured stratigraphic sections.*

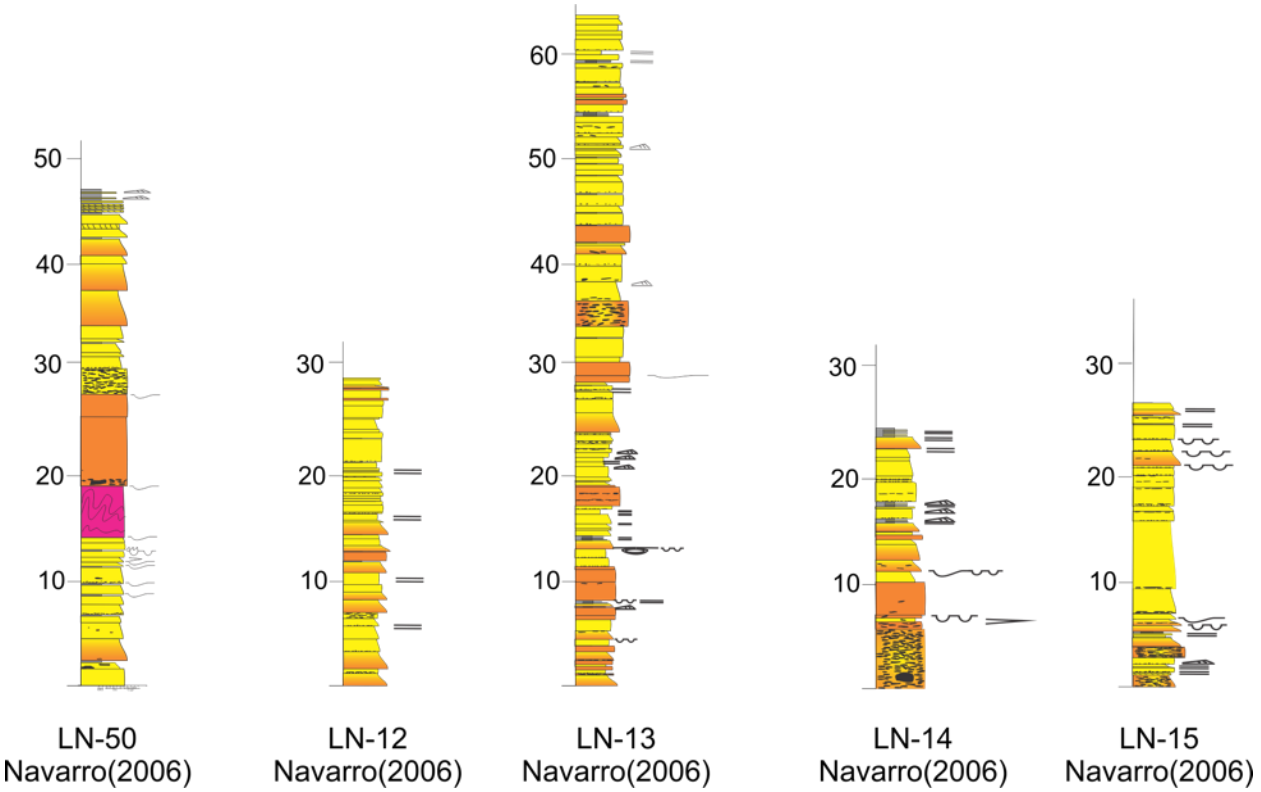

Figure A. 7. *Measured stratigraphic sections in Castle Creek south. For log locations see Figure A.6.*

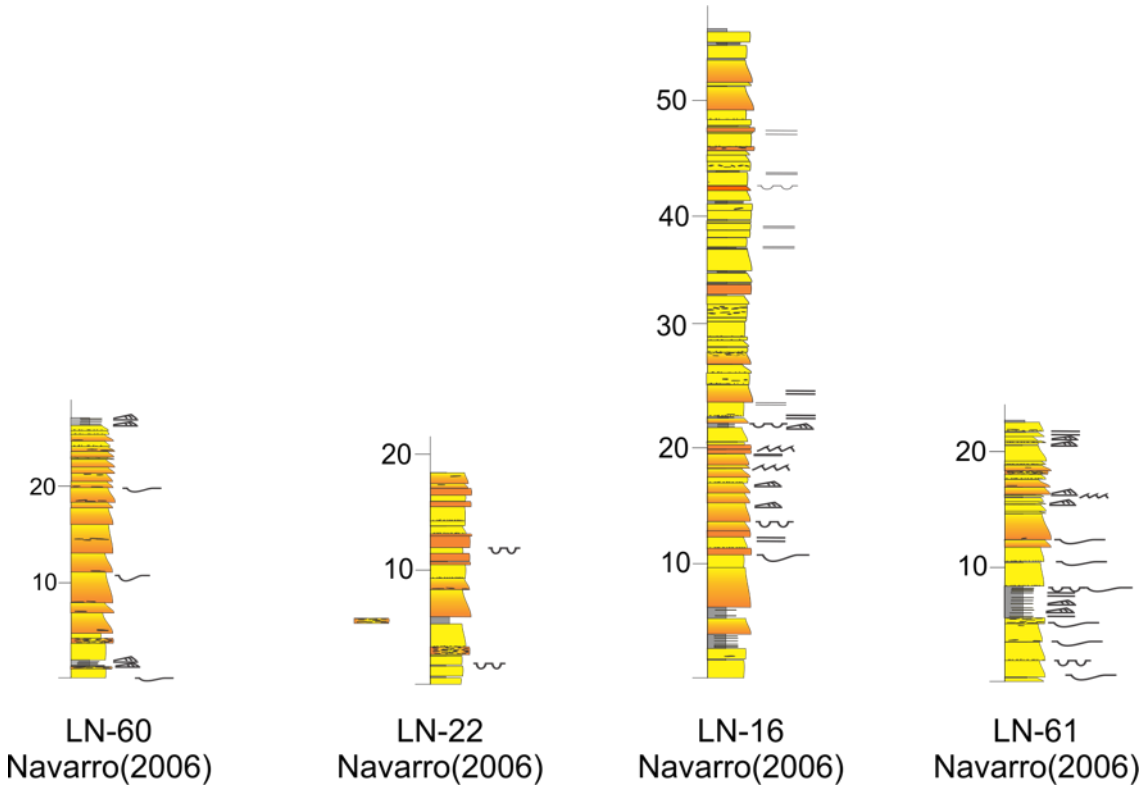

Figure A. 8. *Measured stratigraphic sections in Castle Creek south. For log locations see Figure A.6*

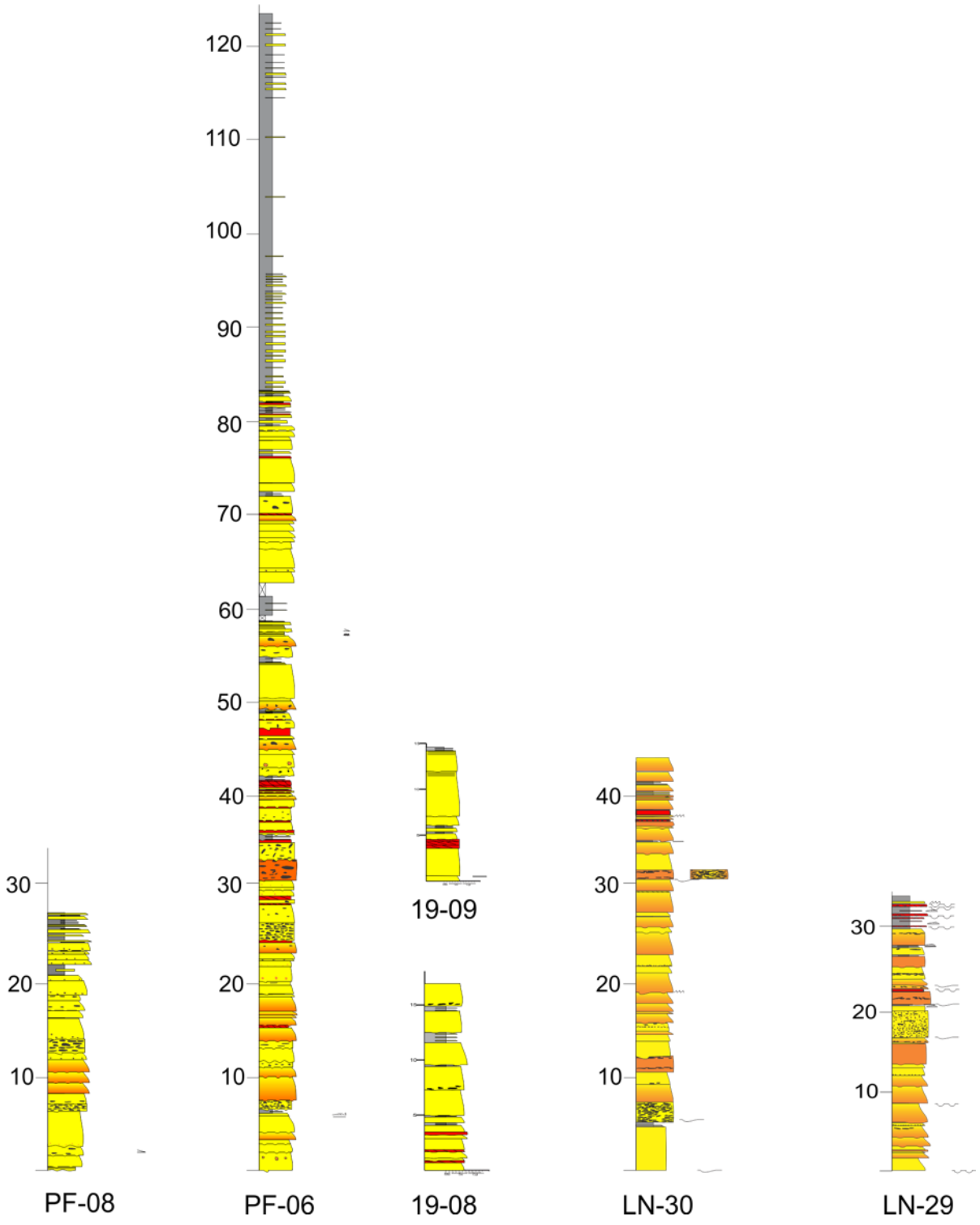

Figure A. 9. *Measured stratigraphic sections in Castle Creek south. For log locations see Figure A.6.*

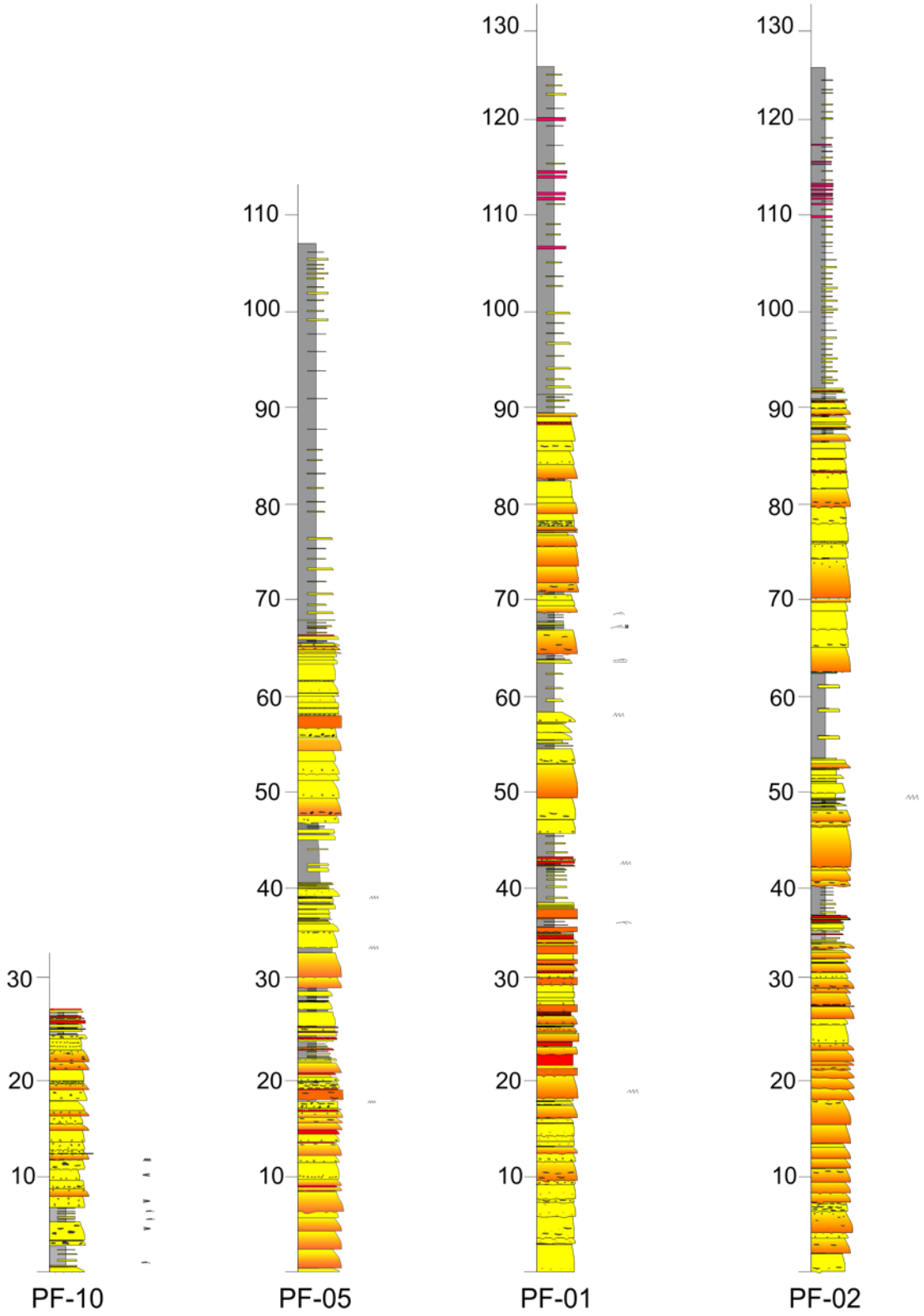

Figure A. 10. *Measured stratigraphic sections in Castle Creek south. For log locations see Figure A.6.*

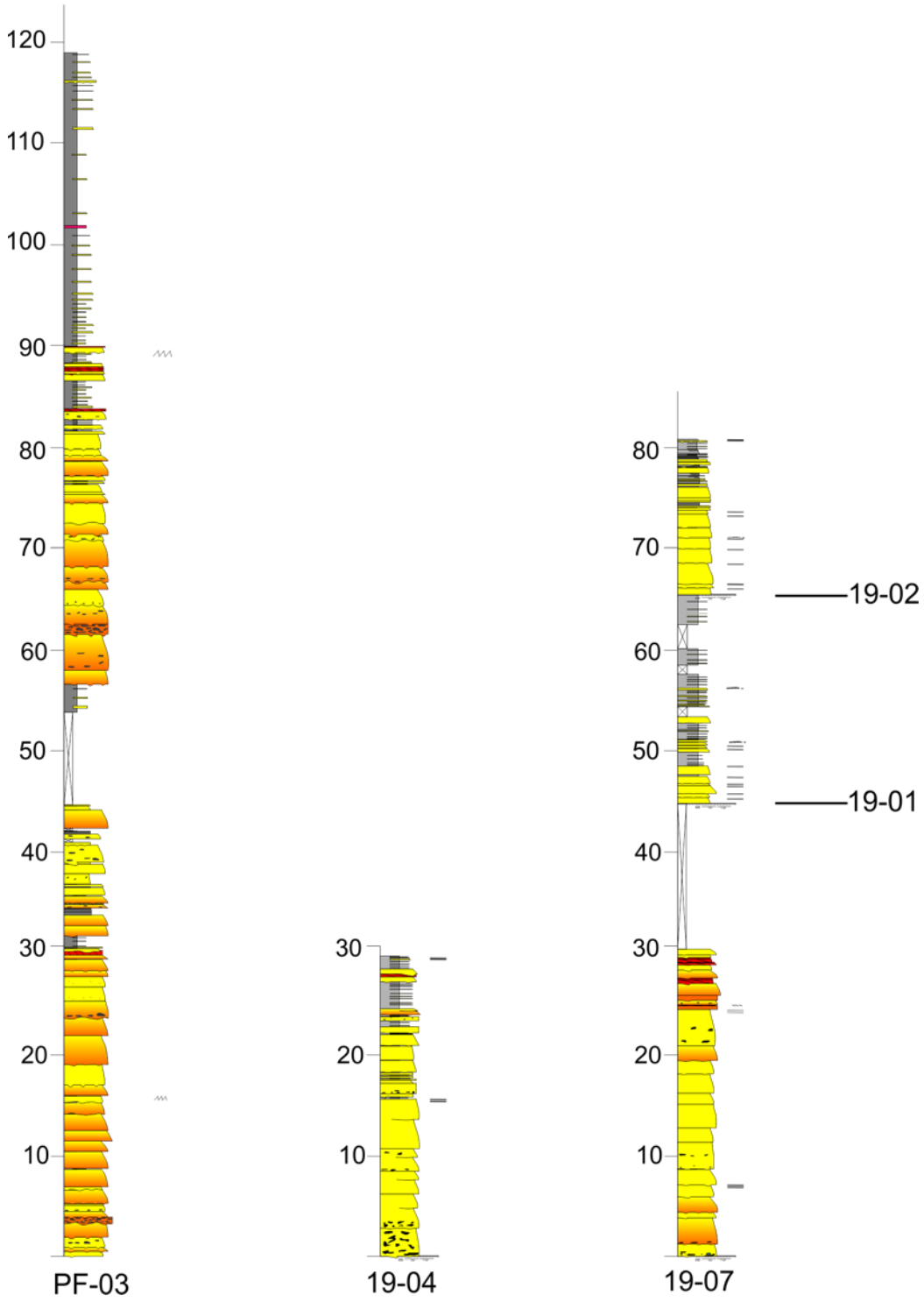

Figure A. 11. *Measured stratigraphic sections in Castle Creek south. For log locations see Figure A.6.*

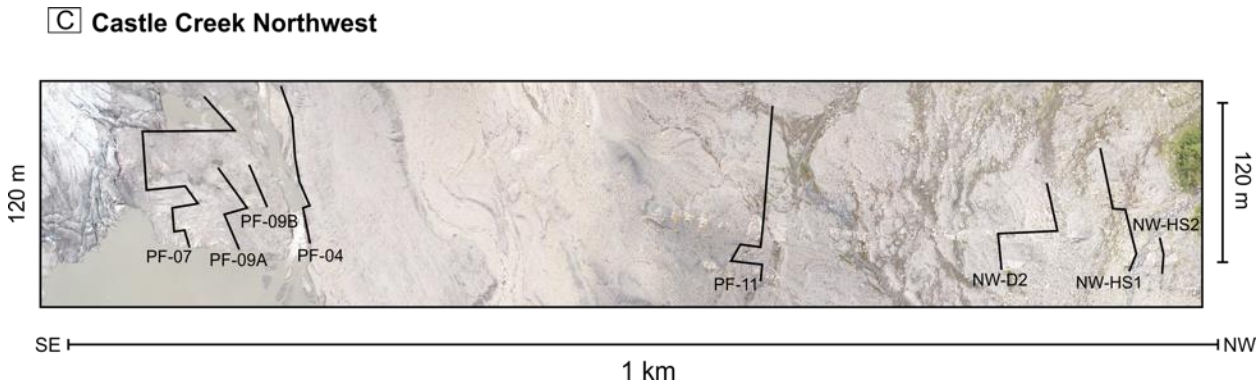

Figure A. 12. *Drone photomosaic from Castle Creek northwest and location of measured stratigraphic sections.*

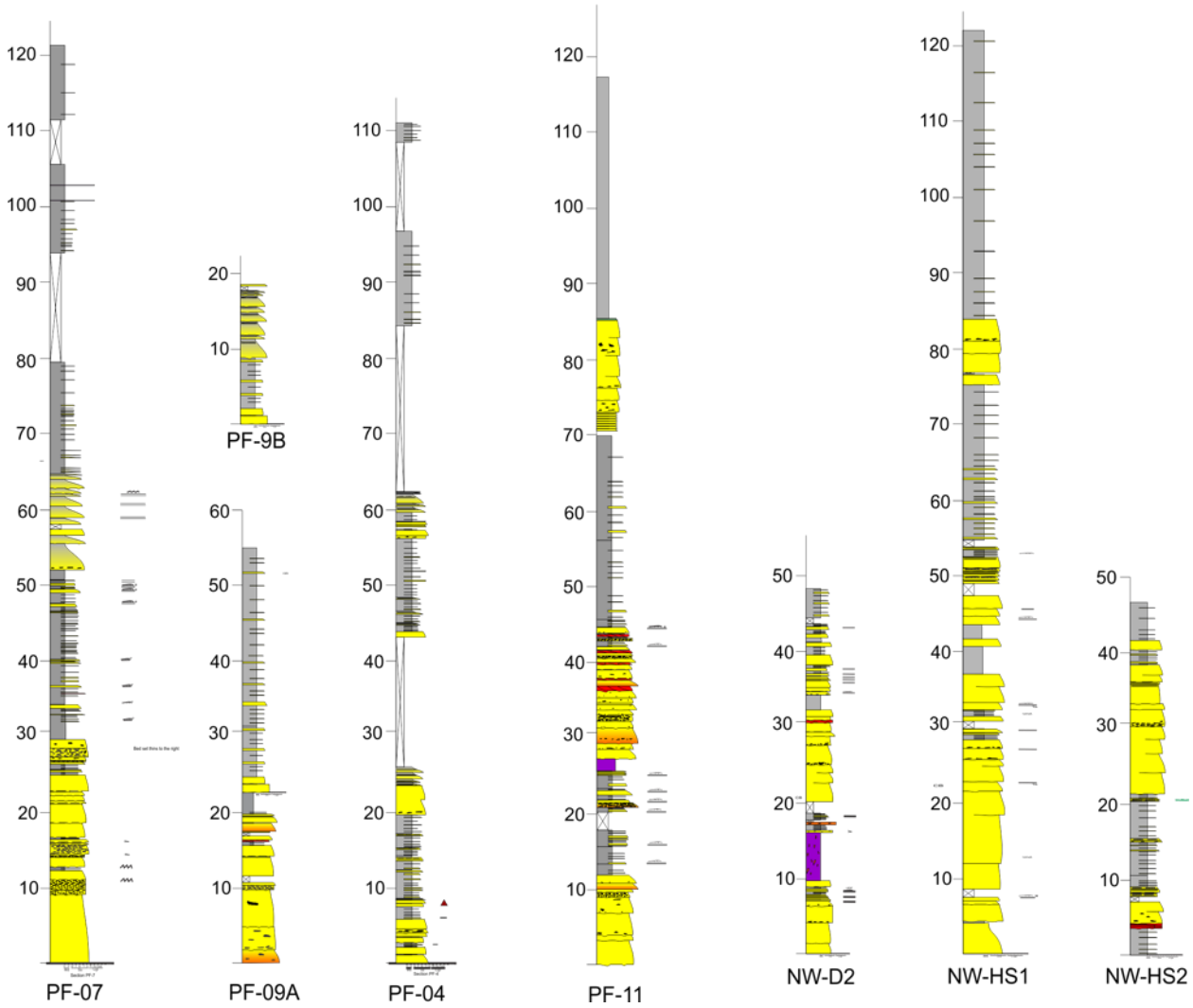

Figure A. 13. *Measured stratigraphic sections in Castle Creek northwest. For log locations see Figure A.12.*

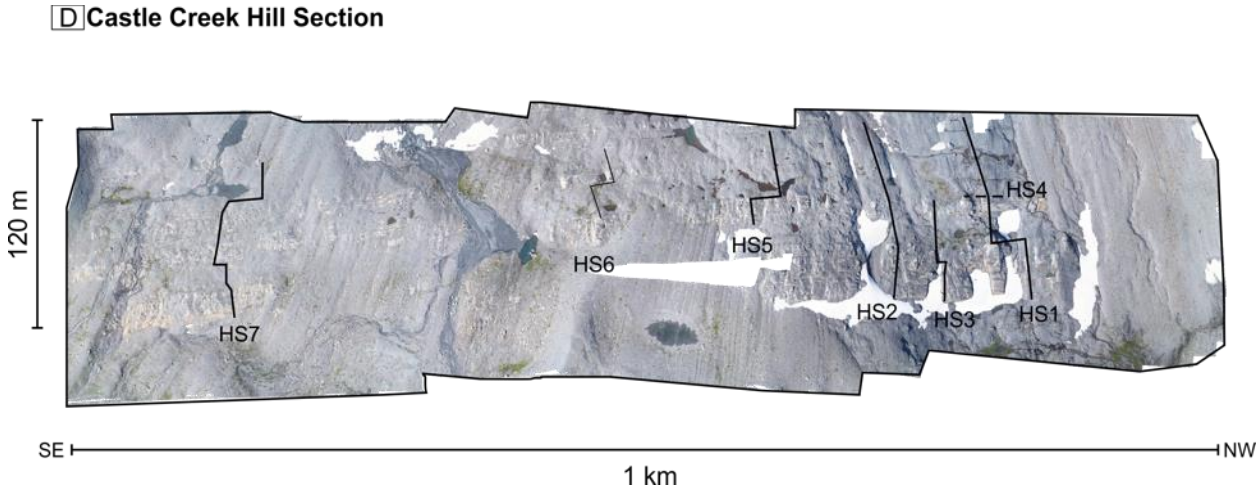

Figure A. 14. *Drone photomosaic from Castle Creek Hill Section and location of measured stratigraphic sections.*

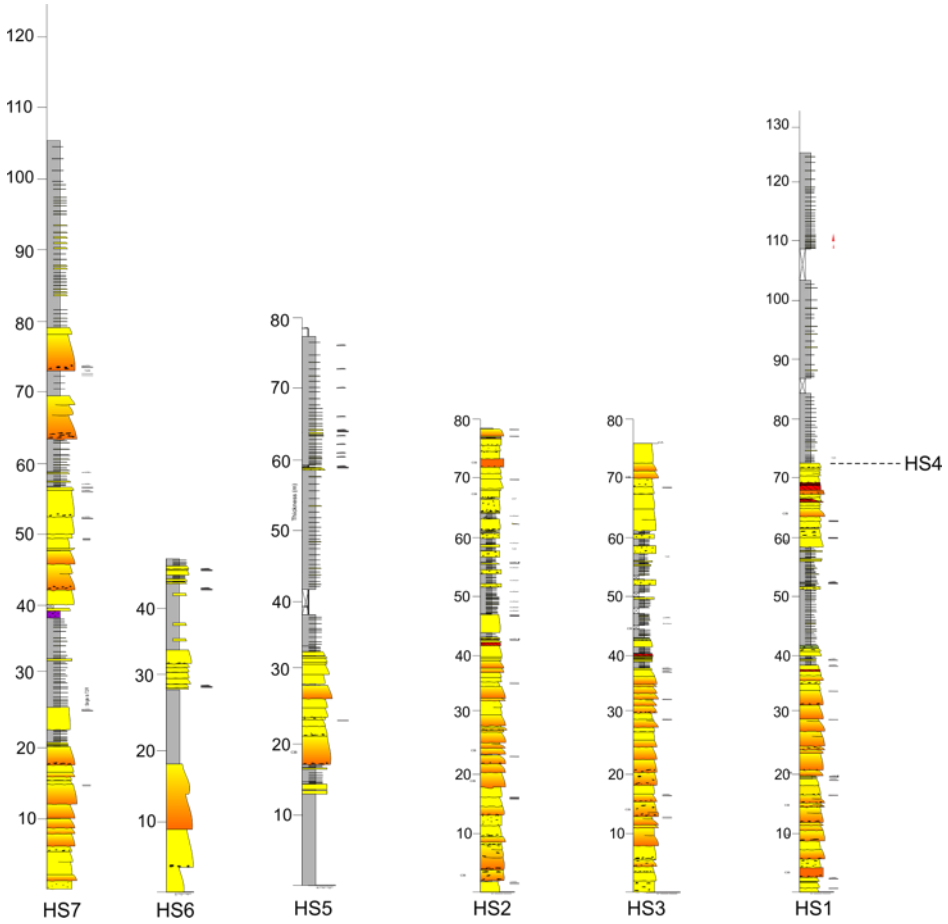

Figure A. 15. *Measured stratigraphic sections in Castle Creek northwest. For log locations see Figure A.14.*

Drone Photomosaic Legend

This study
Navarro (2006)
Anthony (2010)

Stratigraphic Section Legend

Phosphatic-rich claystone


Te= Hemipelagic mudstone or claystone


Tde <1 cm
Tde/Tde's= silty mudstone/silstone/Upper division turbidites


Tcde's= Ripple, Cross-laminated sandstone and siltstone/ Upper division turbidites


Dunes, cross-laminated sandstone


Tb= Parallel-laminated sandstone


Massive Ta= sandstone


Massive Ta= sandstone with granule clasts at the bottom


Mudstone-clast breccia


Normally graded Ta= sandstone


Normally graded sandstone with granule clasts at the bottom


Normally graded, Ta= Granule conglomerate to sandstone


Massive Ta= Granule/Pebbly Conglomerate


Slide deposits


Covered


Parallel lamination

Cross-lamination, single sets of ripples

Cross-lamination, multiple sets of ripples


Flame Structures

Appendix B: Point Counting Analysis

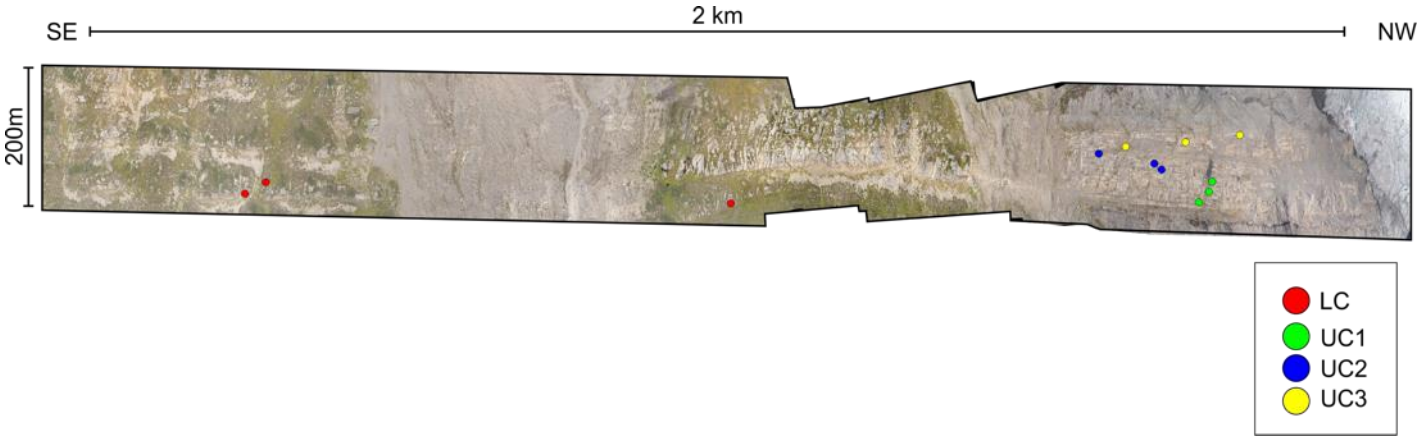

Figure B. 1. *Drone photomosaic of Castle Creek southeast and south with sample location of thick-bedded, coarse-grained sandstone channel fills.*

Samples	Grain Size	Grain Count	Frequency (%)	Cumulative Count	Cumulative Frequency (%)	Φ	Values
Lower Channel Unit Sample LC.1	Pebble	11	4.01	11	4.01	Φ5	-1.98
	Granule	43	15.69	54	19.71	Φ16	-1.4
	Very Coarse	57	20.8	111	40.51	Φ25	-0.73
	Coarse	71	25.91	182	66.42	Φ50	0.21
	Medium	50	18.25	232	84.67	Φ75	1.39
	Fine	24	8.76	256	93.43	Φ84	1.94
	Very Fine	18	6.57	274	100	Φ95	3.09
Lower Channel Unit Sample LC.2	Pebble	25	8.33	25	8.33	Φ5	-2.31
	Granule	54	18	79	26.33	Φ16	-1.39
	Very Coarse	74	24.67	153	51	Φ25	-1.06
	Coarse	62	20.67	215	71.67	Φ50	-0.02
	Medium	47	15.67	262	87.33	Φ75	1.18
	Fine	32	10.67	294	98	Φ84	1.81
	Very Fine	6	2	300	100	Φ95	2.61
Lower Channel Unit Sample LC.2	Pebble	10	3.72	10	3.72	Φ5	-1.89
	Granule	56	20.82	66	24.54	Φ16	-1.27
	Very Coarse	66	24.54	132	49.07	Φ25	-0.99
	Coarse	59	21.93	191	71	Φ50	0.05
	Medium	30	11.15	221	82.16	Φ75	1.38
	Fine	34	12.64	255	94.8	Φ84	2.25
	Very Fine	14	5.2	269	100	Φ95	3.07

Table B. 1 *Lower Channel Unit point count analysis values.*

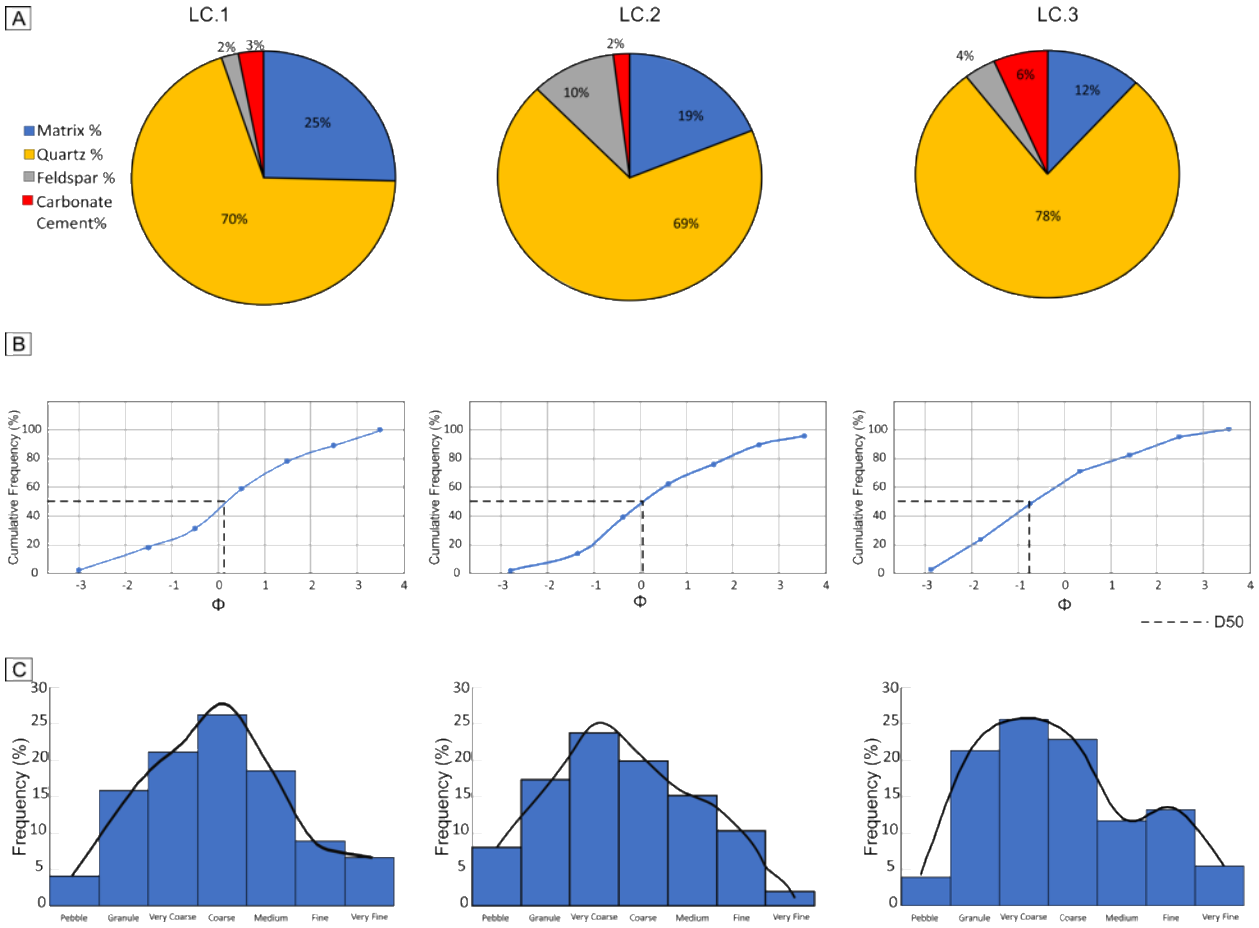

Figure B. 2. Grain size distribution in three thick-bedded, coarse-grained, structureless sandstones from the Lower Channel Unit (LC). (A) Pie graphs showing the mineralogy of constituent components. (B) Cumulative frequency curve. Note that grain size is presented in phi values, which from left to right, changes from pebble (-3) to very fine sand (+3). (C) Histograms of framework grain size.

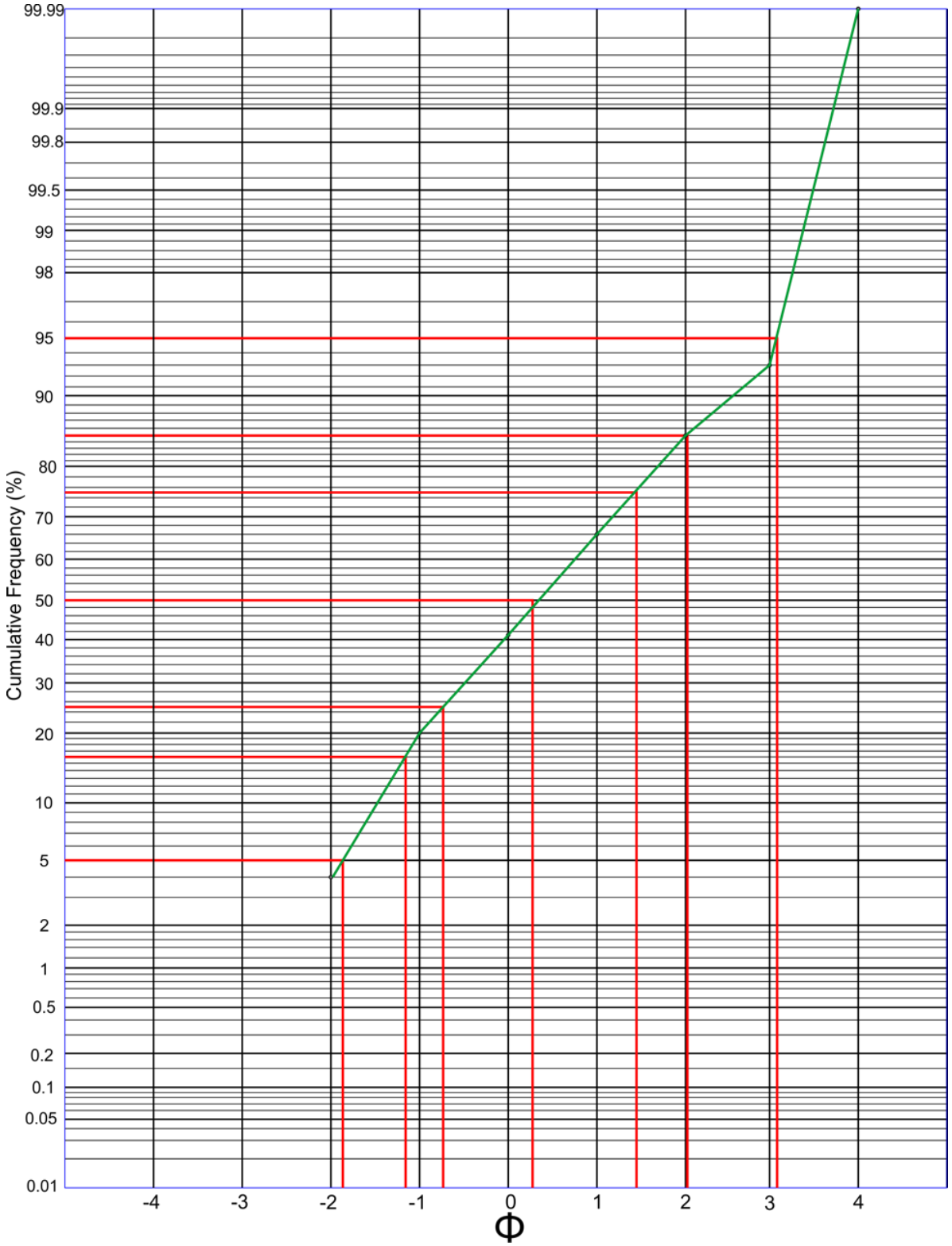

Figure B. 3. *Cumulative Frequency percentage (%) crossed-plotted to phi values using a log probability scale for sample LC.1. Green line represents the cumulative curve, while the red lines yield phi values needed for statistical analysis. For frequency percentage (%) see Table B.1 and for statistical measurement see Table B.5.*

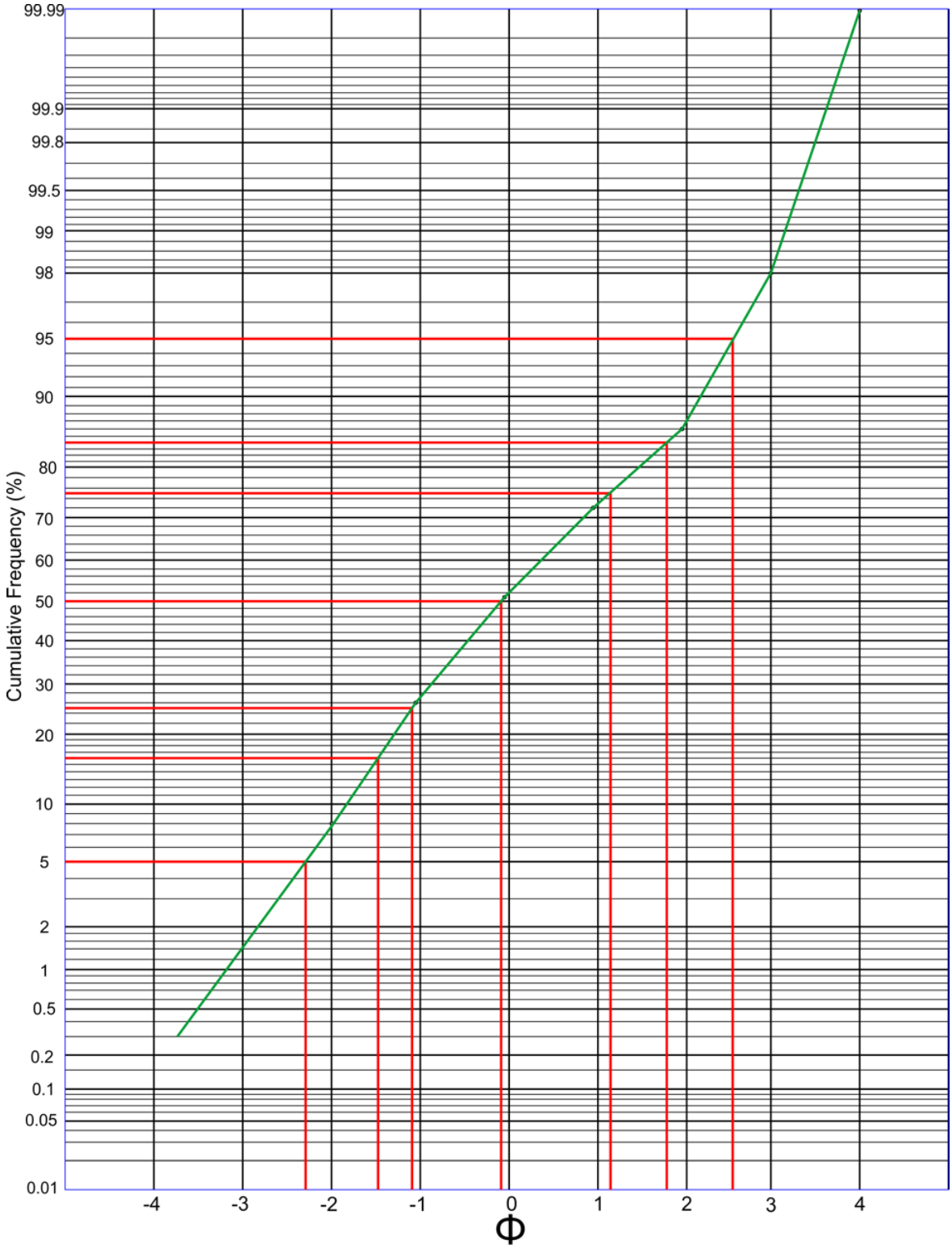

Figure B. 4. Cumulative Frequency percentage (%) crossed-plotted to phi values using a log probability scale for sample LC.2. Green line represents the cumulative curve, while the red lines yield phi values needed for statistical analysis. For frequency percentage (%) see Table B.1 and for statistical measurement see Table B.5.

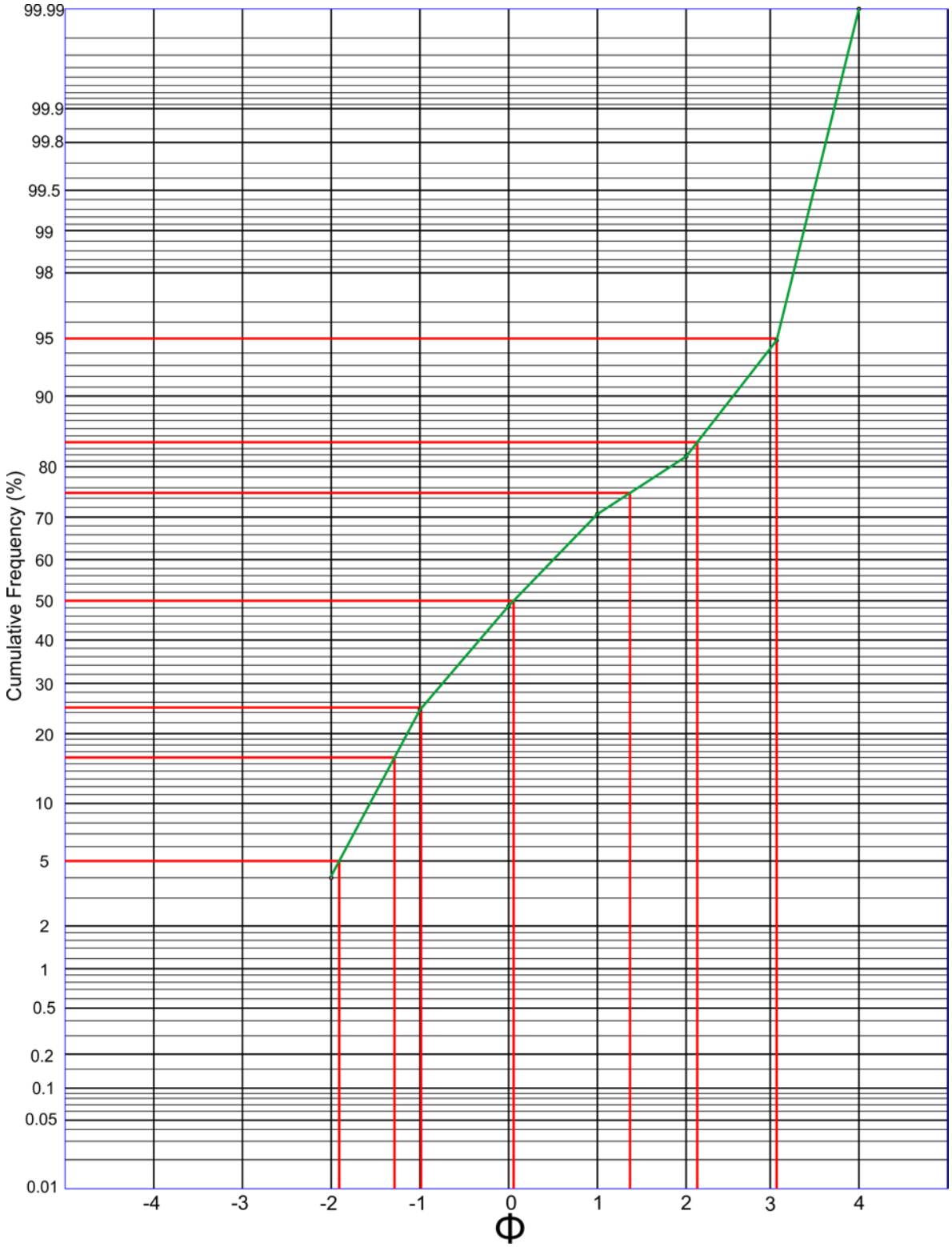

Figure B. 5. *Cumulative Frequency percentage (%) crossed-plotted to phi values using a log probability scale for sample LC.3. Green line represents the cumulative curve, while the red lines yield phi values needed for statistical analysis. For frequency percentage (%) see Table B.1 and for statistical measurement see Table B.5.*

Samples	Grain Size	Grain Count	Frequency (%)	Cumulative Count	Cumulative Frequency (%)	Φ	Values
Upper Channel Unit 1 Sample UC1.1	Pebble	14	7.035	14	7.04	Φ5	-2.19
	Granule	31	15.578	45	22.61	Φ16	-1.38
	Very Coarse	47	23.618	92	46.23	Φ25	-0.92
	Coarse	46	23.116	138	69.35	Φ50	0.13
	Medium	25	12.563	163	81.91	Φ75	1.28
	Fine	26	13.065	189	94.97	Φ84	2.03
	Very Fine	10	5.025	199	100	Φ95	2.95
Upper Channel Unit 1 Sample UC1.2	Pebble	10	3.56	10	3.56	Φ5	-1.88
	Granule	60	21.35	70	24.91	Φ16	-1.37
	Very Coarse	85	30.25	155	55.16	Φ25	-1
	Coarse	69	24.56	224	79.72	Φ50	-0.25
	Medium	29	10.32	253	90.04	Φ75	0.77
	Fine	23	8.19	276	98.22	Φ84	1.35
	Very Fine	5	1.78	281	100	Φ95	2.54
Upper Channel Unit 1 Sample UC1.3	Pebble	4	1.61	4	1.61	Φ5	-1.18
	Granule	16	6.43	20	8.03	Φ16	-0.51
	Very Coarse	67	26.91	87	34.94	Φ25	-0.23
	Coarse	77	30.92	164	65.86	Φ50	0.35
	Medium	37	14.86	201	80.72	Φ75	1.42
	Fine	36	14.46	237	95.18	Φ84	2.17
	Very Fine	12	4.82	249	100	Φ95	2.95

Table B. 2. *Upper Channel Unit 1(UC1) point count analysis values.*

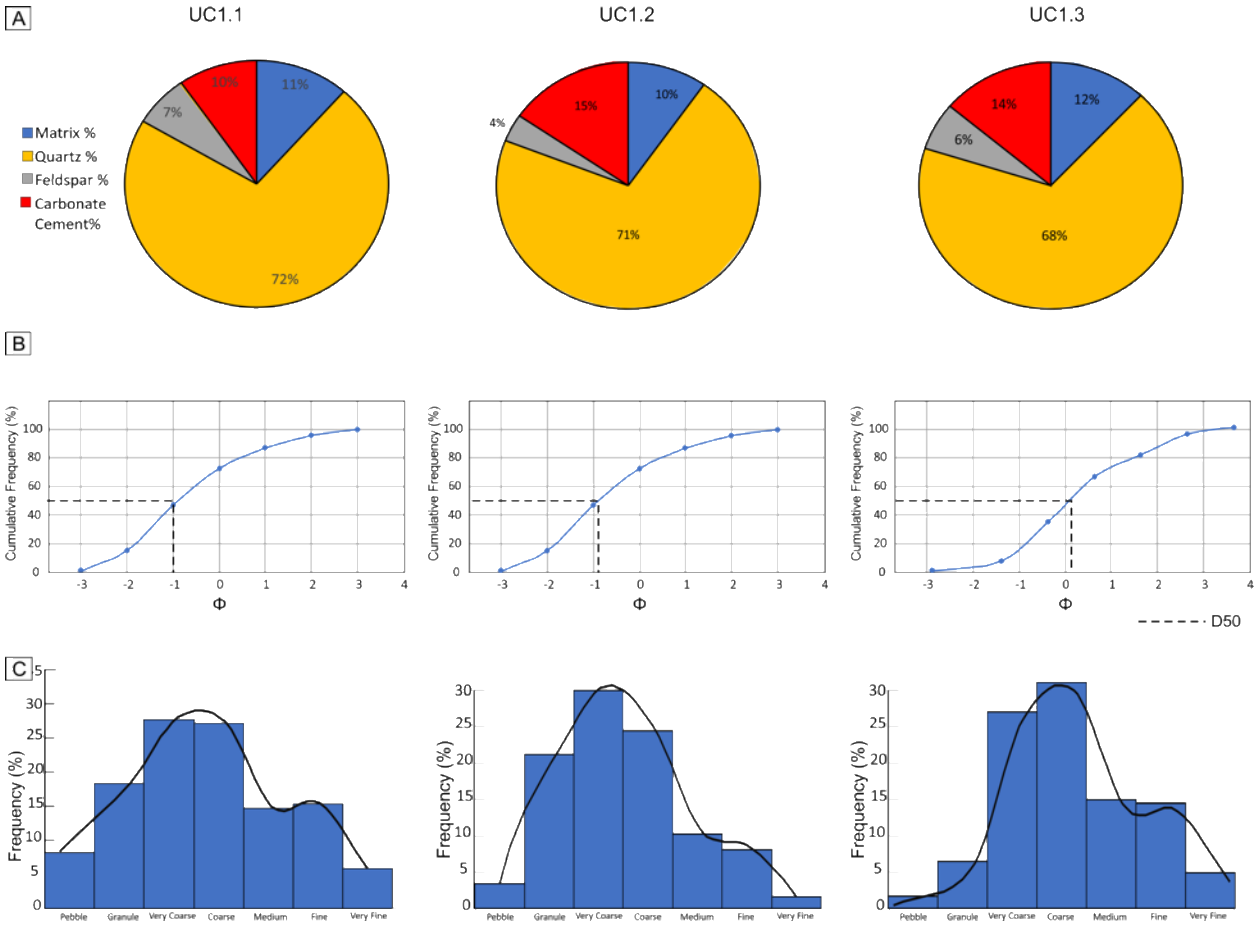

Figure B. 6. *Grain size distribution in three thick-bedded, coarse-grained, structureless sandstones from the Upper Channel Unit 1 (UC1). (A) Pie graphs showing the mineralogy of constituent components. (B) Cumulative frequency curve. Note that grain size is presented in phi values, which from left to right, changes from pebble (-3) to very fine sand (+3). (C) Histograms of framework grain size.*

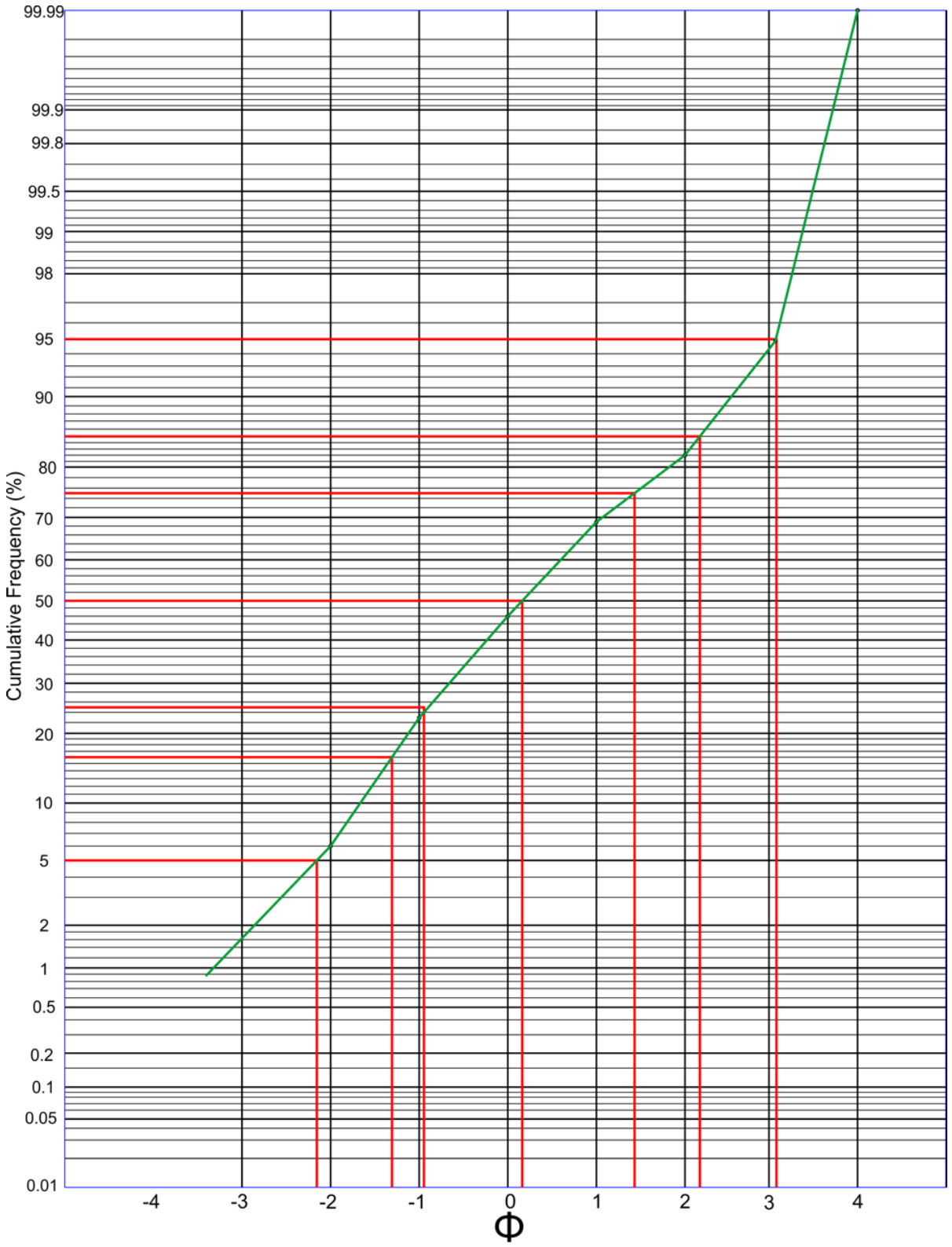

Figure B. 7. *Cumulative Frequency percentage (%) crossed-plotted to phi values using a log probability scale for sample UC1.1. Green line represents the cumulative curve, while the red lines yield phi values needed for statistical analysis. For frequency percentage (%) see Table B.2 and for statistical measurement see Table B.5.*

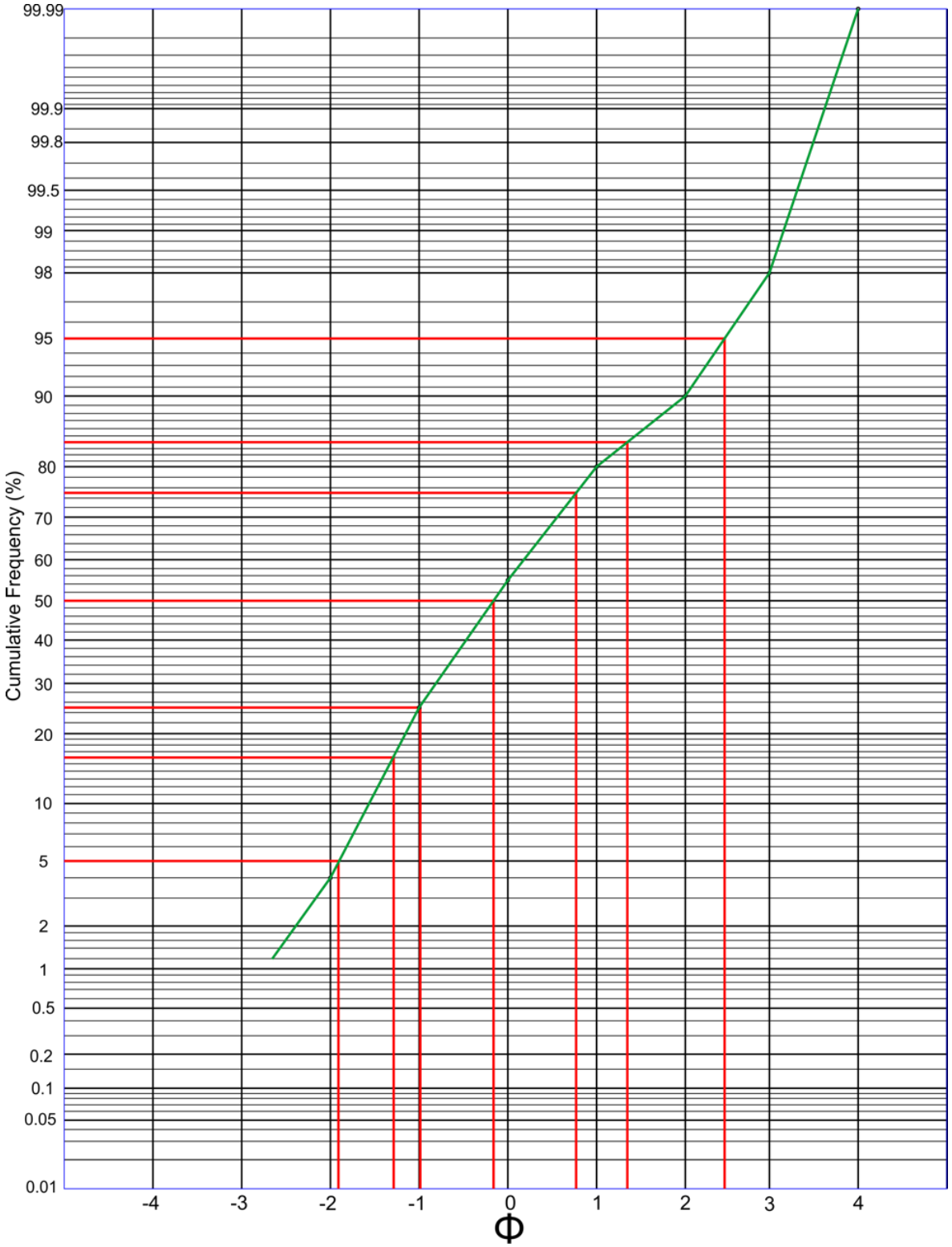

Figure B. 8. *Cumulative Frequency percentage (%) crossed-plotted to phi values using a log probability scale for sample UC1.2. Green line represents the cumulative curve, while the red lines yield phi values needed for statistical analysis. For frequency percentage (%) see Table B.2 and for statistical measurement see Table B.5.*

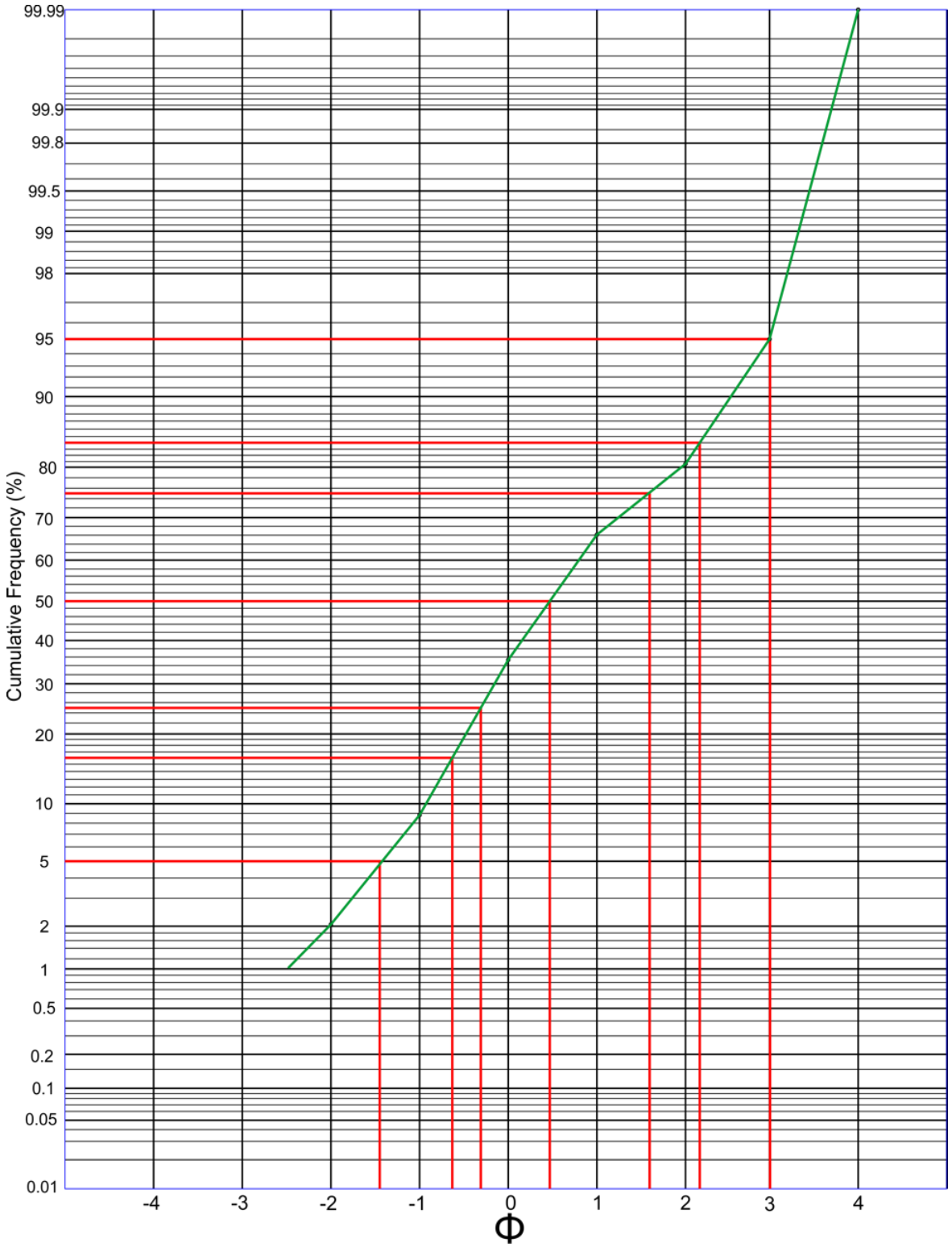

Figure B. 9. *Cumulative Frequency percentage (%) crossed-plotted to phi values using a log probability scale for sample UC1.3. Green line represents the cumulative curve, while the red lines yield phi values needed for statistical analysis. For frequency percentage (%) see Table B.2 and for statistical measurement see Table B.5.*

Samples	Grain Size	Grain Count	Frequency (%)	Cumulative Count	Cumulative Frequency (%)	Φ	Values
Upper Channel Unit 2 Sample UC2.1	Pebble	6	2.41	6	2.41	Φ5	-1.43
	Granule	29	11.65	35	14.06	Φ16	-0.84
	Very Coarse	76	30.52	111	44.58	Φ25	-0.52
	Coarse	69	27.71	180	72.29	Φ50	0.26
	Medium	47	18.88	227	91.16	Φ75	1.14
	Fine	17	6.83	244	97.99	Φ84	1.63
	Very Fine	5	2.01	249	100	Φ95	2.36
Upper Channel Unit 2 Sample UC2.2	Pebble	3	0.73	3	0.73	Φ5	-1.6
	Granule	54	13.17	57	13.9	Φ16	-0.91
	Very Coarse	125	30.49	182	44.39	Φ25	-0.62
	Coarse	116	28.29	298	72.68	Φ50	0.19
	Medium	70	17.07	368	89.76	Φ75	1.09
	Fine	36	8.78	404	98.54	Φ84	1.55
	Very Fine	6	1.46	410	100	Φ95	2.56
Upper Channel Unit 2 Sample UC2.3	Pebble	6	1.95	6	1.95	Φ5	-1.71
	Granule	42	13.64	48	15.58	Φ16	-0.92
	Very Coarse	90	29.22	138	44.81	Φ25	-0.51
	Coarse	93	30.19	231	75	Φ50	0.18
	Medium	34	11.04	265	86.04	Φ75	1
	Fine	31	10.06	296	96.1	Φ84	1.73
	Very Fine	12	3.9	308	100	Φ95	2.77

Table B. 3*. Upper Channel Unit 2 (UC2) point count analysis values.*

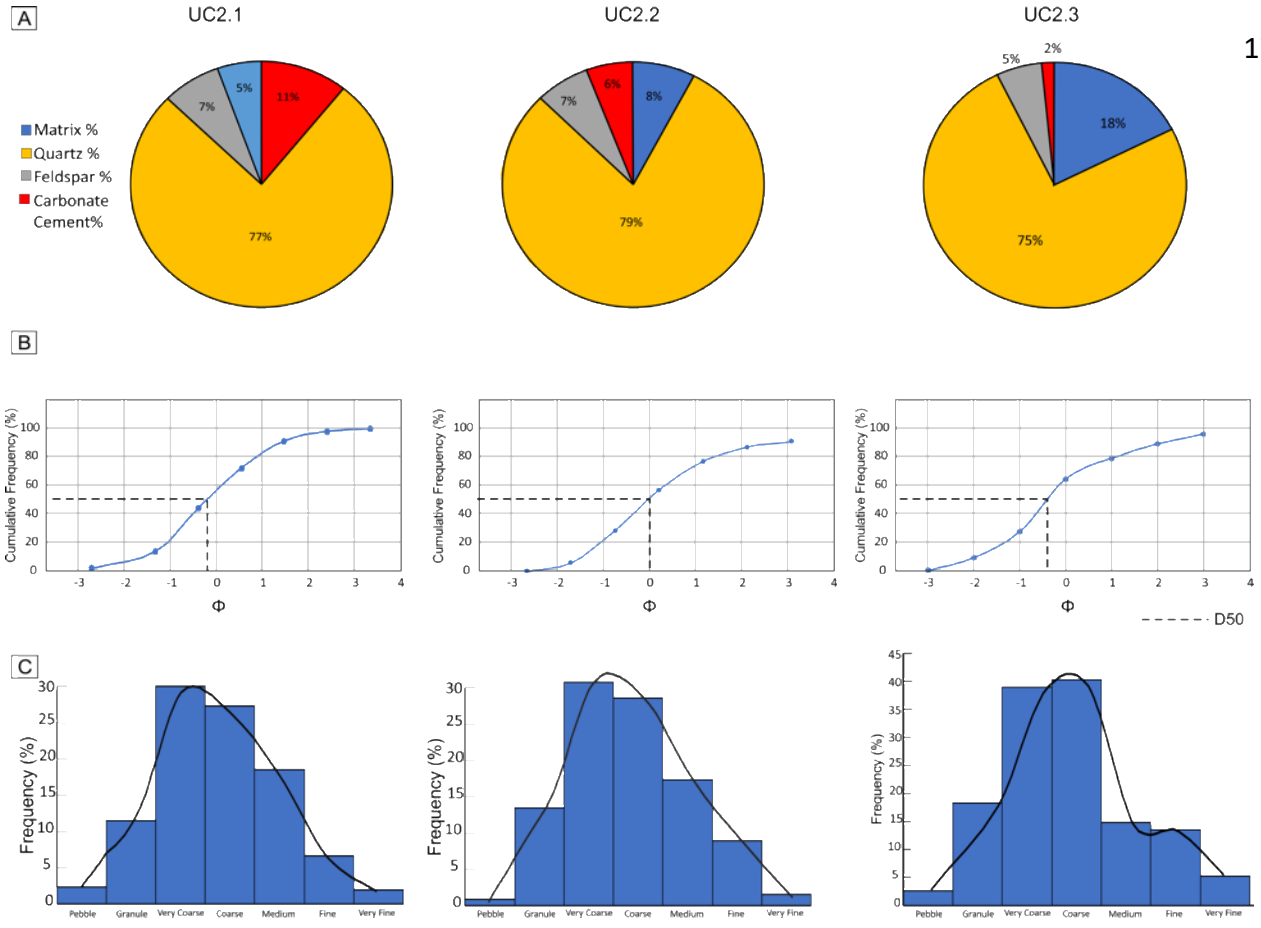

Figure B. 10. *Grain size distribution in three thick-bedded, coarse-grained, structureless sandstones from the Upper Channel Unit 2 (UC2). (A) Pie graphs showing the mineralogy of constituent components. (B) Cumulative frequency curve. Note that grain size is presented in phi values, which from left to right, changes from pebble (-3) to very fine sand (+3). (C) Histograms of framework grain size.*

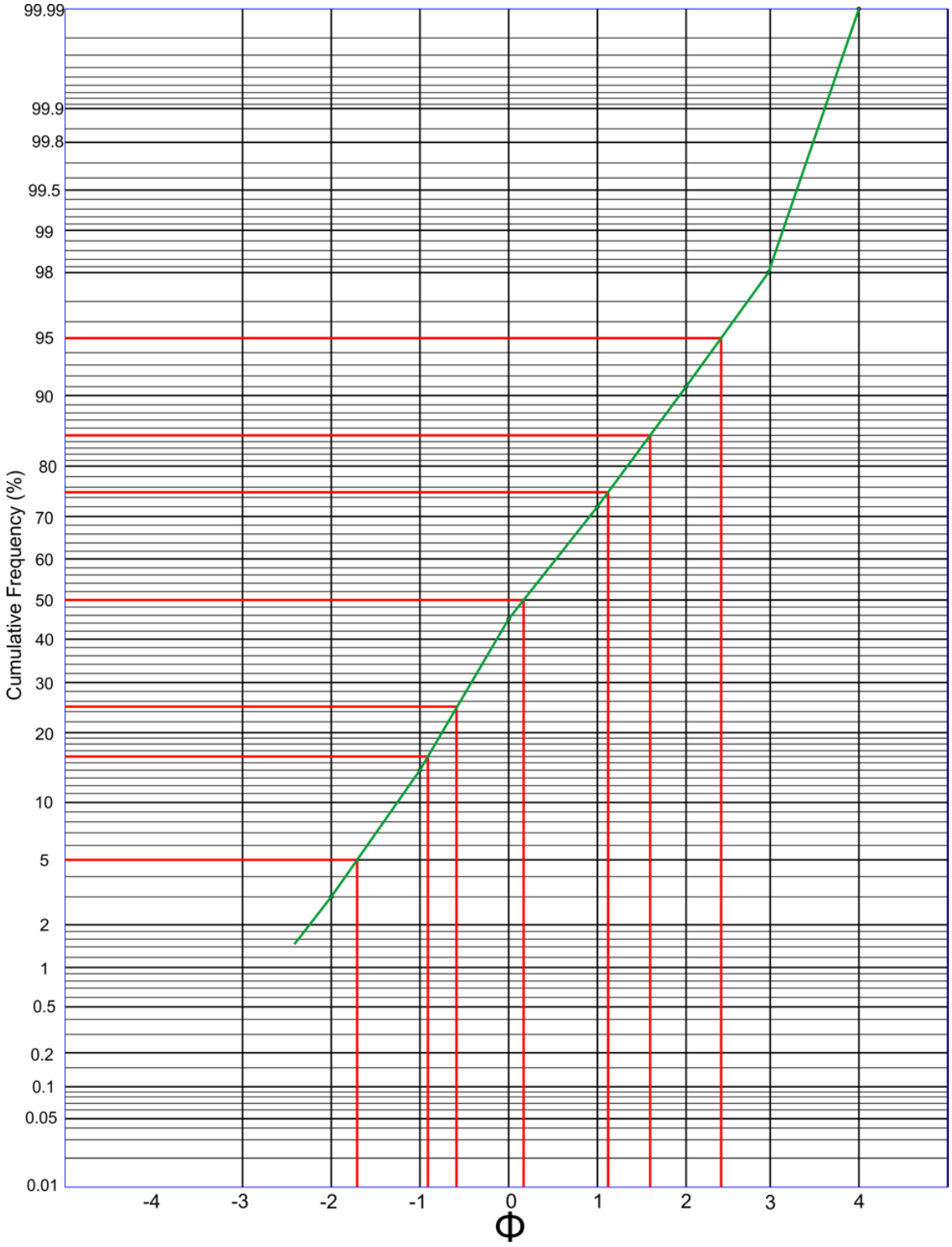

Figure B. 11. *Cumulative Frequency percentage (%) crossed-plotted to phi values using a log probability scale for sample UC2.1. Green line represents the cumulative curve, while the red lines yield phi values needed for statistical analysis. For frequency percentage (%) see Table B.3 and for statistical measurement see Table B.5.*

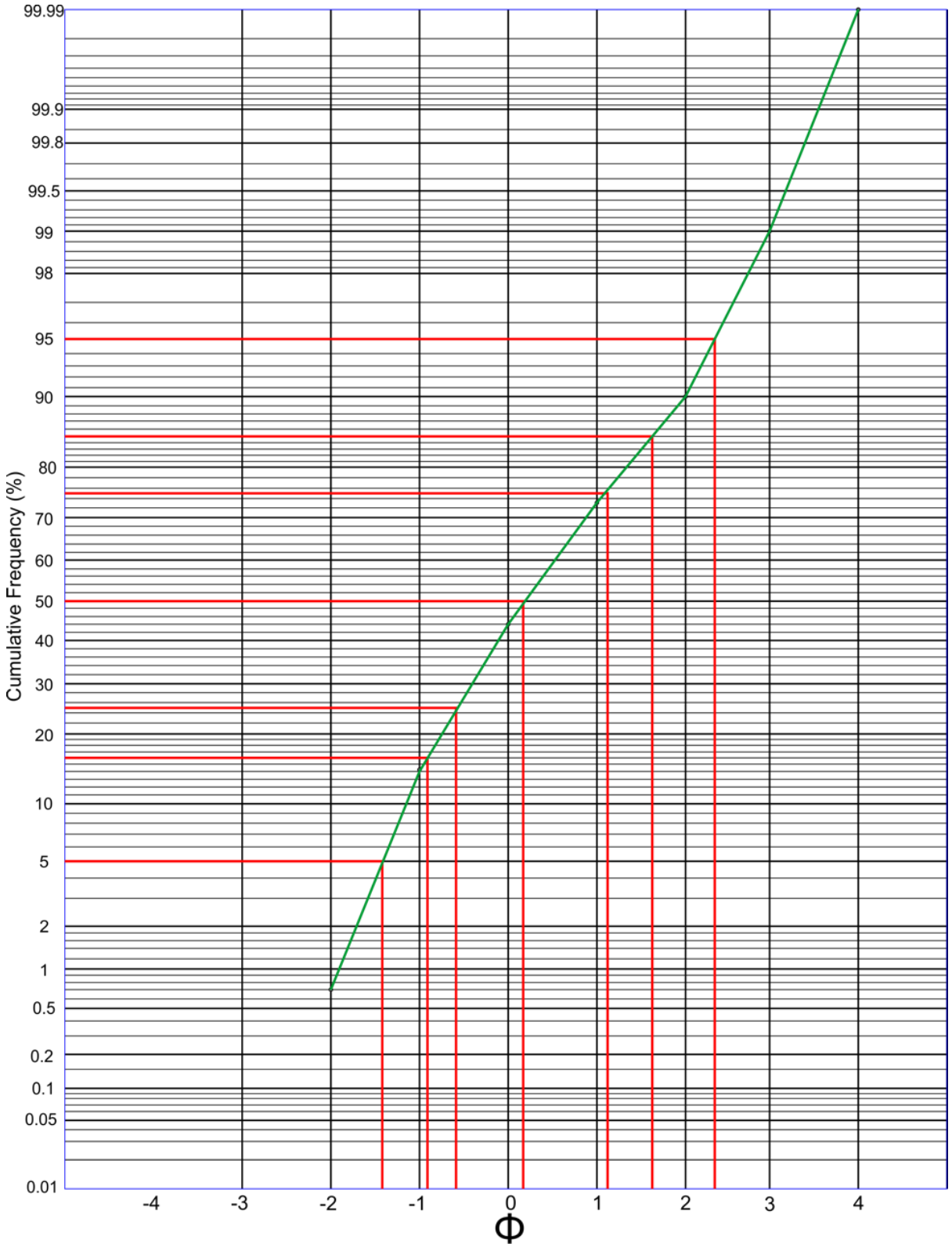

Figure B. 12. *Cumulative Frequency percentage (%) crossed-plotted to phi values using a log probability scale for sample UC2.2. Green line represents the cumulative curve, while the red lines yield phi values needed for statistical analysis. For frequency percentage (%) see Table B.3 and for statistical measurement see Table B.5.*

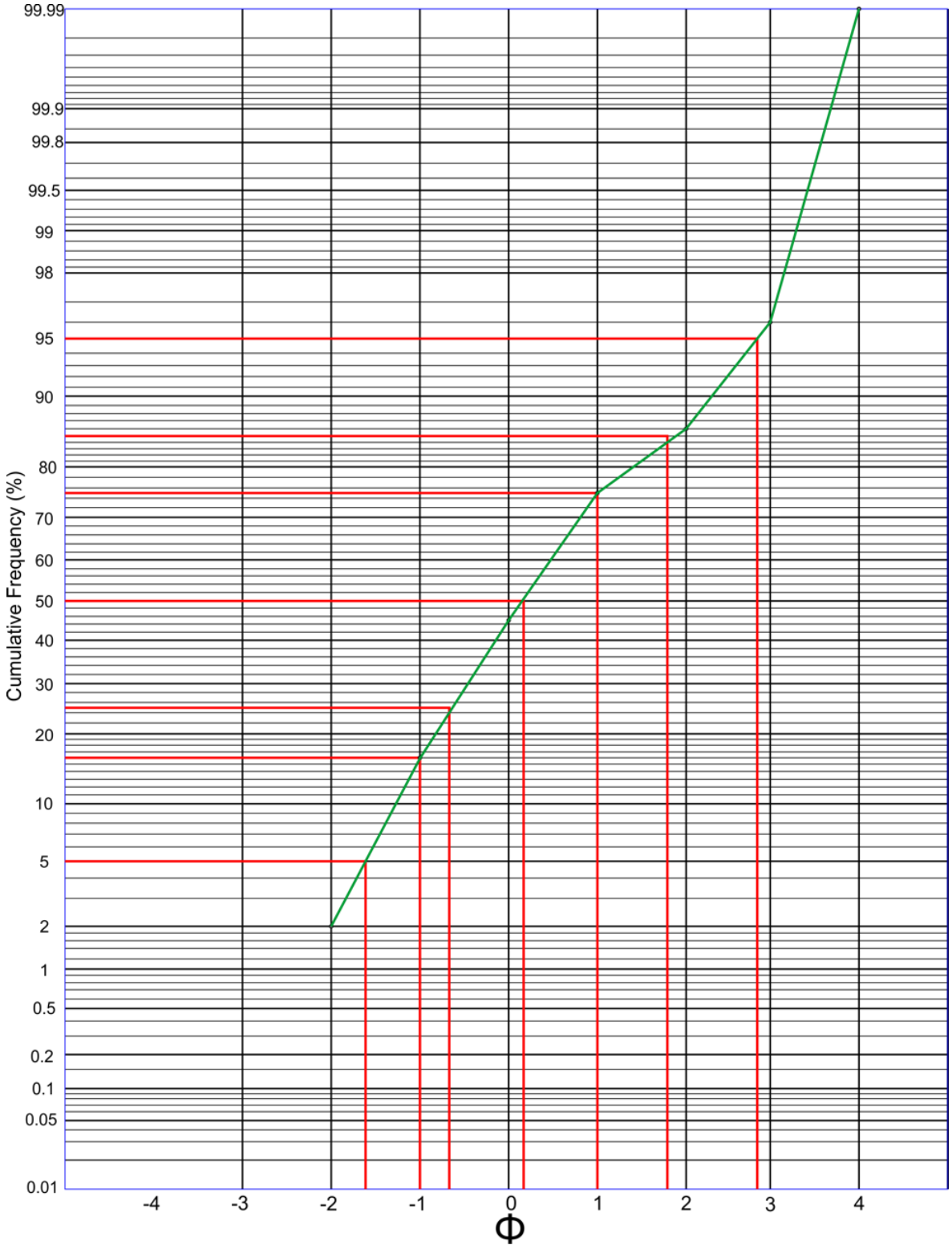

Figure B. 13. *Cumulative Frequency percentage (%) crossed-plotted to phi values using a log probability scale for sample UC2.3. Green line represents the cumulative curve, while the red lines yield phi values needed for statistical analysis. For frequency percentage (%) see Table B.3 and for statistical measurement see Table B.5.*

Samples	Grain Size	Grain Count	Frequency (%)	Cumulative Count	Cumulative Frequency (%)	Φ	Values
Upper Channel Unit 3 Sample UC3.1	Pebble	0	0	0	0	Φ5	-0.39
	Granule	2	0.54	2	0.54	Φ16	0.01
	Very Coarse	56	15.22	58	15.76	Φ25	0.22
	Coarse	159	43.21	217	58.97	Φ50	0.8
	Medium	96	26.09	313	85.05	Φ75	1.47
	Fine	42	11.41	355	96.47	Φ84	1.93
	Very Fine	13	3.53	368	100	Φ95	2.93
Upper Channel Unit 3 Sample UC3.2	Pebble	0	0	0	0	Φ5	-0.7
	Granule	8	2.44	8	2.44	Φ16	-0.27
	Very Coarse	78	23.78	86	26.22	Φ25	-0.02
	Coarse	130	39.63	216	65.85	Φ50	0.56
	Medium	69	21.04	285	86.89	Φ75	1.31
	Fine	29	8.84	314	95.73	Φ84	1.8
	Very Fine	14	4.27	328	100	Φ95	2.98
Upper Channel Unit 3 Sample UC3.3	Pebble	0	0	0	0	Φ5	-0.48
	Granule	3	1.1	3	1.1	Φ16	-0.15
	Very Coarse	62	22.79	65	23.9	Φ25	0.03
	Coarse	118	43.38	183	67.28	Φ50	0.5
	Medium	60	22.06	243	89.34	Φ75	1.29
	Fine	17	6.25	260	95.59	Φ84	1.64
	Very Fine	12	4.41	272	100	Φ95	2.82

Table B. 4. *Upper Channel Unit 3 (UC3) point count analysis values*

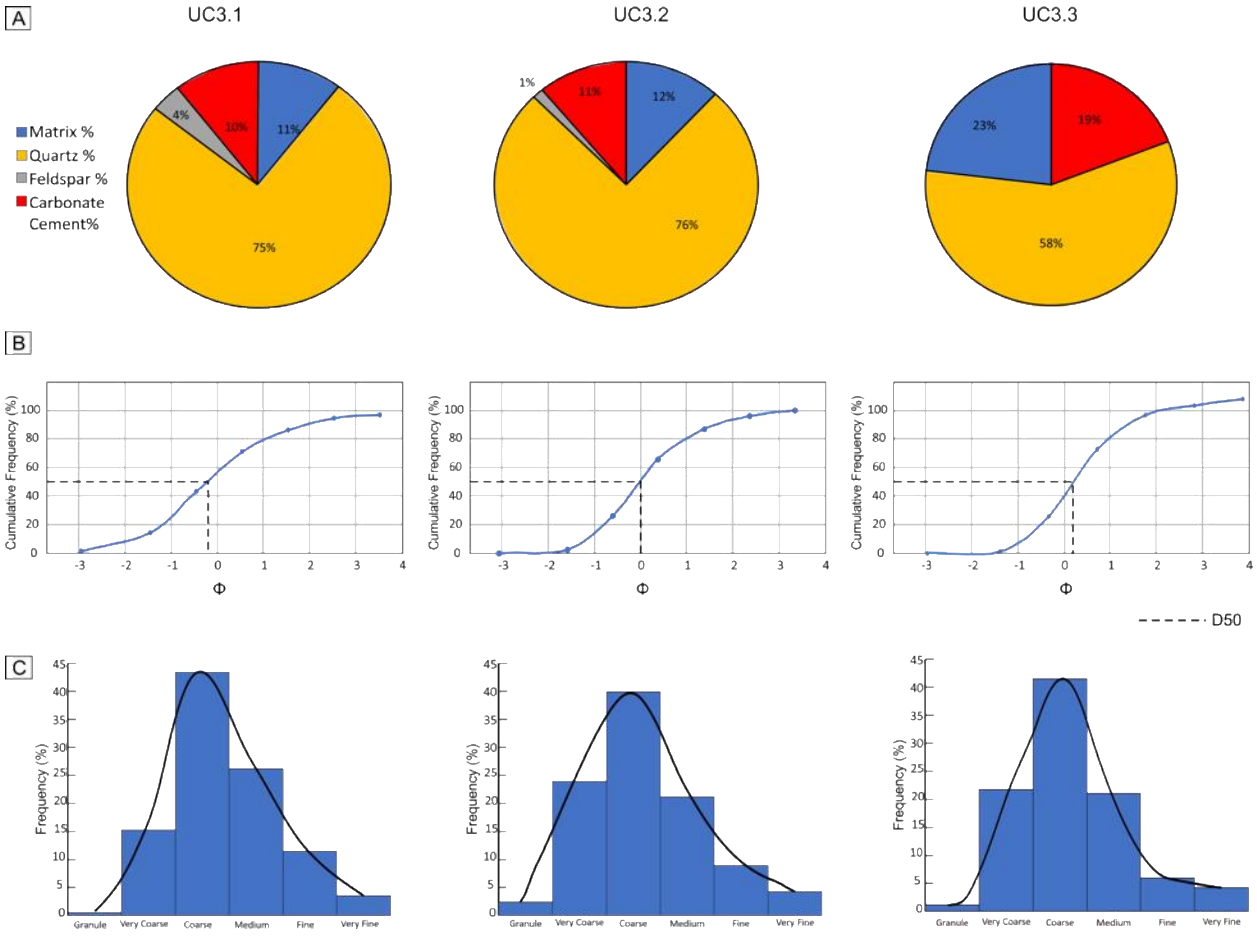

Figure B. 14. *Grain size distribution in three thick-bedded, coarse-grained, structureless sandstones from the Upper Channel Unit 3 (UC3). (A) Pie graphs showing the mineralogy of constituent components. (B) Cumulative frequency curve. Note that grain size is presented in phi values, which from left to right, changes from pebble (-3) to very fine sand (+3). (C) Histograms of framework grain size.*

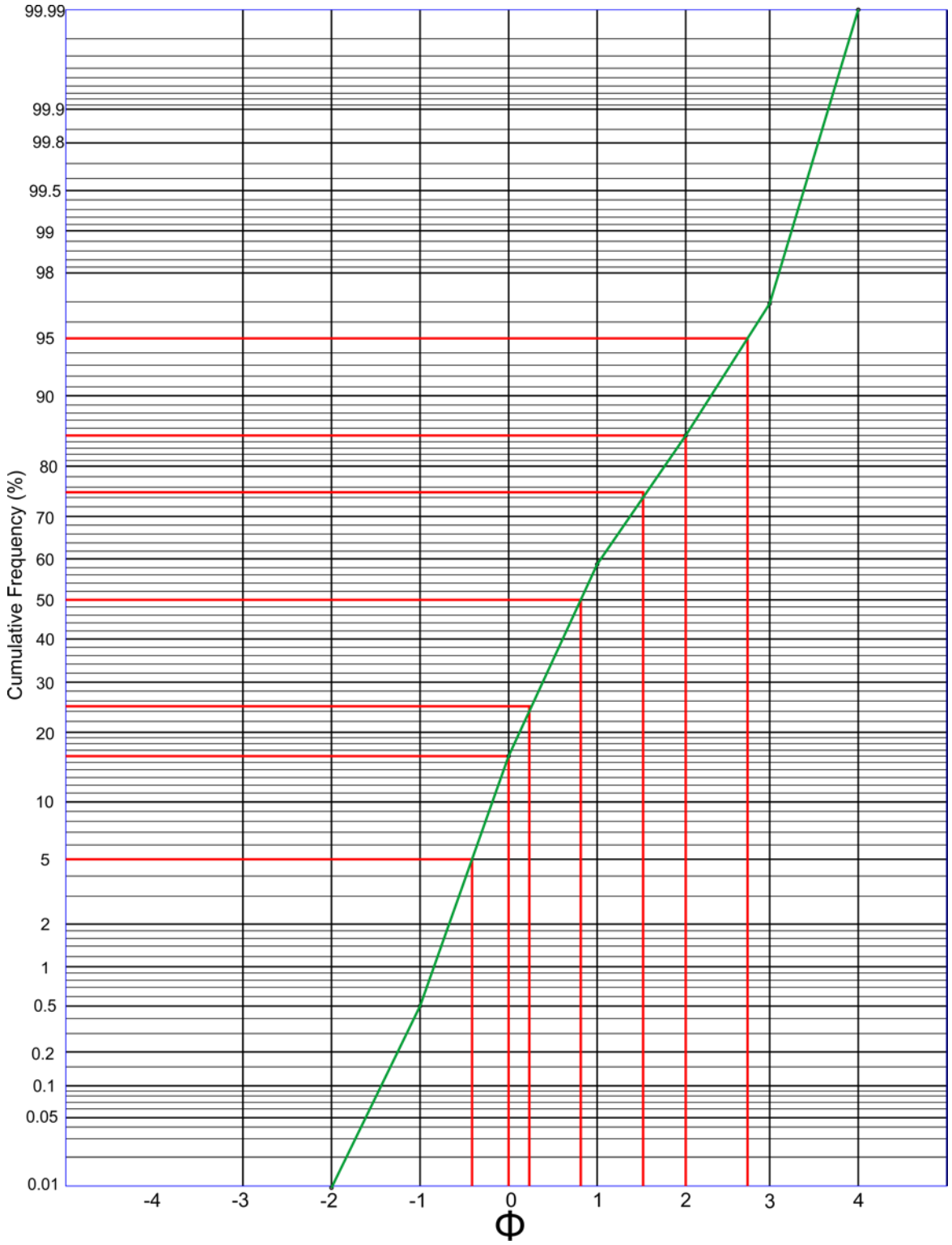

Figure B. 15. *Cumulative Frequency percentage (%) crossed-plotted to phi values using a log probability scale for sample UC3.1. Green line represents the cumulative curve, while the red lines yield phi values needed for statistical analysis. For frequency percentage (%) see Table B.4 and for statistical measurement see Table B.5.*

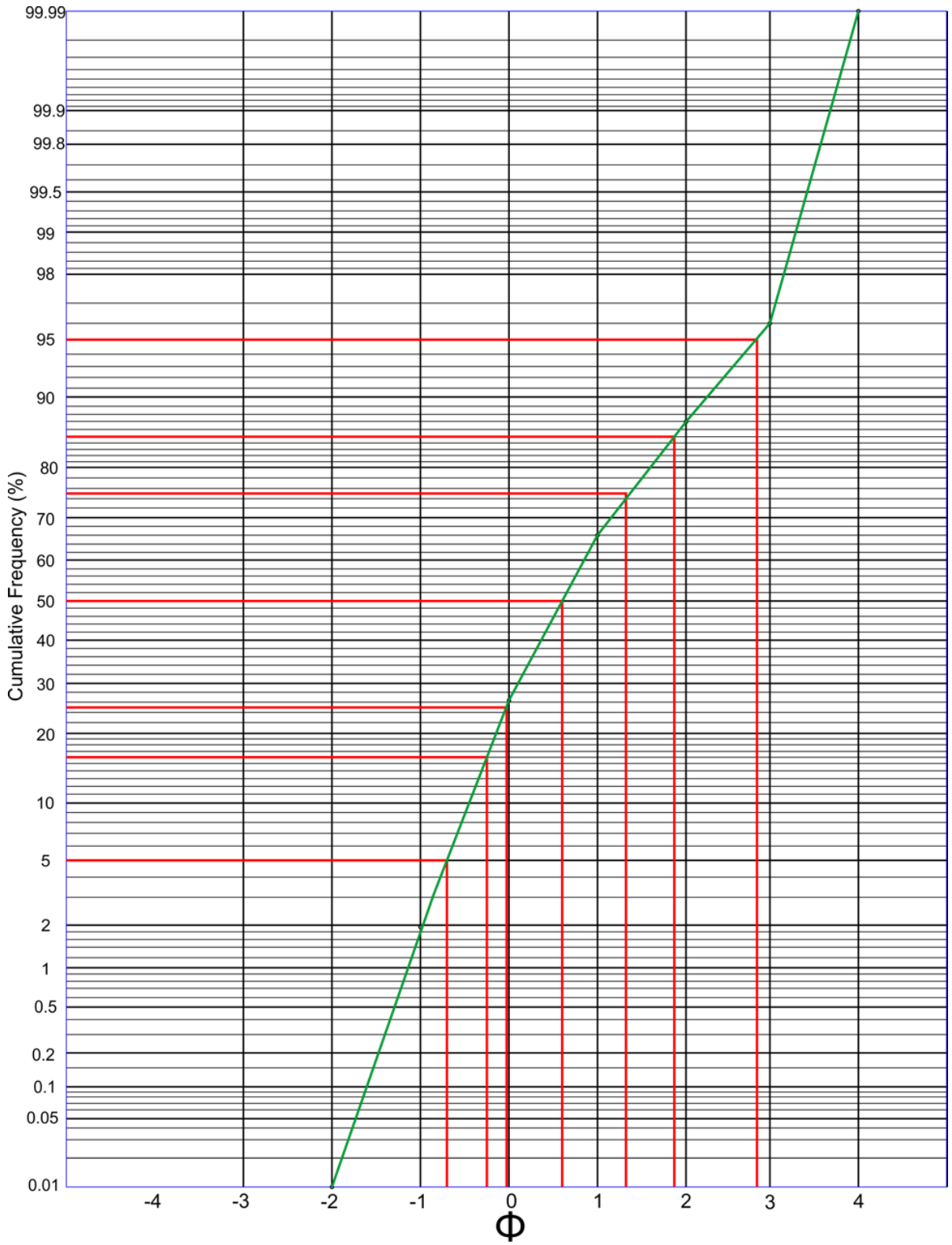

Figure B. 16. *Cumulative Frequency percentage (%) crossed-plotted to phi values using a log probability scale for sample UC3.2. Green line represents the cumulative curve, while the red lines yield phi values needed for statistical analysis. For frequency percentage (%) see Table B.4 and for statistical measurement see Table B.5.*

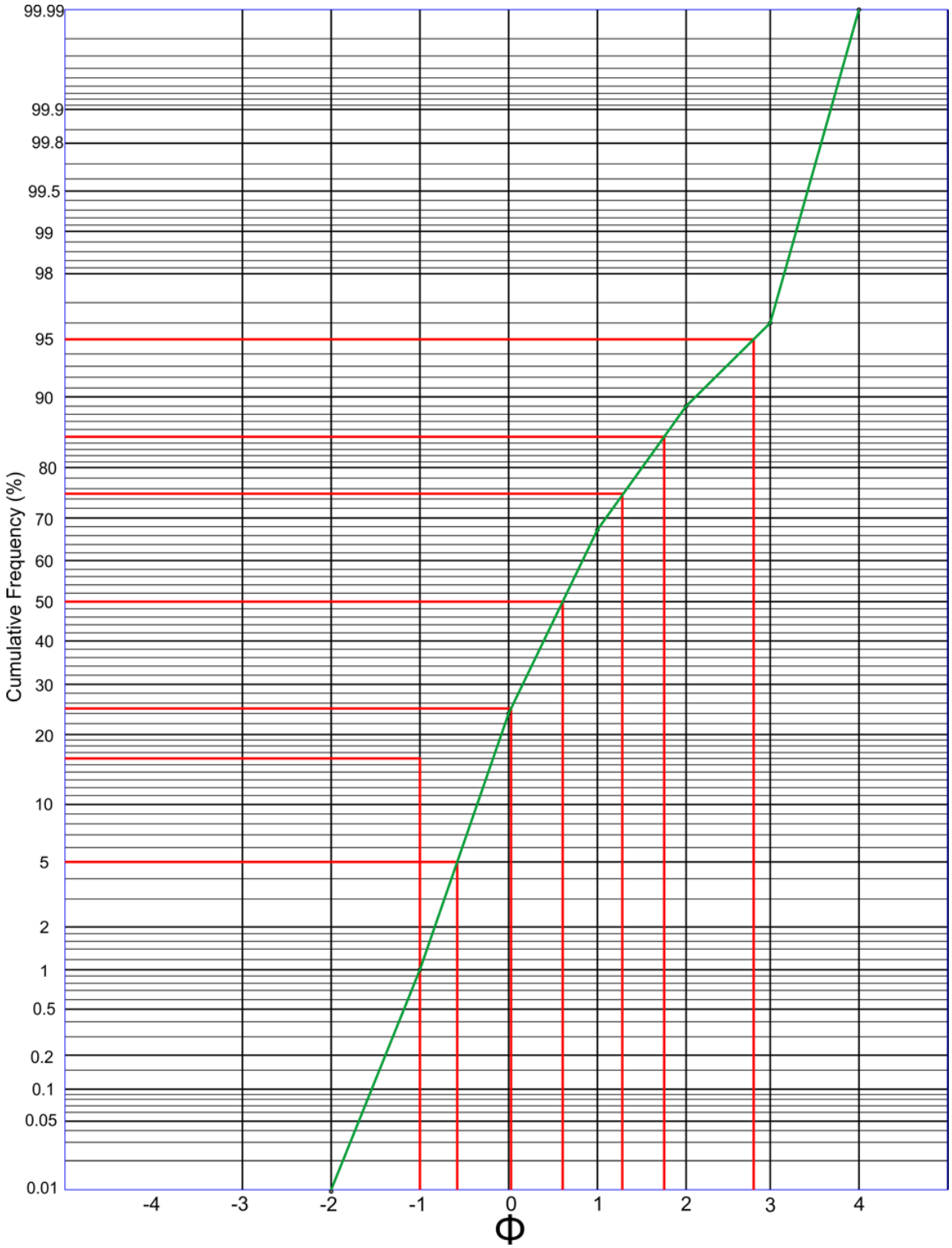

Figure B. 17. Cumulative Frequency percentage (%) crossed-plotted to phi values using a log probability scale for sample UC3.3. Green line represents the cumulative curve, while the red lines yield phi values needed for statistical analysis. For frequency percentage (%) see Table B.4 and for statistical measurement see Table B.5.

Channel Unit	Channel Unit Sample	Facies	Mean (mm)	Median	Mode	STDV	SK	K
Lower Channel Unit (LC)	LC.1	F1.1	0.84	0.86	0.71	1.6	0.07	0.98
	LC.2	F1.1	0.91	1.01	1.4	1.55	-0.01	0.9
	LC.3	F1.1	0.79	1.6	1.57	1.63	0.27	0.86
Combined LC			0.87	0.93	1.32	1.58	0.12	0.91
Upper Channel Unit 1 (UC1)	UC1.1	F1.1	0.84	0.88	1.14	1.63	0.04	0.96
	UC1.2	F1.1	1.06	1.20	1.41	1.35	0.34	1.02
	UC1.3	F1.1	0.63	0.78	0.84	1.3	0.16	1.03
Combined UC1			0.81	0.90	1.15	1.47	0.15	1.0
Upper Channel Unit 2 (UC2)	UC2.1	F1.1	0.78	0.87	1.16	1.19	0.09	0.93
	UC2.2	F1.1	0.82	0.86	1.07	1.24	0.29	1
	UC2.3	F1.1	0.79	0.89	0.93	1.34	0.51	1.08
Combined UC2			0.81	0.88	1.18	1.27	0.26	1.00
Combined aggradational Channel fill	LC through UC2		0.83	0.9	1.17	1.45	0.16	1.02

Channel Complex	Channel Unit Sample	Facies	Mean (mm)	Median	Mode	STDV	SK	K
Upper Channel Unit 3 (UC3)	UC3.1	F1.1	0.53	0.57	0.68	0.98	0.51	1.08
	UC3.2	F1.1	0.62	0.68	0.71	1.02	0.57	1.13
	UC3.3	F1.1	0.63	0.71	0.71	0.95	0.74	1.21
Combined laterally accreting channel fill	UC3		0.58	0.64	0.71	1.02	0.57	1.14

Table B. 5. *Statistical measurements for each individual sample and combined for aggradational and laterally-accreting channel fills using logarithmic graphical measurements of Folk and Ward (1957). STDV= standard deviation, SK= skewness and K= kurtosis.*